Development and Application of Synthetic Lipid Probes to Study and Mimic Lipid Function

A Dissertation Presented for the
Doctor of Philosophy
Degree
The University of Tennessee, Knoxville

Heidi Elizabeth Bostic
August 2012

Copyright © 2012 by Heidi Elizabeth Bostic
All rights reserved.

Dedication

This dissertation is dedicated in loving memory of Grandma Carolyn. I will never forget all of the thoughts, love, and prayers that were delivered to my door because of you; always right when I needed it most. I can only hope to live a Godly life in the way you have set the example before me.

Acknowledgements

First and foremost I would like to thank my Heavenly Father for loving me unconditionally and showing me that with Him, nothing is impossible, including earning a PhD. Secondly, I would like to thank my family and friends, the folks responsible for keeping me (sort of) sane. You are the best I could've ever asked for! I am luckier to have y'all than any person deserves to be. You have been there when I needed you as an ear to listen, a shoulder to cry on, and a giver of tough love when I was in the wrong; whatever I needed at the time, you were it. Mom and Dad, you have been two of the most supportive and loving parents anyone could ask for. Hollie and Heather, you guys paved the way before me and showed me that I really could achieve whatever I set my mind to, exactly the way I hope to prove to Alyssa that she can also achieve anything!

My advisor, Dr. Best, I am most appreciative of all that you have done to help mold me into the proud chemist I am today. You have taught me so much and always worked patiently with me, which I know has not always been easy for either of us. Drs. Campagna, Jenkins, and Reynolds, thank you guys for taking your time to serve on my committee and holding me to the high standards expected of the recipient of a doctorate degree.

Abstract

Lipids are biologically important molecules as they regulate a litany of key cellular processes that, when aberrant, result in disease. Since lipids control these regulation pathways, it is imperative to understand their properties and exploit them for use in advancing therapeutic strategies. The complex environments in which lipids exist have historically complicated their understanding, but recent advancements have facilitated this effort. In the chapters that follow, we have used synthetic lipid probes to investigate the role of signaling lipids as site-specific ligands in the binding of protein effectors and developed a high-throughput platform that can be used to rapidly classify protein-binding partners to phosphoinositide lipids. Using microarray analysis, we have achieved high-throughput binding results for the Akt-PH domain to phosphatidylinositol-(3,4,5)-trisphosphate. In addition, preliminary results from an investigation of how multivalency affects profilin binding to phosphatidylinositol-(4,5)-bisphosphate are discussed. We have also developed the first known example of liposome modification *via* copper-free click chemistry as an ideal bioorthogonal approach to intact membrane derivatization towards targeting applications. Using a microplate surface-based immobilization technique, we have reported the derivatization of intact azido-liposomes with a biotinylated cyclooctyne by copper-free click chemistry and performed various control reactions to ensure labeling is specific and reliable. Additionally, we have reported initial findings for the advancement of this liposome immobilization strategy to be performed in high-throughput fashion via microarray. In the final chapter, we briefly discuss our involvement in a few collaborative efforts including the optimization of a

non-lipid autotaxin inhibitor, synthesis of porphyrin-lipid conjugates for use in photocurrent generation systems, and synthesis of several rhodamine dyes for use in surface enhanced hyper Raman spectroscopy (SEHRS).

Table of Contents

Chapter 1: Introduction 1
1.1 Phospholipids 2
1.2 Signaling Lipids that Bind Proteins 3
1.3 Assays for Studying Lipid Interactions 5
1.3.1 Dot-Blot Assays 5
1.3.2 Direct Fluorescence Assays 6
1.3.3 FRET Assays 6
1.3.4 Surface Plasmon Resonance Assays 7
1.3.5 Calorimetry Assays 8
1.3.6 Lipid Monolayer Penetration Assays 8
1.3.7 Separation Assays 9
1.4 Membrane Interactions and Fusion 10
1.5 Bioorthogonal Reactions 11
1.5.1 Staudinger Ligation 11
1.5.2 Copper Catalyzed Azide–Alkyne Cycloaddition 13
1.5.3 Copper-Free Click Chemistry 15
1.5.4 Examples of Bioorthogonal Labeling Using Lipid Probes 17
Chapter 2: Microarray Analysis of Protein Binding Employing Synthetic Biotinylated Analogs of the Phosphoinositides 22
2.1 Background and Significance 22
2.1.1 Lipid–Binding Domains and Important Pathways 22
2.1.2 Effective Strategies for Studying Protein–PIP_n Binding 24
2.1.3 Previous Protein–Binding Results 28
2.2 Probe Design 31
2.3 $PI(3,4,5)P_3$ Probe Synthesis 34
2.4 Results and Discussion 38
2.4.1 Microarray Analysis of Akt-PH Domain with Biotinylated PIP_3 38
2.5 Probing the Affects of Multivalency on Protein-Lipid Binding 43
2.6 Profilin Microarray 45
2.7 Problems with Microarray 47
2.8 Experimental 49
2.8.1 General Considerations 49
2.8.2 Synthetic Procedures 50
2.8.3 Assay Procedure 62
Chapter 3: Exploiting Copper-Free Click Chemistry for Membrane Derivatization 88
3.1 Background and Significance 88
3.2 Results and Discussion 94
3.3 Modification of glass slides 106
3.4 Experimental 111
3.4.1 General Considerations 111
3.4.2 Synthetic Procedures 112
3.4.3 Assay Procedures 116
Chapter 4: Miscellaneous Synthetic Targets 119
4.1 Optimization of a Pipemidic Acid Autotaxin Inhibitor 119
4.1.1 Synthetic Procedures 123
4.2 Porphyrin–Lipid Conjugates 134

4.2.1 Synthetic Procedures 138
4.3 Rhodamines 143
4.3.1 Synthetic Procedures 145
References 187
Vita 206

Table of Figures

Figure 1.1. Structures of bulk and signaling lipids where the tail has been represented generically since this can consist of different combinations of fatty acids in nature. 3
Figure 1.2. Depiction of the binding modes of the three soluble protein types. 4
Figure 1.3. General scheme for protein–lipid binding. 4
Figure 1.4. Bioorthogonal reactions that have been used for labeling biomolecules. 12
Figure 1.5. Scheme for the incorporation of ManNAc into the biosynthetic pathways and labeling via Staudinger ligation.[74] 13
Figure 1.6. Structures of some of the recently reported cyclooctynes. 17
Figure 1.7. Alkyne derivatized sphingomyelin and phosphatidylcholine probes used to label cells by CuAAC with a fluorophore.[122] 17
Figure 1.8. Types of bolaamphiphiles generated by Smith and co-workers.[124] 19
Figure 1.9. Lipid probes containing click moieties in the acyl chains.[125-127] 20
Figure 1.10. Types of DAG and PA probes generated by our lab which contain a modification at the lipid headgroup and are still able to bind proteins.[130,131] 21
Figure 2.1. Structures of seven phosphatidylinositol polyphosphate isomers. 23
Figure 2.2. Akt binds PIP_3, which is generated by phosphorylation of PIP_2 by PI-3K. Activated Akt regulates many downstream pathways including cell proliferation. This is an important protein–lipid binding pathway as the over-stimulation of Akt results in disease. 28
Figure 2.3. Cartoon depiction of immobilization assay performed. 30
Figure 2.4. Binding results of β-spectrin and $PI(4,5)P_2$ 2.20 based on the immobilization and chemiluminescence assay performed. 31
Figure 2.5. Structures of seven amino-tagged analogs of the PIP_ns. 33
Figure 2.6. Synthetic scheme for the formation of the amino-tagged $PI(3,4,5)P_3$ 2.1. 35
Figure 2.7. Binding curves obtained from a microplate-based immobilization assay of all seven biotinylated PIP_ns with Akt-PH.[213] 38
Figure 2.8. Cartoon depiction of the fluorescence based assay performed via microarray on glass slides. 40
Figure 2.9. Left: image of a robotic pin printer containing 32 pins. Right: Close up image of a pin and the channel that holds the solution while printing. 40
Figure 2.10. Results of Akt-PH binding via microarray assay. Left: Fluorescent image obtained by printing constant concentration of PIP_3-biotin 2.19. Right: Graphed results of mean fluorescence intensity of each column on the left with error bars depicting the standard error. 41
Figure 2.11. Results of Akt-PH binding via microarray assay. Left: Fluorescent image obtained by printing varied concentration of PIP_3-biotin 2.19. Right: Graphed results of mean fluorescence intensity of each column on the left with the error bars depicting the standard error. 43
Figure 2.12. Best PIP_2-profilin binding results to date where PIP_2 concentration increases in each grid from left to right (0–400 uM) and profilin concentration increases from left to right for each set of four grids (3 nM, 30 nM, 300 nM, and 3 μM). 46

Figure 3.1. Cartoon depiction of the assay performed. Fluorescent azido-liposomes (containing fluorescent NBD-PE, azido-lipid 3.12, and PC) were incubated with ADIBO-biotin in a streptavidin-coated 96-well microplate for 4 hours, wells were washed and fluorescence was measured. 95
Figure 3.2. Synthesis of the azido-lipid 3.18 used as a common scaffold for various lipid analogs. 96
Figure 3.3. Synthesis of azido-lipid 3.12 for incorporation into liposomes. 97
Figure 3.4. Results from liposome derivatization and immobilization studies and control experiments. 100
Figure 3.5. Acyclic alkyne-biotin used in a control reaction. 101
Figure 3.6. Synthesis of Bertozzi's octyne 1.1.[108] 102
Figure 3.7. Synthesis of the original octyne-lipid 3.32. 102
Figure 3.8. Cartoon depiction of the FRET-based approach using octynyl liposomes and an azido-fluorophore. 103
Figure 3.9. NBD-azide used for FRET assay.[229] 104
Figure 3.10. Original ADIBO succinimidyl ester 3.35 and steps for preparing ADIBO lipid via triazole and ADIBO-PE. 105
Figure 3.11. Fluorescent image of printed liposomes containing biotinylated tags. 107
Figure 3.12. Cartoon depiction of the immobilization of liposomes by copper-free click chemistry using microarray. 109
Figure 3.13. Fluorescent image of the liposome assay that has been incubated with increasing liposome concentrations from left to right for each set of four grids, 125 μM, 250 μM, 500 μM, and 1 mM. 109
Figure 3.14. Plot of fluorescence intensity of the top leftmost grid from Figure 3.13. ..110
Figure 3.15. Fluorescent image of the liposome microarray assay with ADIBO-biotin 3.13 (columns 2, 4, 6 and 8) and alkyne biotin 3.23 (columns 1, 3, 5, and 7) printed from 0–5 nM and then incubated with azido-liposomes. 110
Figure 4.1. Structure of the lead compound 4.1 used as the basis for generating other potential inihibitors and their effectiveness. 120
Figure 4.2. Model of autotaxin (ATX) with the lead compound 4.1 in the binding pocket that is normally used for the conversion of *lyso*-phosphatidyl choline (LPC) to *lyso*-phosphatidic acid (LPA).[245] 121
Figure 4.3. Compounds synthesized in round I (green box), round II (red box), and round III (blue box) as potential autotaxin inhibitors. 122
Figure 4.4. Structures of three lipids synthesized. 135
Figure 4.5. Synthetic scheme for synthesizing the two porphyrin lipids. 137
Figure 4.6. Synthesis of ferrocene-lipid. 138
Figure 4.7. Synthetic target for use in SEHRS. 143
Figure 4.8. Deuterated tetramethyl rhodamine target to be used in SEHRS. 144
Figure 4.9. Previous synthetic rhodamine target. 145

Abbreviations

ADIBO	aza-dibenzocyclooctyne
Ag_2O	silver oxide
ATX	autotaxin
Bn	benzyl
Boc	*tert*-butoxycarbonyl
BOM	benzyloxymethyl
BOMCl	benzyl chloromethyl ether
BSA	bovine serum albumin
Bz	benzoyl
BzCl	benzoyl chloride
Cbz	benzyloxycarbonyl
CH_2Cl_2	dichloromethane
$CHCl_3$	chloroform
$Cu(OTf)_2$	copper (II) triflate
CuAAC	copper catalyzed azide–alkyne cycloaddition
$CuSO_4$	copper (II) sulfate
Cy3	cyanine 3
DAG	diacylglycerol
DCC	dicyclohexylcarbodiimide
DCE	1,2-dichloroethane
DCM	dichloromethane
DIEA	*N*,*N*'-diisopropylethylamine
DIFO	difluorinated cyclooctyne
DLS	dynamic light scattering
DMAP	4-dimethylaminopyridine
DMF	*N*,*N*'-dimethylformamide
DMSO	dimethyl sulfoxide
EDC	1-(3-dimethylaminopropyl)-3-ethylcarbodiimide
ELISA	enzyme-linked immunosorbent assay
ER	endoplasmic reticulum
Et_2O	ethyl ether
EtOAc	ethyl acetate
EtOH	ethanol
FRET	Förster resonance energy transfer
H_2O	water
H_2SO_4	sulfuric acid
HCl	hydrochloric acid
HEPES	4-(2-hydroxyethyl)-1-piperazineethanesulfonic acid
HOBt	1-hydroxybenzotriazole

HRP	horse radish peroxidase
ITC	isothermal calorimetry
LPA	*lyso*-phosphatidic acid
LPC	*lyso*-phosphatidylchloride
m-CPBA	*meta*-chloroperoxybenzoic acid
MeCN	acetonitrile
MeOH	methanol
$MgSO_4$	magnesium sulfate
MS	mass spectra
Ms	methanesulfonyl
MsCl	methanesulfonyl chloride
NaCl	sodium chloride
$NaHCO_3$	sodium bicarbonate
NaN_3	sodium azide
NaOH	sodium hydroxide
NaOMe	sodium methoxide
NBD	7-nitrobenzofurazan
NBDCl	4-chloro-7-nitrobenzofurazan
NEt_3	triethylamine
NMM	*N*-methylmorpholine
NMR	nuclear magnetic resonance
p-TsOH	*para*-toluenesulfonic acid
PA	phosphatidic acid
PBS	phosphate buffered saline
PC	phosphatidylcholine
$Pd(OH)_2$	palladium (II) hydroxide
PE	phosphatidylethanolamine
PEG	polyethylene glycol
PG	phosphatidylglycerol
PH	pleckstrin homology
PI-3K	phosphoinositide 3-kinase
$PI(3,4,5)P_3$	phosphatidylinositol trisphosphate
PIP_2	phosphatidylinositol bisphosphate
PIP_3	phosphatidylinositol trisphosphate
PIP_ns	phosphatidylinositol polyphosphates
PKB	protein kinase B
PKC	protein kinase C
PMB	*para*-methoxybenzyl
PMBCl	*para*-methoxybenzyl chloride
POPC	1-palmitoyl-2-oleoyl-*sn*-glycero-3-phosphocholine
PS	phosphatidylserine

SEC	size exclusion chromatography
SEHRS	surface enhanced hyper Raman spectroscopy
SERS	surface enhanced Raman spectroscopy
SMSEHRS	single molecule surface enhanced hyper Raman spectroscopy
SPAAC	strain-promoted azide–alkyne cycloaddition
SPR	surface plasmon resonance
TBAF	tetrabutylammonium fluoride
TBDPS	*tert*-butyldiphenyl silyl
TBDPSCl	*tert*-butyldiphenyl chlorosilane
TEG	tetraethylene glycol
Tf	trifluoromethanesulfonyl
TFA	trifluoroacetic acid
THF	tetrahydrofuran
Ts	toluenesulfonyl
TsCl	toluenesulfonyl chloride

Chapter 1: Introduction

Lipids are often overlooked biomolecules that were originally thought to simply have a structural role in membranes, but they are now known to play critical roles in a plethora of physiological events.[1-4] Historically, lipid functions have been difficult to study because they exist within complex living systems, residing in cellular membranes, which complicates matters even further. Lipids have a diverse range of biological functions, including recruitment of proteins to membrane surfaces, actions as small-molecule ligands, and covalent protein modification through lipidation.[1,5,6] Lipids are also responsible for the transport and localization of many biomolecules through membrane budding and fusion.[7-9] Defects in these lipid and membrane functions often result in disease, and therefore it is imperative to understand and harness the activities of lipids.

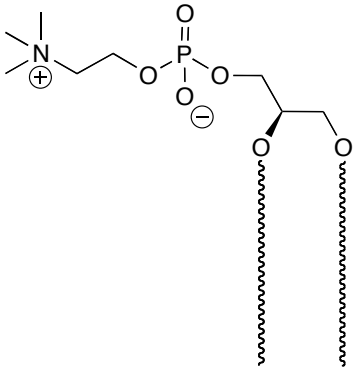
Broadly classified, lipids are hydrophobic or amphipathic small molecules. According to the LIPID MAPS database, there are eight categories of lipids: fatty acyls, glycerolipids, glycerophospholipids, sphingolipids, sterol lipids, prenol lipids, saccarolipids, and polyketides.[10] The research herein focuses on the category of glycerophospholipids, or simply phospholipids, as they are the most abundant of the lipid species.[11,12] A phospholipid is a molecule that consists of a polar region, called a headgroup, and a non-polar region, two long chain fatty acid tails. When exposed to water, these molecules self-assemble into bilayers, a lipid sheet comprised of two layers of interacting lipids. This bilayer is formed because the tails align to maximize their

hydrophobic interactions, resulting in the polar headgroups facing outward, toward the external aqueous environment.

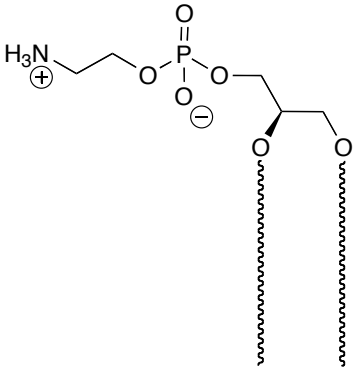
1.1 Phospholipids

Phospholipids can be divided into two main categories, signaling lipids and bulk lipids. The bulk lipids include the lipids that primarily play structural role, such as phophatidylcholine (PC), phosphatidylethanolamine (PE), and phosphatidylserine (PS), although these lipids have also been reported to be involved in protein interactions.[13-15] Examples of signaling lipids include diacylglycerol (DAG), phosphatidic acid (PA) and the family of seven phosphatidylinositol polyphosphates (PIP_ns) (Figure 1.1). These lipids are found in much lower concentration than the bulk lipids, which further complicates their ability to be characterized. For example, a member of the PIP_n family is found in roughly 0.5-1.0% of the total phospholipid concentration on the inner leaflet of the plasma membrane, while PS is present at 25-35%.[4] The signaling lipids often act as site-specific ligands in interactions that enforce membrane association of proteins that play important roles in cell signaling and membrane trafficking.[1,4] The subcellular localization of these signaling lipids and their binding partners is tightly regulated. However, upon stimulation, the amount of localized signaling lipid can increase up to 30 fold.[4]

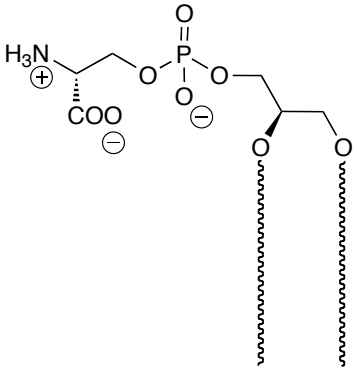
Bulk Lipids



phosphatidylcholine (PC)

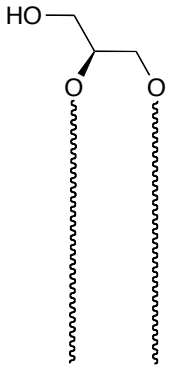


phosphatidylethanolamine (PE)

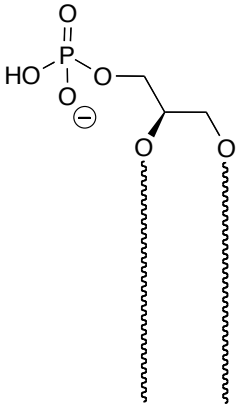


phosphatidylserine (PS)

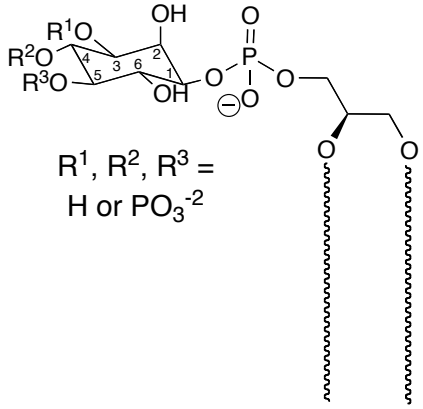
Signaling Lipids



diacylglycerol (DAG)



phosphatidic acid (PA)



phosphoinositides (PIP_ns)

Figure 1.1. Structures of bulk and signaling lipids where the tail has been represented generically since this can consist of different combinations of fatty acids in nature.

1.2 Signaling Lipids that Bind Proteins

Protein-lipid binding lies at the heart of many of the most important cellular pathways, primarily due to the ability to transmit information from the membrane into signaling cascades. Proteins exhibit significant variation in the mode by which they bind to lipids present within membranes. Figure 1.2 shows a cartoon depiction of the ways three types of proteins interact with signaling lipids. S-type proteins are soluble proteins

that interact primarily with the headgroups of signaling lipids. H- and I-type are also soluble proteins, but their mechanism of protein binding also involves insertion of hydrophobic residues into the interfacial region of the membrane. The phosphoinositides, mainly the heavily phosphorylated PIP_2s and PIP_3, bind predominantly S-type proteins, but also have interactions with both H- and I-type. Some of the specifics of phosphoinositide–protein binding and their pathways associated with disease will be further discussed in Chapter 2. A general scheme depicting the way these proteins interact with signaling lipids is shown in Figure 1.3, whereby an inactive peripheral protein that is located in the cytosol can be recruited to the membrane surface by signaling lipids, become activated, and then regulate many downstream pathways.

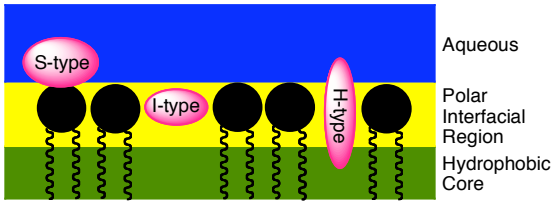


Figure 1.2. Depiction of the binding modes of the three soluble protein types.

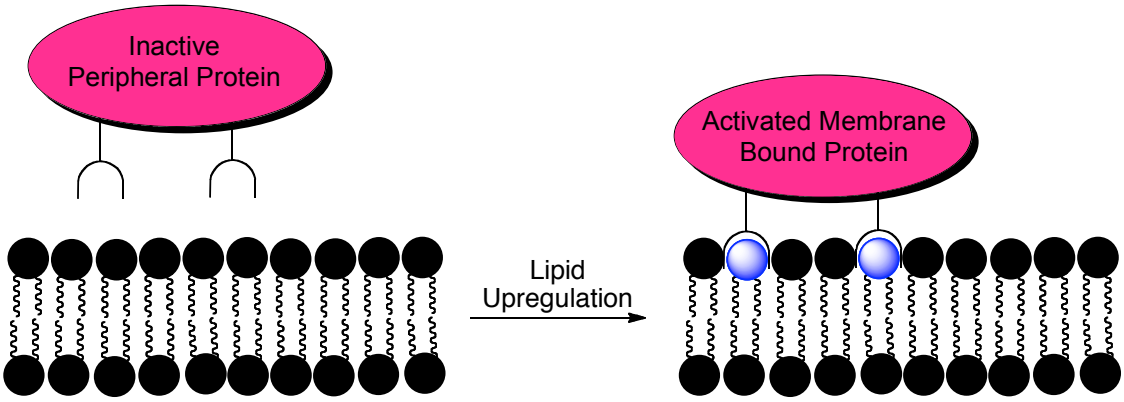


Figure 1.3. General scheme for protein–lipid binding.

1.3 Assays for Studying Lipid Interactions

Since the cellular activities of peripheral proteins depend on their membrane binding affinities, a sensitive and quantitative assay for membrane affinity is an essential tool for understanding the function and regulation of these proteins. Many cellular proteins that participate in signaling pathways translocate to cellular membranes in response to various stimuli, including lipid second messengers. There are two ways of measuring membrane affinity of peripheral proteins: direct assays and separation assays. Examples of direct assays include fluorometric, surface plasmon resonance (SPR), and calorimetric methods. These assays provide experimental convenience but often require protein or lipid modification. Separation assays do not generally require modification but require the laborious task of separation.

1.3.1 Dot-Blot Assays

One of the most commonly used methods of assessing lipid binding specificity uses nitrocellulose membranes that have been spotted with pure lipids and the extent to which any protein of interest binds is determined by its interaction with the lipid spots.[16-19] These dot-blot methods are very sensitive, however, they cannot be quantitated reliably and a positive result in these assays may only be the result of very low affinity binding that has no physiological relevance in the context of a real membrane. Therefore, dot-blot assays should only be used as an initial measure to assess binding specificity before moving forward with more involved techniques.

1.3.2 Direct Fluorescence Assays

Another sensitive and more informative method for detecting membrane–protein binding has been fluorescence assays.[20] Direct fluorescence assays have been performed by using the intrinsic tryptophan fluorescence found on proteins that changes due to environmental differences, such as a shorter wavelength, blue shift, and fluorescence intensity increase when found in hydrophobic environments as in cell membranes. This direct fluorescence method has been used to study the vesicle affinity of many proteins including phospholipases, annexin, and synaptotagmin.[21-25] Of course, these assays require that a tryptophan residue be present in the vicinity of the binding domain, which can also be introduced through mutation but may greatly affect the protein–binding affinity.

1.3.3 FRET Assays

In addition to the direct fluorescence method, there have been Förster resonance energy transfer (FRET) based detection methods. FRET is a mechanism for transferring the energy from one fluorophore to another based on proximity (10–75 Å, the Förster distance). This works by using a FRET-donor and a FRET-acceptor. The donor molecule absorbs and transfers energy to the acceptor. If the donor and acceptor are in close proximity, FRET is activated, and excitation at the donor wavelength yields a fluorescent peak at the acceptor's emission wavelength.

FRET assays often use a tryptophan residue as well, but rather than direct fluorescence, a fluorescent acceptor lipid is used in tandem. In these assays, the protein solution is titrated into a fixed concentration of vesicles or vice versa and the

fluorescence changes are monitored. FRET assays have been used to study the interactions of proteins such as phospholipases, protein kinases C, and annexins.[22,26-34] These FRET-based assays suffer the same drawback as the direct fluorescence assay in that it also requires a tryptophan residue on the protein of interest, but in this case its position is not as strictly defined because it does not have to be located in the hydrophobic membrane core upon binding, only found within the Förster distance of the FRET-partner lipid in the membrane.

1.3.4 Surface Plasmon Resonance Assays

In recent years, surface plasmon resonance (SPR) assays have become popular for measuring membrane–protein binding interactions. In these assays, lipids are immobilized onto the surface of a sensor chip either by attachment of biotinylated vesicles via streptavidin interaction or using a sensor chip with hydrophobic anchors in which membranes are immobilized directly. A protein solution is then washed over the sensor chip and any proteins that bind the lipids remain behind, bound to the lipid. These bound proteins are then detected because of the changes in refractive index near the surface cause a change in the resonance angle of the incident light. These methods are advantageous in that they do not require labeling of the membrane or protein and require only a small amount of sample. SPR assays can provide rapid and direct determination of dissociation constants, but their determination may not be valid when a Langmuir-type binding curve is not valid. Additionally, kinetics of SPR data can be quite complex, these experiments require expensive instrumentation, and it is not a high-throughput technique. Nevertheless, SPR has been used to determine affinity and

specificity of many peripheral proteins including 3-phosphoinositide dependent kinase-1, protein kinase C, phospholipase A_2, FYVE domain of EEA1, C2 domains of synaptotagmin II, mitochondrial creatine kinase, apolipophorin, cytochrome *c*, recoverin, rabbit C-reactive protein, and phosphatidylserine synthase.[35-45]

1.3.5 Calorimetry Assays

Isothermal titration calorimetry (ITC) is another protein–binding assay technique, but it has not been used as extensively. In this case, a solution of protein is titrated into a cell containing a lipid solution, or vice versa, and the heat released or absorbed is measured. This heat exchange is directly proportional to the extent of binding and has been used to evaluate binding of several peripheral proteins such as apolipoprotein A-I, PDC-109, P-glycoportein and serum albumin.[46-49] ITC assays require a relatively large amount of sample, which poses a disadvantage for determining high affinity binding, as well as requiring expensive instrumentation.

1.3.6 Lipid Monolayer Penetration Assays

An assay involving the use of lipid monolayers has also been used to study the binding of peripheral proteins to lipids, whereby a monolayer of lipids is formed on the aqueous interface in a small trough and the surface pressure is measured. Following this, a protein solution is injected into the aqueous layer and the changes in surface pressure are measured over time. If a protein binds the lipid and inserts into the membrane, the surface pressure is altered and can accurately be measured by this technique. This monolayer penetration technique has been used to measure the membrane affinity of phospholipases and protein kinases C.[50-53] Unfortunately, this

assay requires high protein concentrations and cannot be used to determine dissociation constants.

1.3.7 Separation Assays

In addition to these direct assays, there are other assays involving the separation of a protein–lipid complex by centrifugation or chromatography. In the centrifugation assays, cell fractionation is performed in which homogenized cell suspensions are separated by centrifugation into the supernatant and pellet fractions and the proteins in each fraction are quantified. This has been used to study peripheral proteins such as protein kinases C, phospholipases, annexins, and synaptotagmins.[36,51,54-67] However, the long centrifugation in this assay may disturb the delicate equilibriums often seen in these protein–lipid complexes, and therefore, determined dissociation constants may not represent a true equilibrium constant. Also, based on the lipid composition of the vesicles, the pelleting efficiency may vary greatly, as PC vesicles have much lower pelleting efficiency than that of anionic vesicles.[50] Size-based chromatography assays have also been used because they easily separate protein–ligand complexes from large vesicles and have been applied to study phospholipases and protein kinase C.[23,30,54,68] This assay is quite easy to perform, but it is not very sensitive. Additionally, it requires large protein and lipid samples and an appreciable amount of sample is lost on the column in the purification process. Because of these negative aspects of separation assays in that they do not always directly represent a protein–ligand equilibrium in true cellular context, we have chosen to use a direct assay when investigating our protein–lipid binding activities. Additionally, prior assays are not high-throughput, which is a

driving force for the development of our microarray assay that is further discussed in Chapter 2.

1.4 Membrane Interactions and Fusion

There are also protein–membrane interactions that regulate other cellular pathways and membrane actions such as vesicle budding and fusion.[7-9] SNARE proteins regulate the fusion of membranes and have been the subject of recent research.[7,8] The SNARE mechanism works by forming coiled protein strands from SNARE proteins embedded within the bilayer of two opposing membranes to bring the membranes into proximity and then fuse. Interactions such as this are commonplace in nature, but prove to be quite challenging to study in a laboratory setting, as there are many complex variables that are difficult to control. For studying these interactions, model membrane systems, such as liposomes, micelles, supported lipid monolayers (SLMs) and supported lipid bilayers (SLBs), are commonly used to mimic for lipids in their native membrane environment and as delivery systems for drugs, genes, and imaging agents.[16,69-73] There has been a growing interest in understanding and harnessing the power of lipid interactions in recent years, but these efforts have met significant challenges because of the complex environment in which lipids reside. There is, however, a significant need to advance the understanding of lipid function and provide new strategies for utilizing lipids for beneficial applications.

1.5 Bioorthogonal Reactions

As mentioned, the study of the actions and involvements of lipids in biological systems has been hampered by the complex environment in which they exist, but advancement in bioorthogonal reactions have greatly impacted the ability to study these systems. Bioorthogonal reactions involve two complimentary functional groups that are not present in biological systems and do not react with biomolecules, but react well with one another. This allows for selective derivatization in complex biological samples. The azide group has been the subject for most bioorthogonal reactions because it is a small chemical tag that does not cause a large disturbance in the behavior of a molecule, has limited inherent reactivity with any existing biological molecule, and has little-to-no presence in nature. The three most heavily used bioorthogonal reactions with azides have been outlined in Figure 1.4.

1.5.1 Staudinger Ligation

The Staudinger ligation came about as the first example of a bioorthogonal reaction and has been effective for *in vivo* labeling.[74-78] This reaction uses a phosphine reagent to trap the aza-ylide intermediate that is produced through a Staudinger reduction reaction. This first example of a bioorthogonal reaction led to many uses, but a downfall of this technique is the requisite synthesis of the phosphine reagents, which commonly undergoes oxidation.[74,79-83]

Glycans are present in massive quantities on cell surfaces, and they play important roles in cellular process such as immune responses, inflammation, cancer metastasis, and cell-surface recognition, which leads to bacterial and viral cell entry.

Thus, their use in bioorthogonal labeling has been investigated and has provided great insight into these complex systems.[84] A major advancement in the use of bioorthogonal chemistry in living systems has been reported by Bertozzi and co-workers whereby sugar moieties containing azides can be incorporated into glycoproteins via biosynthetic pathways, which her lab then used to perform labeling studies *via* the Staudinger ligation.[74,85] These sugars are easily incorporated into the biosynthetic pathways, resulting in azido-sialic acid derivatives decorating the surface of cancerous cells, an excellent avenue to be exploited for studying and targeting these systems.

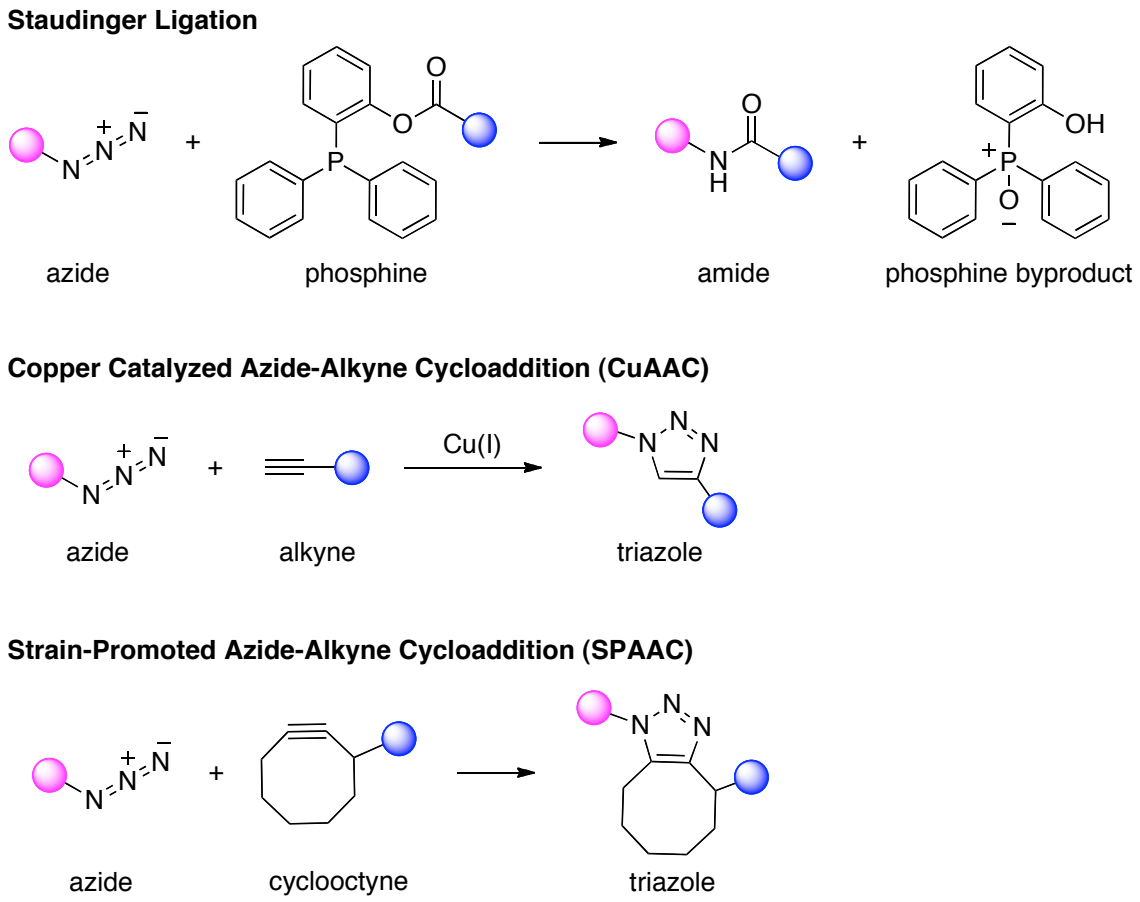


Figure 1.4. Bioorthogonal reactions that have been used for labeling biomolecules.

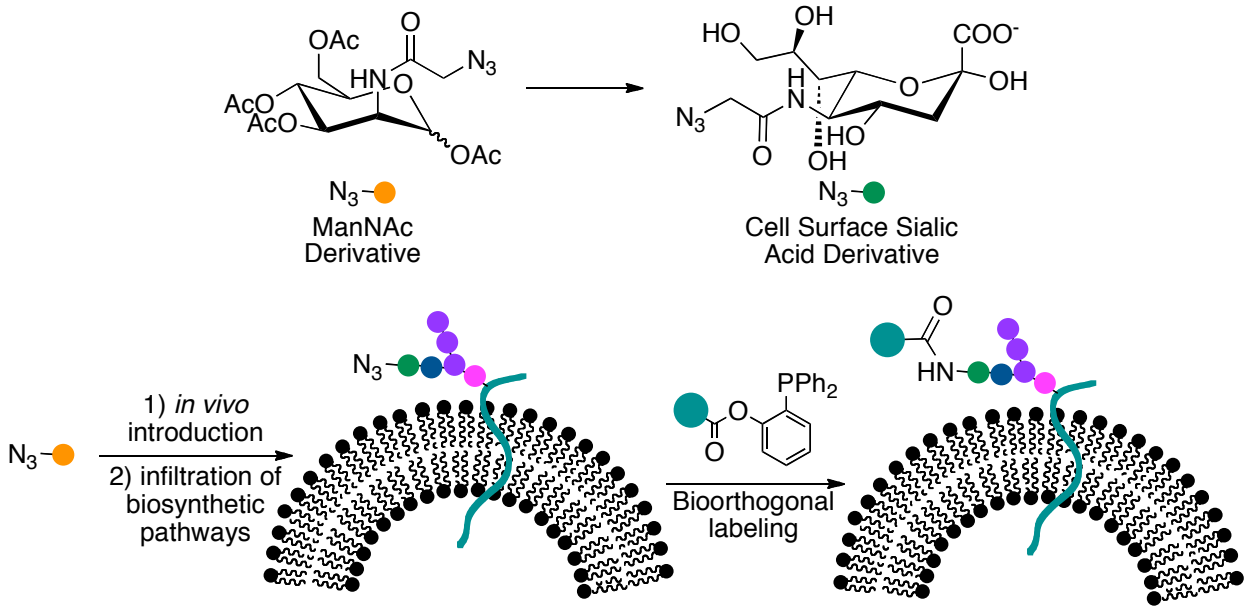


Figure 1.5. Scheme for the incorporation of ManNAc into the biosynthetic pathways and labeling via Staudinger ligation.[74]

1.5.2 Copper Catalyzed Azide–Alkyne Cycloaddition

Another bioorthogonal reaction that has been used in recent years is the copper catalyzed azide–alkyne cycloaddition (CuAAC). First described by Sharpless, Finn, and Kolb, it has now become an invaluable tool for a litany of applications.[86-90] This involves the use of a cycloaddition first reported by Huisgen involving a terminal alkyne and an azide, along with a copper catalyst to join or “click” the two pieces together, yielding a triazole in the resulting product. The purpose of click chemistry is to simplify the task of synthesizing large molecules and identifying molecules with important biological properties. To this end, there have been numerous reports of click chemistry that have been used for a wide range of applications.[86,87,89,90] A few selected examples of the many uses of click chemistry are discussed below.

A report by Tirrell and co-workers showed the incorporation of unnatural amino acids bearing azide and alkyne functional groups into proteins.[91] This group took advantage of lack of differentiation of tRNA synthetases between natural and unnatural amino acids, which allowed the incorporation of click-moiety-bearing unnatural amino acids into proteins. They have used this methodology to replace methionine with homopropargylglycine or azidohomoalanine and phenylalanine with azidophenylalanine.[92-95] This method can be used to globally replace a natural amino acid with its unnatural counterpart, but a more controllable strategy would be the incorporation of the azide or alkyne containing unnatural amino acid at a specific location, which has been reported by Schultz and co-workers.[96-99] They have used this methodology to incorporate azide or alkyne labeled unnatural amino acids into *Escherichia coli*, eukaryotic, and mammalian cells.[100-102]

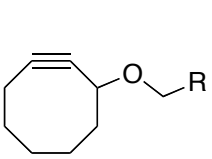
Another example of CuAAC is in the report by Wong and co-workers of the immobilization of carbohydrates for development of platforms for microarray analysis of protein–glycan binding interactions.[103-105] This was then used to characterize the structural requirements for recognition of the tumor antigen Globo H by antibodies MBr1 and VK-9, including direct analysis of serum from breast cancer patients.[106]

While CuAAC has been used in many applications across a very broad spectrum, *in vivo* applications suffer from toxicity of the requisite copper catalyst. There have been efforts in using ligands to first chelate the copper, but even still, cytotoxicity exists.[107] An additional drawback of CuAAC to *in vivo* systems is the need to deliver the catalyst to the reactive site, adding another layer of complexity.

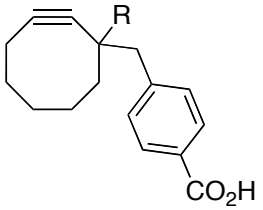
1.5.3 Copper-Free Click Chemistry

To advance click chemistry for *in vivo* applications, Bertozzi and co-workers developed a strain-promoted azide–alkyne cycloaddition (SPAAC), which involves a cyclooctyne moiety and circumvents the need for copper catalyst, and is thus often referred to as copper-free click chemistry.[108] In this system, the click reaction is promoted simply by the strain present in the cyclooctyne ring because it contains an alkyne bond, which typically requires a bond angle of 180° but can only achieve a bond angle of 163° in the cyclooctyne.[109] The initial cyclooctyne **1.1** (Figure 1.6) provided a metal-free bioorthogonal substrate that was less prone to oxidation than the Staudinger ligation reagents and yielded similar reaction rates.[88,108] The recent review by van Delft, Rutjes and co-workers outlines the development of various cyclooctyne reagents by Bertozzi and co-workers and some of their prominent uses.[88] After development of the initial cyclooctyne reagents **1.1** and **1.2**, it was discovered that these compounds decompose even after being stored at -20 °C, so her lab then developed the related alkyl-linked cyclooctyne **1.3**.[108,110,111] This cyclooctyne did not lead to desirable reaction rates, and it drove the introduction of fluorines to increase reactivity providing DIFOs **1.5**, **1.6**, and **1.7**.[112,113] Although these second-generation DIFOs have seen many uses, Boons and co-workers took a different approach for bioorthogonal labeling using cyclooctynes by introducing fused benzenes on either side as in compound **1.8**.[114] This dibenzocyclooctyne (DIBO) was achieved in five synthetic steps and doubled the reaction rate of the DIFO compounds.[114] While the reaction rates of these cyclooctynes are exceptional, all of the previously mentioned cyclooctynes have limited water

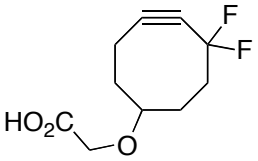
solubility, a necessary attribute if they are to obtain universal applicability in biological systems.[88] Bertozzi and van Delft followed similar strategies to increase the water solubility of these cyclooctynes by including an amine in the cycloooctyne ring providing compounds **1.10** dimethoxyazacyclooctyne (DIMAC) and **1.11** dibenzoazacyclooctyne (DIBAC, also called aza-dibenzocyclooctyne (ADIBO)).[115,116] On the one hand, in DIMAC **1.10**, there was a decrease in the reaction rate over the second generation DIFO compound **1.7**, but when used in Jurkat cells to label metabolically incorporated azido-tagged mannose, **1.10** showed significantly less background signal.[115] On the other hand, in DIBAC (ADIBO) compound **1.11**, there was an increase in the reaction rate over the parent cyclooctyne, DIBO **1.8**, as well as increased water solubility.[116] Continual advancements in the reactivity, stability and synthetic facility of cyclooctyne reagents have led to significant improvements in the efficacy and accessibility of this chemistry.[84,87,114,117-121] The cyclooctynes cited above are meant to provide an overview of the development of strain-promoted click-chemistry in recent years, the reports cited here are representative, not exhaustive.



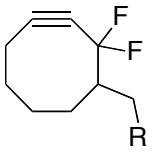
1.1 R = *p*-$HO_2CC_6H_4$
1.2 R = CO_2H



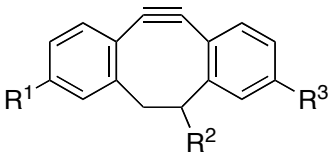
1.3 R = H
1.4 R = F



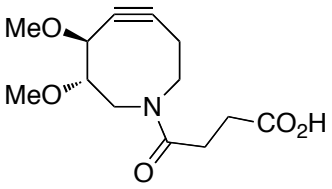
1.5 DIFO



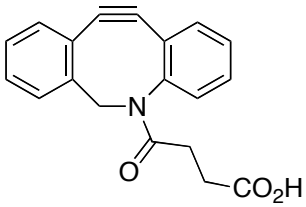
1.6 R = *p*-$HO_2CC_6H_4$
1.7 R = CO_2H



1.8 R^1, R^3 = H, R^2 = OH
1.9 R^1 = OBu, R^2 = H, R^3 = OH



1.10 DIMAC



1.11 DIBAC

Figure 1.6. Structures of some of the recently reported cyclooctynes.

1.5.4 Examples of Bioorthogonal Labeling Using Lipid Probes

Bioorthogonal chemistry has also found uses in lipid probes. Click chemistry has been exploited by Cairo and co-workers in their use of alkyne modified PC and sphingomyelin probes seen in Figure 1.7.[122] In these probes, one of the methyl groups of the choline headgroup has been replaced by an alkyne moiety, and they were then labeled by CuAAC using a benzoxadiazole dye resulting in quantitative yields. In this study, the sphingomyelin derivatives retained activity in sphingomyelinase assays.

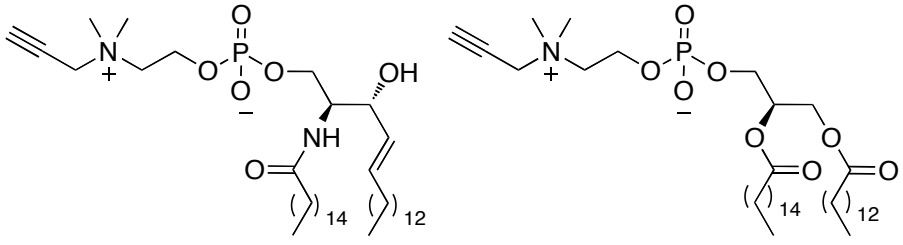


Figure 1.7. Alkyne derivatized sphingomyelin and phosphatidylcholine probes used to label cells by CuAAC with a fluorophore.[122]

In a similar strategy involving an alkyne derivatized choline, Salic and co-workers, instead of synthesizing lipid derivatives, incorporated alkynyl-choline into headgroups via biosynthetic pathways and then used them for labeling in live cells by CuAAC.[123] They successfully hijacked the biosynthetic pathways and incorporated these alkynyl-choline moieties into membrane bilayers as evidenced by a copper catalyzed click reaction with fluorophores that resulted in a fluorescence signal localized and uniformly distributed in the cell membranes. They also investigated the effect of alkynyl-choline labeling on cellular lipids and measured its incorporation into cellular phospholipids by electrospray ionization-tandem mass spectrometry (ESI-MS/MS) analysis of the total lipid suspension. It was discovered that alkynyl-choline does not significantly affect the relative abundance of other phospholipids and thus does not alter their metabolism.

Another PC analog has been reported by Smith and co-workers, but in this case, the click-reactive moieties are located in the acyl tails instead of the choline headgroup.[124] In this report, they used a chemo-enzymatic synthetic strategy in that they selectively cleaved the *sn*-2 acyl chain of PC by the use of phospholipase A2, and then coupled the resulting alcohol to an azide or alkyne-terminated fatty acid. Following this, click chemistry was used to join two of these PC analogs via the use of diazido or dialkynyl linkers to produce bolaamphiphiles of the type seen in Figure 1.8. Unfortunately, these compounds did not form stable membranes, presumably because of the polar triazoles formed from the double click reaction, which must reside in the hydrophobic core if a stable membrane is to be formed.

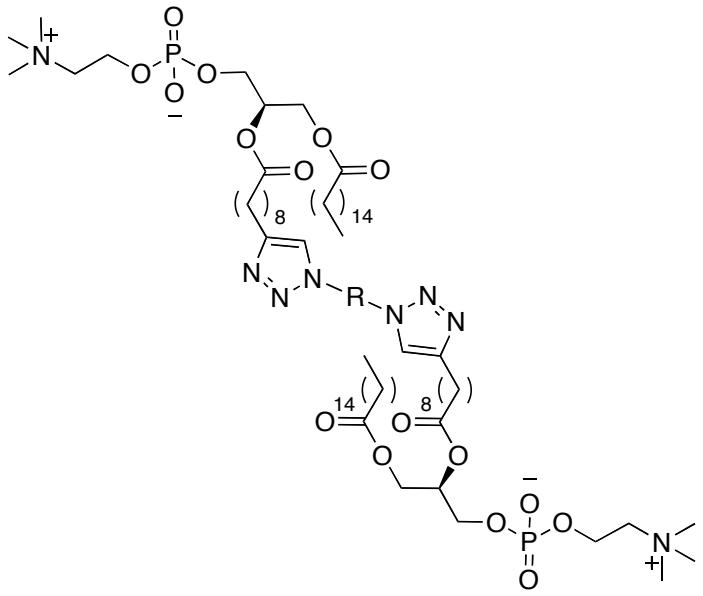


Figure 1.8. Types of bolaamphiphiles generated by Smith and co-workers.[124]

Smith and co-workers have also reported the synthesis of PS probes containing an alkyne at the *sn*-2 terminal end seen in Figure 1.9.[125] Again using a chemoenzymatic approach, a PC derivative was hydrolyzed by phospholipase D (PLD) to form a PA analog, which was then reacted with a protected serine and subsequently deprotected. These PS probes were then derivatized via click chemistry to azide-containing fluorophores, and they have recently been reported for their use in labeling mammalian cells.[126] The PS derivatives in this report containing a neutral coumarin or NBD fluorophore are shown to cross cellular membranes and participate in flippase activity, while the use of a charged fluorophore such as carboxyfluorescein does not cross cellular membranes nor participate in flippase activity.

An example by Schultz and co-workers used phosphatidic acid (PA) probes containing click functional groups in the lipid tails.[127] These lipid probes were protected with an *S*-acetyl-2-thioethyl (SATE) protecting group that enhances cell permeability

and is then cleaved inside cells to yield the active PA probe. These probes were used to label and detect PA in cells, but they discovered that the copper required for the click chemistry is toxic to cells and therefore the cells must be fixed prior to labeling. To circumvent the problem of having to fix cells, Schultz also exploited copper-free click chemistry by incorporating a cyclooctyne in the tail of a PA probe seen in Figure 1.9. In this example, they were able to visualize labeling in live cells by clicking on a coumarin azide. They detected no cytotoxicity and noted that mitosis continued to occur post-labeling.

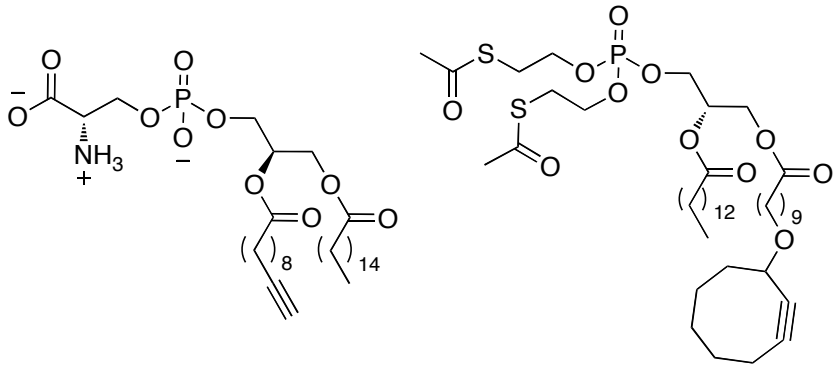


Figure 1.9. Lipid probes containing click moieties in the acyl chains.[125-127]

Our group has also exploited click chemistry to synthesize lipid probes.[5,128-131] Matt Smith of our group has used a modular approach for synthesizing click derived analogs of diacylglycerol (DAG) and phosphatidic acid (PA) seen in Figure 1.10, and through that discovered that such modifications do not have a great affect on the protein binding affinity of those signaling lipids.[130,131] Meng Rowland of our group used PIP_n photoaffinity probes to characterize novel PIP_n binding proteins through the use of activity based protein profiling (ABPP).[128] The synthetic probes contained an azide or alkyne tag as a reactive handle to be used for later attaching a fluorophore for in-gel

detection, or a biotin moiety as a purification handle. The biotin was chosen because it as a well-documented affinity for avidin and has been used for a wide array of applications where a strong and sometimes reversible reaction is needed.[14,38,128,132] Our group has also used biotin as an immobilization anchor for attaching whole liposomes to a microplate surface to then be used for protein–binding studies.[129]

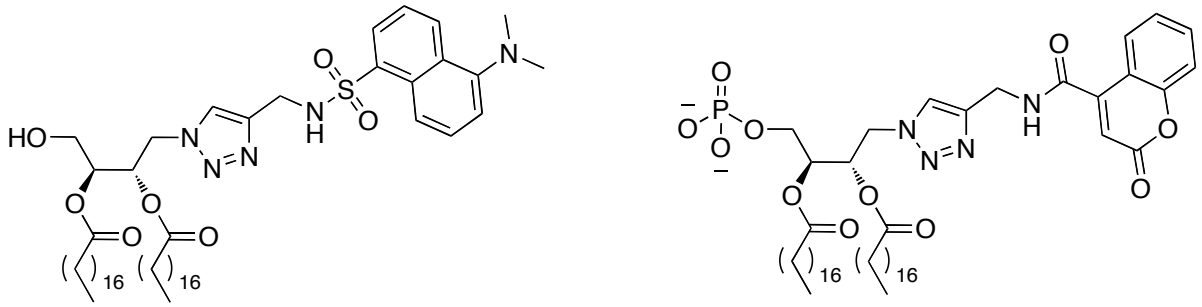


Figure 1.10. Types of DAG and PA probes generated by our lab which contain a modification at the lipid headgroup and are still able to bind proteins.[130,131]

Chapter 2: Microarray Analysis of Protein Binding Employing Synthetic Biotinylated Analogs of the Phosphoinositides

2.1 Background and Significance

The phosphatidylinositol polyphosphates, or phosphoinositides, are a family of compounds that are of great importance within signaling lipids.[4,133,134] Like other signaling lipids, the phosphoinositides act as ligands in the recruitment of peripheral proteins to membrane surfaces, which regulates protein function and subcellular localization.[1] These events are especially important because of their ability to transmit information from the membrane into signaling cascades and since defects in these lipid signaling events have been linked to diseases including diabetes and cancer.[2,133,135,136]

2.1.1 Lipid–Binding Domains and Important Pathways

The phosphoinositides are known to bind an ever-expanding list of cellular proteins, and there are a wide range of phosphoinositide–binding domains present within those proteins including PH, PX, FYVE, ENTH, ANTH, FERM, Tubby, and PROPPIN domains.[4] Among these, there is great diversity in the binding affinities and specificities for each of the seven phosphoinositides. In the PH domain family alone, there are over 250 members reported, with very few being fully characterized, and only about 15% of those bind the phosphoinositides with high affinity.[1,4] It is imperative to discover and characterize the various PIP_n–binding proteins because of their great importance in numerous cellular processes and disease relations. This has previously been hampered by the difficult synthesis of the PIP_n isomers and lack of an appropriate method for screening a large number and wide variety of proteins.

The structural complexity of the phosphoinositides complicates probe synthesis, as these phospholipids consist of phosphodiester-linked *myo*-inositol headgroups that are phosphorylated at every combination of the 3-, 4-, and 5- positions, generating seven naturally occurring isomers that are represented in Figure 2.1. While complex, a number of successful syntheses have been reported which use protecting group chemistry to achieve the enantioselectivity and regioselectivity required to access each isomer.[137-148] There have also been reports by Miller and co-workers of stereoselective phosphorylation of *myo*-inositol substrates using peptide catalysis.[149-153] These strategies have led to successful probe generation and characterization of protein–binding, but require complex synthesis for each reporter probe that therefore limits their broad applicability.

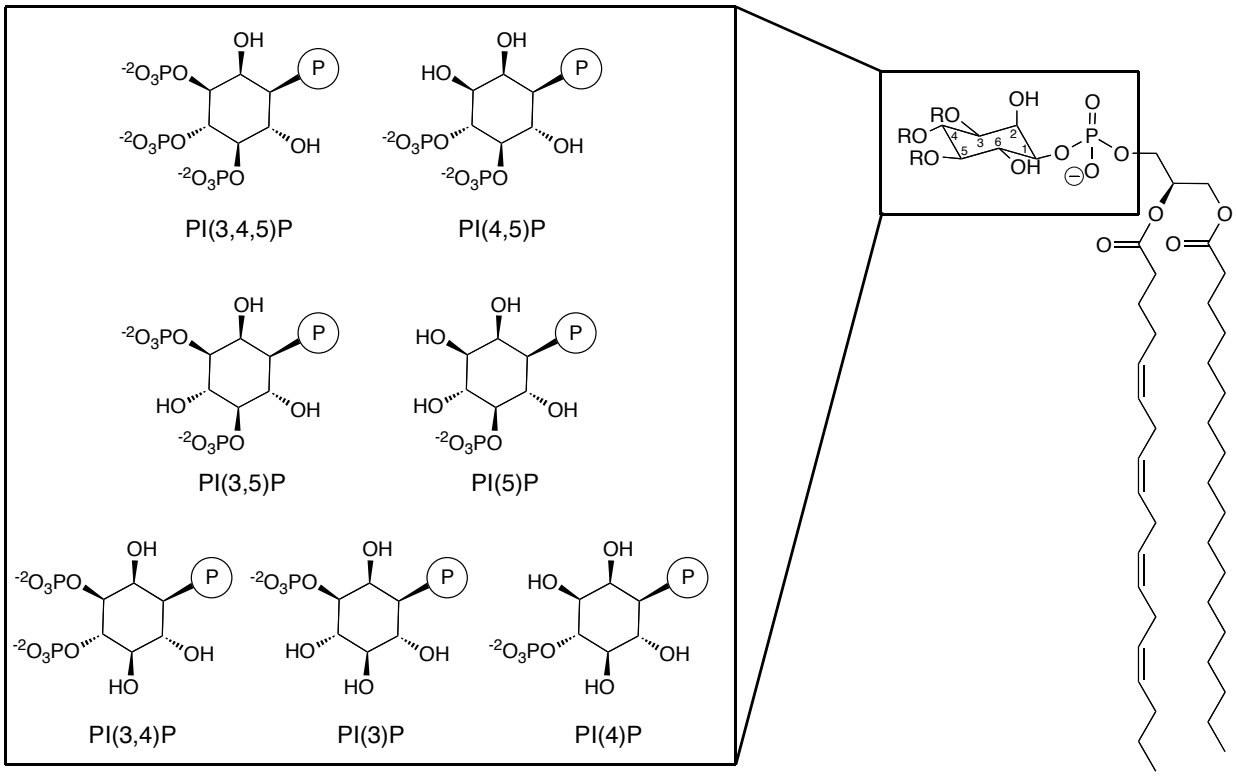


Figure 2.1. Structures of seven phosphatidylinositol polyphosphate isomers.

2.1.2 Effective Strategies for Studying Protein–PIP_n Binding

Due to the complex nature of protein–PIP_n binding interactions, model systems are typically implemented to elucidate the details of binding at the molecular level. As discussed in Chapter 1, a number of effective strategies for characterizing protein–lipid binding have been developed, including SPR analysis employing both membrane and individual lipid motifs, fluorescence, monolayer penetration, vesicle pelleting, monolayer penetration assays, and calorimetry.[16,20] In addition, creative approaches for generating PIP_n-presenting materials have been reported, such as solid supports that have been used for affinity purification of target proteins, polymerized liposomes, and dendrimers.[154-166]

As mentioned, the SPR assay works by immobilizing whole liposomes onto the sensor chip, which is then used for detecting binding and determination of kinetics of the ligand–protein complex formation. Our group has also used whole liposome immobilization as a means of detecting protein binding to DAG though anchoring liposomes to a streptavidin-coated surface via the incorporation of a biotinylated lipid.[129] A similar immobilization approach via biotin-avidin has been used by Gilchrist and co-workers, but it has not yet been used for assessing protein–binding.[167]

Meunier and co-workers reported the use of avidin-coated beads to immobilize $PI(4,5)P_2$-biotin derivatives that were then used to pull down protein effectors from chromaffin granules.[161] After incubation of the PIP-beads with the protein solutions, the protein solutions were separated by SDS-PAGE and visualized by Coomassie blue staining. The bands of interest were excised, subjected to in-gel trypsin digestion, and

mass spectrometry analysis. Using this method, they identified the following proteins of interest: β-spectrin, α2-spectrin, α-adaptin, synaptotagmin-like protein 4, synaptotagmin 1, and synaptotagmin 7. Using the same methodology, Painter and co-workers used a biotinylated $PI(3,5)P_2$ immobilized onto neutravidin beads to pull down binding proteins from the cytosolic extract of adrenal neurosecretory cells.[154] Specifically, they report the elucidation of $PI(3,5)P_2$–binding protein svp1p, a protein known to be involved in membrane trafficking, which was analyzed by SDS-PAGE and Western blotting.

Ferguson and co-workers have used polymerized liposomes containing a single-tailed PIP_n isomer (PIP_3, $PI(4,5)P_2$, and $PI(3,4)P_2$) to detect protein binding to PH-domain bearing nitrocellulose membranes as their initial screening platform.[164] In addition, they performed electrophoresis, Alphascreen binding and competition, and SPR analysis, which complemented previous results using NMR, dot-blots, and affinity resin analyses of the RAG2 protein.[168]

Additionally, PIP_n–protein affinity and multivalency has been studied by Oakley and co-workers through the use of dendrimers displaying multiple $PI(4,5)P_2$ headgroups.[165,166,169] In these reports, polyamidoamine (PAMAM) was used as a core to build out a dendrimer through reaction with 3,4-diethoxy-3-cyclobutene-1,2-dione, which was then reacted with an amine terminated $PI(4,5)P_2$. While their first two reports focused more on the characterization of these dendrimers, the most recent report uses these dendrimers to investigate the multivalent nature of $PI(4,5)P_2$–profilin binding. In this report, they used fourth generation PAMAM dendrimers to assess the protein binding because it is expected that they closely resemble micelles in their size and

headgroup spacing and each dendrimer displays approximately 46 $PI(4,5)P_2$ headgroups. These $PI(4,5)P_2$ dendrimers were then used to assess profilin binding through ELISA (enzyme-linked immunosorbent assay), which resulted in determining the stoichiometry for PIP_2–profiln binding is ~6:1 when using the PIP_2 dendrimers. This result is higher than they observed for profilin binding to PIP_2 liposomes, which may indicate that the micelles are too small to accommodate more protein associations. Nevertheless, their binding stoichiometry is in line with previous reports indicating 5-10 PIP_2s per profilin.[170-175]

The previously discussed PIP_n–binding assays have afforded advantageous information regarding lipid binding, but they each have disadvantages as well. Many of the assays discussed require expensive instrumentation and the detection may be limited to a very specific system, not allowing for rapid quantification of binding partners as in a high-throughput system. In addition, many of these systems are using simplified model membrane systems, but it would be advantageous to study binding in various contexts that mimic different aspects of the cell membrane.

Carbohydrate–protein binding has been studied using surface-based techniques for analyzing recognition, which mirrors certain protein–lipid binding events.[106,176-180] Microarray analysis has proven advantageous for studying the interactions of these carbohydrate systems and has been used to address ligand specificities and structural requirements for recognition among various receptors. These microarray methods have also been used to probe the effect that multivalency has on protein affinity by controlling the carbohydrate density on the surface and for characterizing receptor variations

associated with disease using cell extracts. Since many of these same activities of lipids and their receptors are not well understood and are similar to carbohydrate–protein binding, we sought to exploit the advantages of microarray to apply to lipid binding events. We desired to develop a surface-based platform to rapidly analyze protein–PIP_n binding capable of employing all seven natural isomers.

There is a need to examine the protein–binding partners of the phosphoinositides, but a layer of complexity is added because of the lipid membrane in which they typically exist. There are proteins that bind the PIP_ns that are known to require the membrane environment, while others bind preferentially to the headgroup.[17,134,181-188] For instance, based on the crystal structures of certain PH binding domains, it seems to have a binding pocket to accommodate the phosphorylated *myo*-inositol moiety, which points to strong headgroup association. Because of this evidence, we began our search using the isolated PIP_n headgroups and members of the PH domain family.

A prominent and heavily studied member of the family of proteins that contain PH domains is Akt, also known as protein kinase B (PKB), because its dysregulation is associated with many cancers such as breast, colon, ovarian, pancreatic, lymphoid, and prostate.[2,189-195] Beginning with $PI(4,5)P_2$, phosphoinositide 3-kinase (PI 3-K) phosphorylates the 3-position to form $PI(3,4,5)P_3$, which then recruits Akt to the membrane surface, where it is activated through multiple posttranslational phosphorylation events.[196] Akt then feeds into a number of pathways that control cell proliferation, apoptosis, and growth. The actions of PI 3-K are opposed by the 3-

phosphatase PTEN, whereby PTEN dephosphorylates the 3-position reforming $PI(4,5)P_2$. These enzymes that produce and modify PIP_3, PI 3-K and PTEN, are among the most heavily mutated oncoproteins, and tumor suppressors in cancer.[197-199]

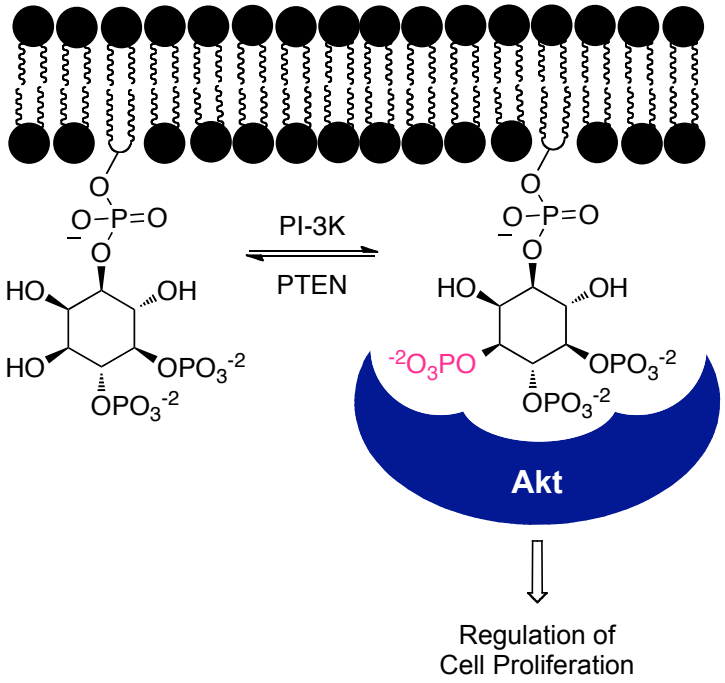


Figure 2.2. Akt binds PIP_3, which is generated by phosphorylation of PIP_2 by PI-3K. Activated Akt regulates many downstream pathways including cell proliferation. This is an important protein–lipid binding pathway as the over-stimulation of Akt results in disease.

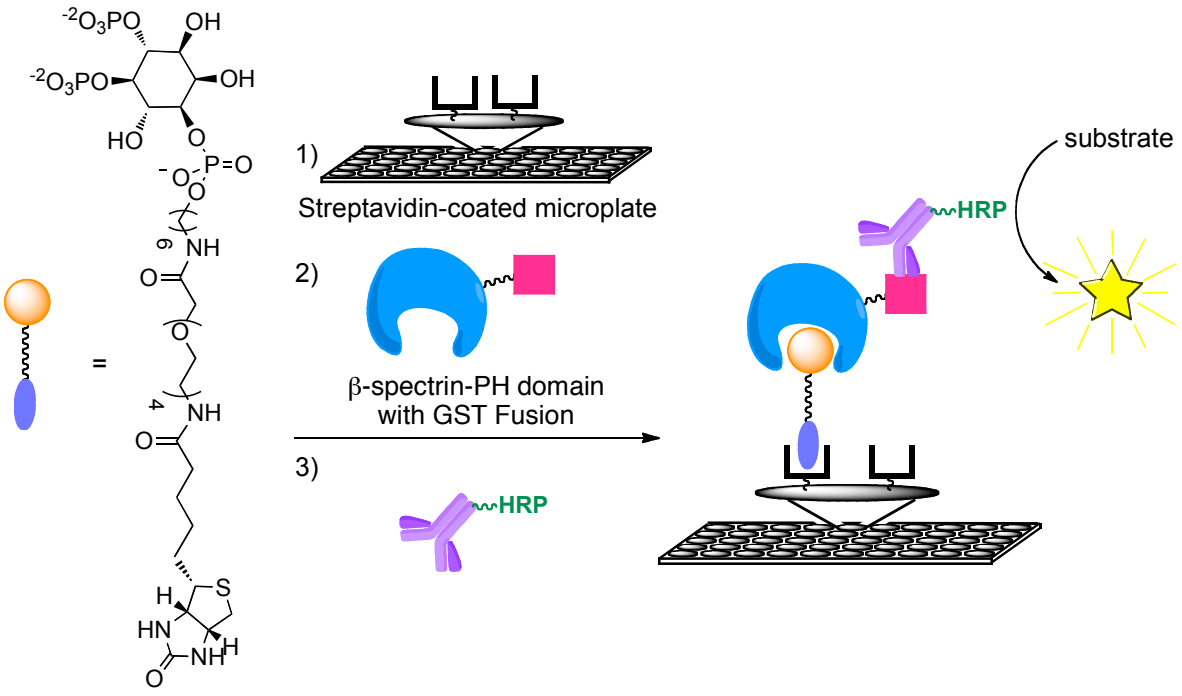
2.1.3 Previous Protein–Binding Results

We chose to exploit a surface-based immobilization strategy because it is a rapid and high-throughput platform for studying the interactions of various proteins with all seven phosphoinositide isomers. Using biotinylated analogs of the PIP_ns, our group has developed a method for detecting the binding of various proteins to the PIP_ns. Our assay uses antibody-based detection, which provides a major advantage because it is amenable to detecting a variety of specific target proteins using the biotinylated probes of all seven PIP_ns by simply using different antibodies.

We first detected the binding of the PH domain of β-spectrin to $PI(4,5)P_2$ following the scheme outlined in Figure 2.3.[134,200] The $PI(4,5)P_2$–biotin analog **2.19** was immobilized onto a streptavidin coated 96-well microplate by placing a solution of the $PI(4,5)P_2$ of a known concentration into each well and incubating at room temperature. Following washes to remove unbound probe, a solution of the GST-tagged PH domain of β-spectrin was added to each well and incubated. Then the microplate was washed and, to each well, horseradish peroxidase (HRP)-tagged anti-GST antibody was added, incubated, and the wells were thoroughly washed. Finally, enzyme-based chemiluminescence detection was used to determine the amount of protein bound to the $PI(4,5)P_2$–biotin ligand. The luminescence results were averaged and plotted versus probe concentration. The results of the β-spectrin PH domain binding are shown in Figure 2.4, which shows a single site saturation curve, as expected. The $K_{d,surf}$ of β-spectrin PH domain was found to be 6 ± 3 nM using this strategy.[201]

Previous to this assay, the binding of the PH domain of β-spectrin was studied by a surface plasmon resonance (SPR) assay and yielded a K_d of 125 ± 18 nM.[201] In this study, the entire $PI(4,5)P_2$ lipid was used and incorporated into liposomes, so it is not unexpected that the value reported by using the isolated lipid headgroup differs. In a membrane environment, the clustering and presentation of the lipid headgroup will be different from a surface immobilized lipid headgroup, and therefore, it is perhaps not surprising that the binding affinity is not equivalent. In this assay, we have termed our dissociation constant $K_{d,surf}$ to acknowledge the differences in membrane and surface affinities, following the example of Wong and co-workers.[176] The PH domain of other

proteins, specifically Btk, GAP1, and Grp1, have been studied with the soluble Ins(1,3,4,5)P_4, the cleaved PIP_3 headgroup.[17,202,203] In an ITC assay using Grp1, a PH-domain-containing protein, a K_d value of 27.3 nM is reported, which is similar to that seen in our surface-based assay.[17]



2.20

Figure 2.3. Cartoon depiction of immobilization assay performed.

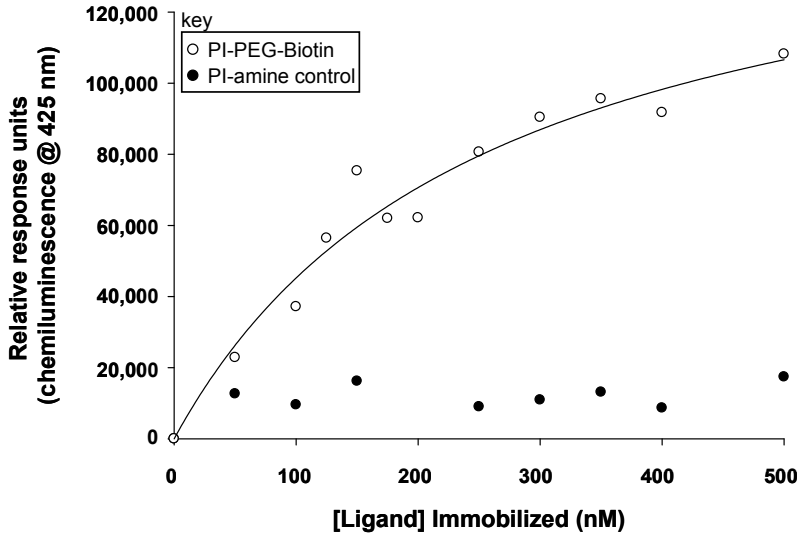


Figure 2.4. Binding results of β-spectrin and PI(4,5)P_2 2.20 based on the immobilization and chemiluminescence assay performed.

2.2 Probe Design

Following initial successful results in lipid microplate analysis, we set out to access all seven isomers of the phosphoinositides from common intermediates and design them in such a way that multiple analogs could be accessed for varying applications. In short, we wanted to be able to identify new protein binding partners as well as quantify the binding affinity of known receptors.

In the natural PIP_ns, the *myo*-inositol is connected *via* a phosphodiester linkage to the glycerolipid backbone, as shown in Figure 2.1, yet it has been shown that the lipid backbone is not always required to achieve protein binding.[4,134] Utilizing this knowledge, we designed our lipid probes to contain a small hydrophobic linker to potentially mimic the glycerolipid backbone while simplifying synthetic access as well as the attachment of reporter groups. We chose to append this short hydrocarbon chain, but instead of the typical methyl group at the terminal end, we desired an amine for easy conversion into

desired probes, following an example set forth by Prestwich and co-workers.[204-212] The structures of our amino-tagged PIP_n analogs are shown in Figure 2.5. For the microarray immobilization assays we wanted to perform, we chose a biotin appendage because of its well-documented affinity for avidin and proven usage in surface-based immobilization assays.[129,200,213] The final feature of our probes is the tetraethylene glycol (TEG) linker to space the headgroup from the biotin and surface of the plate. We chose TEG as a water-soluble linker to ensure that the headgroup would be properly presented as erect, rather than laid horizontally on the surface. Recently, Iyer and co-workers showed that a long tether is critical in studies employing the decoration of streptavidin-coated microplates, as the systematic shortening of this linker led to drastic reductions in binding.[214] Having formulated the design of these probes, we set out to plan the synthesis for achieving them. We wanted our synthetic route to include a final global deprotection step to avoid complicated purification of the highly polar resulting phosphoinositides. Therefore, all of the protecting groups in the next to last step, compound **2.18**, had to be compatible with deprotection *via* hydrogenation, a clean deprotection technique.

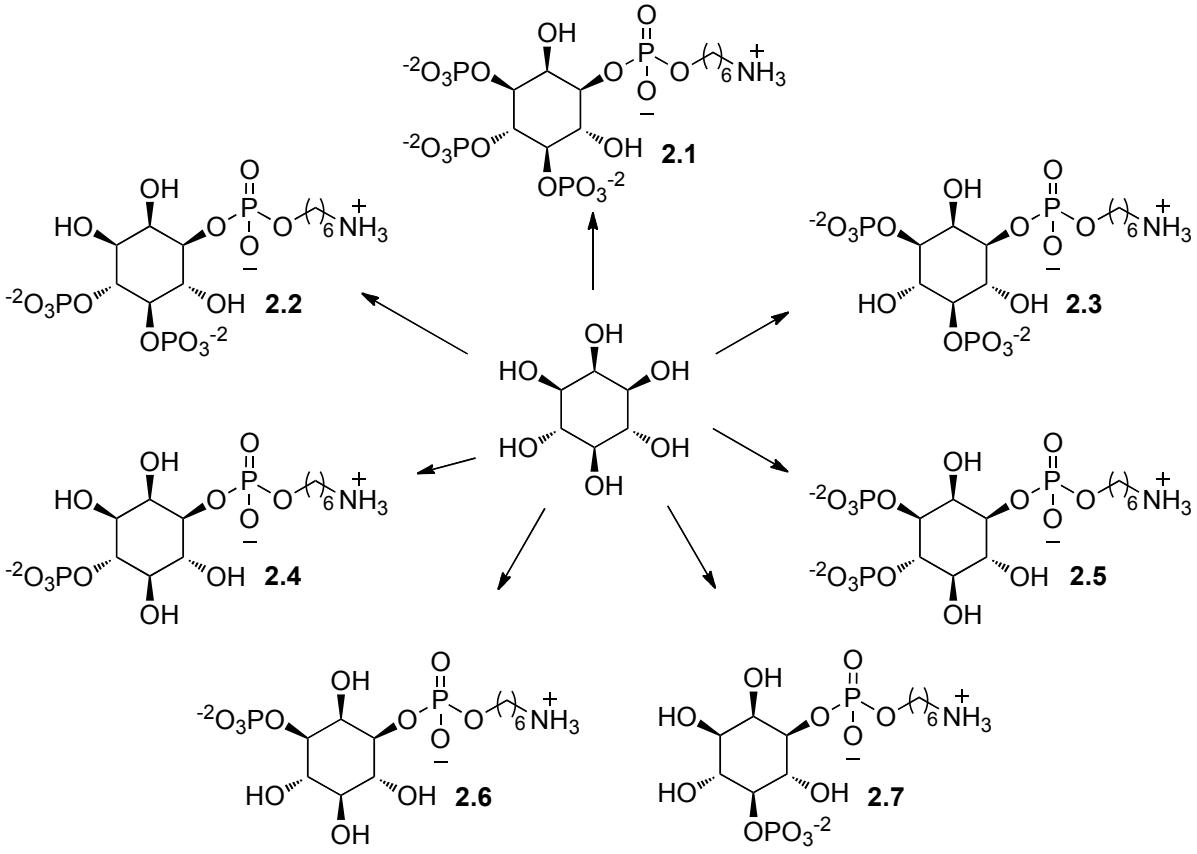


Figure 2.5. Structures of seven amino-tagged analogs of the PIP_ns.

2.3 PI(3,4,5)P_3 Probe Synthesis

In order to synthesize these analogs, we followed the groundwork laid by Bruzik and co-workers and synthesized the amine version of all seven PIP_n isomers beginning with *myo*-inositol.[139,215-217] Taking advantage of the inherent nature of the *myo*-inositol and choosing proper protecting groups has allowed us to synthesize all isomers in good yield with high selectivity. Figure 2.6 shows my role in synthesizing PI(3,4,5)P_3 isomer, which begins by appending (+)-camphor to the 2- and 3- positions of the *myo*-inositol and performing a chiral resolution *via* recrystalization.[217] Beginning with the meso compound, *myo*-inositol has five of the six hydroxyls in an equatorial position in its most stable conformation, with only the 2-position being axial. Because of this axial hydroxyl, the (+)-camphor preferentially protects the 1-2 and the 2-3 hydroxyls, creating diastereomers that can then be separated by recrystallization. Once the appropriate isomer **2.8** was collected, as determined by its optical purity in comparison to literature, the next step was to protect the 1-position using *tert*-butyldiphenylsilyl chloride (TBDPSCl) in the presence of imidazole and pyridine to yield **2.9**. Next, the 4- and 5-positions were protected with benzoyl groups (Bz) to produce compound **2.10** and the camphor acetal was removed with trifluoroacetic acid giving triol **2.11**.

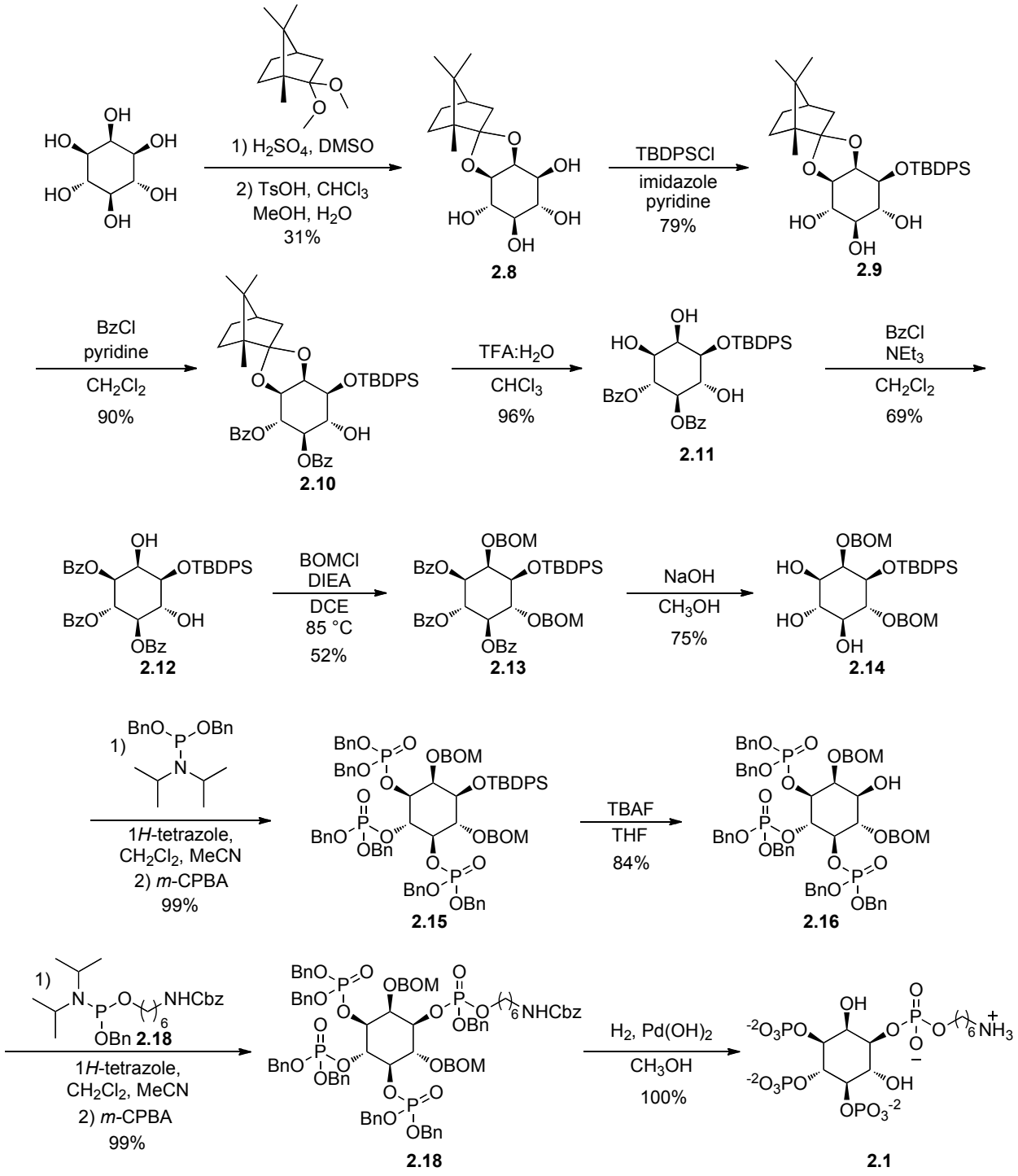


Figure 2.6. Synthetic scheme for the formation of the amino-tagged PI(3,4,5)P_3 2.1.

At this point, the resulting triol **2.11** was used to synthesize both the 4,5- and 3,4,5- analogs, with only a step difference. To generate the 3,4,5-isomer, by using the bulky nature of the TBDPS group to our advantage, we were able to install a third benzoyl group on the 3-position creating 3,4,5-benzoyl protected diol **2.12**. The available alcohols of **2.12** were then protected using benzyloxymethyl chloride (BOMCl), followed by deprotection of the benzoyl groups to generate compound **2.14**. The deprotection of these hydroxyls proved to be somewhat problematic when following methods that were effective for the synthesis of the other PIP_n isomers, such as sodium methoxide in methanol, as the starting material was minimally soluble in methanol. The addition of methylene chloride yielded small amounts of product, but when the reaction scale was increased, the yields declined dramatically. The use of an aqueous solution of sodium hydroxide with methanol and methylene chloride was chosen as a dependable method for generating triol **2.14** on both large and small scale. This triol was then reacted with dibenzyldiisopropyl phosphoramidite in the presence of 1*H*-tetrazole and then oxidized with *meta*-chloroperoxybenzoic acid (*m*-CPBA) to give the protected phosphotriesters of compound **2.15**. Subsequently, the TBDPS protecting group was removed, and more phosphoramidite chemistry installed the benzyloxycarbonyl (Cbz) protected amine tail onto the 1-position to yield the fully protected headgroup **2.18**. The final step to afford the fully deprotected $PI(3,4,5)P_3$ involved a global deprotection with palladium on carbon and hydrogen gas, resulting in pure product. This route minimizes challenges in the purification of the deprotected compound, which is very polar and can cause purification problems. With the amine

version of all seven PIP_ns in hand, we set out to make functionalized derivatives. Our lab has made various probes of the PIP_ns that have been used for a wide array of applications, but the probe **2.19**, seen in Figure 2.8, containing a biotin tag is the molecule of interest here, which was synthesized by Meng Rowland.[5,128,200,213,215]

Following our initial success, we extended our microarray platform technology to detect Akt binding to each of the PIP_ns.[213] Using the purified GST-tagged PH domain of Akt, we performed similar immobilization and protein binding experiments using all seven PIP_n isomers. This approach is advantageous because it can rapidly quantify which isomers are the strongest binders of any protein of choice. The biotinylated headgroups of all seven of the PIP_ns were immobilized in a streptavidin plate as described previously. The wells were then washed and incubated with a constant concentration of GST-tagged Akt PH-domain. After sufficient washing, the ligand–protein binding was then quantified *via* chemiluminescence and the results are shown in Figure 2.7. In agreement with previous reports, it is shown that $PI(3,4,5)P_3$ and $PI(3,4)P_2$ are the strongest binders of Akt, while the remaining PIP_ns do not yield any appreciable signal and essentially double as negative controls.[213,218-220]

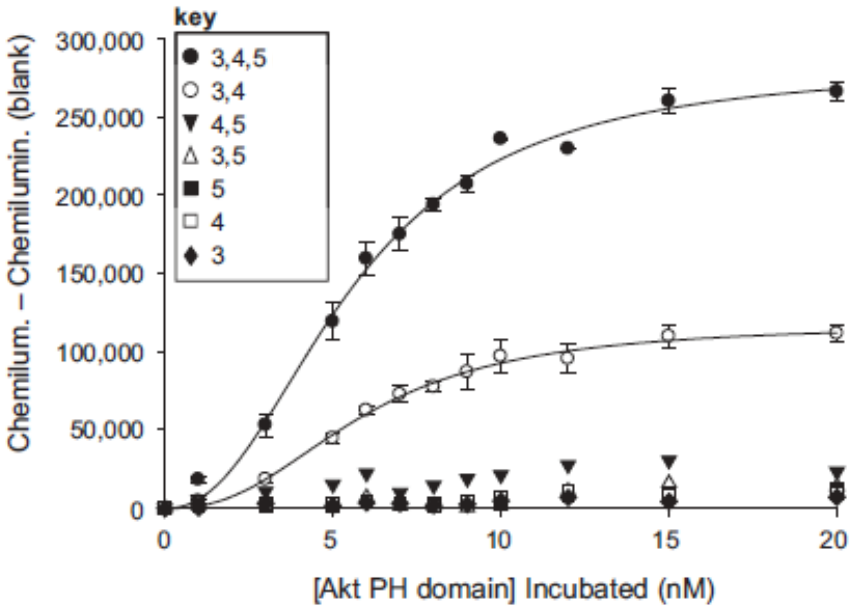


Figure 2.7. Binding curves obtained from a microplate-based immobilization assay of all seven biotinylated PIP_ns with Akt-PH.[213]

2.4 Results and Discussion

While we have achieved success in detecting protein binding to the PIP_ns in microplates using β-spectrin and $PI(4,5)P_2$ and Akt-PH and all seven PIP_ns, this technique requires an appreciable amount of ligand, protein, and antibodies, which are all rather costly. We desired to miniaturize the entire experiment and decided true microarray was an excellent way to accomplish this.

2.4.1 Microarray Analysis of Akt-PH Domain with Biotinylated PIP_3

Microarray generally employs a glass slide that can be derivatized with a variety of groups for immobilizing a number of ligands with various functional tags. These glass slides measure 25 mm X 75 mm and thousands of experiments can be performed on a single slide, greatly minimizing the amount of ligand, protein, and antibodies required. In these experiments, we have employed an avidin coated slide for use with the same

PIP_n-biotin analogs that were used in the previous assays. We began by trying to repeat the microplate Akt-PH binding experiment using the microarray technology. Because of the mobility of the luminescent substrate, fluorescence detection is needed when working with glass slides, so the HRP-tagged antibody was exchanged for a primary and secondary antibody system using rabbit anti-GST and a fluorescent cyanine-3 (Cy3) labeled goat anti-rabbit IgG (Figure 2.8). We began with $PI(3,4,5)P_3$ as our only ligand because it is known as the strongest binder of Akt out of the seven PIP_ns, which is also seen in our previous results.[182,213] Using avidin-coated glass slides, the $PI(3,4,5)P_3$–biotin **2.19** was printed using a robotic pin printing system, which can be seen in Figure 2.9. The pin dips into the solution prepared in a 96-well plate, blots onto a blank slide, and then prints the compound onto the avidin-coated slide the desired number of times depositing ~0.6 femtoliters of sample creating a spot diameter of ~50 μm. Each sample is typically spotted in 20 replicates, resulting in two grids with 10 spots each from the same well.

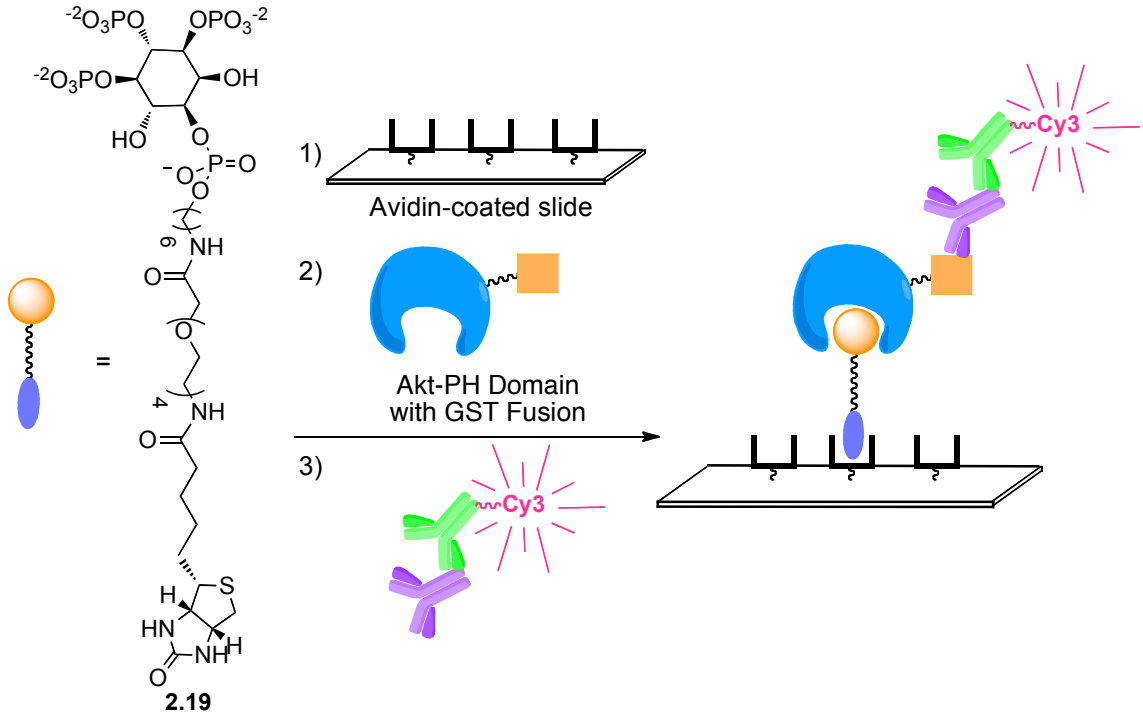


Figure 2.8. Cartoon depiction of the fluorescence based assay performed via microarray on glass slides.

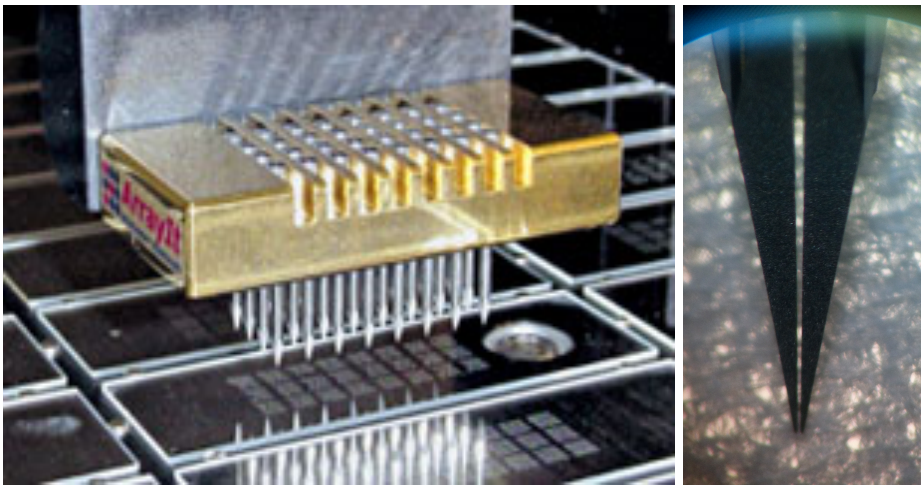


Figure 2.9. Left: image of a robotic pin printer containing 32 pins. Right: Close up image of a pin and the channel that holds the solution while printing.

Beginning with printing a grid where every row and column has PI(3,4,5)P_3–biotin in the same concentration (500 μM) and subjecting the resulting surface to the assay shown in Figure 2.8, we obtained the fluorescent image in Figure 2.10. As can be seen

from the image, there are variations in spot diameter and intensities as you go down the columns, despite the fact that the PI(3,4,5)P_3-biotin was immobilized at a constant concentration, which is a common technical challenge in microarray analysis. The column averages, standard error, and percent error in fluorescence counts for this uniform concentration grid are outlined in Table 2.1. There are several possible reasons for this non-uniformity, such as variations in the density of the reactive functional groups on the slides, the numerous steps that are required for the assay, and variations in the efficacy of pin printing at different locations. In this case, it can be attributed to inconsistencies in the robotic pin printing because, as seen in the image, the effect seems to be most prominent in the lower right of the grid, which corresponds to the spots printed later in the printing sequence. To try and remedy this, shorter print sequences were run and the pin was washed between each printed grid. Overall, the image shows relatively uniform fluorescence, despite the spot morphology differences, providing evidence that our assay worked as expected.

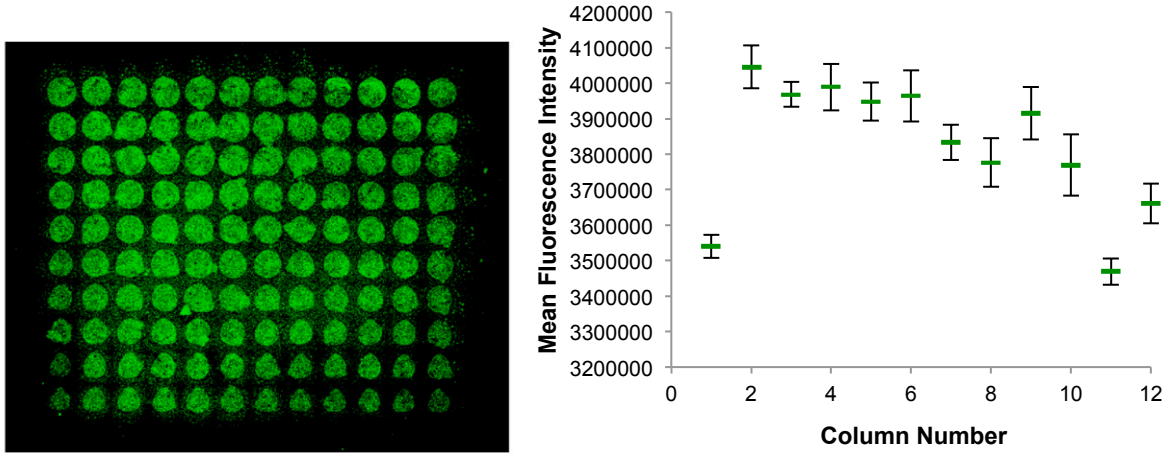


Figure 2.10. Results of Akt-PH binding via microarray assay. Left: Fluorescent image obtained by printing constant concentration of PIP_3-biotin 2.19. Right: Graphed results of mean fluorescence intensity of each column on the left with error bars depicting the standard error.

Table 2.1. Error values for the data plotted in Figure 2.10.

Column	Average Emission (counts)	Standard Error ($x10^4$)	Percent Error
1	3539851	3.28	7.42
2	4046026	6.09	5.82
3	3968459	3.47	3.79
4	3989071	6.55	4.33
5	3948771	5.41	3.27
6	3964619	7.24	3.69
7	3833509	5.01	0.26
8	3776627	6.83	1.23
9	3915266	7.40	2.40
10	3769995	8.67	1.40
11	3469492	3.74	9.26
12	3661295	5.62	4.24
average	3823582	5.78	3.93

Following these initial results, a grid of non-uniform concentration was printed, where the leftmost column contains only buffer and the rightmost has the highest concentration of PI(3,4,5)P_3–biotin at 500 μM. The fluorescent image obtained from this can be seen in the left panel of Figure 2.11. The spot morphology of this grid seems to be improved from previous, but it is still imperfect. The plot of fluorescence versus ligand concentration from this image shows a signal increase as the concentration of the ligand increases. In the microplate assays, the highest concentration of ligand was 500 nM, whereas with the microarray technology, to see an appreciable signal, we had to probe much larger concentrations (up to 500 μM). This could be attributed to the detection limit in microplates because of the higher sensitivity of the chemiluminescence over fluorescence. While we have achieved these initial results, the microarray

techniques still requires further optimization. A further discussion of some of the problems associated with microarray can be found in Section 2.7.

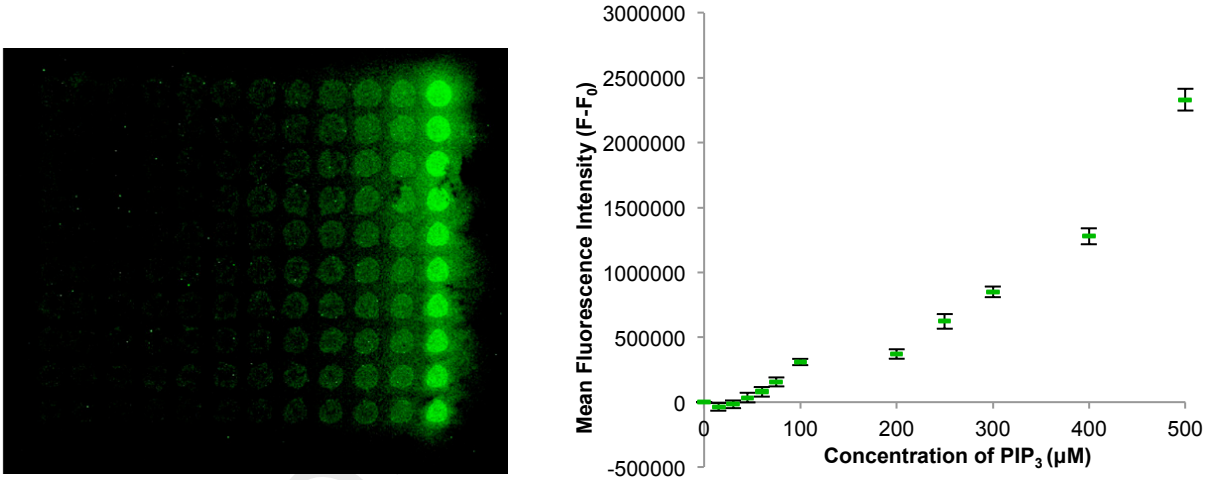


Figure 2.11. Results of Akt-PH binding via microarray assay. Left: Fluorescent image obtained by printing varied concentration of PIP_3-biotin 2.19. Right: Graphed results of mean fluorescence intensity of each column on the left with the error bars depicting the standard error.

2.5 Probing the Affects of Multivalency on Protein-Lipid Binding

While Akt is of immense importance, there is a great need to study the interactions of lipids with multivalent proteins. A protein is classified as multivalent if it can simultaneously bind multiple ligands. In multivalent systems, two typical responses are observed based on the amount and clustering of the ligand on the surface, a threshold or a gradient. A threshold response is essentially an on-off switch in that minimal binding occurs until some threshold is reached, which turns on binding and an immediate response is observed. A gradient response is the result of a linear relationship in that as the ligand density is increased, the binding affinity is gradually enhanced as well.

Multivalent carbohydrate binding has been heavily studied, and it has provided great insight into how multivalency affects carbohydrate binding.[176,221] Surface-based techniques are especially advantageous for carbohydrates and signaling lipids because these ligands are typically displayed on the membrane surfaces and it is in that native environment that they are able to bind soluble proteins. Wong and co-workers have successfully used microarray to study carbohydrate–lectin binding.[106,176,177,221,222] Using four ligands composed of differing numbers of mannose units, his lab probed the binding of concanavalin A, two other mannose binding lectins, *lens culinaris* agglutinin (LCA) and *pisum sativum* agglutinin (PSA), and the human monoclonal antibody 2G12.[176] Based on those results, it is expected that the PIP_ns will behave similarly and analysis of multivalent PIP_n–binding proteins will benefit from a similar surface-based strategy, but it should be noted that profilin has more binding domains than lectin.

Wong and co-workers have also used dendrimers composed of mannose to study carbohydrate–protein binding to the human monoclonal antibody 2G12.[223] As previously mentioned, the use of dendrimers has also proven effective for studying the multivalent binding of $PI(4,5)P_2$ to profilin by Oakley and co-workers.[166] While they have been effective at probing protein binding, dendrimers require difficult synthesis often resulting in minimal product, complex assay conditions that often uses expensive instrumentation, and provide minimal control over ligand density, so we decided that the surface-based immobilization microarray strategy would be an effective one for studying many multivalent protein interactions with the phosphoinositides. A surface-based strategy also affords us control over the surface density of the ligand, a beneficial factor

when exploring multivalent effects. We modeled our multivalent microarray studies after the previously described systems of Wong and co-workers and began by evaluating profilin, a documented binder of $PI(4,5)P_2$. In order to probe multivalent protein binding, the microarray assay must be performed with numerous grids of varying ligand concentration that are then incubated with several protein concentrations. Microarray serves as a beneficial technique for these experiments because the same ligand solutions can be printed onto one glass slide many times to create numerous grids that can all be incubated individually with numerous protein concentrations. From a single successful microarray assay, the $K_{d,surf}$ of many protein concentrations can be determined, providing essential evidence for how multivalency affects protein–lipid binding.

2.6 Profilin Microarray

It is known that profilin preferentially binds $PI(4,5)P_2$ over any other PIP_n isomer, so in these microarray experiments the biotin analog of $PI(4,5)P_2$ has been used, compound **2.20**.[166] In order to probe the multivalency, using experiments similar to those performed by Wong and co-workers for multivalent carbohydrate binding, we desired to print multiple grids with varying concentrations of $PI(4,5)P_2$ and then incubate those grids with varying amounts of profilin. Based on the K_ds determined by curve-fitting the plot of fluorescence versus protein concentration for each $PI(4,5)P_2$ concentration, one can determine the extent to which multivalency affects profilin binding. The best results to date are shown in Figure 2.12, where the $PI(4,5)P_2$-biotin is

printed in increasing concentration (0–400 μM) from left to right in each 12x10 grid, and each set of 4 grids is incubated with increasing profilin concentration (3 nM, 30 nM, 300 nM, and 3 μM). The results show moderately what is expected in that as the concentration of profilin increases, so does the fluorescence. There also seems to be a general trend of increasing fluorescence from left to right across each grid, providing evidence that the higher concentration of ligand binds more profilin. However, these results are only preliminary, and these experiments still need to be further scrutinized and optimized to be used with a wide variety of proteins for eventual use in diagnostic studies.

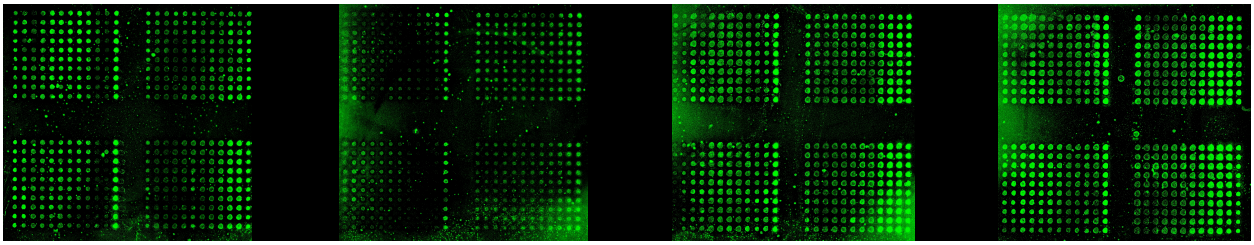


Figure 2.12. Best PIP_2-profilin binding results to date where PIP_2 concentration increases in each grid from left to right (0–400 uM) and profilin concentration increases from left to right for each set of four grids (3 nM, 30 nM, 300 nM, and 3 μM).

2.7 Problems with Microarray

The two aforementioned microarray assays have yielded some initial results, but both could benefit from further optimization. One of the biggest problems with these assays is their consistency. Due to many variables, the actual printing of the ligand on the slide often proves to be temperamental. The buffer used to dissolve the solutions for printing is typically an aqueous solution with a high salt content. The salt serves a nice purpose of being able to visually see spots on the slide after the printing is finished. There are many instances where after running a print sequence, there are no visible spots on the slide. If this is the case, something has gone wrong in the actual slide printing. This could be caused by various issues but is most likely due to the solution that is being spotted evaporating on the pin tip. This evaporation can be addressed in many ways including increasing humidity of the environment while printing, adding solvents such as dimethylsulfoxide or glycerol to enhance the viscosity and printability of the solution, and decreasing the print time by adjusting the number of spots and grids printed from each dipping of the pin. Another important thing to note when printing slides is that the best grids result from printing ligands where the lowest concentration is printed first and the highest last. If the highest concentration of ligand is printed first, there are problems with the pin not washing properly and the higher ligand concentrations bleed over into the next row causing contamination.

Once the printing process is dependable, there is a need to optimize the actual assay as well. Although we have achieved protein–binding results in microplates, there is not necessarily a direct relationship to the microarray assays. The protein

concentrations that have been used have resulted from educated guesses based on the microplate assays, but as discussed, the conditions that have been determined as optimal for microplates are not always directly correlated to the microarray assays. However, an advantage to microarray over microplate analysis is because so many experiments can be performed on a single microarray slide, many protein concentrations can be probed simultaneously. Although the amount of protein used is much lower than the microplate assays, this could benefit from further optimization to determine the ideal concentration window. In the profilin studies, several protein concentrations have been evaluated, including 3 nM, 30 nM, 300 nM, 3 μM, and 33 μM. The appropriate antibody concentrations have been minimally investigated, as the background signal resulting from too much antibody yielded undesirable results, and decreasing this concentration provided a more satisfactory result. The antibody concentrations that have been tested in both the Akt and profilin assays are 1/0.5 μg/mL, 0.5/0.25 μg/mL, and 0.2/0.1 μg/mL. The incubation times and washing procedure were chosen based on literature examples and our previous microplate assays, but these could also benefit from further investigation. Incubation times have generally been 1 hour, but other times such as 2 hours, 4 hours, and even overnight have been used. The washing procedure seems to greatly affect the end results, as in one instance the overall assay yields good spots with minimal background signal, while other times, even when the same procedure is followed, the background is so high that no spots can be seen or the slide is completely black with no spots being detected. The protein concentration, antibody concentrations, washing procedure, and incubation

times are all part of the process that need to be further scrutinized to yield the best possible, dependable microarray assay that has a wide array of applications for many protein-binding studies.

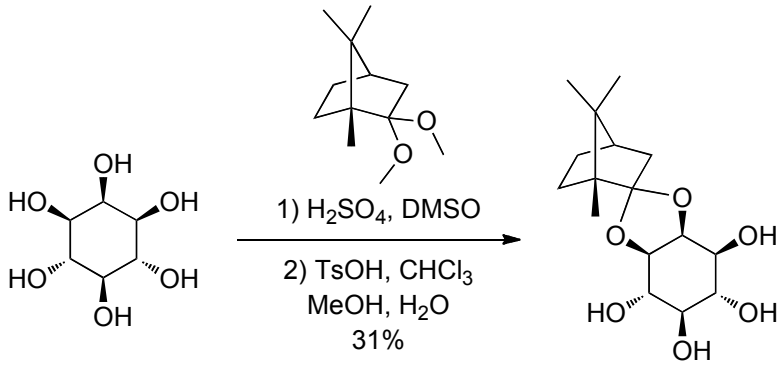
2.8 Experimental

2.8.1 General Considerations

Generally, reagents were purchased from Acros, Aldrich or Advanced ChemTech and used as received. Dry solvents were obtained from a Pure Solv solvent delivery system purchased from Innovative Technology, Inc. Column chromatography was performed using 230-400 mesh silica gel purchased from Sorbent Technologies and C18 (17%) reverse phase SPE columns (6 ml, 2 g) purchased from Silicycle. NMR spectra were obtained using a Varian Mercury 300 spectrometer, a Bruker Avance 400 spectrometer, and a Varian 500 spectrometer. Mass spectra were obtained with JEOL DART-AccuTOF spectrometer and an ABI Voyager DE Pro MALDI spectrometer with high resolution capabilities. Optical rotation values were obtained using a Perkin-Elmer 241 polarimeter. The GST-tagged PH domain of Akt was expressed and purified as previously described.[219] Slide printing was performed using a VersArray ChipWriter Pro obtained from Bio-Rad Laboratories, Inc. (Hercules, CA). Fluorescence on slides was detected using a GenePix 4000B Micorarray Scanner. SuperAvidin coated slides were purchased from Arrayit Corporation (Sunnyvale, CA). The rabbit anti-GST antibody, Cy3 conjugated goat anti-rabbit IgG antibody, anti-profilin antibody, and profilin were obtained from Novus Biologicals (Littleton, CO).

2.8.2 Synthetic Procedures

1D-2,3-*O*-(D-1',7',7'-Trimethyl[2.2.1]bicyclohept-2'-ylidene)-*myo*-inositol (2.8):



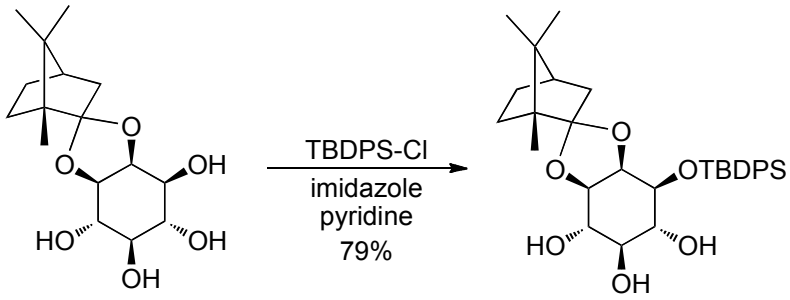
2.8

The following procedure was first described by Bruzik and co-workers[217] whereby D-(+)-camphor (32.6 g, 0.21 mol) was dissolved in methanol (35 mL) and trimethylorthoformate (165 mL) was added and stirred at rt for 48 hours after which sodium methoxide (685 mg) was added. The resulting solution was stirred at rt for 15 minutes, and subsequently concentrated. The remaining residue was dissolved in toluene, filtered, and concentrated once more. The resulting residue was then dissolved in dimethyl sulfoxide (DMSO, 184 mL). To this solution was added *myo*-inositol (16.86 g, 0.09 mol), and concentrated sulfuric acid (H_2SO_4, 0.95 mL) and the reaction was stirred at 75 °C for 3 h. After the allotted time, triethylamine (Et_3N, 6.3 mL) was added. After 20 minutes of stirring, the mixture was then vacuum distilled at 80 °C after which a dark, sticky residue remained. The residue was brought to a weight of approximately 85 g by adding DMSO. Chlororform ($CHCl_3$, 285 mL), methanol (MeOH, 17.9 mL), water (5.7 mL), and *para*-toluene sulfonic acid (*p*-TsOH, 63 mg) were added, and the resulting solution was stirred at rt overnight. The next day, the mixture was filtered through a

Büchner funnel and washed with 400 mL $CHCl_3$ to give the crude product of diastereomers as a white solid cake. This resulting solid was recrystallized by dissolving in hot, refluxing methanol (1.6 L) containing 0.1% triethylamine. The solution was filtered while hot, the volume of solution was reduced by half, then cooled to rt, and finally placed in the freezer. After 2 days, the resulting crystals were collected (22.2 g), and recrystallized once more to afford compound **2.8** (8 g, 27%).

Characterizations match previous reports.[217] $[\alpha]_D^{296\ K}$ = +37.1 (*c* = 1.9, pyr).

1D-1-*O*-(*tert*-Butyldiphenylsilyl)-2,3-*O*-(D-1',7',7'-trimethyl[2.2.1]bicyclohept-2'-ylidene)-*myo*-inositol (2.9):

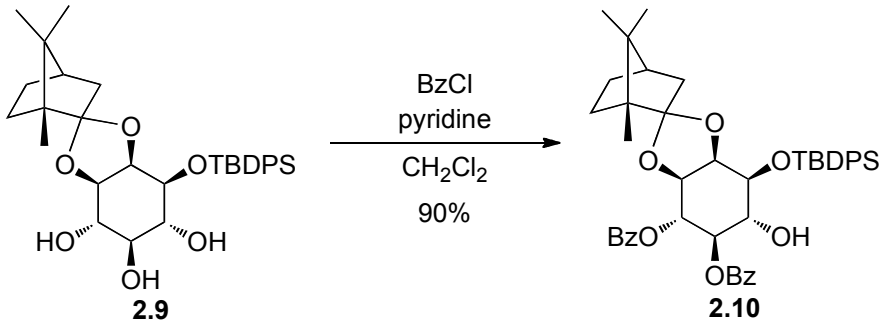


2.8 **2.9**

The following procedure was first described by Bruzik and co-workers[217] whereby protected *myo*-inositol **2.8** (3.5 g, 11.12 mmol) was dissolved in pyridine (35 mL) and imidazole (1.06 g, 15.57 mmol) was added. The mixture was placed under nitrogen, cooled to -10 °C, and *tert*-butyldiphenylsilyl chloride (TBDPSCl, 2.9 mL, 11.12 mmol) was slowly added. The reaction was allowed to warm to 4 °C and stirred overnight. The resulting mixture was concentrated and the residue purified *via* chromatography on silica gel (5 – 25% MeOH/$CHCl_3$) to yield **2.9** (4.77 g, 78%) as a white foam.

Characterizations matched previous reports.[217] $[\alpha]_D^{296\,K}$ = -25.2 (*c* = 4.4, $CHCl_3$). ^1H NMR (300 MHz, $CDCl_3$): δ = 7.75 (dt, *J* = 5.8, 2.0 Hz, 4H), 7.36 (t, *J* = 6.2 Hz, 6H), 4.34 (s, 1H), 3.87–3.70 (m, 3H), 3.59–3.39 (m, 2H), 3.09 (t, *J* = 9.3 Hz, 1H), 1.90 (t, J = 10.0 Hz, 1H), 1.63 (d, J = 10.5 Hz, 3H), 1.36–0.99 (m, 15H), 0.84 (s, 3H), 0.78 (s, 3H) ppm. ^{13}C NMR (75 MHz, $CDCl_3$): δ = 136.27, 135.80, 133.80, 133.30, 127.60, 127.56, 127.41, 123.79, 117.74, 76.88, 76.30, 75.93, 75.75, 73.11, 72.46, 72.27, 51.44, 51.26, 47.91, 45.09, 44.89, 44.69, 29.48, 26.88, 26.71, 20.51, 20.48, 20.32, 19.32, 9.91 ppm.

1D-4,5-*O*-Bisbenzoyl-1-*O*-(*tert*-butyldiphenylsilyl)-2,3-*O*-(D-1',7',7'-trimethyl[2.2.1]bicyclohept-2'-ylidene)-*myo*-inositol (2.10):



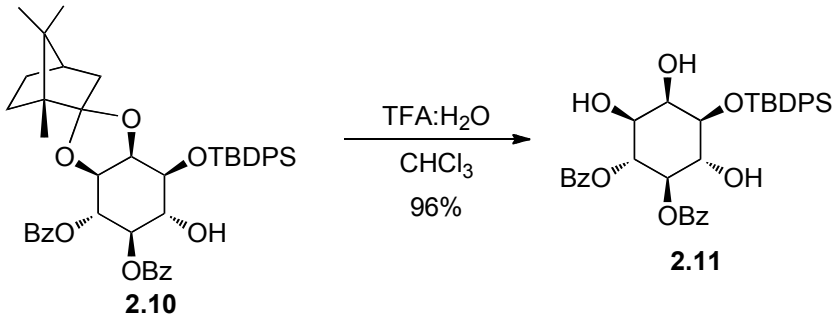
2.9 **2.10**

The following procedure was first described by Bruzik and co-workers[139] whereby triol **2.9** (409 mg, 0.74 mmol) was dissolved in pyridine (4.1 mL) and dichloromethane (CH_2Cl_2, 820 µL) was added. The reaction was placed under nitrogen, cooled to -40 °C, and benzoyl chloride (BzCl, 213 µL, 1.85 mmol) was added dropwise. The mixture was allowed to warm to rt and stirred for 3.5 h. The reaction was concentrated and the residue was extracted from water with dichloromethane (2 x 50 mL), and the organic layers were combined, dried with magnesium sulfate, filtered, and concentrated. The

residue was purified *via* column chromatography on silica (5 – 20% acetone/hexane) to give **2.10** (422 mg, 75%) as a white foam.

Characterizations matched previous reports.[139] ^{1}H NMR (300 MHz, *CDCl$_3$*): δ = 7.95 (d, *J* = 8.3 Hz, 2H), 7.83 (d, *J* = 9.0 Hz, 4H), 7.71 (d, *J* = 7.9 Hz, 2H), 7.52–7.20 (m, 12H), 5.64 (t, *J* = 8.0 Hz, 1H), 5.14 (t, *J* = 8.7 Hz, 1H), 4.22 (t, *J* = 8.5 Hz, 1H), 4.13–3.99 (m, 3H), 1.97–1.59 (m, 5H), 1.48–1.23 (m, 3H), 1.19–1.08 (m, 18H), 0.90 (s, 3H) ppm. ^{13}C NMR (75 MHz, $CDCl_3$): δ = 166.30, 165.28, 136.09, 135.85, 133.12, 132.93, 130.14, 130.04, 130.00, 129.84, 129.67, 129.49, 129.31, 128.43, 128.24, 128.19, 127.91, 127.74, 118.50, 73.39, 72.23, 71.58, 51.80, 48.05, 45.14, 44.46, 29.40, 26.98, 26.90, 20.47, 19.33, 9.79 ppm.

1D-4,5-*O*-Bisbenzoyl-1-*O*-(*tert*-butyldiphenylsilyl)-*myo*-inositol (2.11):



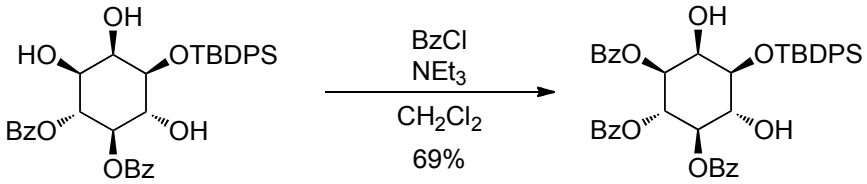
2.10 **2.11**

Protected *myo*-inositol **2.10** (5.41 g, 7.11 mmol) was dissolved in chloroform (55 mL). Water (355 µL) and trifluoroacetic acid (TFA, 6.75 mL) were added and the reaction mixture was allowed to stir at rt overnight. The following day, the reaction was concentrated, neutralized with triethylamine, and concentrated once more. The residue

was then purified via chromatography on silica (15 – 50% acetone/hexane) to afford **2.11** (4.16 g, 93%) as a white foam.

Characterizations matched previous reports.[139] ^{1}H NMR (300 MHz, CD_3OD): δ = 7.87 (dd, *J* = 16.1, 7.0 Hz, 8H), 7.50–7.21 (m, 12H), 5.73 (t, *J* = 10.0 Hz, 1H), 5.23 (t, *J* = 9.8 Hz, 1H), 4.89 (s, 3H), 4.33 (t, J = 9.5 Hz, 1H), 3.88–3.72 (m, 2H), 3.50 (dd, J = 10.0, 2.5 Hz, 1H), 1.13 (s, 9H) ppm. ^{13}C NMR (75 MHz, CD_3OD): δ = 167.62, 167.53, 137.33, 137.04, 135.32, 134.41, 134.03, 131.02, 130.99, 130.81, 130.77, 130.50, 130.47, 129.23, 129.20, 128.64, 128.57, 76.03, 75.33, 74.79, 74.29, 72.24, 71.12, 27.57, 20.31 ppm.

1D-3,4,5-*O*-Tribenzoyl-1-*O*-(*tert*-butyldiphenylsilyl)-*myo*-inositol (2.12):

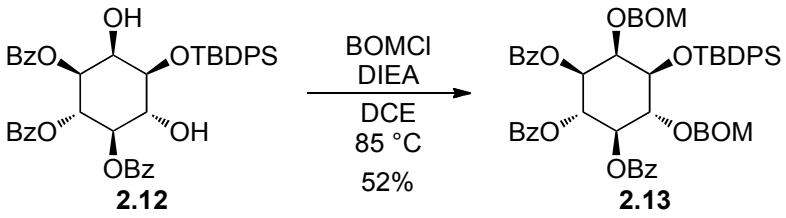


2.11 **2.12**

Triol **2.11** (211.5 mg, 0.337 mmol) was dissolved in anhydrous dichloromethane (4 mL), and triethylamine (142 µL, 1.01 mmol), and *N*, *N*'-dimethylaminopyridine (DMAP, 41.2 mg, 0.337 mmol) were added. The reaction was placed under nitrogen, cooled to –40 °C, and benzoyl chloride (BzCl, 58 µL, 0.51 mmol) was added dropwise. The mixture was allowed to warm to rt over 4 h and subsequently stirred at rt overnight. The reaction mixture was concentrated, dissolved in a solution of 35% acetone/hexane and filtered through a silica plug. Removal of the solvent yielded **2.12** (237 mg, 96%) as a white foam.

Characterizations matched previous reports.[217] ^{1}H NMR (300 MHz, $CDCl_3$): δ = 7.97–7.87 (m, 4H), 7.80–7.65 (m, 6H), 7.54–7.28 (m, 13H), 7.28–7.14 (m, 2H), 6.19 (t, *J* = 9.6 Hz, 1H), 5.38 (t, *J* = 9.9 Hz, 1H), 5.16 (ddd, *J* = 10.5, 2.6, 1.2 Hz, 1H), 4.40 (t, *J* = 9.5 Hz, 1H), 4.22 (s, 1H), 3.93–3.80 (m, 1H), 1.11 (s, 9H) ppm. ^{13}C NMR (75 MHz, $CDCl_3$): δ = 166.18, 165.65, 165.54, 135.87, 135.62, 133.26, 133.14, 132.95, 132.87, 132.29, 130.34, 130.18, 129.81, 129.79, 129.51, 129.25, 129.10, 129.06, 128.34, 128.26, 128.16, 128.09, 128.04, 74.54, 73.28, 72.19, 71.77, 70.56, 69.87, 26.98, 19.35 ppm.

1D-3,4,5-*O*-Tribenzoyl-2,6-*O*-bis(benzyloxymethyl)-1-*O*-(*tert*-butyldiphenylsilyl)-*myo*-inositol (2.13):

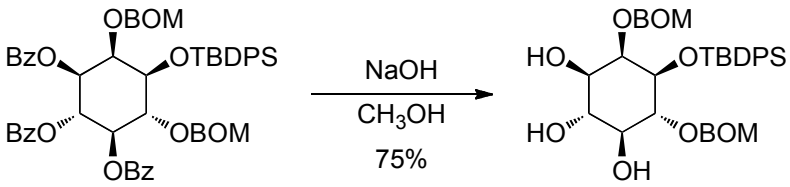


Diisopropylethylamine (0.43 mL, 2.6 mmol) and benzyl chloromethyl ether (0.36 mL, 2.6 mmol) were added to a solution of **2.12** (0.236 g, 0.323 mmol) in 1,2-dichloroethane (3 mL). The reaction mixture was stirred at reflux for 24 h. After the reaction was finished, water was added and the mixture extracted with dichloromethane (2 × 50 mL). The combined organic phases were dried with magnesium sulfate, filtered and concentrated. The crude product was purified by chromatography on silica gel (hexane/acetone, 10:1) to yield **2.13** (0.158 g, 52%) as a syrup.

$[\alpha]_D^{296\,K}$ = +68.9 (*c* = 4.8, $CHCl_3$). Other characterizations match previous reports.[224] ^{1}H NMR (400 MHz, $CDCl_3$): δ = 7.89 (d, *J* = 7.1 Hz, 2H), 7.84–7.69 (m, 8H), 7.49–7.29 (m,

10H), 7.29–7.09 (m, 11H), 7.05 (dd, *J* = 6.9, 2.6 Hz, 2H), 6.91 (dd, *J* = 6.5, 3.0 Hz, 2H), 6.13 (t, *J* = 10.2 Hz, 1H), 5.58 (t, *J* = 9.6 Hz, 1H), 5.02 (d, *J* = 12.9 Hz, 1H), 4.92 (d, *J* = 6.9 Hz, 1H), 4.80 (q, *J* = 6.5 Hz, 2H), 4.62–4.38 (m, 4H), 4.32–4.23 (m, 2H), 4.18 (d, *J* = 12.3 Hz, 1H), 3.99 (s, 1H), 1.11 (s, 9H) ppm. ^{13}C NMR (101 MHz, $CDCl_3$): δ = 165.88, 165.77, 165.34, 137.69, 137.65, 135.92, 133.22, 132.99, 132.86, 132.81, 130.14, 129.94, 129.71, 129.63, 129.54, 129.30, 129.12, 128.18, 128.09, 128.04, 127.85, 127.40, 127.29, 127.21, 127.18, 96.74, 95.80, 72.53, 71.62, 71.00, 69.97, 69.63, 27.24, 19.33 ppm.

1D-2,6-*O*-Bis(benzyloxymethyl)-1-*O*-(*tert*-butyldiphenylsilyl)-*myo*-inositol (2.14):



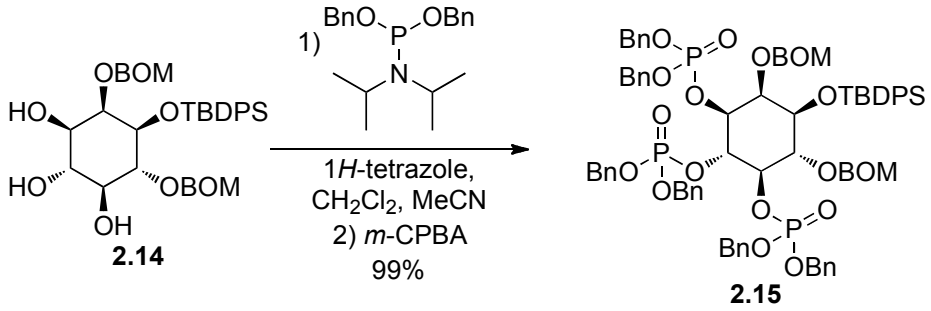
2.13 **2.14**

A 1% sodium hydroxide solution (2 mL) and dichloromethane (2 mL) were added to a solution of **2.13** (0.13 g, 0.134 mmol) in methanol (5 mL). The mixture was stirred at rt under nitrogen for 18 h. The solvent was removed and the residue purified by chromatography on silica gel (hexane/acetone, 4:1) to give **2.14** (0.66 g, 75%) as a syrup.

$[\alpha]_D^{296\,K}$ = +60.5 (*c* = 2.6, $CHCl_3$). ^{1}H NMR (400 MHz, $CDCl_3$): δ = 7.68 (t, *J* = 7.2 Hz, 4 H), 7.45–7.25 (m, 16 H), 4.94 (d, *J* = 6.8 Hz, 1 H), 4.75–4.65 (m, 3 H), 4.54–4.51 (m, 3 H), 4.42 (d, *J* = 11.6 Hz, 1 H), 4.30 (br. s, 1 H), 3.81–3.72 (m, 2 H), 3.66–3.54 (m, 3 H), 3.20–3.13 (m, 2 H), 2.75 (br. s, 1 H), 1.04 (s, 9 H) ppm. ^{13}C NMR (100.6 MHz, $CDCl_3$): δ

= 136.3, 136.2, 135.4, 135.3, 133.1, 129.6, 129.3, 128.1, 127.6, 127.5, 127.3, 127.1, 96.5, 96.2, 84.7, 82.6, 73.3, 72.2, 70.4, 70.0, 69.9, 26.5, 18.9 ppm. DART-HRMS: calcd. for $C_{38}H_{45}O_8Si$ $[M - H]^-$ 657.2884; found 657.2888.

1D-2,6-*O*-Bis(benzyloxymethyl)-1-*O*-(*tert*-butyldiphenylsilyl)-*myo*-inositol 3,4,5-Tris(dibenzyl phosphate) (2.15):

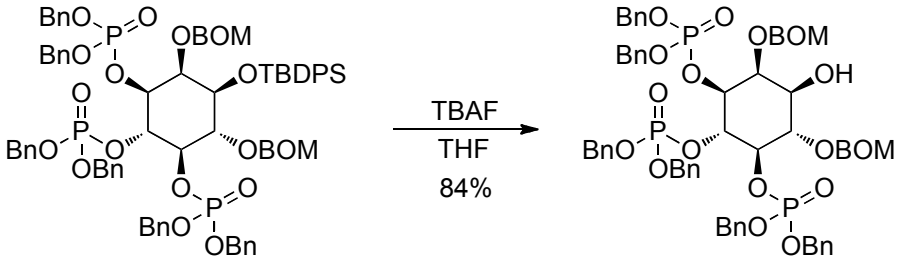


Dibenzyl *N*,*N*-diisopropylphosphoramidite (0.40 mL, 1.22 mmol) was added to a solution of alcohol **2.14** (0.134 g, 0.203 mmol) and 1*H*-tetrazole (4.0 mL, 1.8 mmol, 0.45 M in acetonitrile) in dichloromethane (4 mL) under nitrogen, and the mixture was stirred at rt for 18 h. The reaction solution was cooled to –20 °C, and *m*-CPBA (0.315 g, 57– 86%) was added. The mixture was warmed to rt and stirred for 3 h. The solvent was removed and the residue purified by flash chromatography on silica gel (hexanes/acetone, 8:1) to access **2.15** (0.289 g, 99%) as a syrup.

$[\alpha]_D^{296\ K}$ = +15.5 (*c* = 2.6, $CHCl_3$). ^{1}H NMR (400 MHz, CDCl3): δ = 7.76–7.67 (m, 4 H), 7.38–7.05 (m, 46 H), 5.15–4.88 (m, 12 H), 4.83–4.64 (m, 7 H), 4.54–4.48 (m, 2 H), 4.37–4.26 (m, 2 H), 4.08 (t, *J* = 12 Hz, 1 H), 3.98–3.91 (m, 2 H), 1.07 ppm. ^{13}C NMR (100.6 MHz, $CDCl_3$): δ = 138.2, 137.8, 136.2, 136.2, 136.1, 136.1, 136.0, 135.9, 135.9, 135.8, 135.7, 133.3, 132.5, 130.1, 130.0, 128.5, 128.5, 128.4, 128.4, 128.3, 128.3,

128.3, 128.2, 128.2, 128.1, 128.0, 128.0, 128.0, 127.9, 127.9, 127.9, 127.8, 127.7, 127.6, 127.4, 127.3, 96.6, 96.0, 75.1, 75.1, 75.1, 73.4, 70.7, 69.9, 69.6, 69.5, 69.5, 69.4, 69.3, 69.2, 69.1, 69.0, 27.2, 19.4 ppm. ^{31}P NMR (121.5 MHz, $CDCl_3$): δ = 0.07, –0.04, –0.28 ppm. MALDI-HRMS: calcd. for $C_{80}H_{85}O_{17}P_3SiNa$ $[M + Na]^+$ 1461.4666; found 1461.4603.

1D-2,6-*O*-Bis(benzyloxymethyl)-*myo*-inositol 3,4,5-Tris(dibenzyl phosphate) (2.16):



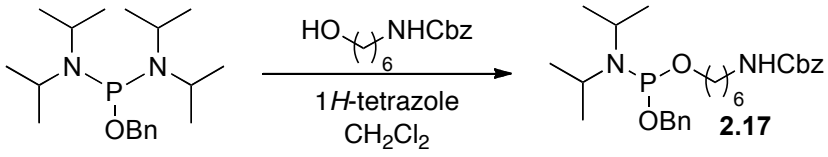
2.15 **2.16**

A solution of fully protected inositol **2.15** (0.027 g, 0.019 mmol) in tetrahydrofuran (1 mL) was treated with tetrabutylammonium fluoride trihydrate (0.018 g, 0.056 mmol) and stirred at rt for 18 h. Following concentration, the residue was purified by chromatography on silica gel (hexanes/acetone, 3:1) to give alcohol **2.16** (0.019 g, 84%) as a syrup.

$[\alpha]_D^{296\ K}$ = –15.4 (*c* = 0.8, $CHCl_3$). ^{1}H NMR (400 MHz, $CDCl_3$): δ = 7.32–7.15 (m, 40 H), 5.14–4.84 (m, 16 H), 4.70–4.60 (m, 5 H), 4.48–4.40 (m, 3 H), 4.28– 4.19 (m, 2 H), 3.85 (t, *J* = 9.4 Hz, 1 H), 3.48–3.44 (m, 1 H) ppm. ^{13}C NMR (100.6 MHz, $CDCl_3$): δ = 137.6, 136.9, 136.1, 136.0, 135.9, 135.9, 135.8, 135.7, 135.6, 135.6, 128.5, 128.4, 128.3, 128.1, 128.1, 128.0, 128.0, 127.9, 127.8, 127.6, 97.1, 96.2, 82.4, 78.7, 76.8, 76.3, 75.4, 70.4, 70.1, 69.7, 69.6, 69.6, 69.5, 69.4, 69.3, 69.3 ppm. ^{31}P NMR (121.5 MHz, $CDCl_3$): δ

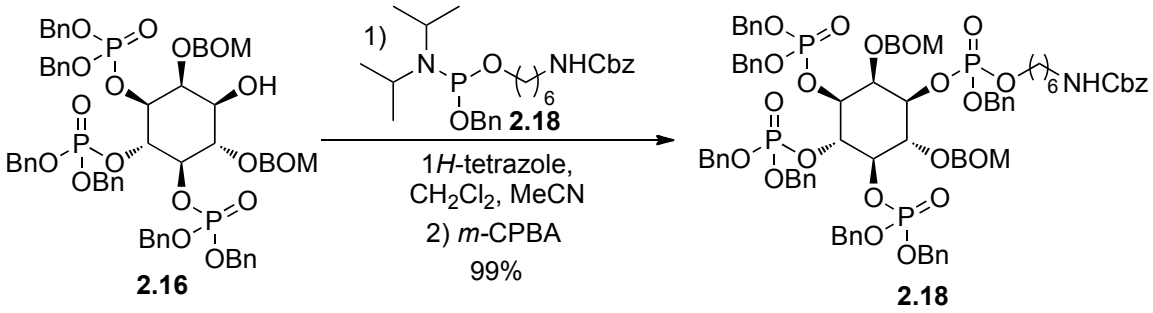
= –0.04, –0.48, –0.58 ppm. MALDI-HRMS: calcd. for $C_{64}H_{67}O_{17}P_3Na$ $[M + Na]^+$ 1223.3489; found 1223.3498.

Cbz-Aminohexanol Phosphoramidite (2.17):



1*H*-Tetrazole (4.6 mL of a 0.45 M solution in acetonitrile, 2.07 mmol) and 1-(benzyloxy)-*N*,*N*,*N*',*N*'-tetraisopropylphosphinediamine (1.392 g, 4.11 mmol) were added to a solution of Cbz-aminohexanol (0.694 g, 2.76 mmol) in dichloromethane (30 mL) under nitrogen. This mixture was stirred at rt for 2 h, at which point the solution was extracted with dichloromethane (3 × 80 mL) from saturated sodium hydrogen carbonate (80 mL). The combined organic phases were dried with magnesium sulfate, filtered, and concentrated, and the residue was purified by chromatography on silica gel (hexane/ethyl acetate/triethylamine, 100:10:1). The resulting colorless liquid **2.17** (0.983 g, 2.0 mmol) was passed on to the next step without further purification.

1D-Benzyl (6-Benzyloxycarbonylaminohexyl) 2,6-*O*-Bis(benzyloxymethyl)-*myo*-inosit-1-yl Phosphate 3,4,5-Tris(dibenzyl phosphate) (2.18):

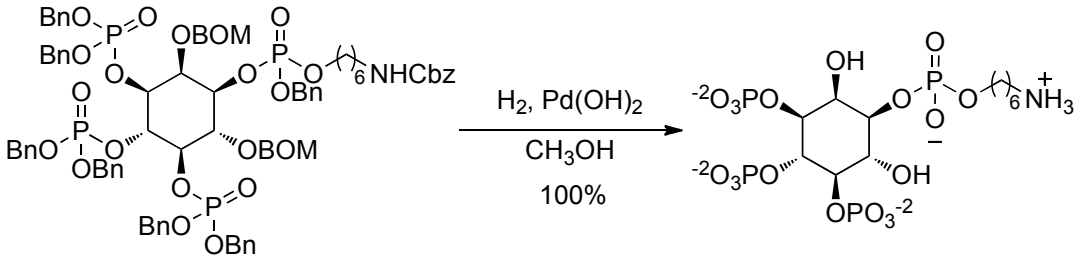


Cbz-aminohexanol phosphoramidite **2.17** (0.183 g, 0.375 mmol) was added to a solution of alcohol **2.16** (0.180 g, 0.15 mmol), and 1*H*-tetrazole (1.0 mL, 0.45 mmol, 0.45 M in acetonitrile) in dichloromethane (15 mL) under nitrogen, and the mixture was stirred at rt for 18 h. The reaction solution was cooled to **–**60 °C, and *m*-CPBA (0.78 g, 57**–**86%) was added. The mixture was stirred at this temperature for 60 min and slowly warmed to rt, after removal of the cooling bath. The solution was diluted to 60 mL with dichloromethane, washed with saturated aqueous sodium hydrogen carbonate (2 × 30 mL), and the aqueous phase was extracted with dichloromethane (60 mL). The combined organic phases were dried with magnesium sulfate, filtered, and concentrated. The residue was purified by chromatography on silica gel (hexanes/acetone, 3:1) to afford product **2.18** (0.238 g, 99%) as a syrup.

$[\alpha]_D^{296\ K}$ = **–**14.7 (*c* = 5.6, $CHCl_3$). ^{1}H NMR (400 MHz, $CDCl_3$): *δ* = 7.32– 7.17 (m, 50 H), 5.13–4.81 (m, 21 H), 4.76–4.52 (m, 5 H), 4.45–4.17 (m, 4 H), 3.94–3.82 (m, 2 H), 3.09–3.03 (m, 2 H), 1.46–1.18 (m, 8 H) ppm. ^{13}C NMR (100.6 MHz, $CDCl_3$): *δ* = 155.9, 137.6, 137.3, 136.3, 135.6, 135.6, 135.5, 135.3, 135.2, 135.2, 135.1, 128.0, 128.0, 127.9, 127.8, 127.8, 127.6, 127.2, 127.0, 126.9, 96.0, 95.7, 95.6, 81.9, 77.5, 75.1, 75.0, 74.8,

74.7, 74.3, 74.1, 74.0, 70.0, 69.9, 69.6, 69.3, 69.1, 69.0, 68.9, 68.9, 68.8, 67.7, 67.6, 67.5, 67.4, 66.0, 52.9, 40.4, 29.5, 29.4, 29.1, 25.5, 24.4 ppm. ^{31}P NMR (121.5 MHz, $CDCl_3$): δ = 0.13, –0.03, –0.21, –0.56 ppm. MALDI-HRMS: calcd. For $C_{85}H_{93}NO_{22}P_4Na$ $[M + Na]^+$ 1626.5032; found 1626.5042.

1D-1-(6-Aminohexyl sodium phosphate)-*myo*-inositol 3,4,5-Tris(disodium phosphate) (2.1):



2.18 **2.1**

Palladium hydroxide (20%) on charcoal (0.30 g) was added to a solution of a compound **2.18** (0.23 g, 0.143 mmol) in methanol (15–40 mL). The mixture was then stirred at rt with 1 atm of hydrogen (balloon) for 3 days. The catalyst was removed by filtration and the residue washed with methanol. The solvent was removed in vacuo, and the crude product was dissolved in water and stirred with Chelex 100 resin (Sigma, Na^+ form) for 3 h. The resin was removed by filtration and the filtrate lyophilized to give the corresponding amino conjugate **2.1** (88 mg, 100%) as a white solid.

$[\alpha]_D^{296\ K}$ = –7.2 (*c* = 0.68, H_2O). ^{1}H NMR (400 MHz, D_2O): δ = 4.04 (br. s, 2 H), 4.22–3.95 (m, 6 H), 3.02 (br. s, 2 H), 1.68 (br. s, 4 H), 1.44 (br. s, 4 H) ppm. ^{13}C NMR (100.6 MHz, D_2O): δ = 78.2, 76.1, 75.3, 74.5, 70.9, 70.7, 66.3, 39.5, 29.4, 26.6, 25.1, 24.4

ppm. ^{31}P NMR (121.5 MHz, D_2O): δ = 2.75, 2.54, 1.78, 0.89 ppm. MALDI-HRMS: calcd. for $C_{12}H_{31}NO_{18}P_4Na$ $[M + Na]^+$ 624.0389; found 624.0301.

2.8.3 Assay Procedure

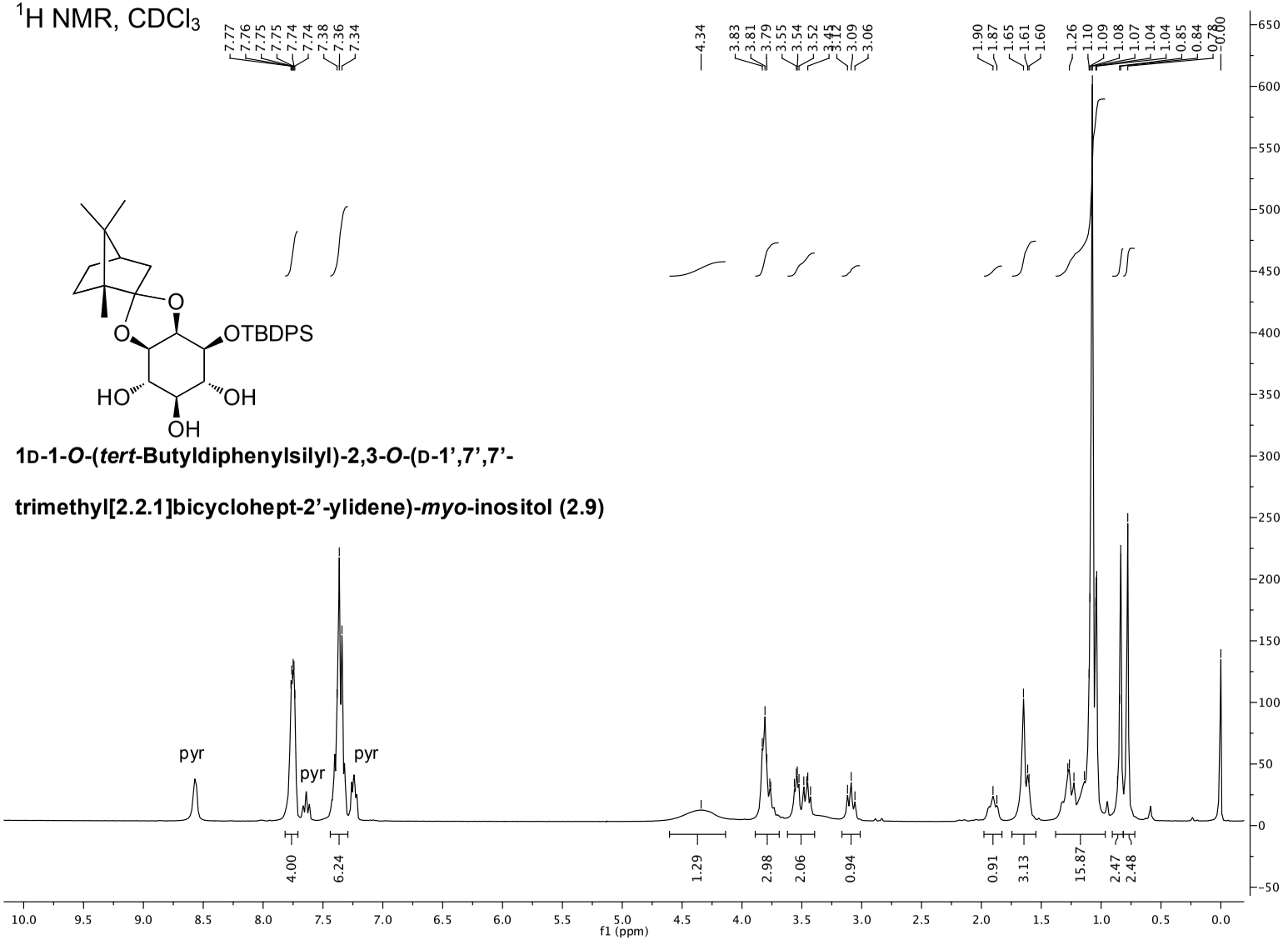
Microarray Assay with Akt-PH:

The wash buffer employed for all glass slide experiments was 20 mM Tris buffer at pH 7.74, with 0.05% tween and all washings were done in petri dishes with agitation. For the uniform concentration grids, 12 solutions of **2.19** at 500 μM were printed onto the slide in 20 replicates (2 grids of 12x10) and then incubated in a humidifying chamber overnight. For the varying concentration grids, 12 solutions of **2.19** at 0, 15, 30, 45, 60, 75, 100, 200, 250, 300, 400, and 500 μM were printed onto the slide in 20 replicates (2 grids of 12x10) and incubated in a humidifying chamber overnight. The grids were outlined with a marker, and the slide was washed 3x with wash buffer. It was then dried under a stream of nitrogen, 50 μg/mL Akt-GST in wash buffer was added, and incubated for 1 h in a humidifying chamber. The slide was washed 3x with wash buffer, dried under a stream of nitrogen, and a solution of 0.2 μg/mL rabbit anti-GST and 0.1 μg/mL goat anti-rabbit–Cy3 in wash buffer was added and incubated in a humidifying chamber for 1 h. Following the incubation, the slide was washed 2x with wash buffer, 3x with deionized water, dried under a stream of nitrogen and then scanned for fluorescence detecting at 532 nm.

Microarray Assay for Profilin:

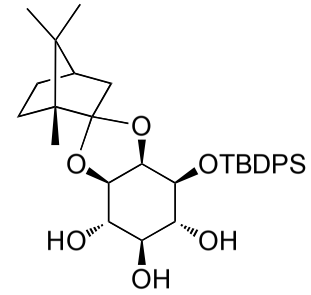
The wash buffer employed for all glass slide experiments was 20 mM Tris buffer at pH 7.74, with 0.05% tween and all washings were done in petri dishes with agitation. Twelve solutions of **2.20** at 0, 10, 25, 50, 75, 100, 150, 200, 250, 300, 350, and 400 μM were printed onto the slide in 20 replicates (2 grids of 12x10) and incubated in a humidifying chamber overnight. The grids were outlined with a marker, and the slide was washed 2x with wash buffer. It was then dried under a stream of nitrogen. From left to right in sets of 4 grids, 0.05 μg/mL, 0.5 μg/mL, 5 μg/mL, and 50 μg/mL profilin in wash buffer was added, and incubated for 1 h in a humidifying chamber. The slide was washed 2x with wash buffer, dried under a stream of nitrogen, and a solution of 0.2 μg/mL rabbit anti-profilin and 0.1 μg/mL goat anti-rabbit–Cy3 in wash buffer was added and incubated in a humidifying chamber for 1.5 h. Following the incubation, the slide was washed 3x with deionized water, dried under a stream of nitrogen and then scanned for fluorescence detecting at 532 nm.

^{1}H NMR, $CDCl_3$

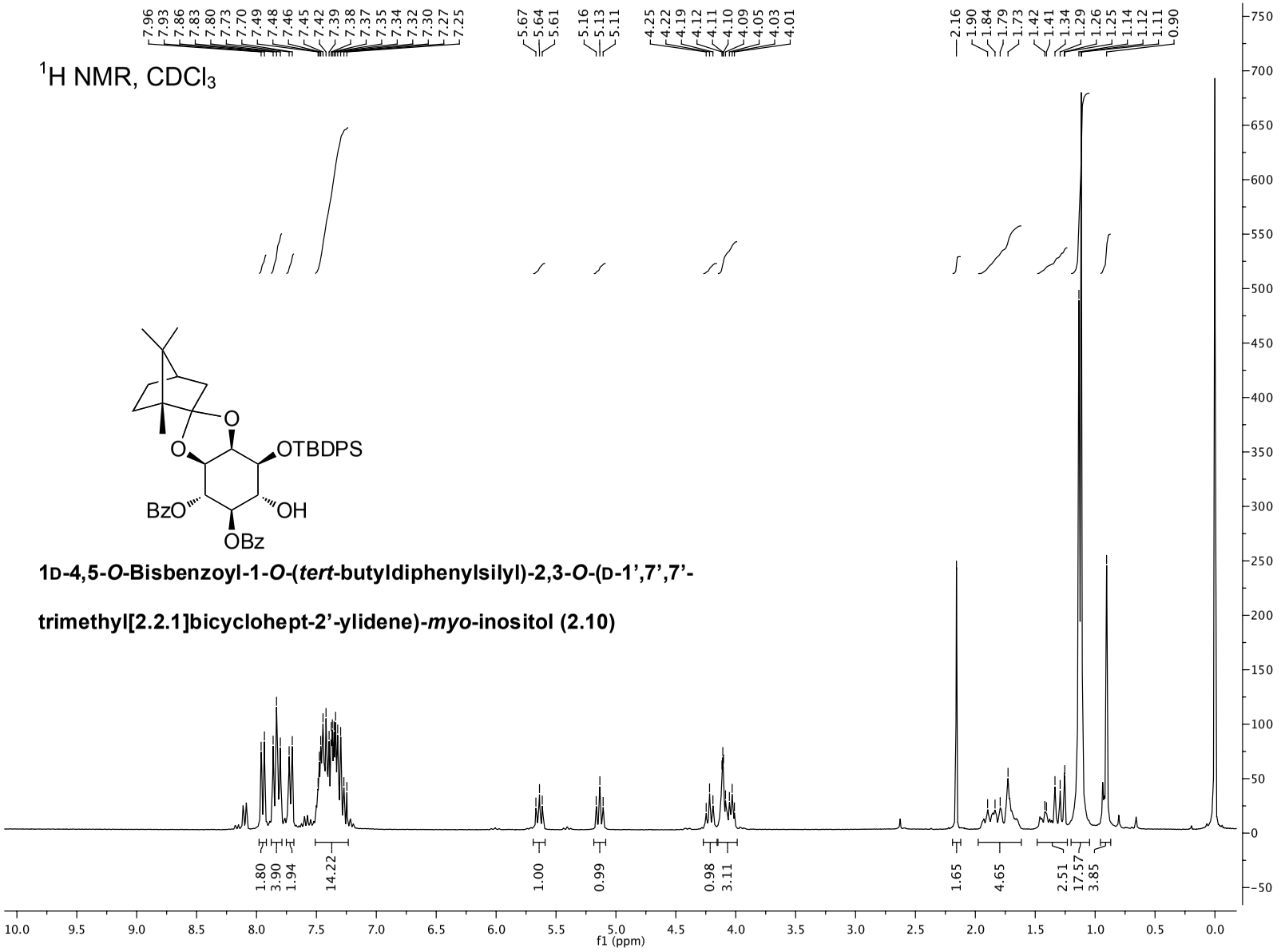


1D-1-*O*-(*tert*-Butyldiphenylsilyl)-2,3-*O*-(D-1',7',7'-trimethyl[2.2.1]bicyclohept-2'-ylidene)-*myo*-inositol (2.9)

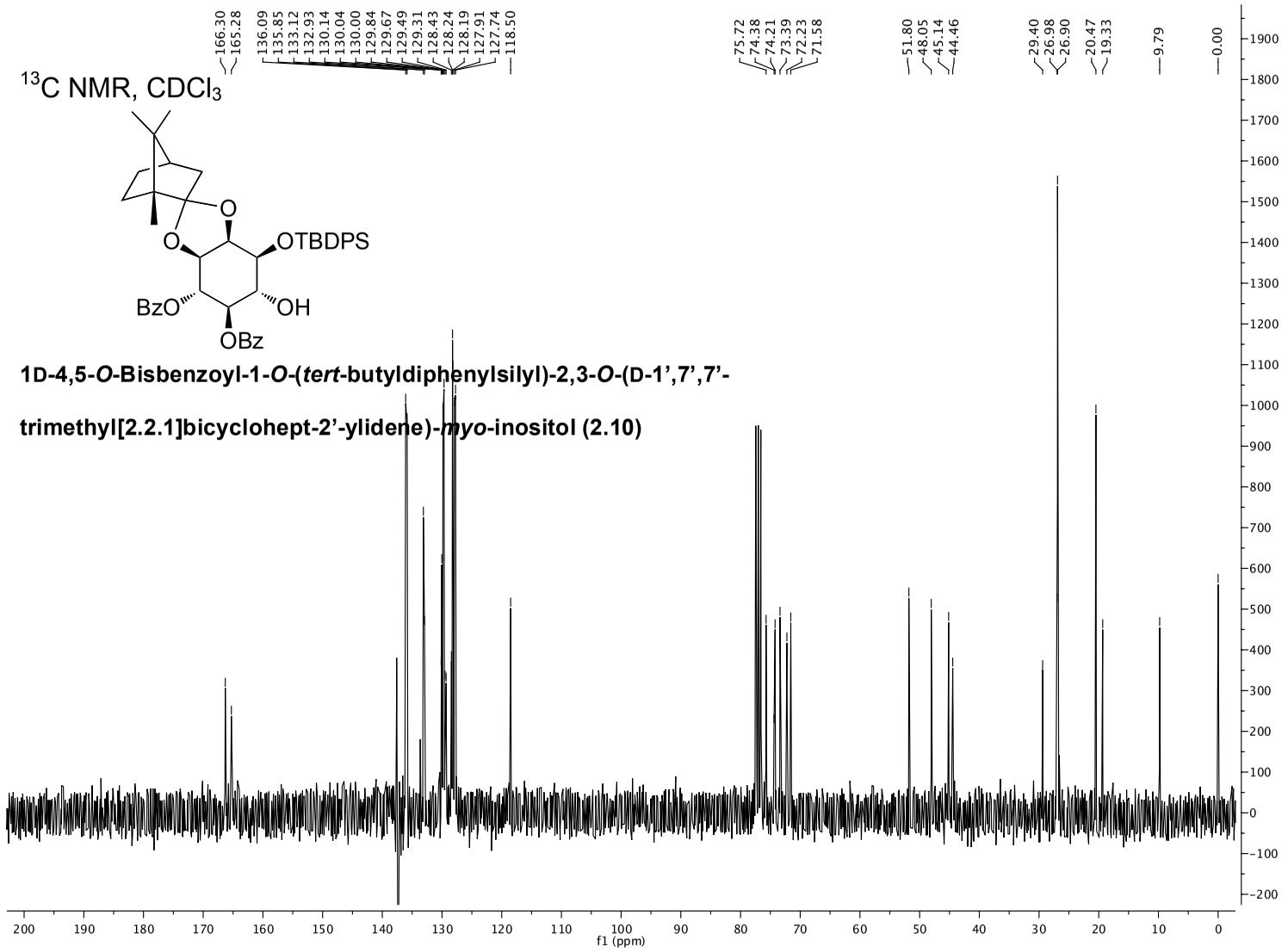
^{13}C NMR, $CDCl_3$



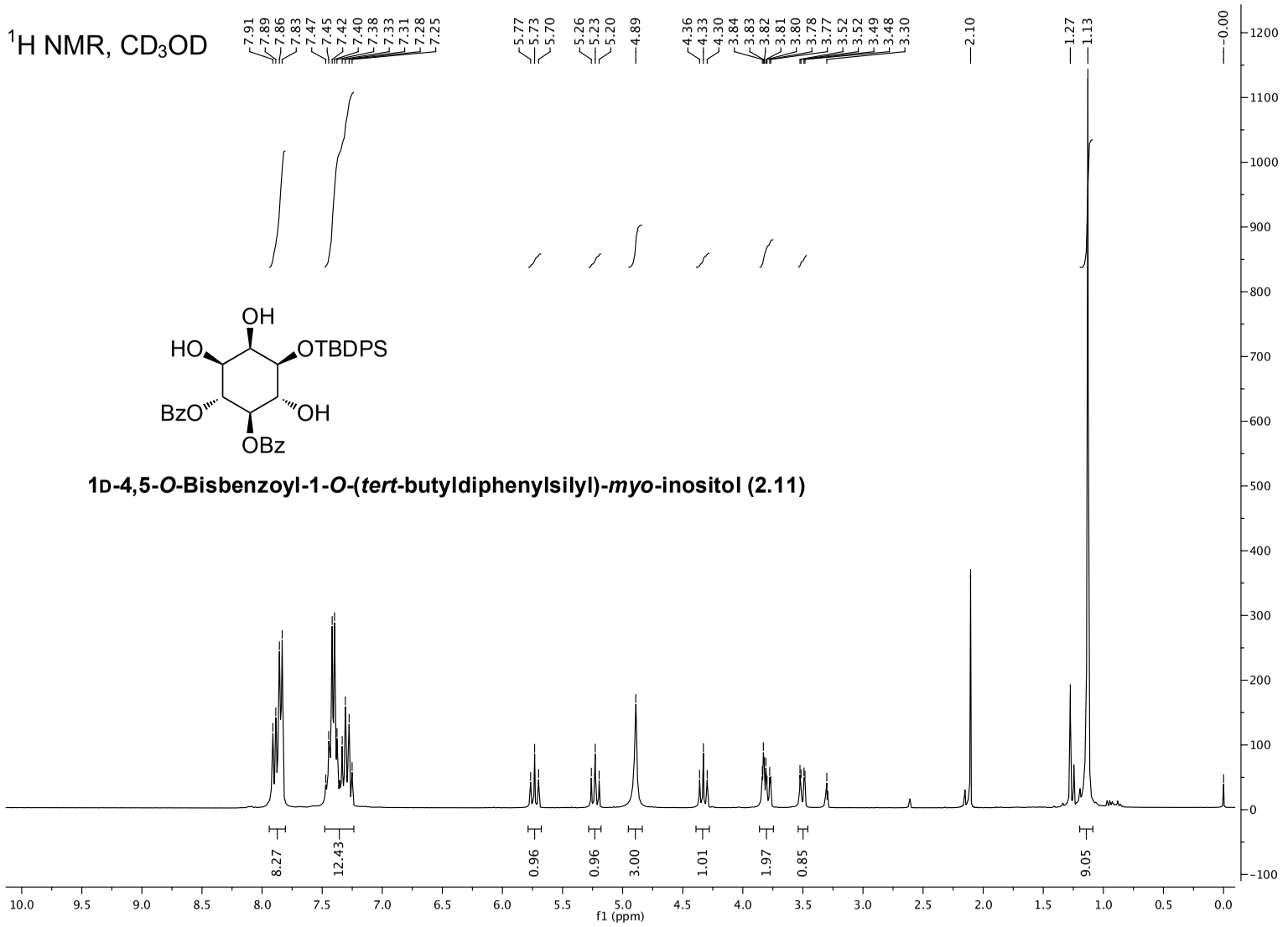
1D-1-*O*-(*tert*-Butyldiphenylsilyl)-2,3-*O*-(D-1',7',7'-trimethyl[2.2.1]bicyclohept-2'-ylidene)-*myo*-inositol (2.9)



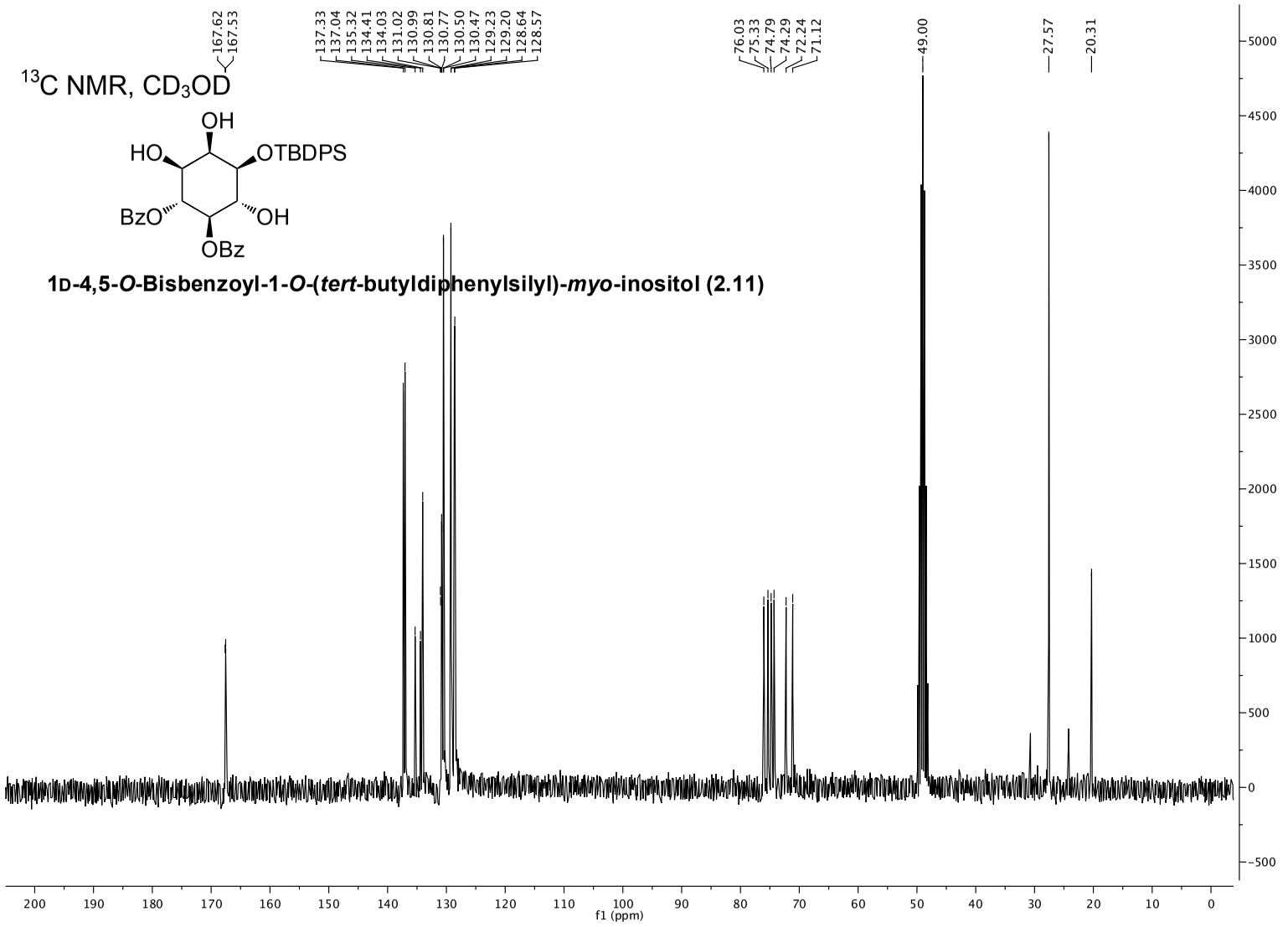
1D-4,5-*O*-Bisbenzoyl-1-*O*-(*tert*-butyldiphenylsilyl)-2,3-*O*-(D-1',7',7'-trimethyl[2.2.1]bicyclohept-2'-ylidene)-*myo*-inositol (2.10)



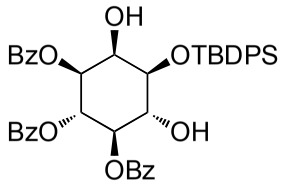
1D-4,5-*O*-Bisbenzoyl-1-*O*-(*tert*-butyldiphenylsilyl)-2,3-*O*-(D-1',7',7'-trimethyl[2.2.1]bicyclohept-2'-ylidene)-*myo*-inositol (2.10)



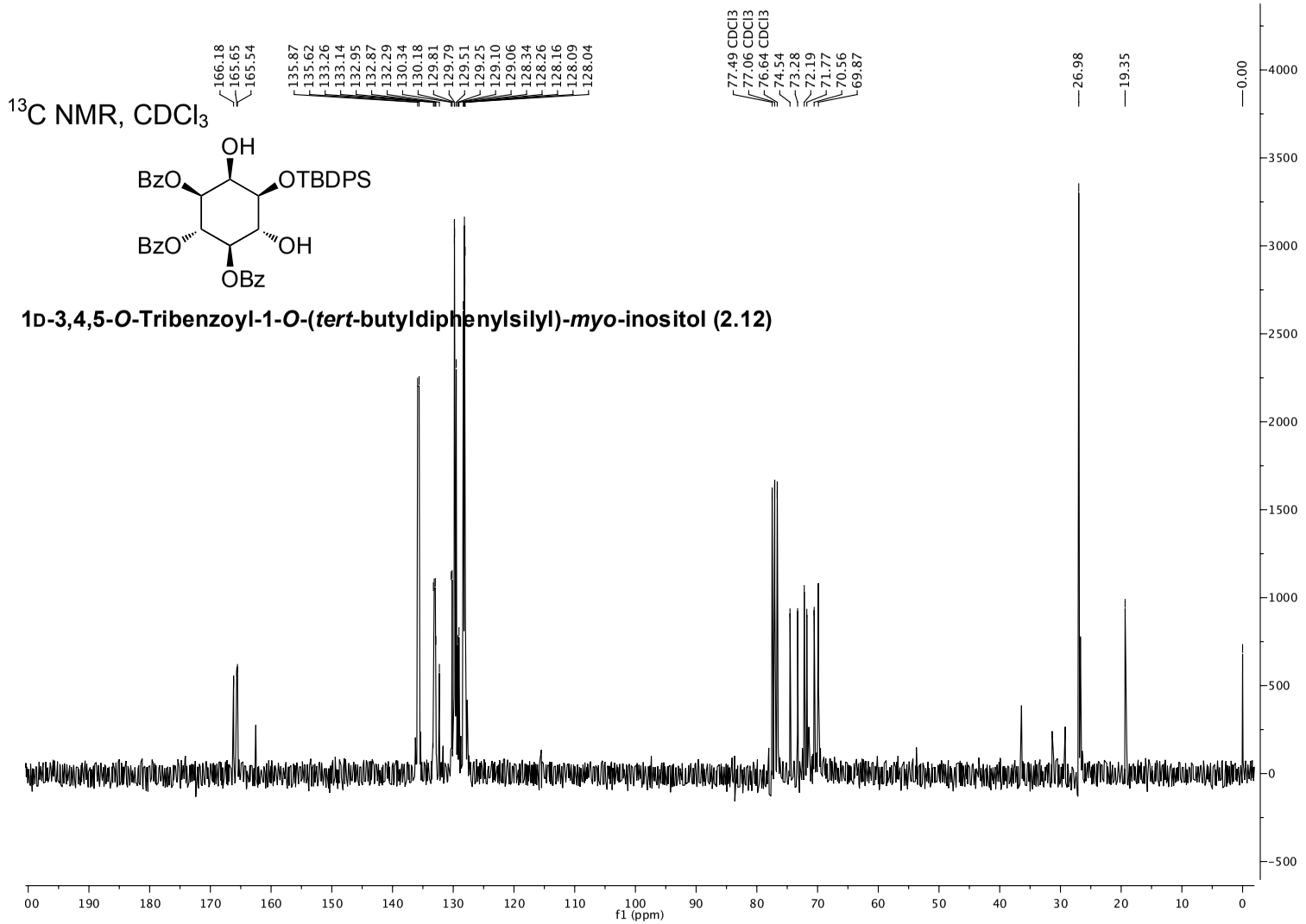
1D-4,5-*O*-Bisbenzoyl-1-*O*-(*tert*-butyldiphenylsilyl)-*myo*-inositol (2.11)

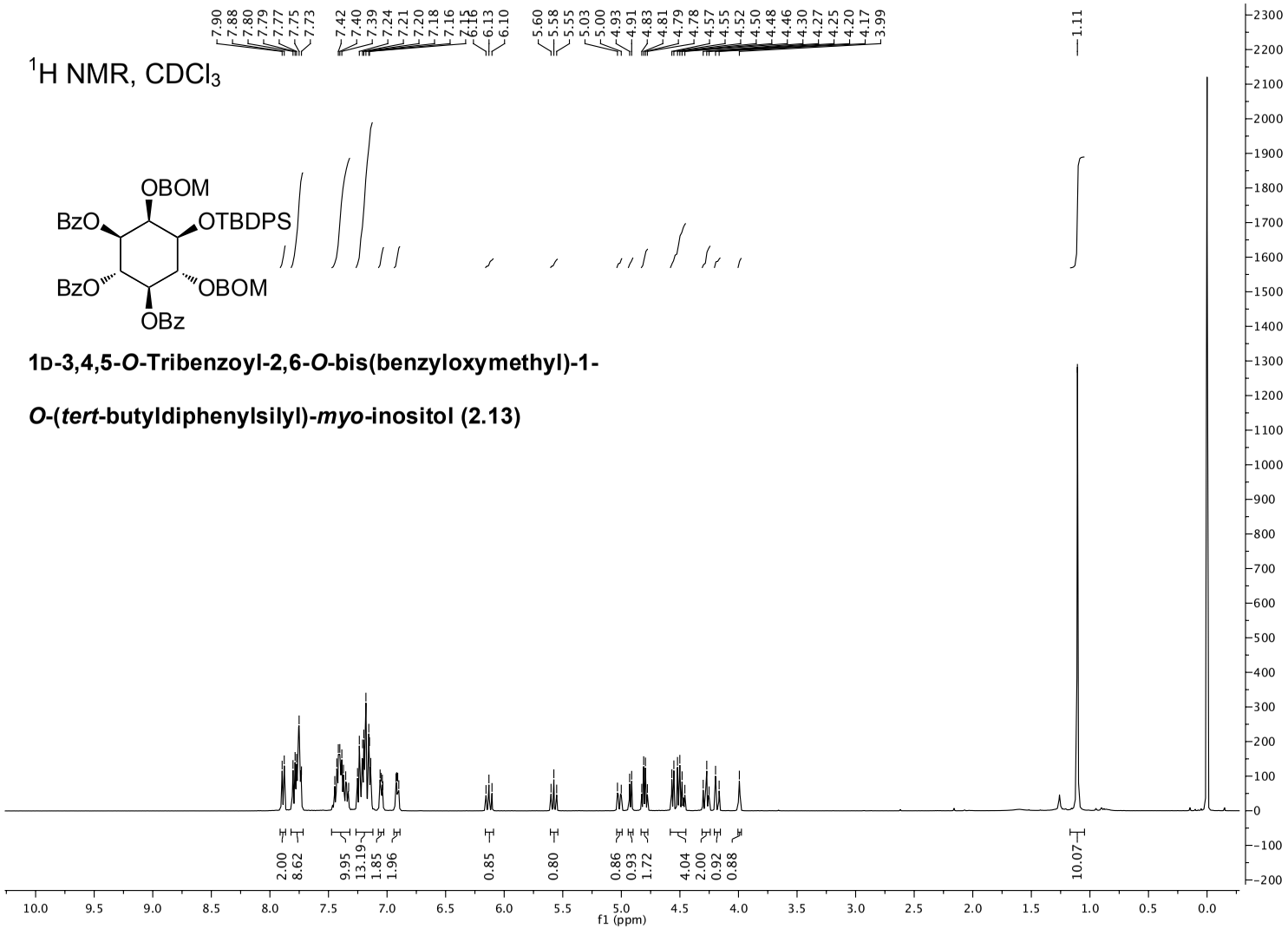

167.62
167.53
137.33
137.04
135.32
134.41
134.03
131.02
130.99
130.81
130.77
130.50
130.47
129.23
129.20
128.64
128.57
76.03
75.33
74.79
74.29
72.24
71.12
49.00
27.57
20.31
^{13}C NMR, CD_3OD
OH
HO
OTBDPS
BzO
OH
OBz
1D-4,5-*O*-Bisbenzoyl-1-*O*-(*tert*-butyldiphenylsilyl)-*myo*-inositol (2.11)
f1 (ppm)

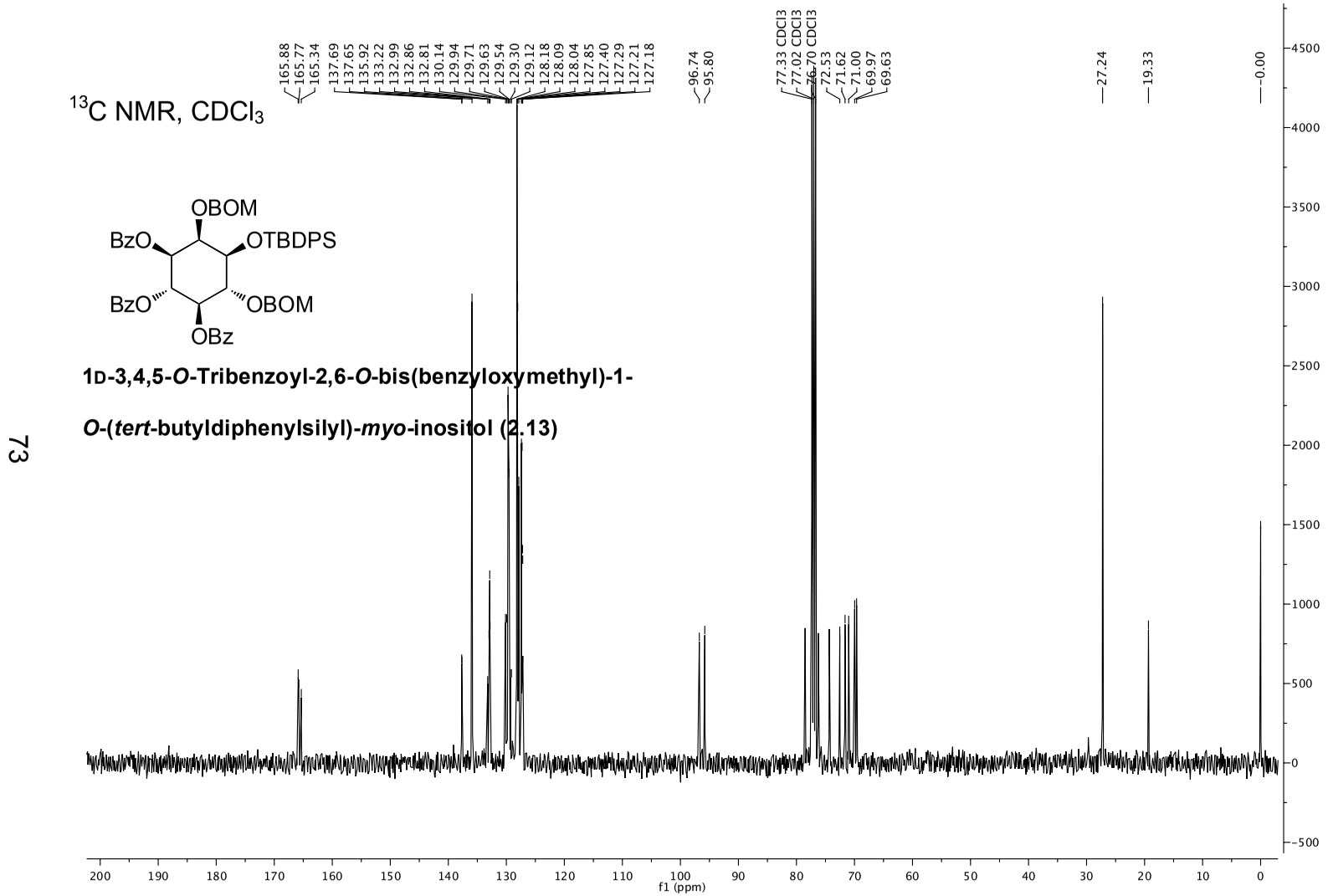
^{1}H NMR, $CDCl_3$

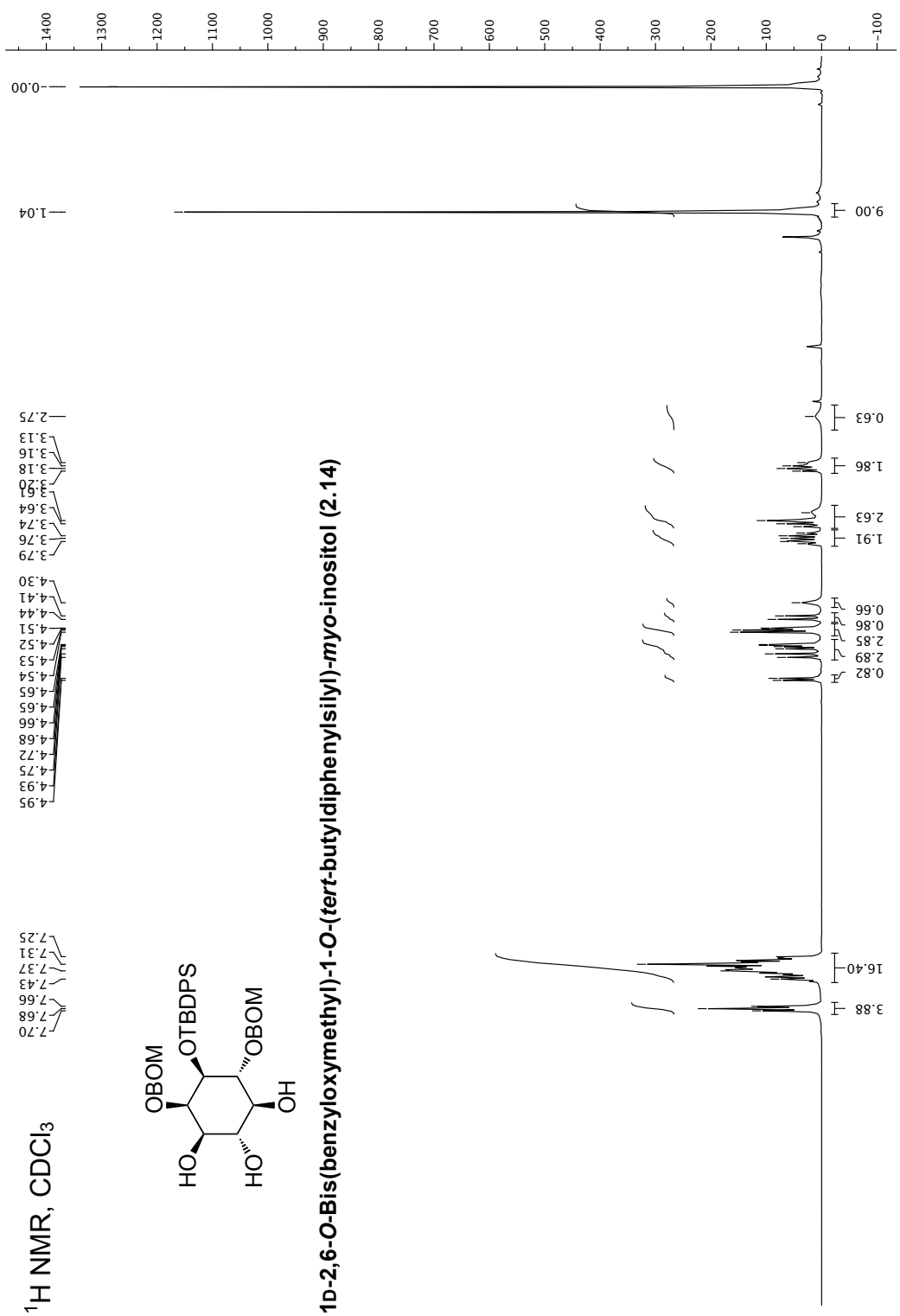


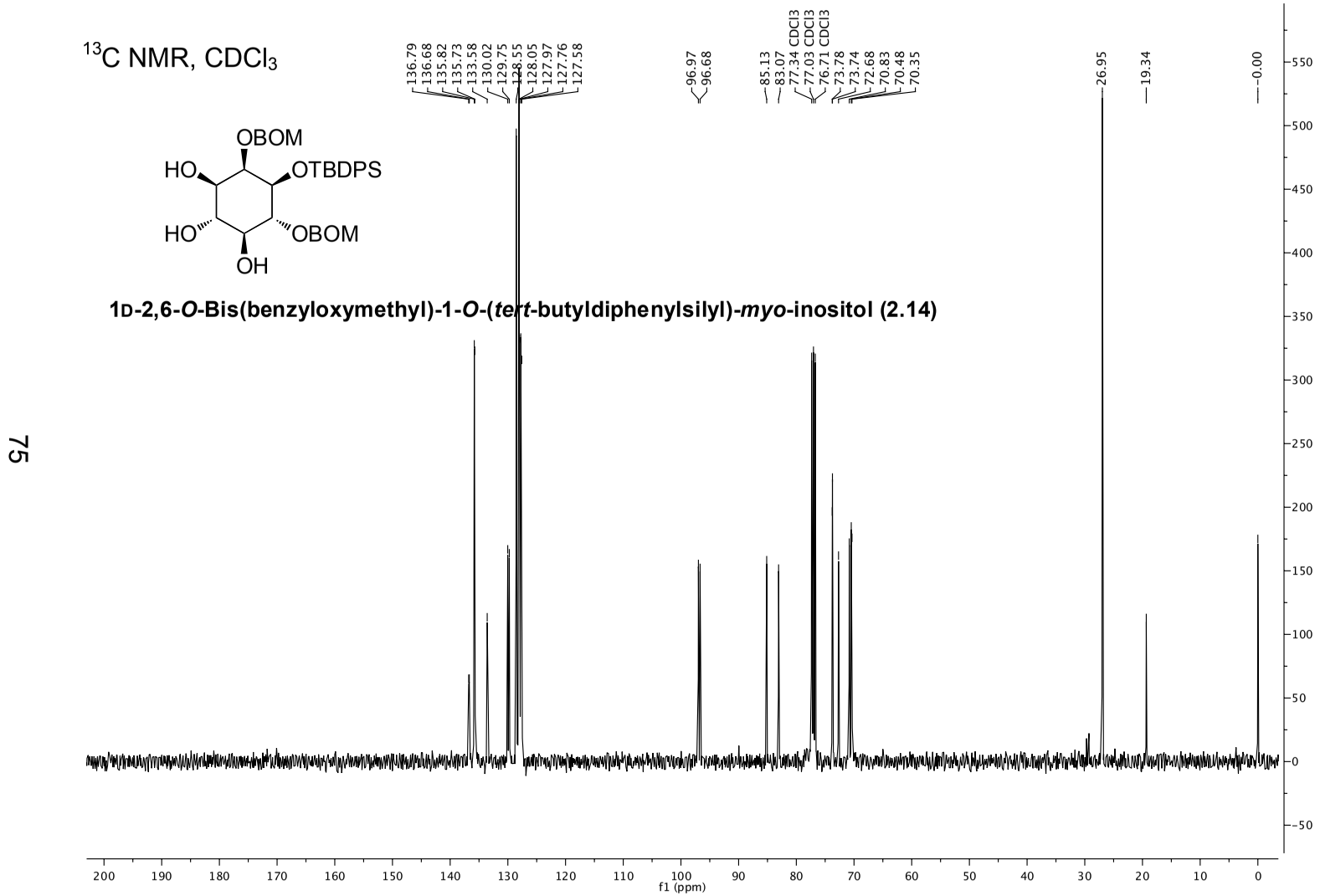
1D-3,4,5-*O*-Tribenzoyl-1-*O*-(*tert*-butyldiphenylsilyl)-*myo*-inositol (2.12)

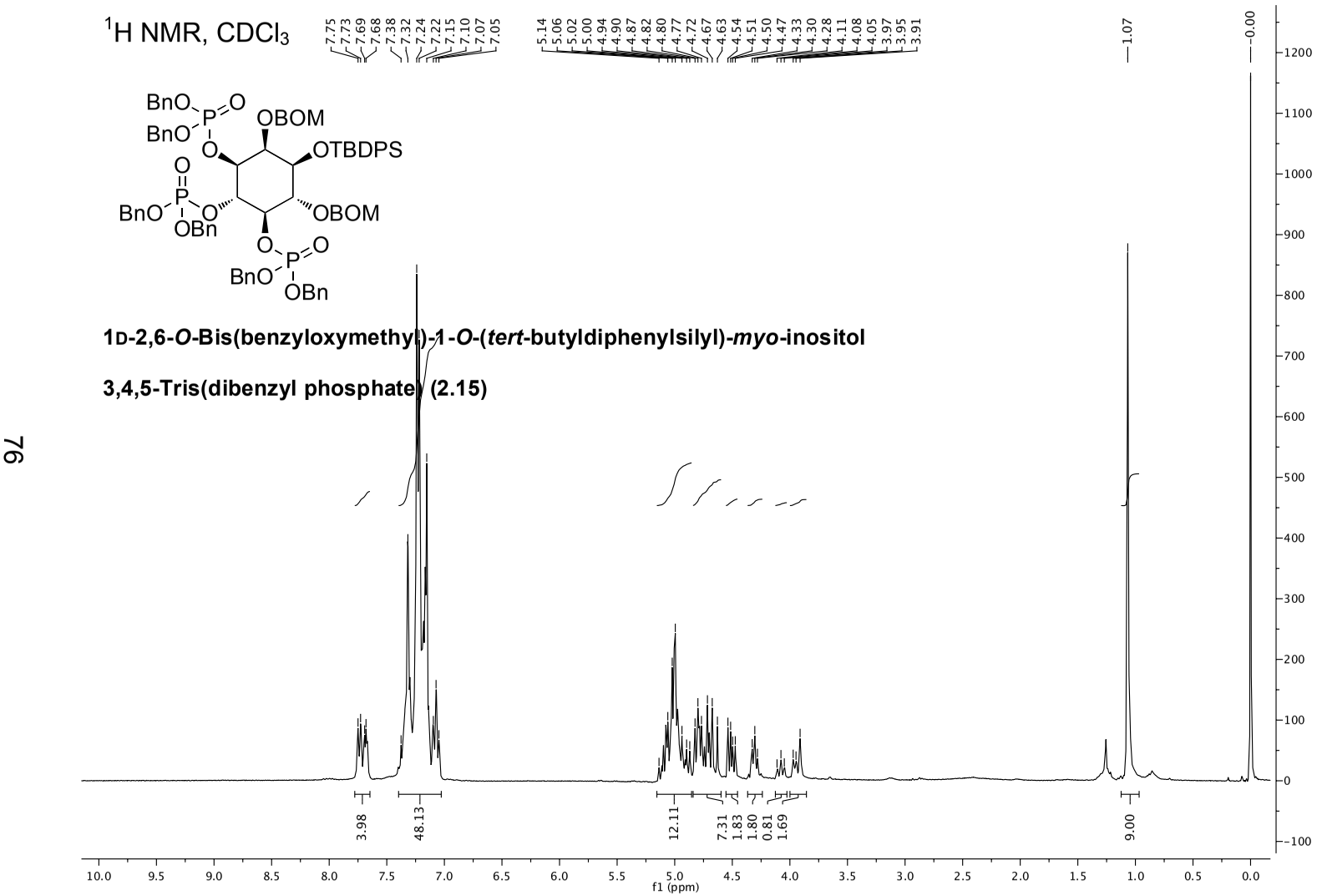

166.18
165.65
165.54
135.87
135.62
133.26
133.14
132.95
132.87
132.29
130.34
130.18
129.81
129.79
129.51
129.25
129.10
129.06
128.34
128.26
128.16
128.09
128.04
77.49 CDCl3
77.06 CDCl3
76.64 CDCl3
74.54
73.28
72.19
71.77
70.56
69.87
26.98
19.35
0.00
^{13}C NMR, CDCl$_3$
OH
BzO
OTBDPS
BzO
OH
OBz
1D-3,4,5-O-Tribenzoyl-1-O-(tert-butyldiphenylsilyl)-myo-inositol (2.12)
f1 (ppm)


^{1}H NMR, CDCl$_3$
OBOM
BzO
OTBDPS
BzO
OBOM
OBz
1D-3,4,5-O-Tribenzoyl-2,6-O-bis(benzyloxymethyl)-1-
O-(tert-butyldiphenylsilyl)-myo-inositol (2.13)
f1 (ppm)

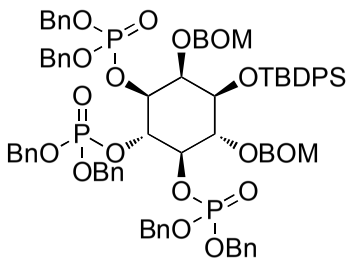

^{13}C NMR, CDCl$_3$
OBOM
BzO
OTBDPS
BzO
OBOM
OBz
1D-3,4,5-O-Tribenzoyl-2,6-O-bis(benzyloxymethyl)-1-
O-(tert-butyldiphenylsilyl)-myo-inositol (2.13)
165.88
165.77
165.34
137.69
137.65
135.92
133.22
132.99
132.86
132.81
130.14
129.94
129.71
129.63
129.54
129.30
129.12
128.18
128.09
128.04
127.85
127.40
127.29
127.21
127.18
96.74
95.80
77.33 CDCl3
77.02 CDCl3
76.70 CDCl3
72.53
71.62
71.00
69.97
69.63
27.24
19.33
0.00
f1 (ppm)


1H NMR, CDCl3
OBOM
OTBDPS
HO
HO
OBOM
OH
1D-2,6-O-Bis(benzyloxymethyl)-1-O-(tert-butyldiphenylsilyl)-myo-inositol (2.14)
f1 (ppm)


^{13}C NMR, CDCl$_3$
OBOM
HO
OTBDPS
HO
OBOM
OH
1D-2,6-O-Bis(benzyloxymethyl)-1-O-(tert-butyldiphenylsilyl)-myo-inositol (2.14)
136.79
136.68
135.82
135.73
133.58
130.02
129.75
128.55
128.05
127.97
127.76
127.58
96.97
96.68
85.13
83.07
77.34 CDCl3
77.03 CDCl3
76.71 CDCl3
73.78
73.74
72.68
70.83
70.48
70.35
26.95
19.34
0.00
f1 (ppm)

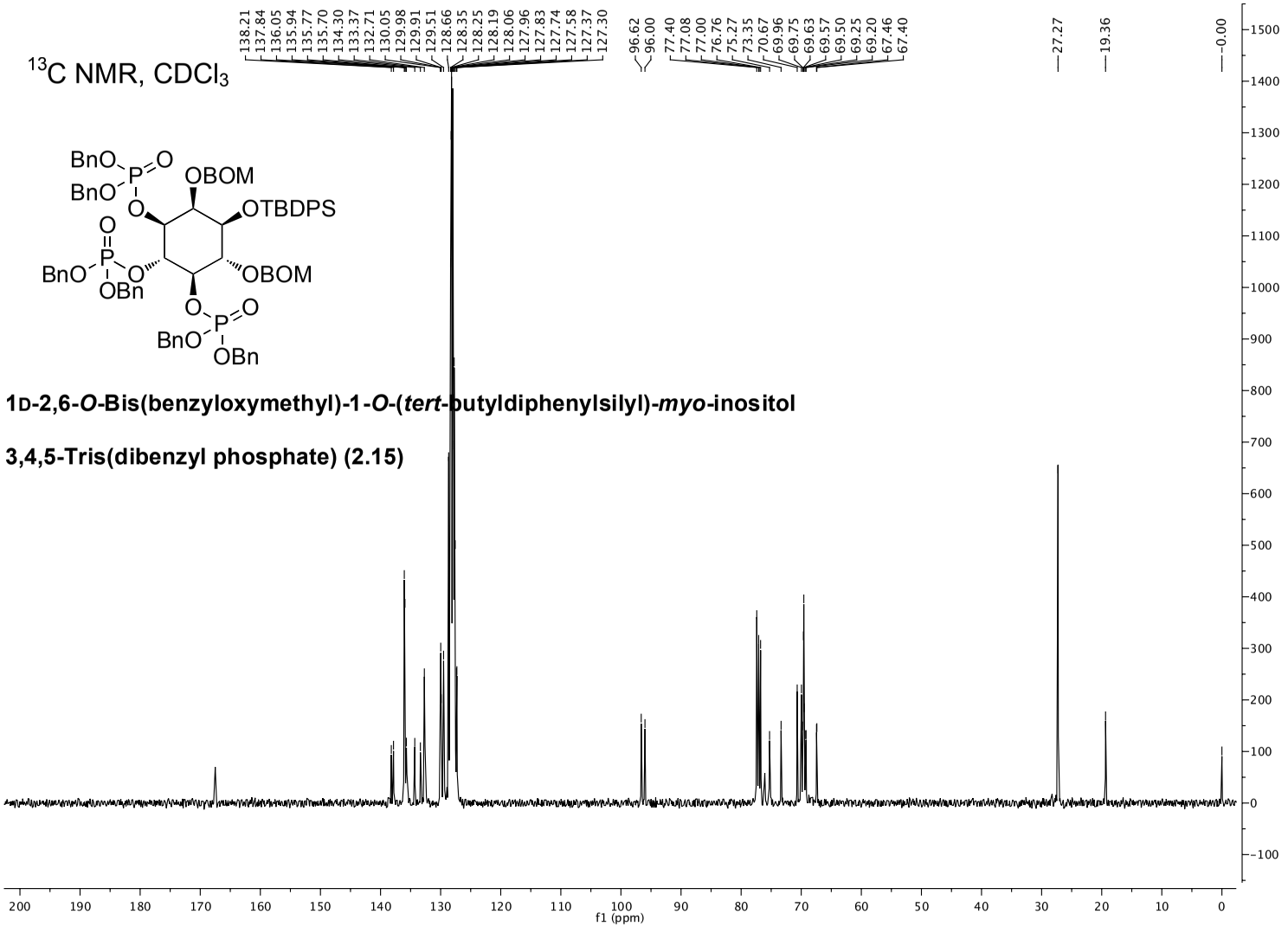

1H NMR, CDCl3
1D-2,6-O-Bis(benzyloxymethyl)-1-O-(tert-butyldiphenylsilyl)-myo-inositol
3,4,5-Tris(dibenzyl phosphate) (2.15)
f1 (ppm)

^{31}P NMR, $CDCl_3$



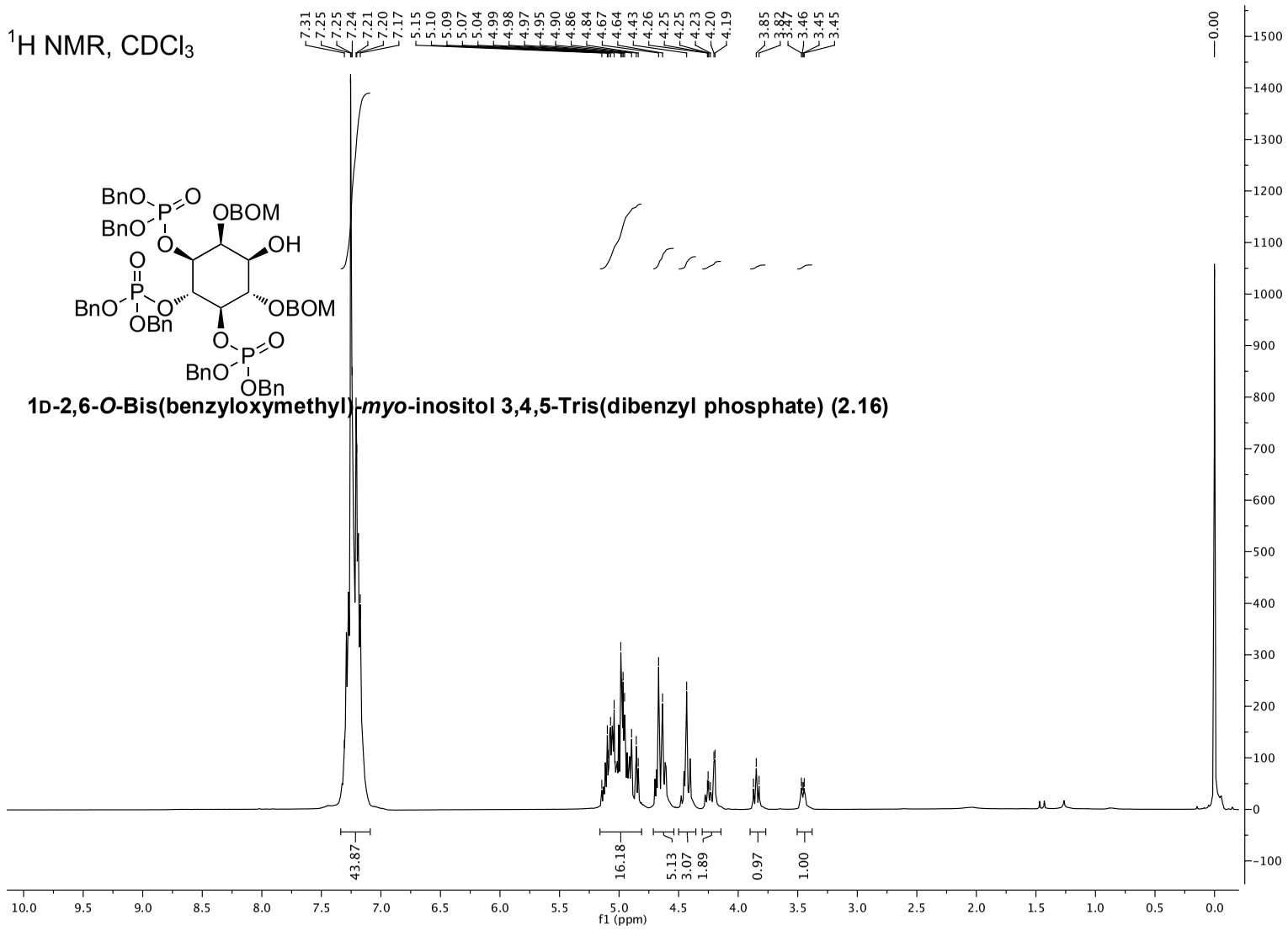
1D-2,6-*O*-Bis(benzyloxymethyl)-1-*O*-(*tert*-butyldiphenylsilyl)-*myo*-inositol

3,4,5-Tris(dibenzyl phosphate) (2.15)

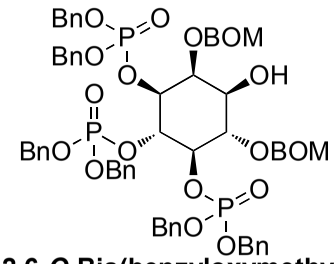


1D-2,6-*O*-Bis(benzyloxymethyl)-1-*O*-(*tert*-butyldiphenylsilyl)-*myo*-inositol

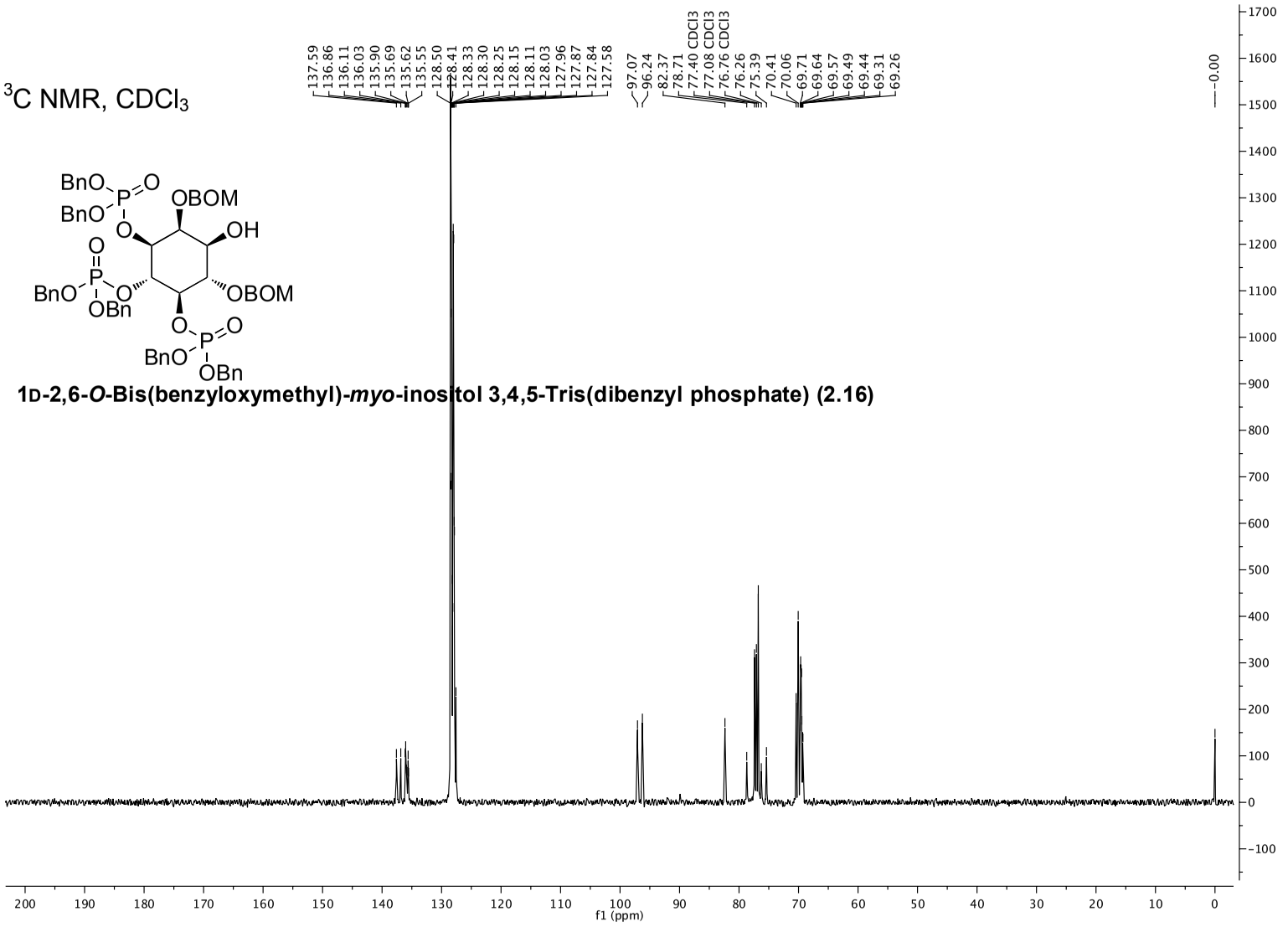
3,4,5-Tris(dibenzyl phosphate) (2.15)


1H NMR, CDCl3
7.31
7.25
7.25
7.24
7.21
7.20
7.17
5.15
5.10
5.09
5.07
5.04
4.99
4.98
4.97
4.95
4.90
4.86
4.84
4.67
4.64
4.43
4.26
4.25
4.25
4.23
4.20
4.19
3.85
3.82
3.47
3.46
3.45
3.45
0.00
BnO
BnO
OBOM
OH
OBOM
BnO
OBn
BnO
OBn
1D-2,6-O-Bis(benzyloxymethyl)-myo-inositol 3,4,5-Tris(dibenzyl phosphate) (2.16)
43.87
16.18
5.13
3.07
1.89
0.97
1.00
f1 (ppm)

^{31}P NMR, $CDCl_3$

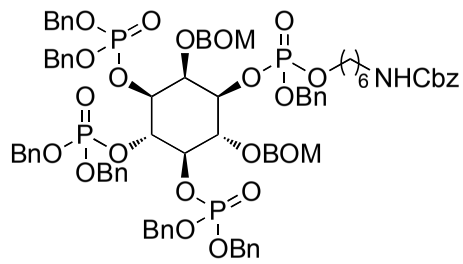


1D-2,6-*O*-Bis(benzyloxymethyl)-*myo*-inositol 3,4,5-Tris(dibenzyl phosphate) (2.16)



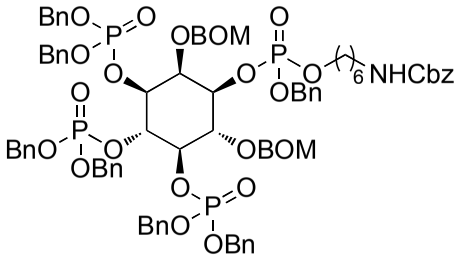
1D-2,6-*O*-Bis(benzyloxymethyl)-*myo*-inositol 3,4,5-Tris(dibenzyl phosphate) (2.16)

^{1}H NMR, $CDCl_3$

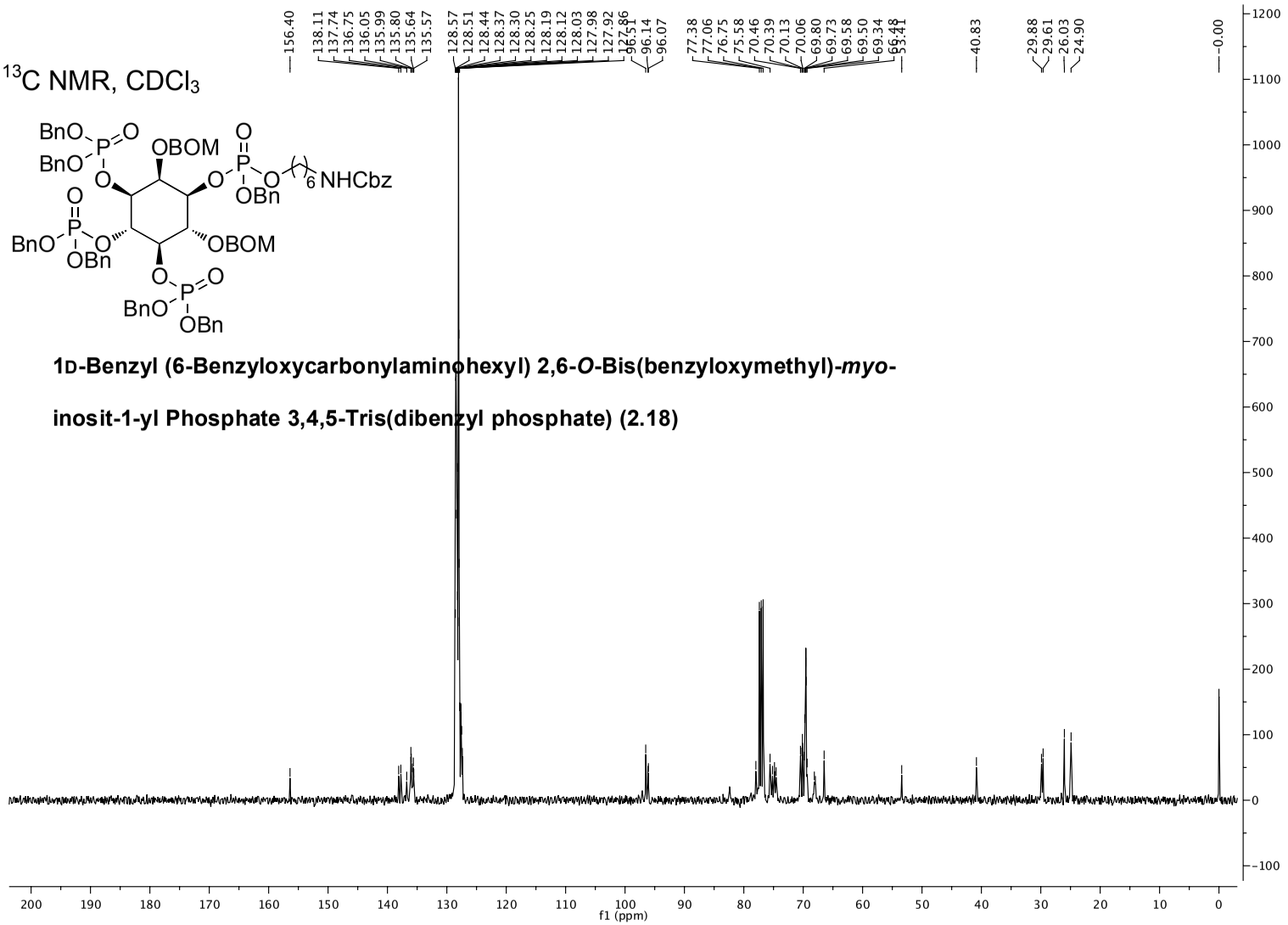


1D-Benzyl (6-Benzyloxycarbonylaminohexyl) 2,6-*O*-Bis(benzyloxymethyl)-*myo*-inosit-1-yl Phosphate 3,4,5-Tris(dibenzyl phosphate) (2.18)

^{31}P NMR, $CDCl_3$

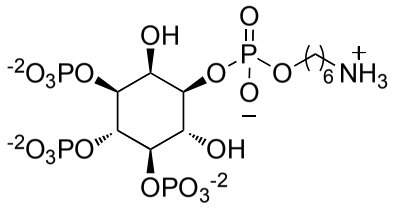


1D-Benzyl (6-Benzyloxycarbonylaminohexyl) 2,6-*O*-Bis(benzyloxymethyl)-*myo*-inosit-1-yl Phosphate 3,4,5-Tris(dibenzyl phosphate) (2.18)



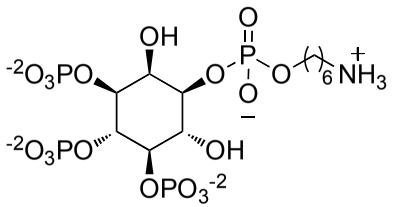
1D-Benzyl (6-Benzyloxycarbonylaminohexyl) 2,6-*O*-Bis(benzyloxymethyl)-*myo*-inosit-1-yl Phosphate 3,4,5-Tris(dibenzyl phosphate) (2.18)

^{1}H NMR, D_2O



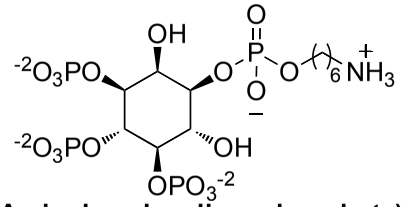
1D-1-(6-Aminohexyl sodium phosphate)-*myo*-inositol 3,4,5-Tris(disodium phosphate) (2.1)

^{31}P NMR, D_2O



1D-1-(6-Aminohexyl sodium phosphate)-*myo*-inositol 3,4,5-Tris(disodium phosphate) (2.1)

^{13}C NMR, D_2O



1D-1-(6-Aminohexyl sodium phosphate)-*myo*-inositol 3,4,5-Tris(disodium phosphate) (2.1)

Chapter 3: Exploiting Copper-Free Click Chemistry for Membrane Derivatization

3.1 Background and Significance

Functionalizing the surface of intact membrane bilayers has been a topic of recent interest because of the wide range of applications that can be achieved by exploiting membranes, including their use as pharmaceutical carriers with gene delivery and cancer therapy as the main attractors to this field.[225-227] These systems typically involve the use of varying targeting groups for *in vivo* delivery, and liposomes are effective for these applications because they are biologically inert and are intrinsic containers for a variety of cargo.[69-71,227] The choice of targeting groups to use is an important one because of the complex environments in which these membranes exist. Proper execution of controlled membrane derivatization should ideally combine several features. For example, the reactive group that allows functionalization must be presented on the surface of the membrane, so it must be stable and compatible with the exterior aqueous environment, and the conjugations should occur under mild reaction conditions and result in high yields and chemoselectivity.

As mentioned in Chapter 1, in recent years, copper catalyzed azide–alkyne cycloaddition (CuAAC), also known as click chemistry, has become an invaluable tool for a litany of applications.[86-89] Although there have been numerous reports of click chemistry in biological systems, the first example of click chemistry in liposomes was reported in 2006 by Schuber and co-workers.[228] They reported derivatizing the surface of alkynyl-containing liposomes with azido-mannose moieties by the use of copper-

catalyzed click chemistry. In this report, they first performed a model reaction using simplified click partners, a tetraethyleneglycol (TEG) azide and 5-hexynoic acid. They hoped that the reaction conditions used in this model system would be capable of being extended to the liposome surface derivatization reaction, but this was not the case. When the same model reaction conditions were used for the liposome click reaction, they saw no appreciable yield of conjugated liposomes, but instead, they observed liposome decomposition. In the end, they remedied this by the addition of a copper(I) stabilizing ligand, bathophenanthrolinedisulfonate, which led to much improved conjugation yields. In a final study, they evaluated the turbidity increase (agglutination) of the liposome suspensions upon the addition of concanavalin A resulting from clustering and multivalent binding of the mannosylated liposomes to con A, providing evidence that the mannose moieties are exposed and available for binding.

In the same year, Kros and co-workers also reported the use of copper-catalyzed click chemistry on the surface of liposomes and the reaction was monitored by a FRET assay.[229] In this study, a fluorescent azido-tagged peptide was synthesized by solid phase peptide synthesis that was subsequently conjugated to the surface of liposomes through the use of copper(I) bromide. The azido-peptide contained a fluorescent NBD, and the liposomes contained a fluorescent, commercially available rhodamine-PE. These two fluorophores were used to monitor the reaction by FRET, whereby upon click conjugation to the liposome surface, the FRET signal is activated because of the near proximity of the fluorophores. This reaction was even visible to the naked eye and could be monitored by a colorimetric assay after dialyzing away any of the unreacted dye.

While this report only uses the FRET assay and azido-NBD peptide, the assay could be extended to append other azido-peptides to liposome surfaces for targeting purposes.[230]

In a later report, Sun and co-workers have used the Staudinger ligation to attach azido-lactose moieties to membrane surfaces containing a phosphine conjugated PE.[83] They reported that the integrity of the liposomes was unaffected after being exposed to their reaction conditions as monitored by dynamic light scattering (DLS), and the leakiness was evaluated by encapsulation of a self-quenching concentration of 5(6)-carboxyfluorescein (CBF) and fluorescence monitoring. An agglutination assay was performed by the addition of *Arachis hypogea*, which showed an accumulation of large particles, as determined by DLS, providing evidence that the lactose residues were conjugated to the liposome surfaces and were available to bind the protein multivalently. Finally, the stability of the liposomes was assessed through particle size observation over a period of fifteen days, and the sugar-conjugated liposomes proved to be stable for longer periods than the unreacted liposomes, supporting that sugar moieties such as GM1 affect the ability for liposomes to aggregate and therefore prolong their lifetimes.[231]

Following these initial reports, Boxer and co-workers have used copper-catalyzed click chemistry to study DNA-mediated membrane docking.[232] Building off of a previous report, they successfully observed vesicle collision and docking onto a fluid-supported bilayer as mediated by complimentary DNA strands bearing click partners to prevent reversibility.[233] The DNA strands on the vesicles are modified with an alkyne while the fluid-supported bilayer contains an azido-PE. In the reaction, the complimentary strands

presented on the vesicle and fluid-supported bilayer easily interact in solution and zipper together. This tethers the vesicle to the fluid-supported bilayer surface, and upon the addition of copper(I) catalyst, the click reaction takes place between the fluid-supported bilayer and the vesicle, covalently linking them together. When the salt concentration is lowered, the DNA uncoils, but the vesicle remains docked on the surface because of this covalent triazole linkage.

CuAAC has also been used by Cai and co-workers for the attachment of RGD-peptides and AMP-peptides to polymerized liposomes that were then used for *in vivo* delivery.[234,235] In their initial findings, they used polymerized liposomes (made by UV irradiation of lipids containing diacetylene tails) displaying alkyne moieties from an alkynyl-TEG-diacetylene lipid and then clicked on a fluorogenic coumarin to optimize the click conditions.[234] Next, they clicked on a GRGD peptide, which targets integrin receptors on cell membranes, and carboxyfluorescein to visualize the liposomes that are targeted to the cells. An important note is that those liposomes were used for *in vivo* delivery, but the click reaction was not performed *in vivo* but prior to the delivery. In an additional report, Cai et al. have formulated polymerized liposomes composed of 10,12-pentacosadiynoic acid that they then coupled to propargylamine, resulting in polymerized liposomes displaying terminal alkynes on their surfaces.[235] These liposomes underwent a click reaction to append an antimicrobial peptide, IG-25, to the surface and were then tested for effectiveness against *Pseudomonas aeruginosa*, the most common culprit of contact lens related eye infection.

Zumbuehl and co-workers have recently reported the use of copper-catalyzed click chemistry to fuse vesicles.[236] Ether tailed lipids are synthesized containing an azide and a terminal alkyne that are then incorporated into liposomes. They discovered that upon the addition of these click partner-containing liposomes, when formulated with PC, no vesicle aggregates formed, but when a positively charged lipid was incorporated into the alkyne-containing liposomes, they formed aggregates and spontaneously fused.

While copper-catalyzed click chemistry has been used in a handful of reports functionalizing the surface of liposomes, this research has also uncovered some problems associated with CuAAC in membrane systems. For example, initial attempts at functionalization using standard copper-catalyzed click chemistry led to liposome decomposition and very low conjugation yields.[228] Even the use of polymerized liposomes, which are formed via cross-linking of the lipid tails and are inherently more stable than their non-polymerized counterparts, led to membrane decomposition.[234] The use of polymerized liposomes is also at a disadvantage to normal liposomes as the polymerization and cross-linking of the lipid tails restricts the fluidity and fusion that are beneficial for applications. Because of the expansive applications of click chemistry, it has become imperative to circumvent these problems that impede click chemistry from being applicable *in vivo*. There have been efforts for ligand-based methods of chelating the requisite copper catalyst to circumvent the aforementioned problems, but these approaches are also hampered by the need to deliver the copper and ligands to the reactive site, and even still, cytotoxicity exists.[107] Because of the copper catalyst cytotoxicity and our desire to eventually move into in vivo labeling and delivery, we

chose to exploit copper-free click chemistry for use as a targeting moiety in a liposome-based delivery system.

Among the reported cyclooctynes, the aza-dibenzocyclooctynes (ADIBOs) boast fast kinetics, synthetic ease, and have proven to be quite robust.[88,116,237-239] After some unsuccessful attempts with Bertozzi's initial cyclooctyne moiety **1.1**, we found the recently published report by Popik and co-workers, where they reported surface functionalization onto modified glass slides *via* copper-free click chemistry.[238] In this report, they accomplished clicking onto a glass surface modified with either an azide or aza-dibenzocyclooctyne (ADIBO), which was then detected *via* a fluorescent avidin binding to the appended biotin moiety. Since we desire to use click-driven membrane reactions, this seemed the perfect system to extend to our membrane systems.

With the goal of copper-free click driven vesicle fusion in mind, we set out to prove that we could exploit copper-free click chemistry to derivatize the surfaces of intact liposomes. We chose an immobilization-based strategy for validating surface derivatization as a high-throughput method that we have previously had success with.[129] In our previous assay, we were able to anchor whole, intact liposomes onto a streptavidin surface through the use of a synthetic biotinylated lipid incorporated into the liposomes. The use of a fluorescent lipid in those liposomes resulted in a fluorescent signal that increased with increasing amounts of immobilized liposomes. In this study, in order to prove that the liposomes remained intact after surface deposition we performed the immobilization assay using dye-loaded liposomes. In the dye-encapsulated liposomes, the fluorophore inside the liposome is self-quenched, but upon detergent

addition, the fluorophore is released resulting in a dramatic fluorescence increase. This provides evidence that the liposomes remain intact when deposited and immobilized on the streptavidin-coated microplate surface, since the use of detergent is required to rupture the liposomes.

3.2 Results and Discussion

Since we knew that intact liposomes could be immobilized on streptavidin-coated microplate surfaces, we approached a copper-free click-driven immobilization in a similar fashion. To achieve this, we designed an experiment where we could make liposomes that contained an azido-lipid and a fluorophore, in addition to the normal phosphatidylcholine (PC) as the structural backbone of the membrane.[240] Figure 3.1 outlines the copper-free click-driven immobilization assay performed, in which a cycloooctyne that is tethered to a biotin is placed in a streptavidin-coated 96-well plate and then the fluorescent, azido-tagged liposomes are added and incubated. The liposomes that have achieved a successful click reaction will display a biotin on their surface, and because of the well-known high affinity interaction of biotin and avidin, the entire liposome will be immobilized, resulting in fluorescence observed on the microplate surface. After several washings to remove unbound liposomes, the fluorescence is then measured to quantify the reaction.

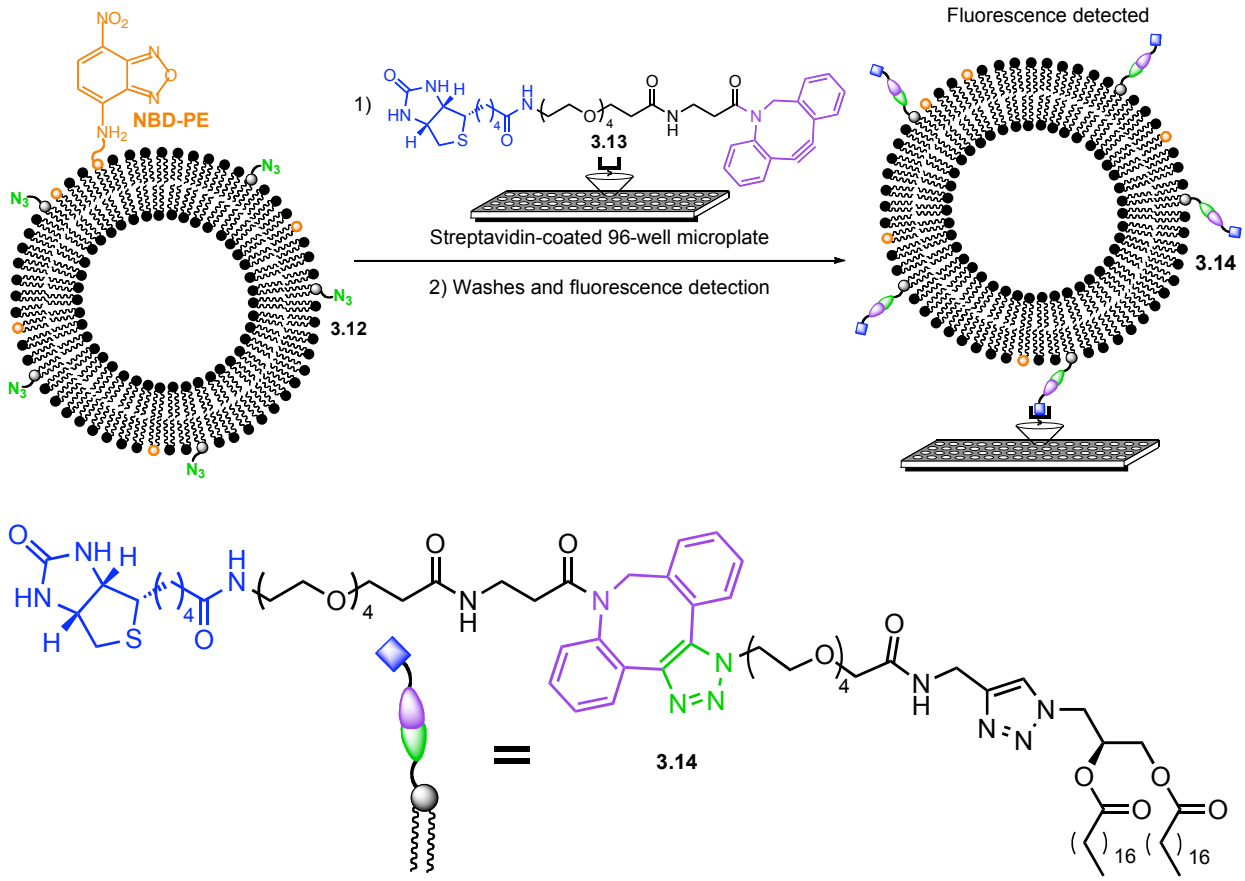


Figure 3.1. Cartoon depiction of the assay performed. Fluorescent azido-liposomes (containing fluorescent NBD-PE, azido-lipid 3.12, and PC) were incubated with ADIBO-biotin in a streptavidin-coated 96-well microplate for 4 hours, wells were washed and fluorescence was measured.

To make the azido-tagged lipid **3.12**, we began with a modular lipid **3.18** that has afforded us previous success.[129] This lipid is beneficial because it can be used to easily derive a number of compounds through the use of click chemistry with any alkyne. The resulting triazole in the product provides the needed polarity to keep the lipid headgroup properly oriented toward the aqueous exterior and is easily purified. The use of a natural phospholipid, such as PE, could be used as a synthetic precursor but yields much more difficult purification.

The synthesis of azido lipid scaffold **3.18** begins by tosylating *S*-glyceroacetonide followed by azide displacement to give **3.16**. The acetonide is then removed under acidic conditions and coupled to stearic acid with the use of coupling reagents to give the azido-lipid scaffold **3.18**. Our group has used this lipid scaffold in the aforementioned liposome immobilization assay for synthesizing the biotinylated lipid as well as the fluorescent lipid that is incorporated in those liposomes.[129]

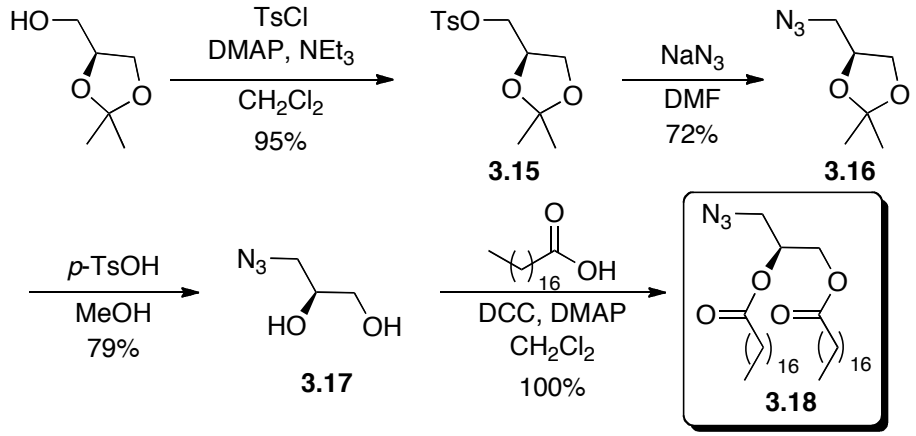


Figure 3.2. Synthesis of the azido-lipid 3.18 used as a common scaffold for various lipid analogs.

The azido-tagged lipid **3.12** was initially synthesized by Matt Smith in our group, as outlined in Figure 3.3, beginning with the reaction of tetraethylene glycol with ethyldiazoacetate in the presence of copper (II) triflate to afford the previously reported tetraethylene glycol (TEG) ethyl ester **3.19**.[129] The ester was then deprotected using sodium hydroxide and coupled to propargylamine with the use of coupling reagents to provide the TEG-alkyne **3.20**. A click reaction was performed using the alkyne **3.20** and the azide–lipid **3.18**[129] to give the lipid alcohol **3.21**. The alcohol of **3.21** was then converted to a mesylate and finally displaced by azide to give the azido-tagged lipid **3.12**, which was then used in liposome studies.

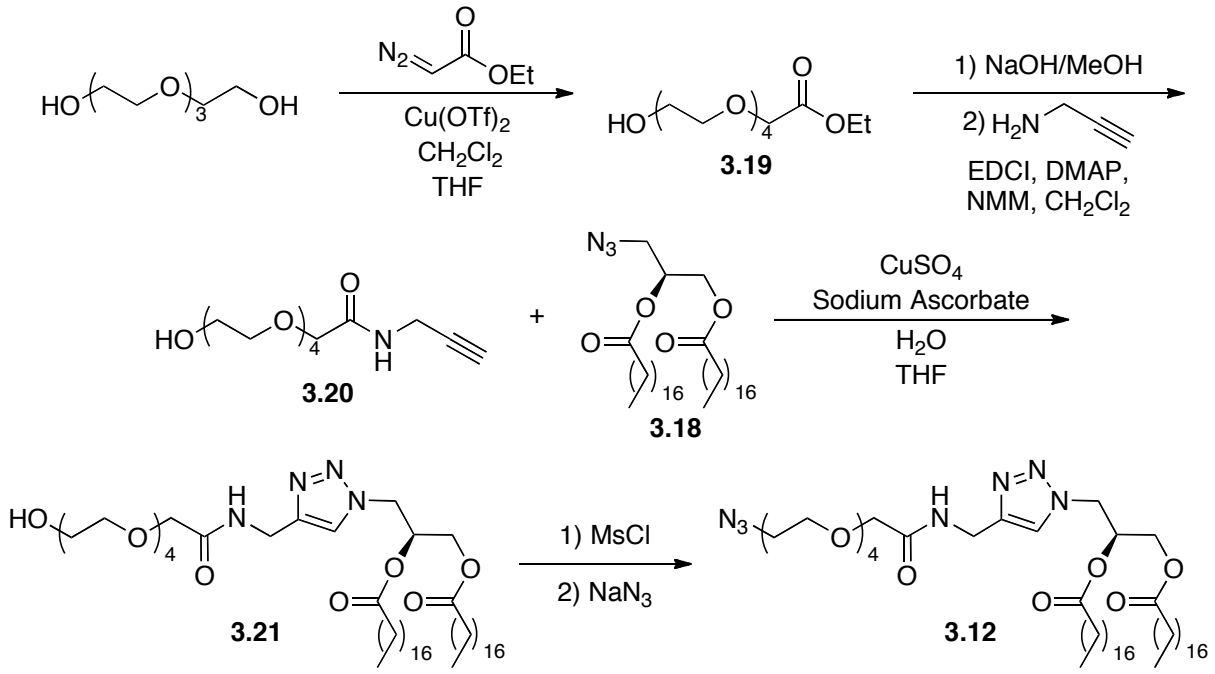


Figure 3.3. Synthesis of azido-lipid 3.12 for incorporation into liposomes.

In addition to this azido-lipid **3.12**, we needed to include a fluorescent lipid. In our previous liposome assay, we used a synthetic 7-nitrobenzo-2-oxa-1,3-diazole (NBD) lipid to make the liposomes fluorescent. In this assay, we chose to use the same fluorophore but in a commercially available format, a phosphatidylethanolamine derivative, NBD-PE.

The liposomes were prepared by measuring out an amount of each dried lipid (azido-lipid **3.12**, NBD-PE, and PC) and dissolving them in chloroform to provide individual stock solutions. These chloroform solutions were then used to measure out a known volume of each lipid into a glass vial to give the proper ratios (1% azido-lipid **3.12**, 1% NBD-PE, and 98% PC) of each lipid in the final liposome concentration. The chloroform was evaporated under a stream of nitrogen, and the dried lipid film was placed under vacuum for further drying. This lipid film was then hydrated by the addition

of 500 µL of buffer and rotating on a rotary evaporator for 40 minutes at 40 °C. Following this hydration, the liposomes were subjected to 10 freeze-thaw cycles in a dry ice/acetone bath and 40 °C water bath. The resulting liposome suspension was extruded through a 200 nm polycarbonate membrane to provide uniform sized, unilamilar liposomes as evidenced by DLS. Initally, we attempted to synthesize multiple cyclooctyne compounds, but after limited success, we settled on the ADIBO-biotin **3.13** compound that was generously donated by Popik and co-workers.[238] The assay begins with diluting a stock solution of the ADIBO-biotin **3.13** in buffer to twelve concentrations (0, 0.05, 0.15, 0.30, 0.45, 0.60, 0.75, 1.0, 1.25, 1.50, 1.75, and 2.0 µM). After washing the streptavidin-coated microplate with buffer, the twelve solutions of ADIBO-biotin **3.13** were placed in the wells, immediately followed by 250 µM liposomes, which provides final ADIBO-biotin concentrations of 0, 0.025, 0.075, 0.15, 0.225, 0.3, 0.375, 0.5, 0.625, 0.75, 0.875, and 1.0 µM and 125 µM total liposomes, containing 1.25 µM azido-lipid **3.12** and 1.25 µM NBD-PE. The concentration of liposomes was held constant across the varied concentration of the ADIBO-biotin so that any fluorescence that was detected was from the clicked product, not residual liposomes.

The fluorescence results of the immobilization and several controls are shown in Figure 3.4. There is a dose-dependent response (blue diamond) showing the fluorescence results obtained from incubating the fluorescent, azido-tagged liposomes with the ADIBO-biotin **3.13**. The results show that the increase of cyclooctyne correlated to an increase in fluorescence, resulting from a greater amount of immobilized liposomes, and therefore more of the click product. To conclude that the increased

fluorescence is directly a result of the click reaction and immobilization of the liposomes, we performed several control reactions. Firstly, we incubated the fluorescent, azido-tagged liposomes with an acyclic alkyne–biotin **3.23**, which should not yield reaction in the absence of copper, as was observed (red square). Secondly, we incubated fluorescent liposomes that did not contain the azido-lipid **3.12**, which also abrogated the fluorescence signal (green triangle). These two controls show the lack of appreciable fluorescence signal, allowing us to conclude that the click reaction is taking place on the surface of the azido-tagged liposomes only in the presence of the strained cyclooctyne moiety.

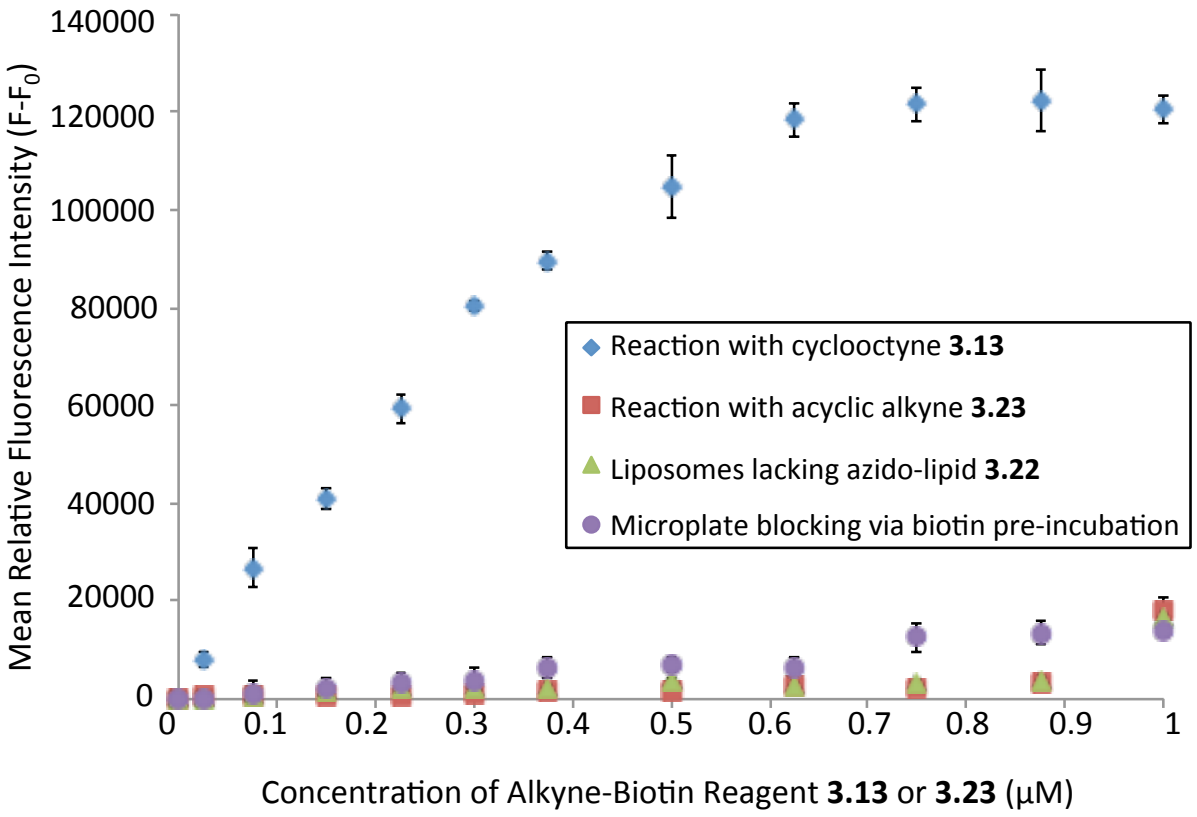
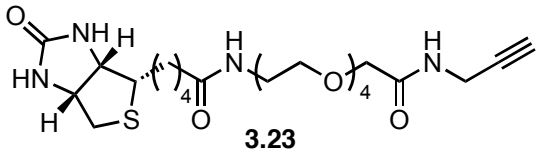


Figure 3.4. Results from liposome derivatization and immobilization studies and control experiments.

The last remaining control reaction was undertaken by repeating the same process with the ADIBO–biotin **3.13** and fluorescent azido-tagged liposomes, only this time the microplate was first incubated with biotin alone. This step blocked the surface of the microplate with natural biotin, which has a documented higher affinity for avidin than amide-linked biotin and therefore would not be displaced upon addition of the biotinylated liposomes, resulting in loss of fluorescence signal (purple circle).



3.23

Figure 3.5. Acyclic alkyne-biotin used in a control reaction.

Previous to this successful liposome surface derivatization, we tried various avenues that did not yield success. We initially tried to synthesize a cyclooctyne-lipid to be incorporated into liposomes that could then be labeled via various azide-containing reagents. This strategy was desired since the previously discussed azido-sugars and their exclusive incorporation into cancer cells already prove the bioorthogonality that we wished to exploit as our targeting moiety.[74] Our initial attempt was using a different cyclooctyne, based off of the original cyclooctyne reported by Bertozzi and co-workers,[108] in which we synthesized compound **1.1**. This synthetic octyne was then appended to the end of a lipid molecule as outlined in Figure 3.7. Using this octyne-lipid **3.32**, we attempted FRET-based assays. The assay works as depicted in Figure 3.8, whereby the liposome is loaded with one of the FRET pairs, a donor or acceptor lipid, cyclooctyne-lipid **3.32**, and PC. The remaining FRET partner is tethered to an azide and the click reaction is attempted. These assays were carried out on the fluorimeter whereby, based on the click of the azide and cyclooctyne, the FRET signal should increase.

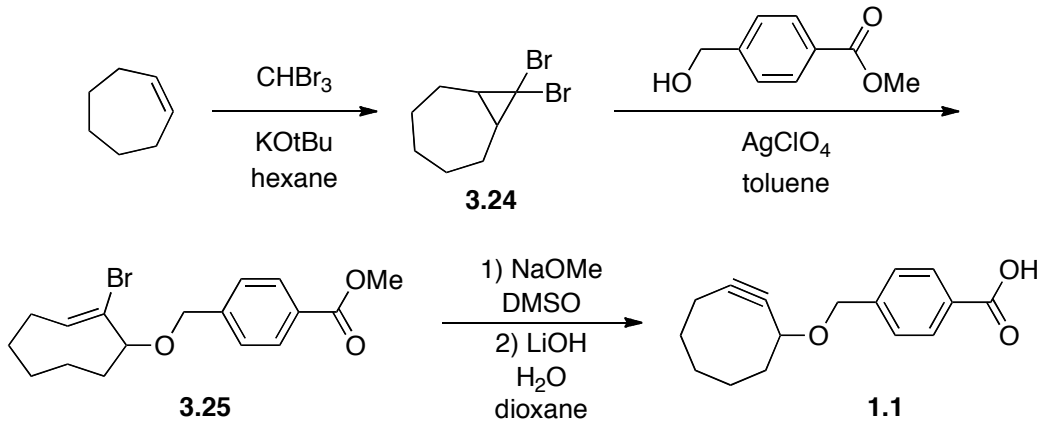


Figure 3.6. Synthesis of Bertozzi's octyne 1.1.[108]

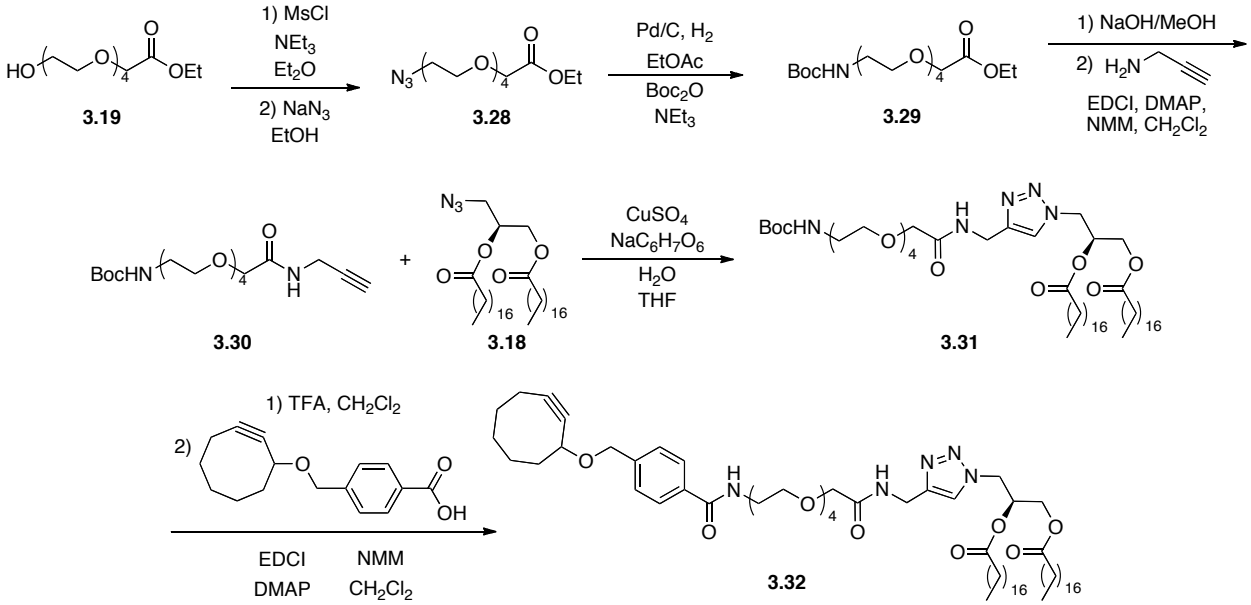


Figure 3.7. Synthesis of the original octyne-lipid 3.32.

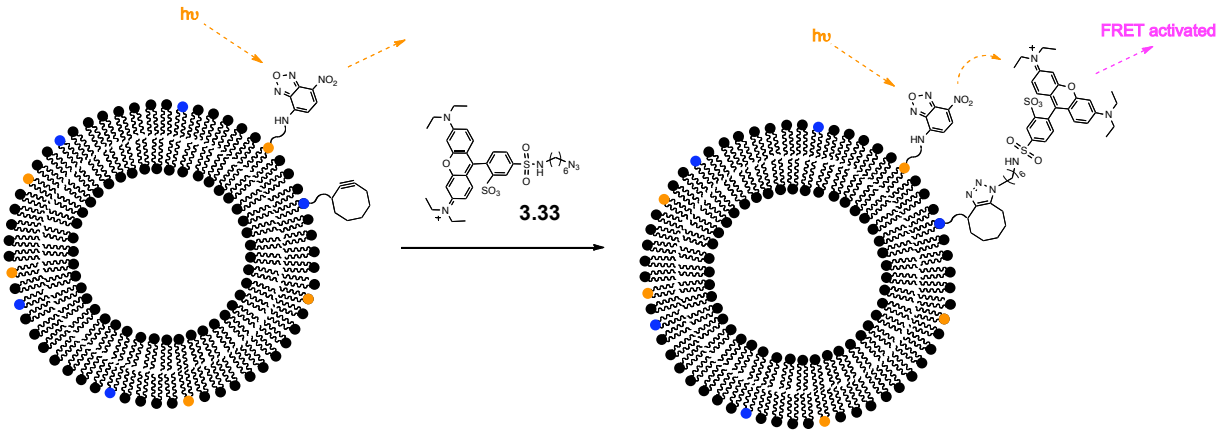
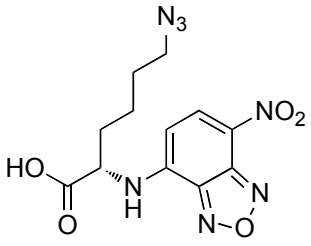


Figure 3.8. Cartoon depiction of the FRET-based approach using octynyl liposomes and an azido-fluorophore.

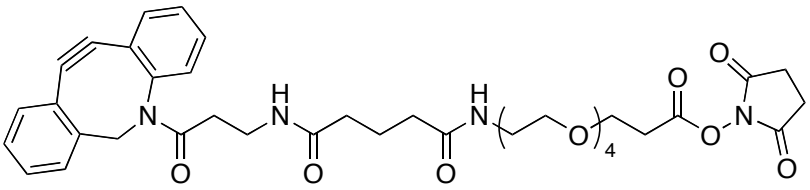
Our initial attempts with this FRET-based approach used rhodamine–azide **3.33**, which contains a six carbon linker between the dye and azide. This assay never yielded dependable results. The fluorescence signal often looked the same regardless of whether the cyclooctyne-lipid **3.32** was included, which could have been caused by the six-carbon chain on the rhodamine–azide burying into the membrane. This rhodamine–azide also suffered from poor water solubility. Attempts to overcome this included differing buffers with varying pH ranges, heating and sonication. The addition of dimethylsulfoxide (DMSO) solubilized the rhodamine–azide but still failed to produce desirable results. Because of these fluorophore downfalls, we investigated other routes. Based on the report by Kros and co-workers where they employed an amino acid based fluorophore–azide for clicking onto liposome surfaces followed by FRET detection,[229] we synthesized a peptide version of an NBD-azide and attempted our assay. Since they used the FRET-donor (NBD) with the azide, the FRET-acceptor (rhodamine) must be included as a lipid in the liposome. This attempt also did not lead to success under our scrutiny. It was after these attempts that we discovered the cyclooctyne **1.1** that we had

been using is susceptible to decomposing, even after being stored at -20 ºC.[111] Upon this discovery, we investigated other cyclooctyne moieties and since aza-dibenzocyclooctynes had been reported at that time, to benefit from their reported synthetic ease, stability, and fast kinetics, we chose them. Having seen the previously mentioned paper by Popik and co-workers, we acquired some of the aza-dibenzocyclooctyne as a succinimidyl ester to get our assays started. Attempts at putting this onto phosphatidylethanolamine (PE) or a triazole-based lipid were not successful, and our FRET-based approach hinged on the cyclooctyne being part of the membrane. A potential problem in this ADIBO-based cyclooctyne being incorporated into membranes is the hydrophobicity of the cyclooctyne moiety. It is possible that this cyclooctyne is not presented properly on the membrane surface, facing the aqueous exterior, but instead may be buried in the hydrophobic membrane core, complicating the click derivatization. To eventually use this system for *in vivo* delivery by membrane labeling and fusion, it will be necessary to create a cyclooctyne lipid that can be incorportated in the liposomes for use as a targeting moiety.

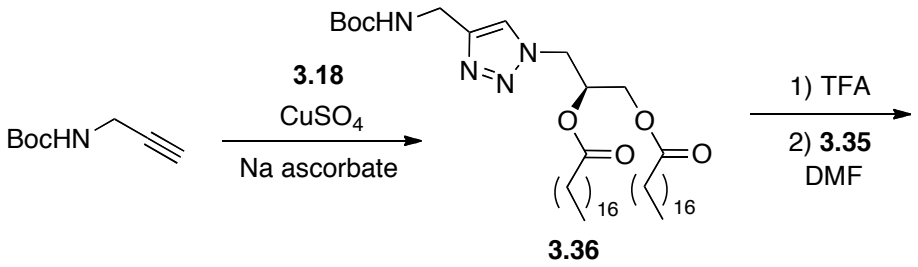


3.34

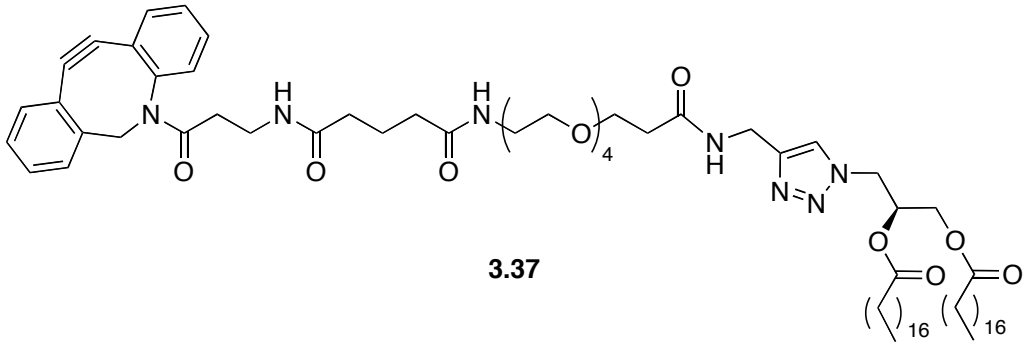
Figure 3.9. NBD-azide used for FRET assay.[229]



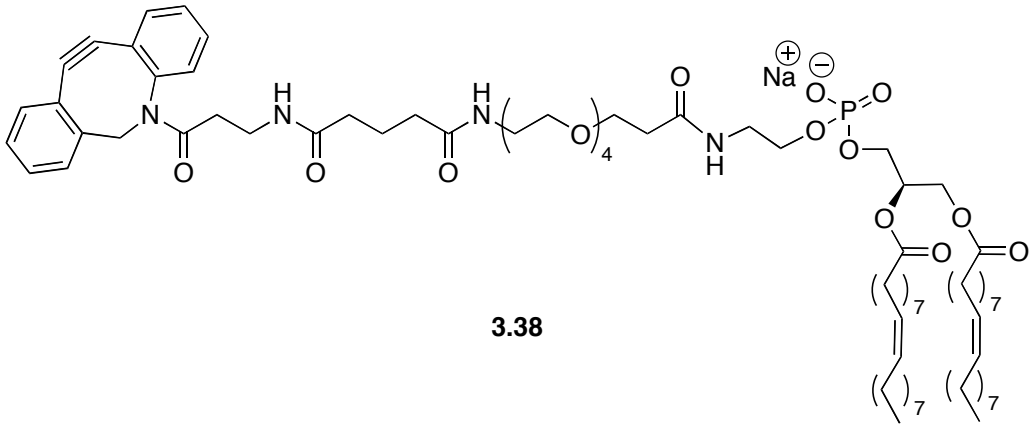
3.35



3.36



3.37



3.38

Figure 3.10. Original ADIBO succinimidyl ester 3.35 and steps for preparing ADIBO lipid via triazole and ADIBO-PE.

3.3 Modification of glass slides

In addition to the previously discussed microplate assay, we have attempted to miniaturize this assay to be performed on avidin-modified glass slides in true microarray format. We have previously reported the use of immobilized whole liposomes to study DAG binding of protein kinase C, and we would like to exploit this system of studying protein–binding in a native membrane environment to be achieved through microarray analysis.[129] While in the previously discussed assay we used NBD-PE as our fluorescent lipid, based on the wavelength detection limits of the slide scanner, it only recognizes fluorophores that emit at 533 or 650 nm. Thus, the fluorophore used in these studies is commercially available rhodamine-PE.

We initially attempted to simplify the system by printing intact liposomes. An attempt at this assay is shown in Figure 3.11. The image shown here contains different reactions in each column. The first and second columns were obtained by printing diluted stock solutions of the reaction of alkynyl-liposomes with azido-biotin and octynyl-liposomes with azido-biotin. In the third and fourth columns, the roles are reversed and azido-liposomes are incubated with alkynyl-biotin and octynyl-biotin, respectively. The fifth column is a control reaction where liposomes containing an already biotinylated lipid were printed. Columns six and seven contain control reactions with only liposomes (azido and octynyl) being printed, which, as seen, still yields a fluorescent signal. These last two columns provide evidence that the liposomes may not remain intact when printed on the surface, but instead are being ruptured. It seems that the mechanical impact of the robot pin may be the cause of these ruptured liposomes, which is not

surprising considering that liposomes are quite fragile. There is also a possibility that the washing procedure performed on this slide is insufficient. Recently, Sun and co-workers reported the printing of intact liposomes and use of control studies that seem to indicate that their liposomes are not ruptured upon contact from pin printing.[241] Their washing procedure is much more intensive than the one that has been used here in that they wash for a total of 6 hours, while we have only washed for 1–2 hours. Because of the directly printed fluorophore, it requires extensive washing to remove any unbound species, so this printing of the intact liposomes should be reinvestigated with more rigorous washing procedures.

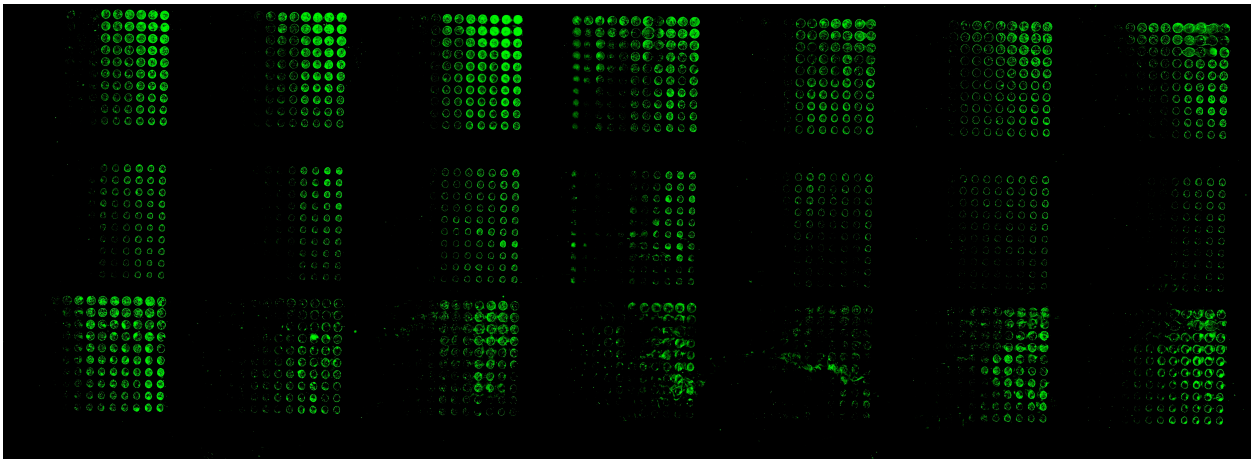


Figure 3.11. Fluorescent image of printed liposomes containing biotinylated tags.

Upon the initial observed failure of the printing of intact liposomes, we chose to instead print the click ligands, and then incubate with liposomes containing the appropriate click partner, as outlined in Figure 3.12. So far, we have seen fluorescence on the slide that appears to be a result of a clicked product as seen in Figure 3.13 and Figure 3.15. In Figure 3.13, the ADIBO-biotin **3.13** has been printed and the slide incubated with fluorescent, azido-lipid **3.12**-containing liposomes in increasing

concentrations from left to right for each set of four grids, 125 μM, 250 μM, 500 μM, and 1 mM liposomes containing 1.25, 2.5, 5, and 10 μM azido-lipid **3.12**. The plot of the fluorescence of the first (top, leftmost) grid is shown in Figure 3.14. This plot shows a general dose-dependent response, as expected. Plots of the other grids display a similar curve and have been excluded for clarity. Following this, a control similar to the previous assay was undertaken. Figure 3.15 shows the results of the assay performed where the ADIBO-biotin **3.13** was printed along with the same acycylic alkyne **3.23** from the previous assay. In this case, the background is very high, but the grids remain visible. The plot of the fluorescence of these grids yields a dose-dependent response for the acyclic alkyne **3.23** but the plot for the ADIBO-biotin **3.13** is not as desired, it is very flat. This may not necessarily mean the assay is futile, as fluorescence quenching may cause the problem here, which may mean the ADIBO-biotin reaction is performing as expected, but the concentration of liposomes and fluorophore in any region is too high. This can be remedied by incubating with a much lower concentration of liposomes and printing the alkyne reagents at even lower concentrations. Because of inconsistencies in microarray printing, attempts at this have been unsuccessful to date.

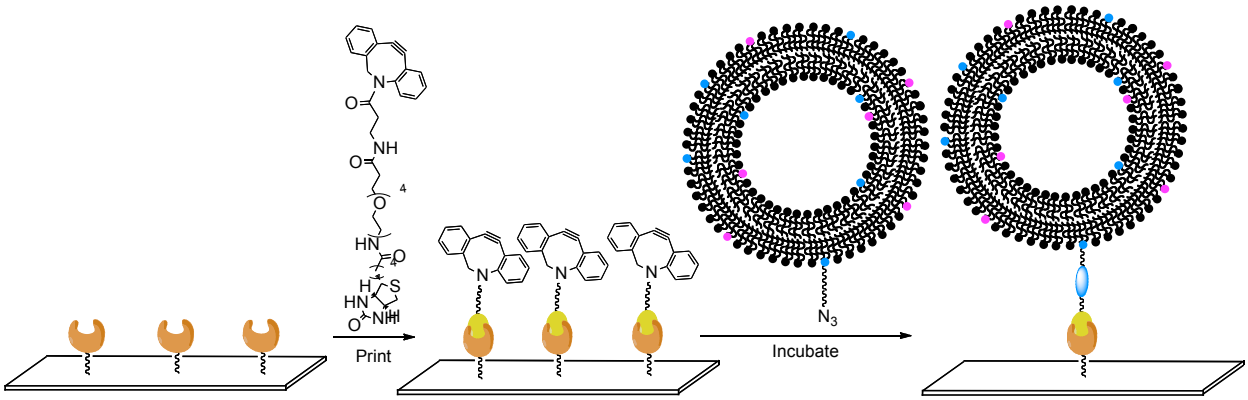


Figure 3.12. Cartoon depiction of the immobilization of liposomes by copper-free click chemistry using microarray.

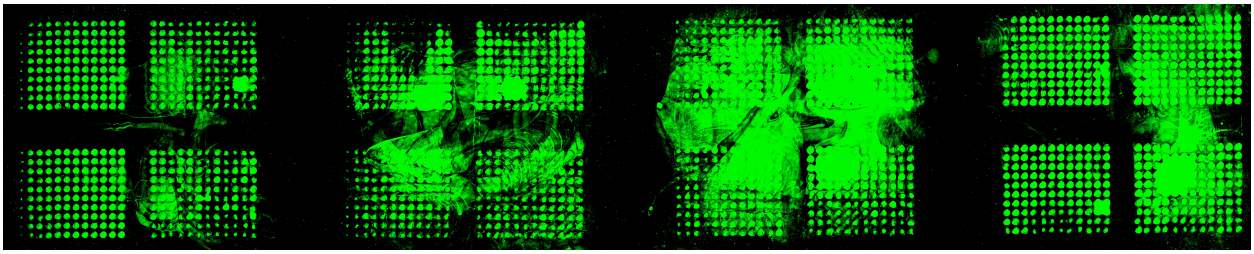


Figure 3.13. Fluorescent image of the liposome assay that has been incubated with increasing liposome concentrations from left to right for each set of four grids, 125 μM, 250 μM, 500 μM, and 1 mM.

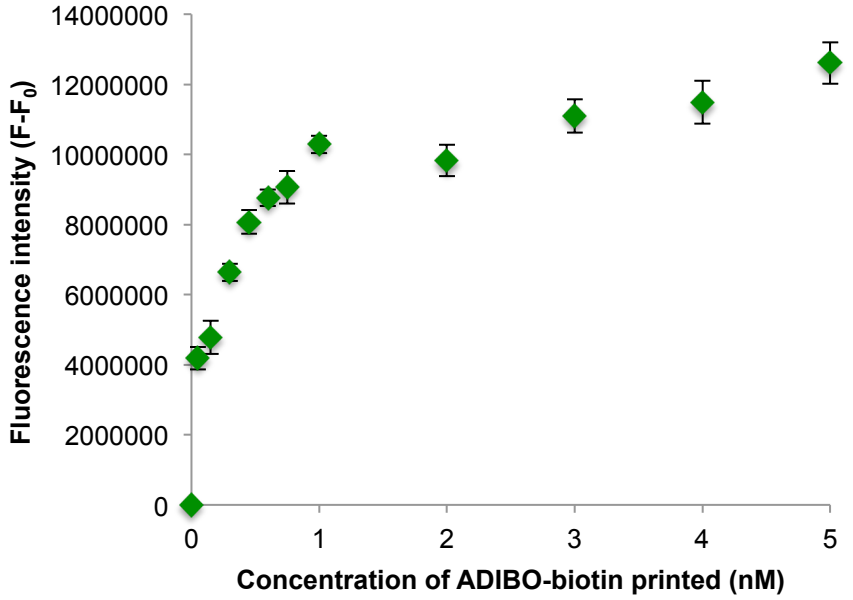


Figure 3.14. Plot of fluorescence intensity of the top leftmost grid from Figure 3.13.

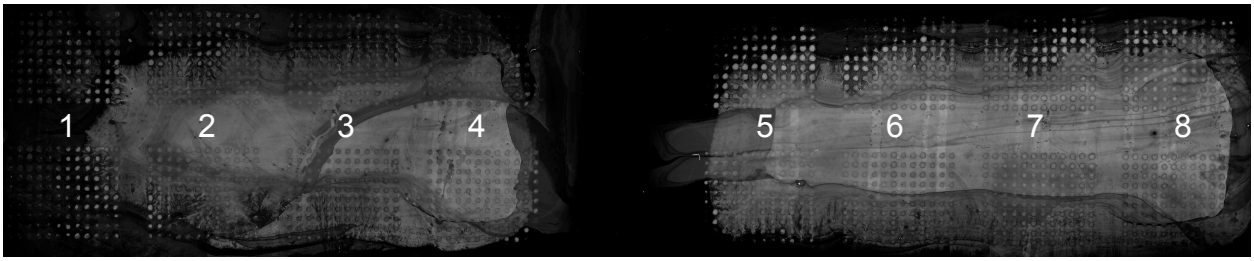


Figure 3.15. Fluorescent image of the liposome microarray assay with ADIBO-biotin 3.13 (columns 2, 4, 6 and 8) and alkyne biotin 3.23 (columns 1, 3, 5, and 7) printed from 0–5 nM and then incubated with azido-liposomes.

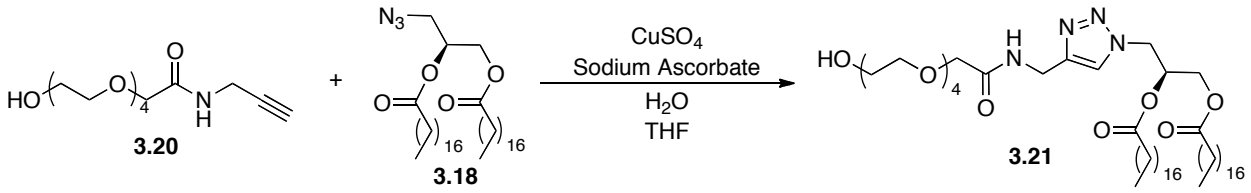
3.4 Experimental

3.4.1 General Considerations

Reagents were generally purchased from Acros, Aldrich or AK Scientific and used as received. Dry solvents were obtained from a Pure Solv solvent delivery system purchased from Innovative Technology, Inc. Column chromatography was performed using 230–400 mesh silica gel purchased from Sorbent Technologies and C18 (17%) reverse phase SPE columns (6 mL, 2g) purchased from Silicycle. NMR spectra were obtained using a Varian Mercury 300 spectrometer, a Bruker Avance 400 spectrometer, and a Varian 500 spectrometer. Mass spectra were obtained with JEOL DART-AccuTOF spectrometer and ABI Voyager DE Pro MALDI spectrometer with high resolution capabilities. Optical rotation values were obtained using a Perkin-Elmer 241 polarimeter. L-α-phosphatidylcholine (PC) and 1,2-dioleoyl-*sn*-glycero-3-phosphoethanolamine-*N*-(7-nitro-2-1,3-benzoxadiazol-4-yl) (ammonium salt) (NBD-PE) were obtained from Avanti Polar Lipids, Inc. (Alabaster, AL). Liposome extruder and polycarbonate membranes were obtained from Avestin (Ottawa, Canada). Microplate-based fluorescence measurements were performed using a BioTek Synergy 2 multi-detection microplate reader. Black reacti-bind streptavidin high binding capacity (HBC) coated 96-well microplates were purchased from Pierce Biotechnology (Rockford, IL). SuperAvidin slides were purchased from Arrayit Corporation (Sunnyvale, CA). Slide printing was performed using a BioRad VersArray ChipWriter Pro robotic pin printer (Hercules, CA). Fluorescence slide scans were performed using a GenePix 4000B Microarray Scanner.

3.4.2 Synthetic Procedures

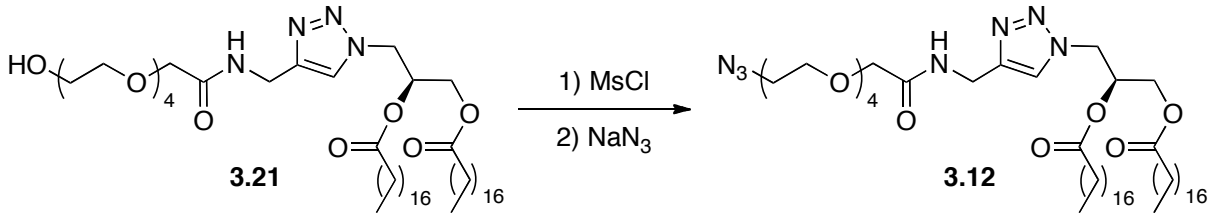
(*S*)-3-(4-(16-Hydroxy-3-oxo-5,8-11,14-tetraoxa-2-azahexadecyl)-1*H*-1,2,3-triazol-1-yl)propane-1,2-diyl distearate (3.21):



Alkyne-alcohol **3.20** (69 mg, 0.238 mmol) and (*S*)-3-azidopropane-1,2-diyl distearate (**3.18**, 155 mg, 0.238 mmol) were dissolved in tetrahydrofuran (1.5 mL). Copper sulfate pentahydrate (173 mg, 0.693 mmol) and sodium ascorbate (275 mg, 1.386 mmol) were then added, along with water (0.5 mL). The reaction was stirred at rt overnight, and the solvent was then removed under reduced pressure. Column chromatography with silica gel and a solvent system of 10% methanol-chloroform afforded **3.21** as a white solid (131 mg, 59%).

$[\alpha]_D^{296\ K}$ = +1.22 (*c* = 5.25, $CHCl_3$). ^{1}H NMR (300 MHz, $CDCl_3$) δ = 7.97 (t, *J* = 5.6 Hz, 1H), 7.65 (s, 1H), 5.39–5.36 (m, 1H), 4.64–4.54 (m, 4H), 4.32 (dd, *J* = 4.1, 12 Hz, 1H), 4.08–4.01 (m, 3H), 3.73–3.43 (m, 17H), 2.36–2.27 (m, 4H), 1.62–1.57 (m, 4H), 1.26 (*b* s, 56H), 0.88 (t, *J* = 6.3 Hz, 6H) ppm. ^{13}C NMR (75.5 MHz, $CDCl_3$) δ = 173.1, 172.6, 145.3, 123.6, 72.6, 70.9, 70.5, 70.4, 70.22, 70.18, 69.3, 62.0, 61.5, 50.0, 34.2, 34.0, 31.9, 29.72, 29.67, 29.5, 29.4, 29.3, 29.1, 29.0, 24.8, 24.7, 22.7, 14.1 ppm. MALDI–HRMS $[M + Na]^+$ calcd: 961.7175, found: 961.7190.

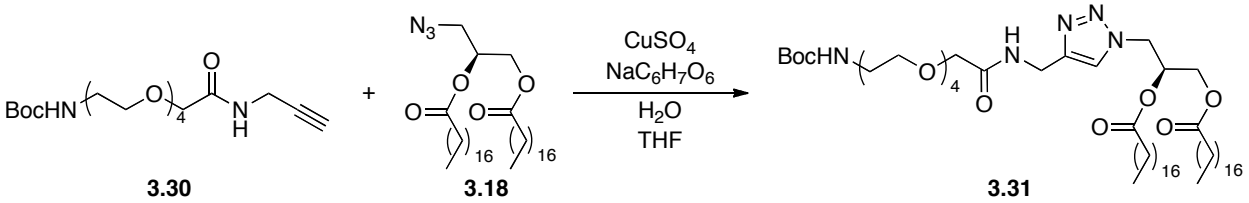
(S)-3-(4-(16-Azido-3-oxo-5,8-11,14-tetraoxa-2-azahexadecyl)-1H-1,2,3-triazol-1-yl)propane-1,2-diyl distearate (3.12):



Lipid alcohol **3.21** (129 mg, 0.137 mmol) was dissolved in tetrahydrofuran (3 mL) and cooled to 0 ºC under nitrogen. With stirring, triethylamine (57 µL, 0.411 mmol) and methanesulfonyl chloride (10.8 µL, 0.138 mmol) were added. Stirring was continued at 0 ºC for 1 h. The solvent was removed under reduced pressure and the residue was dissolved in *N*,*N*-dimethylformamide. Sodium azide (17.8 mg, 0.274 mmol) was added and the reaction was heated at 85 ºC overnight. The solvent was next removed under reduced pressure and column chromatography with silica gel and a solvent system of 5% methanol-chloroform afforded **3.12** as a tan solid (103 mg, 78%).

$[\alpha]_D^{296\ K} = -0.17$ (*c* = 4.12, $CHCl_3$). ^1H NMR (300 MHz, $CDCl_3$) δ = 7.72 (*b* s, 1H), 7.62 (s, 1H), 5.39–5.35 (m, 1H), 4.62–4.50 (m, 4H), 4.31 (dd, *J* = 4.2, 12 Hz, 1H), 4.08–4.00 (m, 3H), 3.77–3.61 (m, 14H), 3.39 (t, *J* = 4.8 Hz, 2H), 2.36–2.27 (m, 4H), 1.62–1.57 (m, 4H), 1.25 (*b* s, 56H), 0.88 (t, *J* = 6.3 Hz, 6H) ppm. ^{13}C NMR (75.5 MHz, $CDCl_3$) δ = 173.1, 172.5, 145.2, 123.4, 71.3, 71.1, 70.7, 70.6, 70.4, 70.2, 70.0, 69.3, 62.0, 50.6, 50.0, 42.8, 34.2, 34.0, 31.9, 29.72, 29.68, 29.6, 29.5, 29.4, 29.3, 29.1, 29.0, 24.8, 24.7, 22.7, 14.1 ppm. MALDI–HRMS $[M + Na]^+$ calcd: 986.7240, found: 986.7200.

(*S*)-3-(4-(11,11-dimethyl-3,9-dioxo-5,10-dioxa-2,8-diazadodecyl)-1*H*-1,2,3-triazol-1-yl)propane-1,2-diyl dipropionate (3.31):

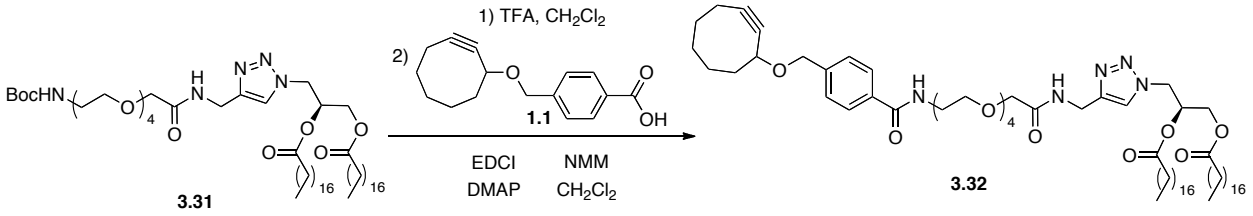


3.30 **3.18** **3.31**

Alkyne **3.30** (164 mg, 0.422 mmol) and (*S*)-3-azidopropane-1,2-diyl distearate **3.18** (329 mg, 0.507 mmol) were dissolved in THF (2.5 mL). Copper sulfate pentahydrate (127 mg, 0.507 mmol) and sodium ascorbate (201 mg, 1.02 mmol) were added along with water (0.5 mL). The reaction was stirred at rt overnight and the solvent was removed under reduced pressure. Column chromatography with silica gel and a solvent system of 50% acetone-chloroform afforded **3.31** as a white solid (272 mg, 62%).

$[\alpha]_D^{296\ K}$ = + 0.21 (C = 4.24, $CHCl_3$). ^{1}H NMR (300 MHz, $CDCl_3$ + CD_3OD) δ = 7.91 (bs, 1H), 7.70 (bs, 1H), 5.40–5.36 (m, 2H), 4.61–4.55 (m, 4H), 4.33 (dd, *J* = 4.1, 12.2 Hz, 1H), 4.09–4.01 (m, 3H), 3.66–3.52 (m, 14H), 3.31–3.29 (m, 2H), 2.37–2.28 (m, 4H), 1.64–1.55 (m, 4H), 1.44 (s, 9H), 1.26 (bs, 56H), 0.88 (t, *J* = 6.6 Hz, 6H) ppm. ^{13}C NMR (100.6 MHz, $CDCl_3$ + CD_3OD) δ = 173.1, 172.5, 170.2, 156.0, 145.4, 123.6, 79.1, 71.1, 70.5, 70.3, 69.4, 69.3, 62.0, 50.1, 40.3, 34.0, 31.93, 31.88, 29.7, 28.4, 24.8, 22.7, 14.1 ppm. MALDI–HRMS $[M + Na]^+$ calcd: 1060.7859, found: 1060.7831.

(2*S*)-3-(4-((2-(2-(4-((cyclooct-2-yn-1-yloxy)methyl)benzamido)ethoxy)acetamido) methyl)-1*H*-1,2,3-triazol-1-yl)propane-1,2-diyl dipropionate (3.32):



The Boc protected amine **3.31** (35 mg, 0.034 mmol) was dissolved in dichloromethane (1 mL) and trifluoroacetic acid (1 mL) was added. The reaction was stirred at rt for 2 h. The solvent was removed and the product placed under high vacuum for 2 h. The amine was then dissolved in dichloromethane (1 mL) and *N*-methylmorpholine (26 µL, 0.232 mmol) was added. Separately, the octyne acid **1.1** (6 mg, 0.023 mmol), 1-ethyl-3-(3-dimethylaminopropyl) carbodiimide (9 mg, 0.047 mmol), and 4-dimethylaminopyridine (4.3 mg, 0.035 mmol) were dissolved in CH_2Cl_2 (1 mL) and then added to the amine mixture. The reaction was stirred at rt overnight and the solvent removed under reduced pressure. Column chromatography with silica gel and a solvent system of 0-10% methanol-dichloromethane gave **3.32** as a white solid (31 mg, 77%).

^{1}H NMR (300 MHz, $CDCl_3$) δ = 7.80 (d, *J* = 6 Hz, 2H), 7.71 (bs, 1H), 7.59 (s, 1H), 7.39 (d, *J* = 6 Hz, 2H), 7.06 (bs, 1H), 5.36–5.30 (m, 2H), 4.73–4.69 (m, 1H), 4.55–4.53 (m, 4H), 4.46–4.41 (m, 1H), 4.31–4.22 (m, 2H), 4.07–3.98 (m, 3H), 3.66–3.63 (m, 14H), 2.31 (quint, *J* = 6 Hz, 4H), 2.21–2.07 (m, 2H), 2.05–1.93 (m, 2H), 1.85 (bs, 3H), 1.67–1.55 (m, 6H), 1.27–1.24 (m, 56H), 0.88–0.86 (m, 6H) ppm. MALDI–HRMS $[M + Na]^+$ calcd: 1200.8485, found: 1200.8510.

3.4.3 Assay Procedures

Fluorescent Azido-Labeled Liposome Preparation

Stock solutions were made of synthetic azido-lipid **3.12**, NBD-PE, and PC. Examples of each stock solution used are as follows: 1.5 mg azido-lipid **3.12**, 1.0 mg NBD-PE, and 50 mg PC were each weighed into separate vials and dissolved in 1 mL chloroform to form stock solutions of 1.56 mM azido-lipid **3.12**, 1.08 mM NBD-PE, and 65.8 mM PC. Using these stock solutions, 12.8 µL azido-lipid **3.12** stock (1%), 18.5 µL NBD-PE stock (1%), and 29.8 µL PC stock (98%) were combined in a glass vial. In addition, liposomes lacking azido-lipid **3.12** were prepared by combining 9.3 µL NBD-PE (1%) and 15.0 µL PC (99%). In both, the chloroform was removed under a stream of nitrogen and placed under vacuum for 1 h. The dried lipids were then hydrated by adding 500 µL of 0.5X PBS buffer, pH 7.4, and rotated on a rotary evaporator for 40 min at 40 ºC. The liposomes were then subjected to 10 freeze-thaw cycles and extruded (19 times) to uniform size and lamellarity using a 200 nm polycarbonate filter. The resulting solutions were then diluted to a total volume of 4 mL, which yielded a concentration of 500 µM total liposome suspension.

Membrane Derivatization and Immobilization via Copper-Free Click Chemistry

Stock solutions were made of ADIBO-TEG-biotin **3.13**,[238] and alkyne-TEG-biotin **3.23.**[129] Examples of each stock solution used are as follows: 0.8 mg ADIBO-TEG-biotin **3.13**, and 0.4 mg alkyne-TEG-biotin **3.23** were each weighed into separate vials and dissolved in 1 mL chloroform to form stock solutions of 0.71 mM **3.13**, and 0.78 mM

3.23. In addition, a 500 μM stock solution of D-biotin was made by dissolving 1.4 mg in 11.5 mL of 0.5X PBS buffer, pH 7.4. Using the alkyne stock solutions, 14.1 μL ADIBO-TEG-biotin **3.13** stock and 12.8 μL alkyne-TEG-biotin **3.23** stock were measured into separate glass vials, dried under a stream of nitrogen, and placed under vacuum for 1 h. To the alkyne (**3.13** and **3.23**) containing vials, 2 mL of 0.5X PBS, pH 7.4 buffer was added to provide 5 μM stock solutions of each. These stock solutions were then diluted into 12 solutions – 0, 0.05, 0.15, 0.3, 0.45, 0.6, 0.75, 1.0, 1.25, 1.5, 1.75, and 2.0 μM. In a 96-well streptavidin-coated microplate, 200 μL of wash buffer (0.5X PBS, pH 7.4) was added to each row to be used. The plates were then shaken for 30 min, and the wash buffer was then removed. For the biotin preincubation control, 100 μL of 500 μM D-biotin was added to each well and incubated for 1h. This solution was removed and the wells were washed with 3 x 200 μL wash buffer. In each case, 100 μL of the respective alkyne reagent (**3.13** or **3.23**) was added to the appropriate well. This was immediately followed by addition of 100 μL of 500 μM of the previously described liposome solution to each well. This yielded a final liposome concentration of 250 μM in each well, and alkyne reagent concentrations of 0, 0.025, 0.075, 0.15, 0.225, 0.3, 0.375, 0.5, 0.625, 0.75, 0.875, and 1.0 μM in different wells. These solutions were incubated, with shaking, for 4 h at rt. Following incubation, the solutions were removed and each well was washed with 3 x 200 μL wash buffer. Water (100 μL) was then added to each well and fluorescence was then measured using a microplate reader with a 460 nm (± 40 nm) excitation filter and 528 nm (± 20 nm) emission filter.

Procedure for Membrane Labeling via Fluorescent Octyne-Labeled Liposomes and FRET Assay

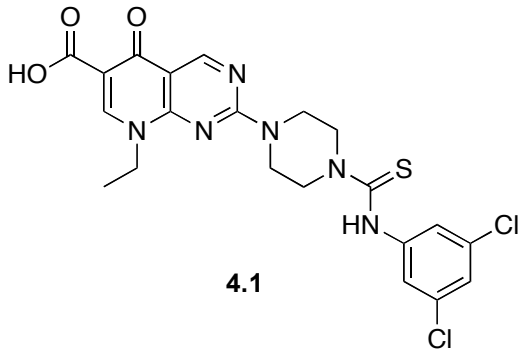
Stock solutions of octyne-lipid **3.32** (3.05 mM), NBD-lipid (3.20 mM), and phosphatidylcholine (65.8 mM) were prepared in chloroform. In a glass vial, NBD-lipid (9.4 µL, 3%), octyne-lipid (19.7 µL, 6%), and PC (13.8 µL, 91%) were measured out and dried under a stream of nitrogen. The dried lipids were placed under vacuum for 1 h. The liposomes were hydrated using 500 µL of 20 mM HEPES, 150 mM NaCl, pH 7.4 buffer to make a final concentration of 2 mM liposomes. The hydrated liposomes were rotated on a rotary evaporator for 40 min at 40 °C, freeze-thawed 10 cycles, extruded through 200 nm filter, and used for studies. The rhodamine-azide **3.33** used for studies was taken from a 0.25 mM stock solution in the same buffer. In a centrifuge tube, 45 µL of buffer and 25 µL of 2 mM liposomes were added and mixed. Immediately following addition of 50 µL of rhodamine-azide stock solution, the mixture was placed in a cuvette and fluorescence read. Fluorescence was measured every 60 seconds for 65 minutes and then plotted.

Chapter 4: Miscellaneous Synthetic Targets

4.1 Optimization of a Pipemidic Acid Autotaxin Inhibitor

In addition to DAG, PA, and the PIP_ns, our group is also interested in *lyso*-phosphatidyl choline (LPC) and *lyso*-phosphatidic acid (LPA). One of the main signaling pathways involving these two *lyso*- lipids is the conversion of LPC into LPA by autotaxin (ATX), which works via hydrolysis of the choline headgroup.[242,243] This is an important interaction because recent research has shown that autotaxin plays critical roles in normal human development and disease.[244] Autotaxin has been linked to cancer progression, multiple sclerosis, obesity, diabetes, Alzheimer's disease, and chronic pain.[245] Because of autotaxin's heavy involvement in aberrant processes, there is a need for specific and potent inhibitors as novel therapeutic leads. There are reported lipid-like inhibitors of autotaxin, but these lack many characteristics seen in 90% of orally bioavailable drugs. We collaborated with Drs. Parrill and Baker from the University of Memphis to investigate a structure–activity relationship for some novel autotaxin inhibitors.[245] Before approaching us, they previously modeled autotaxin and found compound **4.1** as a novel lead inhibitor as shown in Figure 4.1.[245] Working with this knowledge, we designed a library of compounds that could be synthesized and they predicted which of these compounds would be effective inhibitors. This list of predicted compounds greatly benefitted from the basal structure being commercially available, pipemidic acid, and the desired appending groups could be formed through reaction with a rather reactive isothiocyanate. Figure 4.3 shows the structures of all compounds synthesized in round one (green box), round two (red box), and round three (blue box).

The calculations and binding model were adjusted with each set of compounds to generate new lists of compounds to be synthesized and tested. In each of these cases, isothiocyanate compounds were reacted with pipemidic acid in the presence of triethylamine and subsequently purified *via* column chromatography to give the resulting thioureas that were then tested for effectiveness as an inhibitor in a FRET-based assay.



4.1

Figure 4.1. Structure of the lead compound 4.1 used as the basis for generating other potential inihibitors and their effectiveness.

The assays performed showed the *meta*-trifluoromethyl compound as having the strongest inhibition, while the *ortho*-trifluoromethyl shows the least inhibition. This study provides evidence that even small disturbances in chemical structures can lead to dramatically enhanced or decreased inhibition or binding of proteins of interest, so all avenues must be thoroughly investigated.

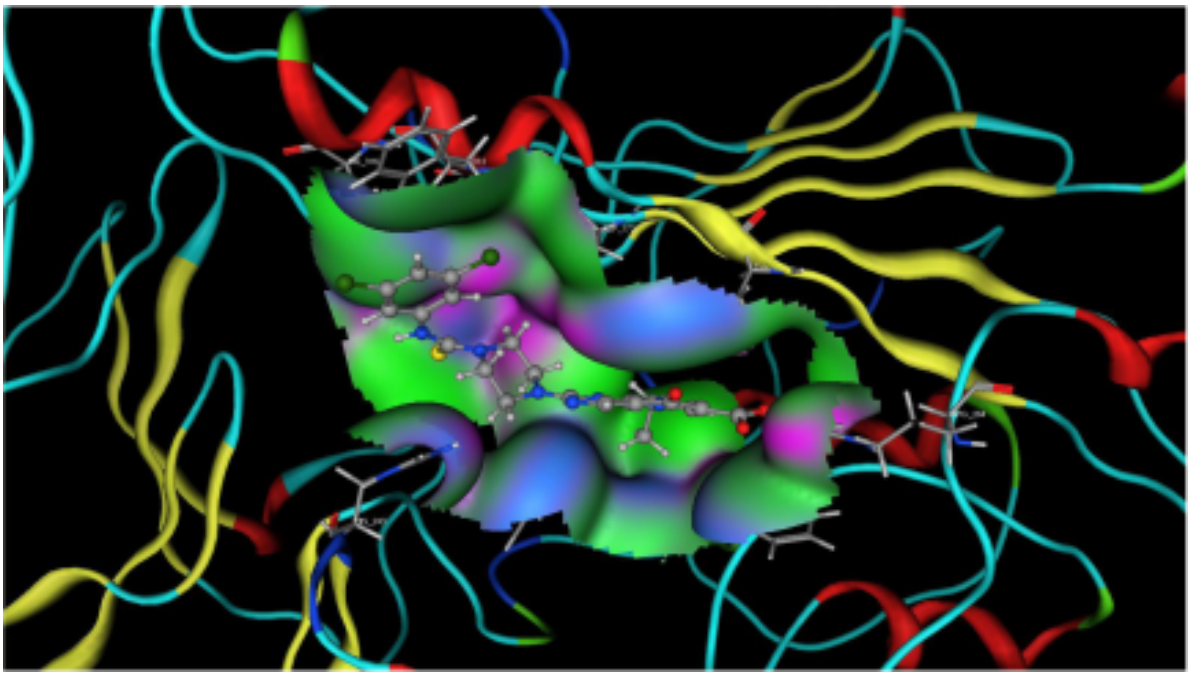


Figure 4.2. Model of autotaxin (ATX) with the lead compound 4.1 in the binding pocket that is normally used for the conversion of *lyso*-phosphatidyl choline (LPC) to *lyso*-phosphatidic acid (LPA).[245]

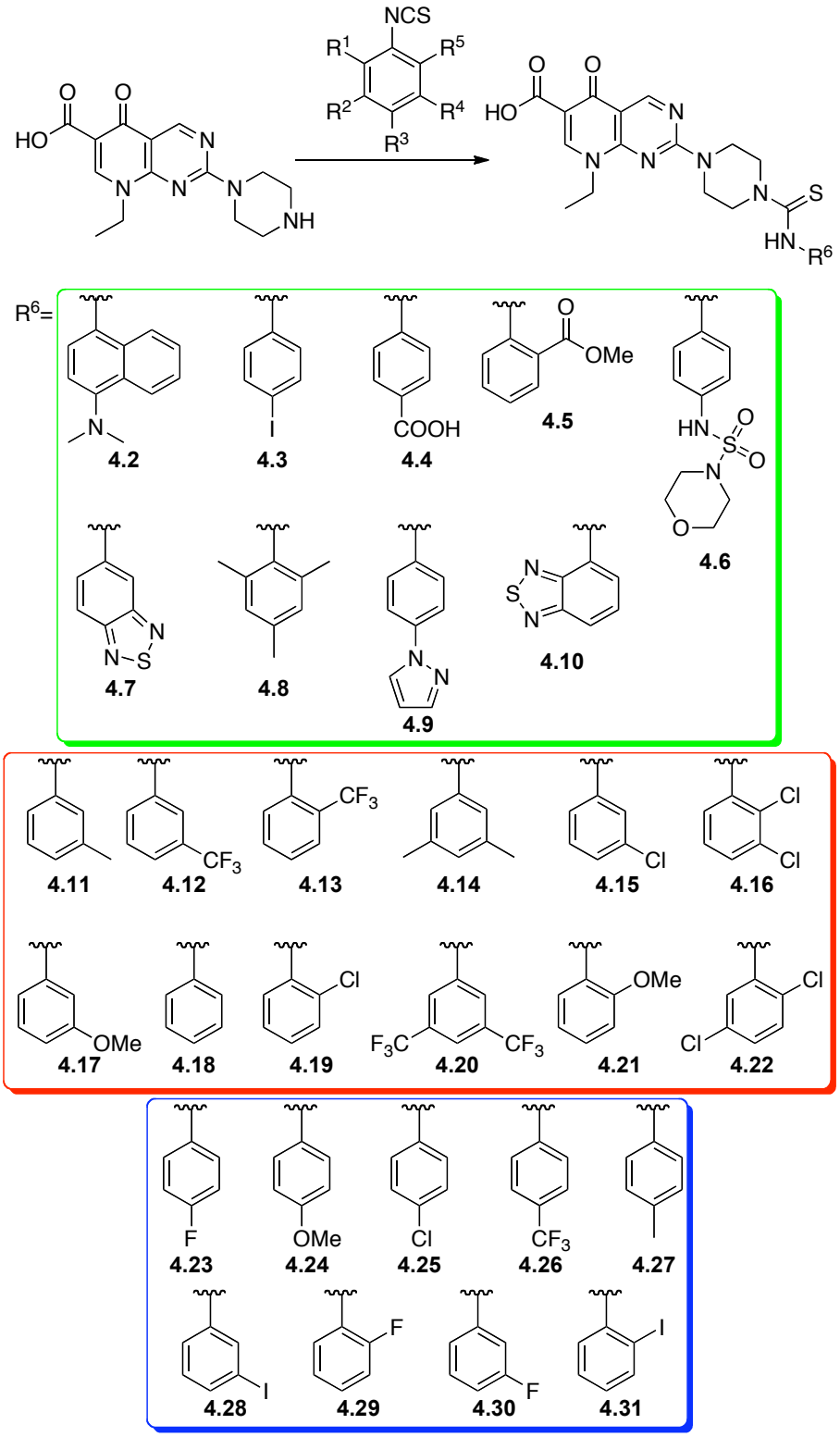


Figure 4.3. Compounds synthesized in round I (green box), round II (red box), and round III (blue box) as potential autotaxin inhibitors.

4.1.1 Synthetic Procedures

General procedure for thiourea formation. To a solution of pipemidic acid in *N,N*-dimethylformamide (1 mL) was added the corresponding substituted phenyl isothiocyanate. In some cases, triethylamine was added to speed up the reaction, while in others, the addition of this base led to the formation of byproducts, and was thus avoided. The mixture was then allowed to stir at room temperature under nitrogen overnight. The solvent was then removed *in vacuo* and the residue was extracted twice with methylene chloride from aqueous saturated ammonium chloride. The organic layers were combined, dried with magnesium sulfate, filtered and concentrated. The resulting crude was then purified by flash chromatography on silica gel eluting with a gradient of methanol in methylene chloride (0-20%) to yield the corresponding thiourea products (**4.2**–**4.31**). Compound purity was determined by HPLC and products were determined to be > 95% purity.

2-(4-((4-(dimethylamino)naphthalen-1-yl)carbamothioyl)piperazin-1-yl)-8-ethyl-5-oxo-5,8-dihydropyrido[2,3-*d*]pyrimidine-6-carboxylic acid (4.2) Pipemidic acid (25 mg, 0.0824 mmol), 4-dimethylamino-1-napthylisothiocyanate (18.8 mg, 0.0824 mmol) and triethylamine (23 µL, 0.165 mmol) were used. Purification on silica yielded **4.2** (23 mg, 53%). ^{1}H NMR (300 MHz, $CDCl_3$) δ 9.29 (s, 1H), 8.63 (s, 1H), 8.32-8.24 (m, 1H), 8.02-7.93 (m, 1H), 7.62-7.46 (m, 3H), 7.02 (d, *J* = 7.95 Hz, 1H), 4.29 (q, *J* = 13.69, 6.79 Hz, 2H), 4.16-3.85 (m, 8H), 2.90 (s, 6H), 1.45 (t, *J* = 7.08 Hz, 3H) ppm.

8-ethyl-2-(4-((4-iodophenyl)carbamothioyl)piperazin-1-yl)-5-oxo-5,8-dihydropyrido[2,3-*d*]pyrimidine-6-carboxylic acid (4.3) Pipemidic acid (25 mg, 0.0824 mmol), 4-iodophenyl isothiocyanate (21.5 mg, 0.0824 mmol) and triethylamine (23 µL, 0.165 mmol) were used. Purification on silica yielded **4.3** (36 mg, 77%). ^{1}H NMR (300 MHz, $CDCl_3$) δ 9.32 (s, 1H), 8.66 (s, 1H), 7.66 (d, *J* = 6.94 Hz, 2H) 7.37 (s, 1H), 7.00 (d, *J* = 6.0 Hz, 2H) 4.33 (q, *J* = 8.0 Hz, 2H), 4.21-3.99 (m, 8H), 1.52 (t, *J* = 7.5 Hz, 3H) ppm.

2-(4-((4-carboxyphenyl)carbamothioyl)piperazin-1-yl)-8-ethyl-5-oxo-5,8-dihydropyrido[2,3-*d*]pyrimidine-6-carboxylic acid (4.4) Pipemidic acid (25 mg, 0.0824 mmol), 4-isothiocyanatobenzoic acid (14.8 mg, 0.0824 mmol) and triethylamine (23 µL, 0.165 mmol) were used. Purification on silica yielded **4.4** (23 mg, 58%). ^{1}H NMR (300 MHz, DMSO) δ 9.71 (s, 1H), 9.24 (s, 1H), 8.98 (s, 1H), 7.87 (d, *J* = 8.53 Hz, 1H), 7.49 (d, *J* = 8.43 Hz, 1H), 4.45-4.39 (m, 2H), 4.10-4.03 (m, 8H), 1.38 (t, *J* = 6.94 Hz, 3H) ppm.

8-ethyl-2-(4-((2-(methoxycarbonyl)phenyl)carbamothioyl)piperazin-1-yl)-5-oxo-5,8-dihydropyrido[2,3-*d*]pyrimidine-6-carboxylic acid (4.5) Pipemidic acid (25 mg, 0.0824 mmol), methyl 2-isothiocyanatobenzoate (16 mg, 0.0824 mmol) and triethylamine (23 µL, 0.165 mmol) were used. Purification on silica yielded **4.5** (24 mg, 59%). ^{1}H NMR (300 MHz, $CDCl_3$) δ 11.14 (s, 1H), 9.35 (d, *J* = 3.14 Hz, 1H), 8.77 (dd, *J* = 8.43, 2.41 Hz, 1H), 8.69 (d, *J* = 2.99 Hz, 1H), 8.01 (d, *J* = 6.95 Hz, 1H), 7.55 (t, *J* =

7.72 Hz, 1H), 7.12 (t, *J* = 7.99 Hz, 1H), 4.40-4.24 (m, 8H), 4.11 (s, 2H), 3.92 (s, 3H), 1.52 (t, *J* = 7.5 Hz, 3H) ppm.

8-ethyl-2-(4-((4-(morpholine-4-sulfonamido)phenyl)carbamothioyl)piperazin-1-yl)-5-oxo-5,8-dihydropyrido[2,3-*d*]pyrimidine-6-carboxylic acid (4.6) Pipemidic acid (14.2 mg, 0.0468 mmol), 4-(morpholinosulfonyl)phenyl isothiocyanate (14 mg, 0.0468 mmol) and triethylamine (13 µL, 0.0935 mmol) were used. Purification on silica yielded **4.6** (24 mg, 85%). ^{1}H NMR (300 MHz, $CDCl_3$) δ 9.28 (s, 1H), 8.65 (s, 1H), 8.09 (s, 1H), 7.64 (d, *J* = 8.71 Hz, 2H), 7.51 (d, *J* = 8.61 Hz, 2H), 4.43-4.01 (m, 10H), 3.80-3.70 (m, 4H), 3.04-2.98 (m, 4H), 1.49 (t, *J* = 7.17 Hz, 3H) ppm.

2-(4-(benzo[c][1,2,5]thiadiazol-5-ylcarbamothioyl)piperazin-1-yl)-8-ethyl-5-oxo-5,8-dihydropyrido[2,3-*d*]pyrimidine-6-carboxylic acid (4.7) Pipemidic acid (25 mg, 0.0824 mmol), 2,1,3-benzothiadiazol-5-yl isothiocyanate (15.8 mg, 0.0824 mmol) and triethylamine (23 µL, 0.165 mmol) were used. Purification on silica yielded **4.7** (24 mg, 58%). ^{1}H NMR (300 MHz, DMSO) δ 9.26 (s, 1H), 8.98 (s, 1H), 7.98-7.82 (m, 3H), 4.51-4.33 (m, 2H), 4.24-3.99 (m, 8H), 1.42-1.32 (m, 3H) ppm.

8-ethyl-2-(4-(mesitylcarbamothioyl)piperazin-1-yl)-5-oxo-5,8-dihydropyrido[2,3-*d*]pyrimidine-6-carboxylic acid (4.8) Pipemidic acid (25 mg, 0.0824 mmol), mesityl isothiocyanate (14.6 mg, 0.0824 mmol) and triethylamine (23 µL, 0.165 mmol) were used. Purification on silica yielded **4.8** (36.6 mg, 92%). ^{1}H NMR (300 MHz, $CDCl_3$) δ

9.32 (s, 1H), 8.64 (s, 1H), 7.05 (s, 1H), 6.92 (s, 2H), 4.41-3.93 (m, 10H), 2.34-2.19 (m, 9H), 1.50 (t, *J* = 6.96 Hz, 3H) ppm.

2-(4-((4-(1H-pyrazol-1-yl)phenyl)carbamothioyl)piperazin-1-yl)-8-ethyl-5-oxo-5,8-dihydropyrido[2,3-*d*]pyrimidine-6-carboxylic acid (4.9) Pipemidic acid (27 mg, 0.0894 mmol) and 4-(1H-pyrazol-1-yl)phenyl isothiocyanate (15 mg, 0.0745 mmol) were used. Purification on silica yielded **4.9** (35.5 mg, 94%). ^{1}H NMR (250 MHz, $CDCl_3$) δ 9.30 (s, 1H), 8.69 (s, 1H), 7.91 (s, 1H), 7.72-7.56 (m, 3H), 7.46-7.30 (m, 2H), 6.46 (s, 1H), 4.36 (dd, *J* = 14.33, 6.78 Hz, 2H), 4.28-3.96 (m, 8H), 1.48 (t, *J* = 7.04 Hz, 3H) ppm.

2-(4-(benzo[c][1,2,5]thiadiazol-4-ylcarbamothioyl)piperazin-1-yl)-8-ethyl-5-oxo-5,8-dihydropyrido[2,3-*d*]pyrimidine-6-carboxylic acid (4.10) Pipemidic acid (25 mg, 0.0824 mmol), 2,1,3-benzothiadiazol-4-yl isothiocyanate (16 mg, 0.0824 mmol) and triethylamine (23 µL, 0.165 mmol) were used. Purification on silica yielded **4.10** (10.8 mg, 26%). ^{1}H NMR (300 MHz, DMSO) δ 9.27 (s, 1H), 9.00 (s, 1H), 7.93 (d, *J* = 8.40 Hz, 1H), 7.77-7.68 (m, 1H), 7.63 (d, *J* = 7.23 Hz, 1H), 4.48-4.41 (m, 2H), 4.24-3.99 (m, 8H), 1.39 (t, *J* = 6.52, 3H) ppm.

8-ethyl-5-oxo-2-(4-(*m*-tolylcarbamothioyl)piperazin-1-yl)-5,8-dihydropyrido[2,3-*d*]pyrimidine-6-carboxylic acid (4.11) Pipemidic acid (54 mg, 0.177 mmol) and m-tolylisothiocyanate (20 µL, 0.148 mmol) were used. Purification on silica yielded **4.11** (67 mg, 100%).^{1}H NMR (300 MHz, $CDCl_3$) δ 9.32 (s, 1H), 8.68 (s, 1H), 7.33 (s, 1H),

7.24 (d, *J* = 9.0 Hz, 1H), 7.05-6.94 (m, 3H), 4.33 (q, *J* = 7.0 Hz, 2H), 4.24-3.87 (m, 8H), 2.35 (s, 3H), 1.49 (t, *J* = 7.19 Hz, 3H) ppm.

8-ethyl-5-oxo-2-(4-((3-(trifluoromethyl)phenyl)carbamothioyl)piperazin-1-yl)-5,8-dihydropyrido[2,3-*d*]pyrimidine-6-carboxylic acid (4.12) Pipemidic acid (25 mg, 0.0824 mmol), 3-(trifluoromethyl)phenyl isothiocyanate (12.5 µL, 0.0824 mmol) and triethylamine (23 µL, 0.165 mmol) were used. Purification on silica yielded **4.12** (31 mg, 75%). ^{1}H NMR (300 MHz, $CDCl_3$) δ 9.32 (s, 1H), 8.74 (s, 1H), 7.63-7.60 (m, 2H), 7.51-7.42 (m, 2H), 4.45-4.37 (m, 2H), 4.23-4.10 (m, 8H), 1.52 (t, *J* = 7.5 Hz, 3H) ppm.

8-ethyl-5-oxo-2-(4-((2-(trifluoromethyl)phenyl)carbamothioyl)piperazin-1-yl)-5,8-dihydropyrido[2,3-*d*]pyrimidine-6-carboxylic acid (4.13) ortho trifluoro (25) Pipemidic acid (48 mg, 0.159 mmol) and 2-(trifluoromethyl)phenyl isothiocyanate (20 µL, 0.132 mmol) were used. Purification on silica yielded **4.13** (55 mg, 82%). ^{1}H NMR (300 MHz, $CDCl_3$) δ 9.32 (s, 1H), 8.69 (s, 1H), 7.74-7.64 (m, 1H), 7.63-7.51 (m, 2H), 7.43-7.33 (m, 1H), 4.39-4.03 (m, 10H), 1.50 (t, *J* = 6.86 Hz, 3H) ppm.

2-(4-((3,5-dimethylphenyl)carbamothioyl)piperazin-1-yl)-8-ethyl-5-oxo-5,8-dihydropyrido[2,3-*d*]pyrimidine-6-carboxylic acid (4.14) Pipemidic acid (45 mg, 0.148 mmol), 3,5-dimethylphenyl isothiocyanate (24 mg, 0.148 mmol) and triethylamine (41 µL, 0.296 mmol) were used. Purification on silica yielded **4.14** (41.6 mg, 67%). ^{1}H

NMR (300 MHz, $CDCl_3$) δ 9.30 (s, 1H), 8.66 (s, 1H), 7.48 (s, 1H), 6.86-6.75 (m, 3H), 4.33 (q, *J* = 7.0 Hz, 2H), 4.22-3.91 (m, 8H), 2.30 (s, 6H), 1.48 (t, *J* = 7.11 Hz, 3H) ppm.

2-(4-((3-chlorophenyl)carbamothioyl)piperazin-1-yl)-8-ethyl-5-oxo-5,8-dihydropyrido[2,3-*d*]pyrimidine-6-carboxylic acid (4.15) Pipemidic acid (25 mg, 0.0824 mmol), 3-chlorophenyl isothiocyanate (11 µL, 0.0824 mmol) and triethylamine (23 µL, 0.165 mmol) were used. Purification on silica yielded **4.15** (8.2 mg, 21%). ^{1}H NMR (300 MHz, $CDCl_3$) δ 9.03 (s, 1H), 8.51 (s, 1H), 7.10 (s, 1H), 7.04-6.93 (m, 2H), 6.90-6.84 (m, 1H), 4.14 (q, *J* = 14.23, 7.04 Hz, 2H), 4.00-3.74 (m, 8H), 1.23 (t, *J* = 7.01 Hz, 3H) ppm.

2-(4-((2,3-dichlorophenyl)carbamothioyl)piperazin-1-yl)-8-ethyl-5-oxo-5,8-dihydropyrido[2,3-*d*]pyrimidine-6-carboxylic acid (4.16) Pipemidic acid (51 mg, 0.168 mmol) and 2,3-dichlorophenyl isothiocyanate (20 µL, 0.141 mmol) were used. Purification on silica yielded **4.16** (15.5 mg, 22%). ^{1}H NMR (300 MHz, DMSO) δ 9.03 (s, 1H), 8.78 (s, 1H), 7.53 (d, *J* = 7.43 Hz, 1H), 7.41-7.26 (m, 2H), 4.51-3.90 (m, 10H), 1.43-1.27 (m, 3H) ppm.

8-ethyl-2-(4-((3-methoxyphenyl)carbamothioyl)piperazin-1-yl)-5-oxo-5,8-dihydropyrido[2,3-*d*]pyrimidine-6-carboxylic acid (4.17) Pipemidic acid (53 mg, 0.175 mmol) and 3-methoxyphenyl isothiocyanate (20 µL, 0.145 mmol) were used. Purification on silica yielded **4.17** (36 mg, 53%). ^{1}H NMR (300 MHz, $CDCl_3$) δ 9.31 (s,

1H), 8.67 (s, 1H), 7.47 (s, 1H), 7.30-7.21 (m, 1H), 6.80-6.68 (m, 3H), 4.32 (q, *J* = 7.05 Hz, 2H), 4.23-3.89 (m, 8H), 3.79 (s, 3H), 1.48 (t, *J* = 7.16 Hz, 3H) ppm.

8-ethyl-5-oxo-2-(4-(phenylcarbamothioyl)piperazin-1-yl)-5,8-dihydropyrido[2,3-*d*]pyrimidine-6-carboxylic acid (4.18) Pipemidic acid (25 mg, 0.0824 mmol), phenyl isothiocyanate (9.8 µL, 0.0824 mmol) and triethylamine (23 µL, 0.165 mmol) were used. Purification on silica yielded **4.18** (16 mg, 43%). ^{1}H NMR (300 MHz, $CDCl_3$) δ 9.33 (s, 1H), 8.68 (s, 1H), 7.41-7.33 (m, 3H), 7.22-7.15 (m, 2H), 4.38-4.28 (m, 2H), 4.24-3.89 (m, 8H), 1.49 (t, *J* = 7.57 Hz, 3H) ppm.

2-(4-((2-chlorophenyl)carbamothioyl)piperazin-1-yl)-8-ethyl-5-oxo-5,8-dihydropyrido[2,3-*d*]pyrimidine-6-carboxylic acid (4.19) Pipemidic acid (56 mg, 0.184 mmol) and 2-chlorophenylisothiocyanate (20 µL, 0.153 mmol) were used. Purification on silica yielded **4.19** (72mg, 99%). ^{1}H NMR (300 MHz, $CDCl_3$) δ 9.34 (s, 1H), 8.68 (s, 1H), 7.75 (dd, *J* = 8.10, 1.43 Hz, 1H), 7.44 (dd, *J* = 8.00, 1.48 Hz, 1H), 7.37-7.27 (m, 2H), 7.15 (dt, *J* = 7.67, 1.53 Hz, 1H), 4.38-4.06 (m, 10H), 1.50 (t, *J* = 7.20 Hz, 3H) ppm.

2-(4-((3,5-bis(trifluoromethyl)phenyl)carbamothioyl)piperazin-1-yl)-8-ethyl-5-oxo-5,8-dihydropyrido[2,3-*d*]pyrimidine-6-carboxylic acid (4.20) Pipemidic acid (40 mg, 0.132 mmol) and 3,5-bis(trifluoromethyl)phenyl isothiocyanate (20 µL, 0.110 mmol) were used. Purification on silica yielded **4.20** (61 mg, 97%). ^{1}H NMR (300 MHz, $CDCl_3$)

δ 9.30 (s, 1H), 8.68 (s, 1H), 8.62 (s, 1H), 7.94 (s, 2H), 7.62 (s, 1H), 4.42-4.10 (m, 10H), 1.51 (t, *J* = 7.07 Hz, 3H) ppm.

8-ethyl-2-(4-((2-methoxyphenyl)carbamothioyl)piperazin-1-yl)-5-oxo-5,8-dihydropyrido[2,3-*d*]pyrimidine-6-carboxylic acid (4.21) Pipemidic acid (25 mg, 0.0824 mmol), 2-methoxyphenyl isothiocyanate (11.6 µL, 0.0824 mmol) and triethylamine (23 µL, 0.165 mmol) were used. Purification on silica yielded **4.21** (21.4 mg, 55%). ^{1}H NMR (250 MHz, $CDCl_3$) δ 9.33 (s, 1H), 8.68 (s, 1H), 7.84 (d, *J* = 7.30 Hz, 1H), 7.54 (s, 1H), 7.20-7.04 (m, 1H), 7.03-6.85 (m, 2H), 4.34 (q, *J* = 8.0 Hz, 2H), 4.24-4.01 (m, 8H), 3.89 (s, 3H), 1.49 (t, *J* = 6.60 Hz, 3H) ppm.

2-(4-((2,5-dichlorophenyl)carbamothioyl)piperazin-1-yl)-8-ethyl-5-oxo-5,8-dihydropyrido[2,3-*d*]pyrimidine-6-carboxylic acid (4.22) Pipemidic acid (51 mg, 0.168 mmol) and 2,5-dichlorophenyl isothiocyanate (20 µL, 0.140 mmol) were used. Purification on silica yielded **4.22** (42.7 mg, 60%). ^{1}H NMR (300 MHz, $CDCl_3$) δ 9.39 (s, 1H), 9.06 (s, 1H), 7.57 (d, *J* = 2.39 Hz, 1H), 7.42-7.36 (m, 1H), 7.20 (d, *J* = 7.35 Hz, 1H), 4.55-4.39 (m, 2H), 4.31-4.02 (m, 8H), 1.52 (t, *J* = 6.88 Hz, 3H) ppm.

8-ethyl-2-(4-((4-fluorophenyl)carbamothioyl)piperazin-1-yl)-5-oxo-5,8-dihydropyrido[2,3-*d*]pyrimidine-6-carboxylic acid (4.23) Pipemidic acid (35 mg, 0.1154 mmol) and 4-fluorophenyl isothiocyanate (17.7 mg, 0.1154 mmol) were used. Purification on silica yielded **4.23** (30 mg, 57%). ^{1}H NMR (300 MHz, $CDCl_3$) δ 9.34 (s,

1H), 8.69 (s, 1H), 7.33 (s, 1H), 7.25-7.16 (m, 2H), 7.13-7.03 (m, 2H), 4.40-4.29 (m, 2H), 4.28-3.96 (m, 8H), 1.50 (t, *J* = 7.36 Hz, 3H) ppm.

8-ethyl-2-(4-((4-methoxyphenyl)carbamothioyl)piperazin-1-yl)-5-oxo-5,8-dihydropyrido[2,3-*d*]pyrimidine-6-carboxylic acid (4.24) Pipemidic acid (30 mg, 0.0989 mmol) and 4-methoxyphenyl isothiocyanate (13.7 µL, 0.0989 mmol) were used. Purification on silica yielded **4.24** (37 mg, 80%). ^{1}H NMR (300 MHz, $CDCl_3$) δ 9.33 (s, 1H), 8.67 (s, 1H), 7.30 (s, 1H), 7.15 (d, *J* = 8.76 Hz, 2H), 6.90 (d, *J* = 8.82 Hz, 2H), 4.34 (q, *J* = 7.10, 6.89 Hz, 2H), 4.25-3.92 (m, 8H), 3.81 (s, 3H), 1.49 (t, *J* = 7.12 Hz, 3H) ppm.

2-(4-((4-chlorophenyl)carbamothioyl)piperazin-1-yl)-8-ethyl-5-oxo-5,8-dihydropyrido[2,3-*d*]pyrimidine-6-carboxylic acid (4.25) Pipemidic acid (58 mg, 0.191 mmol) and 4-chlorophenyl isothiocyanate (27 mg, 0.159 mmol) were used. Purification on silica yielded **4.25** (50 mg, 67%). ^{1}H NMR (300 MHz, $CDCl_3$) δ 9.34 (s, 1H), 8.68 (s, 1H), 7.34 (d, *J* = 14.13 Hz, 2H), 7.17 (d, *J* = 8.70 Hz, 2H), 4.39-4.28 (m, 2H), 4.28-3.93 (m, 8H), 1.49 (t, *J* = 6.68 Hz, 3H) ppm.

8-ethyl-5-oxo-2-(4-((4-(trifluoromethyl)phenyl)carbamothioyl)piperazin-1-yl)-5,8-dihydropyrido[2,3-*d*]pyrimidine-6-carboxylic acid (4.26) Pipemidic acid (30 mg, 0.0989 mmol) and 4-trifluorophenyl isothiocyanate (16.7 mg, 0.0824 mmol) were used. Purification on silica yielded **4.26** (31 mg, 77%). ^{1}H NMR (300 MHz, $CDCl_3$) δ 9.34 (s,

1H), 8.69 (s, 1H), 7.65-7.57 (m, 2H), 7.51 (s, 1H), 7.37-7.31 (m, 2H), 4.34 (q, *J* = 7.46, 7.27 Hz, 2H), 4.27-3.97 (m, 8H), 1.49 (t, *J* = 7.25, 7.25 Hz, 3H) ppm.

8-ethyl-5-oxo-2-(4-(p-tolylcarbamothioyl)piperazin-1-yl)-5,8-dihydropyrido[2,3-*d*]pyrimidine-6-carboxylic acid (4.27) Pipemidic acid (89 mg, 0.293 mmol) and p-tolyl isothiocyanate (40 mg, 0.268 mmol) were used. Purification on silica yielded **4.27** (82 mg, 68%). ^{1}H NMR (300 MHz, $CDCl_3$) δ 9.32 (s, 1H), 8.67 (s, 1H), 7.40 (s, 1H), 7.17 (d, *J* = 7.60 Hz, 2H), 7.09 (d, *J* = 7.44 Hz, 2H), 4.33 (q, *J* = 13.30, 6.75 Hz, 2H), 4.23-3.91 (m, 8H), 2.34 (s, 3H), 1.49 (t, *J* = 7.03 Hz, 3H) ppm.

8-ethyl-2-(4-((3-iodophenyl)carbamothioyl)piperazin-1-yl)-5-oxo-5,8-dihydropyrido[2,3-*d*]pyrimidine-6-carboxylic acid (4.28) Pipemidic acid (40 mg, 0.133 mmol) and 3-iodophenyl isothiocyanate (29 mg, 0.111 mmol) were used. Purification on silica yielded **4.28** (57 mg, 90%). ^{1}H NMR (250 MHz, $CDCl_3$) δ 9.33 (s, 1H), 8.73 (s, 1H), 7.65 (s, 1H), 7.51 (s, 1H), 7.40-7.24 (m, 1H), 7.08 (s, 1H), 4.48-4.31 (m, 2H), 4.27-3.93 (m, 8H), 1.34-1.17 (m, 3H) ppm.

8-ethyl-2-(4-((2-fluorophenyl)carbamothioyl)piperazin-1-yl)-5-oxo-5,8-dihydropyrido[2,3-*d*]pyrimidine-6-carboxylic acid (4.29) Pipemidic acid (25 mg, 0.0824 mmol) and 2-fluorophenyl isothiocyanate (10 µL, 0.0824 mmol) were used. Purification on silica yielded **4.29** (24 mg, 64%). ^{1}H NMR (300 MHz, $CDCl_3$) δ 9.35 (s,

1H), 8.69 (s, 1H), 7.64 (t, *J* = 7.34 Hz, 1H), 7.21-7.12 (m, 3H), 4.35 (q, *J* = 13.56, 7.29 Hz, 2H), 4.28-4.02 (m, 8H), 1.50 (t, *J* = 7.09 Hz, 3H) ppm.

8-ethyl-2-(4-((3-fluorophenyl)carbamothioyl)piperazin-1-yl)-5-oxo-5,8-dihydropyrido[2,3-*d*]pyrimidine-6-carboxylic acid (4.30) Pipemidic acid (25 mg, 0.0824 mmol) and 3-fluorophenyl isothiocyanate (9.9 µL, 0.0824 mmol) were used. Purification on silica yielded **4.30** (22 mg, 59%). ^{1}H NMR (300 MHz, $CDCl_3$) δ 9.32 (s, 1H), 8.66 (s, 1H), 7.41 (s, 1H), 7.37-7.27 (m, 1H), 6.96 (t, *J* = 7.39, 2H), 6.88 (t, *J* = 7.67 Hz, 1H), 4.38-4.27 (m, 2H), 4.27-3.91 (m, 8H), 1.54-1.43 (m, 3H) ppm.

8-ethyl-2-(4-((2-iodophenyl)carbamothioyl)piperazin-1-yl)-5-oxo-5,8-dihydropyrido[2,3-*d*]pyrimidine-6-carboxylic acid (4.31) Pipemidic acid (25 mg, 0.0824 mmol) and 2-iodophenyl isothiocyanate (21.5 mg, 0.0824 mmol) were used. Purification on silica yielded **4.31** (35 mg, 75%). ^{1}H NMR (300 MHz, $CDCl_3$) δ 9.36-9.30 (m, 1H), 8.69-8.65 (m, 1H), 7.89-7.82 (m, 1H), 7.62-7.55 (m, 1H), 7.41-7.32 (m, 1H), 7.00-6.92 (m, 1H), 4.40-4.01 (m, 10H), 1.53-1.44 (m, 3H) ppm.

4.2 Porphyrin–Lipid Conjugates

Photoactive complexes based on porphyrins and fullerenes have been extensively used in building molecular photovoltaic systems owing to efficient electron transfer from porphyrin to fullerene upon photoexcitation.[246] Ground-state porphyrins absorb light very strongly at ~400 nm, but in their excited-state they have long lifetimes and can often exchange electrons readily with redox species in their vicinity. Because of the close redox potential of these excited-state porphyrins and fullerenes, a class of compounds known to have strong electron-accepting capability, they have often been used in tandem. Through collaboration with Dr. Wei Zhan at Auburn University, we have synthesized three lipids (shown in Figure 4.4) for use in photoconversion systems using electrode-supported lipid bilayers, which involves building bilayers composed of a porphyrin-lipid and fullerene molecules buried within the hydrophobic core of the bilayers. For their system, it was desirable to have the porphyrin appended to the headgroup of the lipid, so that it is exposed to the exterior aqueous environment. To achieve this, we coupled the porphyrin moiety in Figure 4.5 to the headgroup of phosphatidylethanolamine (PE).

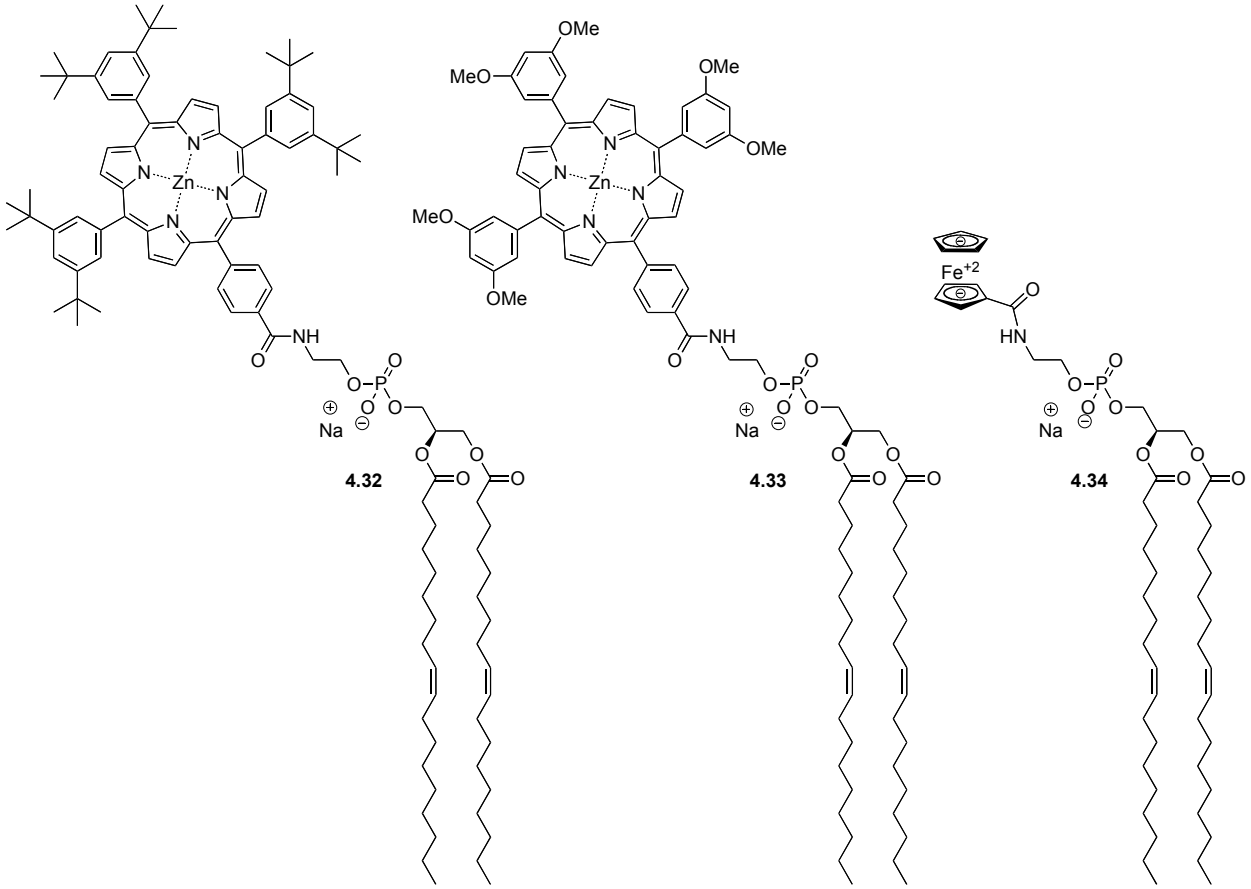


Figure 4.4. Structures of three lipids synthesized.

We received the porphyrin methyl esters, shown in Figure 4.5, from Dr. X. Peter Zhang at the University of South Florida. Beginning there, zinc was inserted into the center of the porphyrin using zinc acetate in *N*,*N*-dimethylformamide and heating at 60 ºC overnight. The methyl ester was then deprotected with sodium hydroxide in methanol. Finally, the acid was coupled to the amine of PE using hydroxybenzyltriazole and HBTU. In addition to these porphryin lipids, Dr. Zhan was interested in the effect of ferrocene on these photovoltaic membrane systems. The synthesis of this ferrocene lipid, Figure 4.6, was a coupling reaction between ferrocene carboxylic acid and PE.

Dr. Zhan began investigating the *tert*-butyl porphyrin lipid, and after some testing, it was thought that the porphyrin portion was not hydrophilic enough to be properly presented outside of the membrane, so we decided a methoxy porphyrin lipid would be a good alternative. Upon further investigation by Dr. Zhan, it was discovered that the *tert*-butyl porphyrin lipid, in fact, was a usable and valuable compound and he obtained promising results.

The studies involved in this report use electrodes as a surface for immobilizing a membrane bilayer. The base layer is composed of a thiol-terminated phospholipid and the upper layer is composed of PC and the *tert*-butyl porphyrin lipid conjugate. They discovered that the fullerene can be incorporated into the top, bottom, or both layers and have obtained different photocurrent responses based on the locale of the fullerene. The sequential formation of the bilayer allows a direct organization of these agents on electrodes. In this report, the best, most stable, photocurrent generation system was determined to be when fullerenes were incorporated in both the upper and lower layer. The results reported here represent the first step toward lipid-based, multicomponent photoconversion systems.

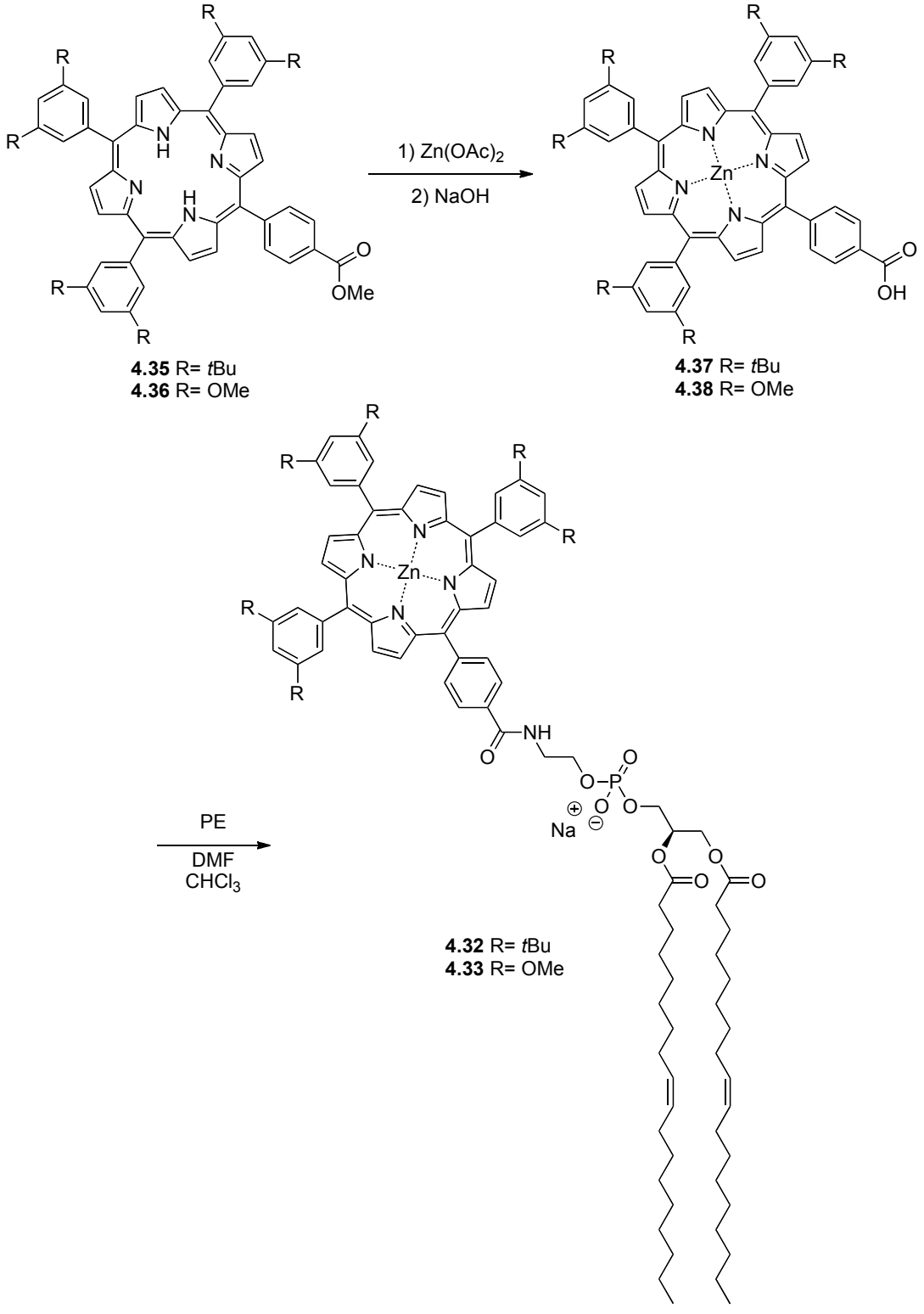


Figure 4.5. Synthetic scheme for synthesizing the two porphyrin lipids.

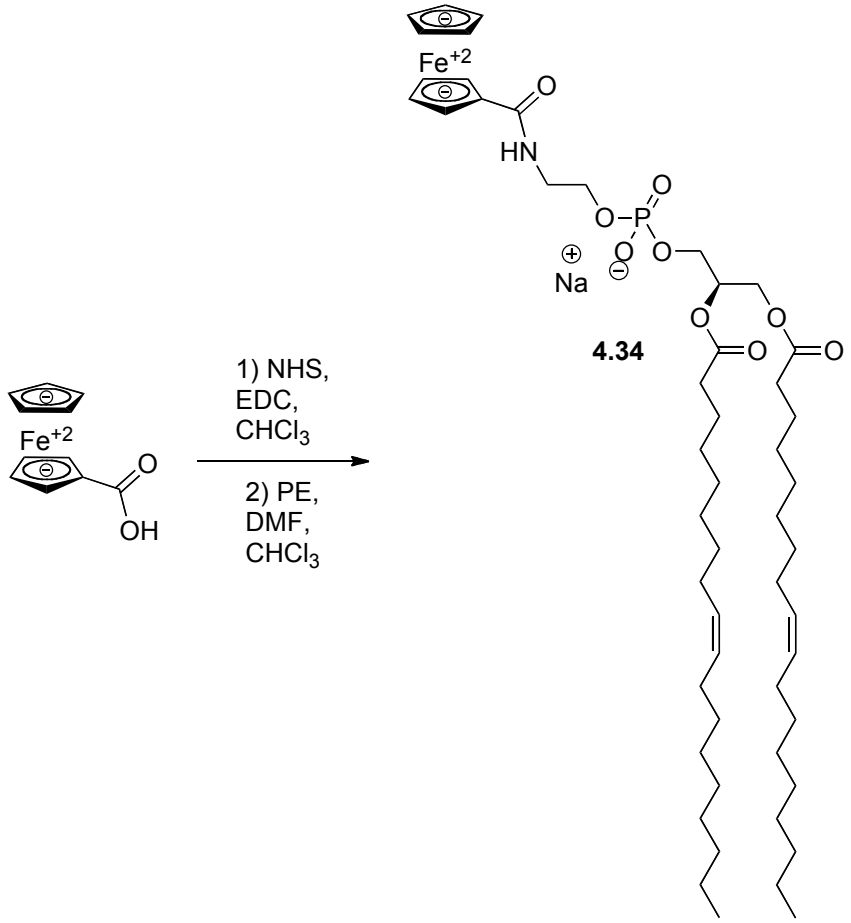


Figure 4.6. Synthesis of ferrocene-lipid.

4.2.1 Synthetic Procedures

5-(4-carboxyphenyl)-10,15,20-tris-(3,5,di-*tert*-butylphenyl)porphyrin zinc complex (4.37): To the methyl ester **4.35** (25 mg, 0.025 mmol) was added 2.5 mL of *N*, *N*-dimethylformamide and zinc(II)acetate (36.4 mg, 0.198 mmol). The solution was heated to 60 °C and stirred overnight. The solvent was then removed under reduced pressure and the residue was extracted with methylene chloride (2 x 10 mL) and water. The organic layers were combined, dried with magnesium sulfate, filtered, and concentrated. The resulting residue was dissolved in ethanol (2.5 mL) and tetrahydrofuran (2.5 mL). Potassium hydroxide was added (500 µL, 2M) and the resulting mixture was stirred at

reflux overnight. The solvent was removed and the residue was extracted with chloroform (3 x 25 mL) and water, following neutralization with 2M hydrochloric acid to pH 4. The organic layers were combined, dried with magnesium sulfate, filtered, and concentrated. The residue was purified by chromatography on silica gel with a gradient of methanol–methylene chloride (0–10%) to afford the zinc-conjugated porphyrin carboxylic acid **4.37** (26 mg, 100%).

^{1}H NMR (300 MHz, $CDCl_3$): δ = 9.07–9.05 (m, 6H), 8.95 (d, *J* = 4.5 Hz, 2H), 8.55 (d, *J* = 7.8 Hz, 2H), 8.44 (d, *J* = 7.8 Hz, 2H), 8.13–8.11 (m, 6H), 7.83–7.81 (m, 3H), 1.55–1.54 (m, 54H) ppm.

5-(4-Carboxyphenyl)-10,15,20-tris-(3,5,di-methoxyphenyl)porphyrin zinc complex (4.38): To the methyl ester **4.36** (25 mg, 0.029 mmol) was added 2.5 mL of *N*, *N*-dimethylformamide and zinc(II)acetate (43 mg, 0.23 mmol). The solution was heated to 60 °C and stirred overnight. The solvent was then removed under reduced pressure and the residue was extracted with methylene chloride (2 x 10 mL) and water. The organic layers were combined, dried with magnesium sulfate, filtered, and concentrated. The resulting residue was dissolved in ethanol (2.5 mL) and tetrahydrofuran (2.5 mL). Potassium hydroxide was added (500 µL, 2M) and the resulting mixture was stirred at reflux overnight. The solvent was removed and the residue was extracted with chloroform (3 x 25 mL) and water, following neutralization with 2M hydrochloric acid to pH 4. The organic layers were combined, dried with magnesium sulfate, filtered, and concentrated. The residue was purified by chromatography on silica gel with a gradient

of methanol–methylene chloride (0–10%) to afford the zinc-conjugated porphyrin carboxylic acid **4.38** (26 mg, 100%).

^{1}H NMR (300 MHz, $CDCl_3$): δ = 9.06–9.02 (m, 6H), 8.89 (d, *J* = 4.5 Hz, 2H), 8.49 (d, *J* = 7.8 Hz, 2H), 8.34 (d, *J* = 7.8 Hz, 2H), 7.40–7.35 (m, 6H), 6.81 (s, 3H), 3.88 (s, 18H) ppm.

Zinc complex 5-(4-carboxyphenyl)-10,15,20-tris-(3,5,di-*t*-butylphenyl)porphyrin phosphatidylethanolamine conjugate (4.32): To the porphyrin carboxylic acid **4.37** (9 mg, 0.0101 mmol) was added *N*, *N*-dimethylformamide (1 mL), hydroxybenzotriazole (HOBt, 1mg, 0.0067 mmol), *O*-benzotriazole-*N*, *N*, *N*', *N*'-tetramethyl-uronium-hexafluro-phosphate (HBTU, 4 mg, 0.0101 mmol), and *N*, *N*-diisopropylethylamine (DIEA, 3.3 µL, 0.0202 mmol). A solution of phosphatidylethanolamine (5 mg, 0.0067 mmol) in chloroform (1 mL) was added to the reaction mixture and the reaction was stirred at room temperature overnight. The solvent was removed and the residue was purified by chromatography on silica gel with a gradient of methanol–methylene chloride (0–30%). The resulting lipid **4.32** was obtained as a purple solid (9.5 mg, 86%).

^{1}H NMR (300 MHz, $CDCl_3$:CD_3OD): δ = 8.94–8.91 (m, 6H), 8.81–8.79 (m, 2H), 8.33 (d, *J* = 7.8 Hz, 2H), 8.25 (d, *J* = 7.8 Hz, 2H), 8.08 (s, 6H) 7.78 (s, 3H), 5.33–5.23 (m, 4H), 4.23–4.17 (m, 3H), 4.08–4.04 (m, 2H), 3.86–3.81 (m, 3H), 3.70–3.65 (m, 5H), 2.36–2.26 (m, 4H), 2.02–1.91 (m, 8H), 1.53 (s, 54H), 1.27–1.22 (m, 40H), 0.85 (t, *J* = 6.5 Hz, 6H) ppm.

Zinc complex 5-(4-Carboxyphenyl)-10,15,20-tris-(3,5,di-methoxyphenyl)porphyrin phosphatidylethanolamine conjugate (4.33): To the porphyrin carboxylic acid **4.38** (9 mg, 0.0101 mmol) was added *N*, *N*-dimethylformamide (1 mL), hydroxybenzotriazole (HOBt, 1mg, 0.0067 mmol), *O*-benzotriazole-*N*, *N*, *N*', *N*'-tetramethyl-uronium-hexafluro-phosphate (HBTU, 4 mg, 0.0101 mmol), and *N*, *N*-diisopropylethylamine (DIEA, 3.3 µL, 0.0202 mmol). A solution of phosphatidylethanolamine (5 mg, 0.0067 mmol) in chloroform (1 mL) was added to the reaction mixture and the reaction was stirred at room temperature overnight. The solvent was removed and the residue was purified by chromatography on silica gel with a gradient of methanol–methylene chloride (0–30%). The resulting lipid **4.32** was obtained as a purple solid (9.5 mg, 86%).

^{1}H NMR (300 MHz, $CDCl_3$:CD_3OD): δ = 8.96 (s, 6H), 8.79 (d, *J* = 6 Hz, 2H), 8.33–8.24 (m, 4H), 7.42–7.40 (m, 6H), 6.91–6.88 (m, 3H), 5.32–5.24 (m, 4H), 4.24–4.15 (m, 3H), 4.10–4.03 (m, 1H), 3.97–3.95 (m, 22H), 3.86–3.80 (m, 4H), 3.68–3.65 (m, 1H), 2.36–2.26 (m, 4H), 2.03–1.91 (m, 8H), 1.63–1.53 (m, 4H), 1.27–1.23 (m, 40H), 0.87–0.83 (m, 6H) ppm. ^{31}P NMR (121.5 MHz, $CDCl_3$:CD_3OD): δ = 2.02 (s, 1P) ppm.

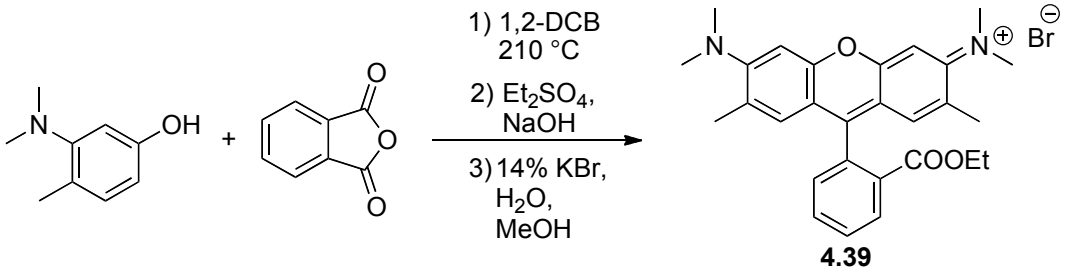
Ferrocene phosphatidylethanolamine (4.34): To ferrocene carboxylic acid **4.37** (2.4 mg, 0.01 mmol) was added *N*, *N*-dimethylformamide (1 mL), hydroxybenzotriazole (HOBt, 1mg, 0.0067 mmol), *O*-benzotriazole-*N*, *N*, *N*', *N*'-tetramethyl-uronium-hexafluro-phosphate (HBTU, 3.8 mg, 0.010 mmol), and *N*, *N*-diisopropylethylamine (DIEA, 3.3 µL, 0.0202 mmol). A solution of phosphatidylethanolamine (5 mg, 0.0067 mmol) in chloroform (1 mL) was added to the reaction mixture and the reaction was stirred at

room temperature overnight. The solvent was removed and the residue was purified by chromatography on silica gel with a gradient of methanol–methylene chloride (0–30%). The resulting lipid **4.34** was obtained as a purple solid (6.4 mg, 98%).

^{1}H NMR (300 MHz, $CDCl_3$:CD_3OD): δ = 5.36–5.32 (m, 4H), 5.26–5.22 (m, 2H), 4.83 (t, *J* = 1.8 Hz, 1H), 4.43–4.38 (m, 2H), 4.22 (s, 3H), 4.19–4.12 (m, 2H), 4.02–3.98 (m, 2H), 3.68–3.66 (m, 1H), 3.60–3.56 (m, 1H), 2.31 (t, *J* = 7.5 Hz, 4H), 2.02 (q, *J* = 6 Hz, 8H), 1.65–1.57 (m, 4H), 1.31–1.27 (m, 40H), 0.89 (t, *J* = 6.3 Hz, 6H) ppm.

4.3 Rhodamines

Surface enhanced hyper raman spectroscopy (SEHRS) is an analytical technique used to detect the vibrational modes in any given molecule. This is done by attaching the molecule to a silver or gold surface, followed by ablation with two lasers at 90º angles to one another, exciting the surface and the attached molecule resulting in a vibrational spectrum. This project has gone through various phases, with the current synthetic target shown in Figure 4.8. Compound **4.39** is an isomer of rhodamine 6G where the ethyl groups of the xanthene nitrogens have been replaced by methyls, which has been synthesized. This rhodamine isomer was made by refluxing 3-dimethylamino-4-methylphenol and phthalic anhydride in 1,2-dichlorobenzene at 210 ºC overnight. This created the acid version of the rhodamine, which was then treated with sodium hydroxide and diethyl sulfate to create the ethyl ester that was then used for SEHRS. A deuterated version of the same molecule, with the methyls of the xanthene nitrogen fully deuterated, began by treating 3-hydroxy-6-methylaniline with dimethyl sulfate–d_6 in acetonitrile overnight, and then repeating the previous rhodamine preparation procedure. These two molecules will be used to detect differences in SEHR spectra, which is a process that is still underway.



4.39

Figure 4.7. Synthetic target for use in SEHRS.

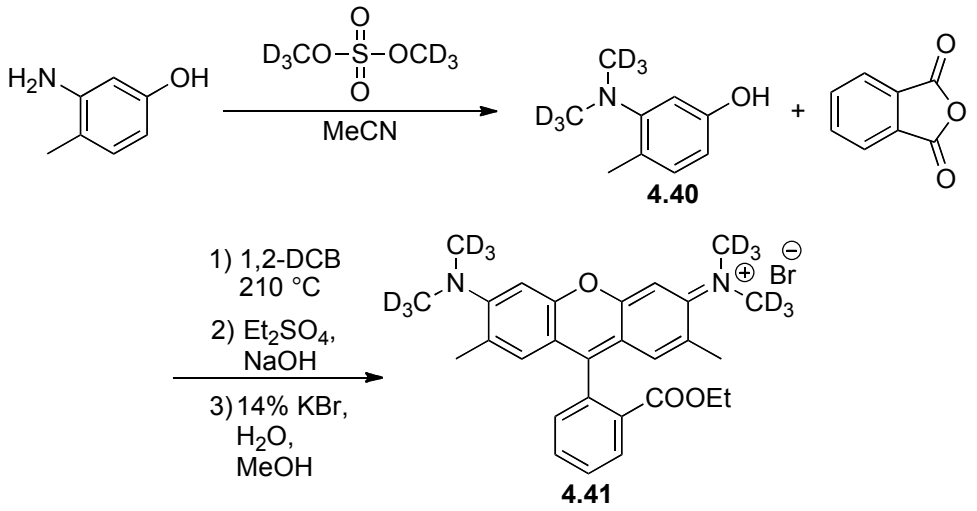


Figure 4.8. Deuterated tetramethyl rhodamine target to be used in SEHRS.

In the previous phases of the project, there were other rhodamine targets, as seen in Figure 4.9. These rhodamines were designed based on calculations of the expected SEHRS spectra performed by the Camden group at the University of Tennessee at Knoxville. Theoretical calculations of the expected SEHRS spectra were performed as the rhodamine isomer **4.45** was being synthesized. There were some complications in the initial synthetic route, which included the protection of the amine with acetate. The removal of this acetate group proved to be problematic; therefore the synthetic route was adjusted to include the more easily cleaved trifluoroacetate protecting group. The removal of this protecting group also led to minimal success, even upon the addition of sodium borohydride. Before the rhodamine isomer **4.45** could be properly purified, an initial SEHRS experiment was undertaken with the impure product and the spectra did not show much difference from rhodamine 6G. Based on theoretical calculations, it was determined that another pair of rhodamine isomers, **4.39** and **4.41**, would be more beneficial. Therefore, the synthetic targets were adjusted.

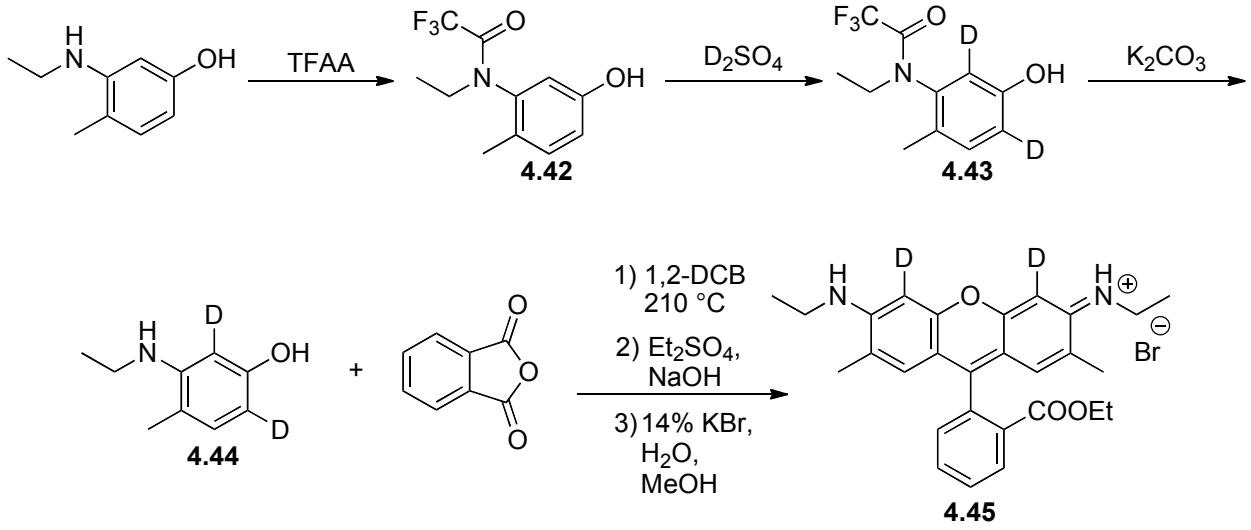


Figure 4.9. Previous synthetic rhodamine target.

4.3.1 Synthetic Procedures

Tetramethylrhodamine (4.39): To 3-(dimethylamino)-4-methylphenol (146 mg, 0.97 mmol) was added phthalic anhydride (72 mg, 0.48 mmol) and 1,2-dichlorobenzene (30 mL). A Dean-Stark trap was placed on the flask, tightly wrapped with glass wool and foil, and stirred at 220 °C overnight. The next day, the reaction was cooled to room temperature, and sodium hydroxide (19 mg, 0.48 mmol) and diethylsulfate (88 µL, 0.67 mmol) were added. The reaction was heated to 110 °C and stirred overnight. The solvent was then removed under reduced pressure and the residue was purified by column chromatography on silica gel with a gradient of ethyl acetate/hexanes (25–100%). The collected product was then dried and then dissolved in ethanol (5 mL). Potassium bromide (10 mL, 14% solution) was added and the reaction mixture was stirred at rt overnight. The reaction mixture was concentrated and the rhodamine bromide salt was filtered to yield rhodamine **4.39** (30 mg).

^{1}H NMR (300 MHz, $CDCl_3$): δ = 8.30 (d, *J* = 9.0 Hz, 1H), 7.83–7.71 (m, 2H), 7.33 (d, *J* = 9.0 Hz, 1H), 7.09 (d, *J* = 9.0 Hz, 2H), 6.94–6.88 (m, 4H), 4.03 (q, *J* = 7.0 Hz, 2H), 3.34 (s, 12H), 1.01 (t, *J* = 7.5 Hz, 3H) ppm. MALDI-HRMS: calcd. for $C_{28}H_{31}N_2O_3$ $[M + H]^+$ 443.2335; found 443.2459.

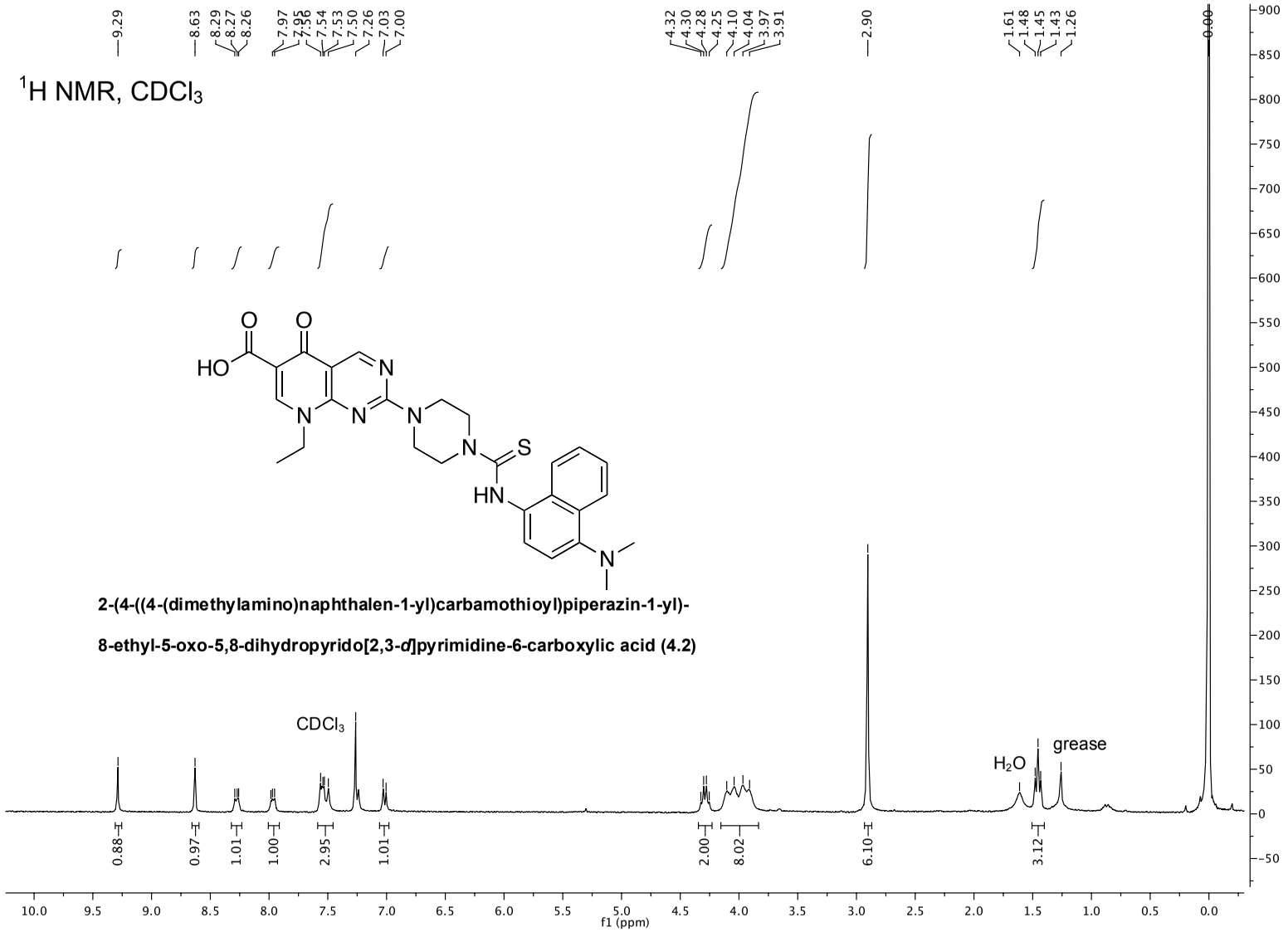
3-(Dimethyl-(d_6)-amino)-4-methylphenol (4.40): To 3-amino-4-methylphenol (200 mg, 1.62 mmol) dissolved in acetonitrile (10 mL) was added dimethyl sulfate-d_6 (154 µL, 1.624 mmol) and the reaction was stirred at rt overnight. The solvent was then removed and the residue purified by chromatography on silica gel with a gradient of ethyl acetate–hexanes (50–100%) to methanol–dichloromethane (3%) to afford **4.40** (98 mg, 38%).

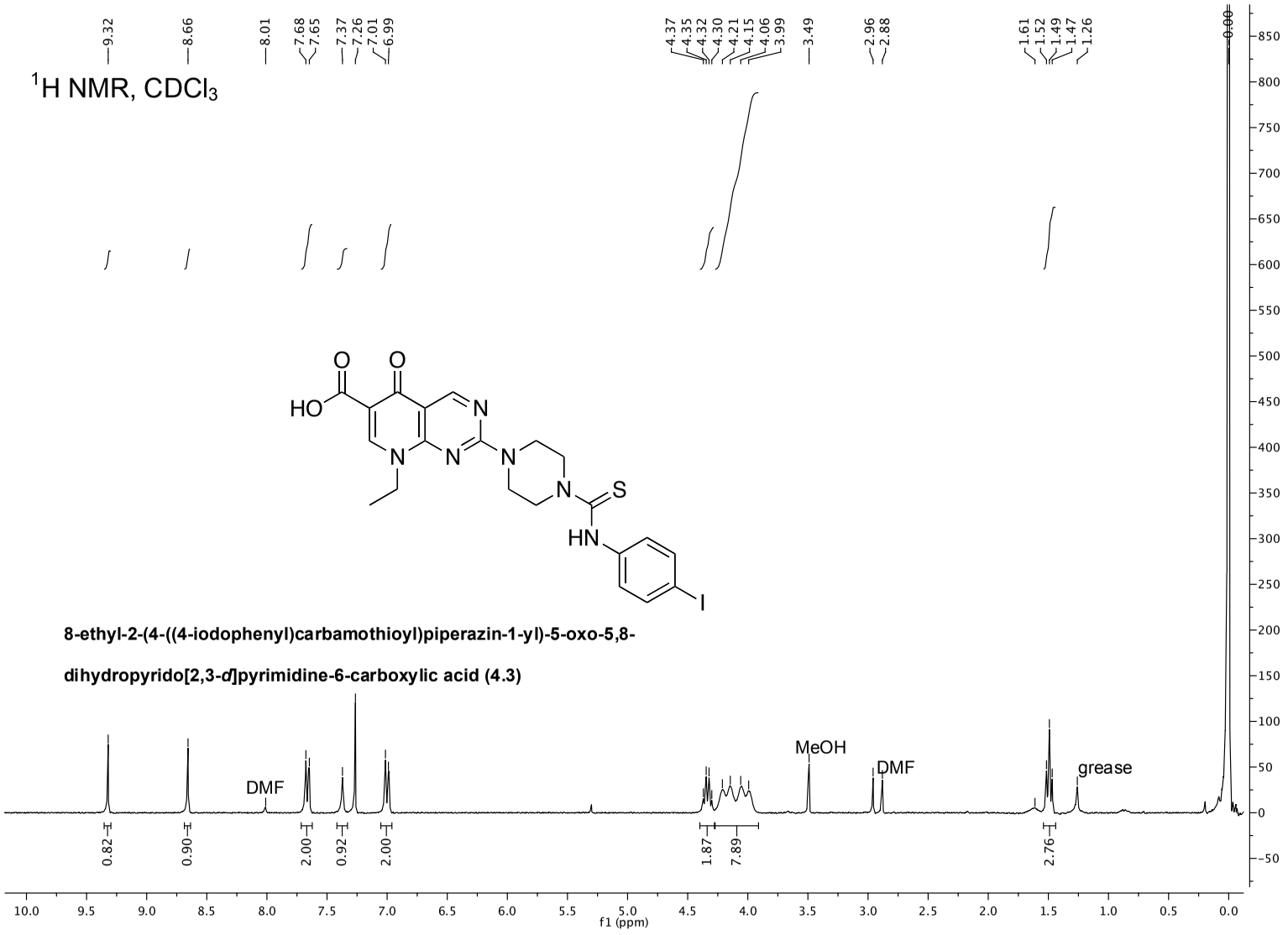
^{1}H NMR (500 MHz, $CDCl_3$): δ = 6.87–6.85 (m, 1H), 6.14 (s, 2H), 2.04 (s, 3H) ppm. ^{2}H NMR (500 MHz, $CDCl_3$:CD_3OD): δ = 2.79 (s, 6D) ppm. ^{13}C NMR (500 MHz, $CDCl_3$): δ = 155.74, 148.34, 130.43, 114.01, 103.37, 97.58, 77.37, 16.51 ppm. DART-HRMS: calcd. for $C_9H_7D_6NO$ $[M + H]^+$ 158.1448; found 158.1452.

***N*-Ethyl-2,2,2-trifluoro-*N*-(5-hydroxy-2-methylphenyl)acetamide (4.42):** To a round bottom flask was added 3-(ethylamino)-4-methylphenol (500 mg, 3.31 mmol) and cooled in an ice bath for 10 mins. Trifluoroacetic anhydride (1.18 mL, 8.47 mmol) was slowly added with stirring. After 3 h, the reaction mixture was concentrated and the resulting residue was purified by chromatography on silica gel with a gradient of ethyl acetate–hexanes (20–60%) to obtain the product **4.42** (496 mg, 61%).

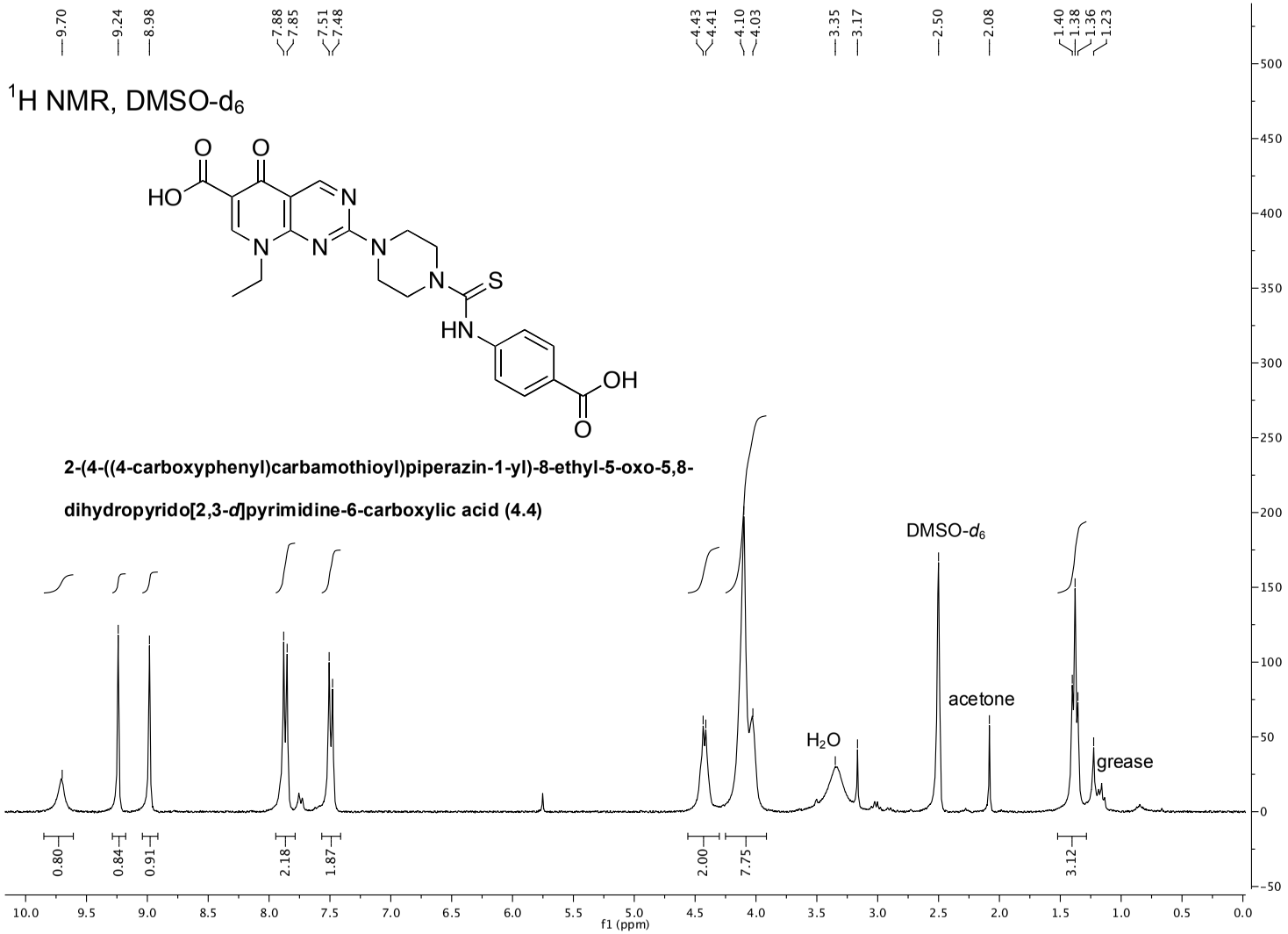
^{1}H NMR (300 MHz, $CDCl_3$): δ = 7.13 (t, *J* = 4.5 Hz, 1H), 6.88 (d, *J* = 8.3, 2.6 Hz, 1H), 6.69–6.66 (m, 1H), 4.25–4.13 (m, 1H), 3.23–3.19 (m, 1H), 2.12 (s, 3H), 1.18 (t, *J* = 7.2 Hz, 3H) ppm. ^{19}F NMR (272 MHz, $CDCl_3$): δ = -68.92 ppm.

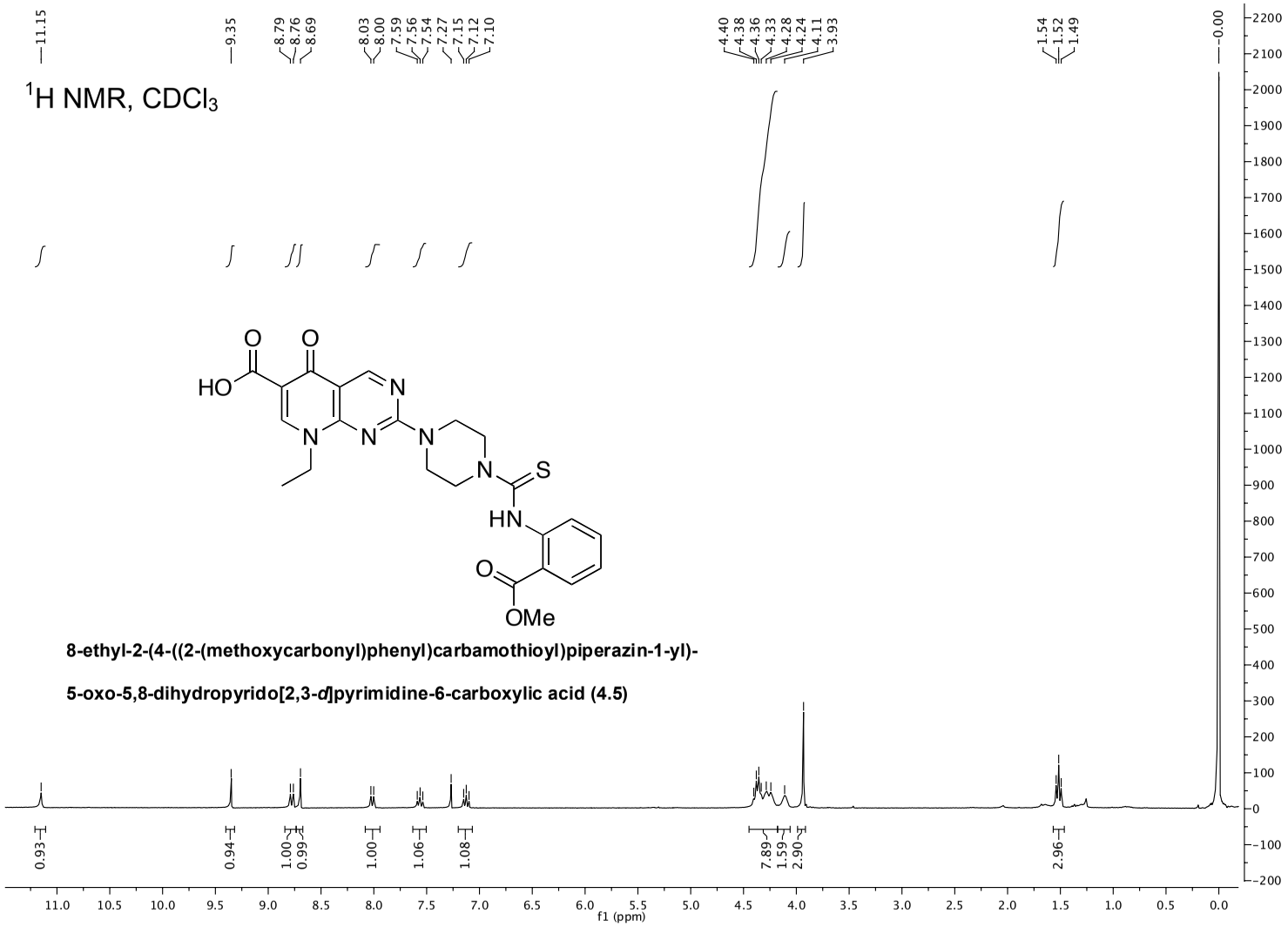
***N*-Ethyl-2,2,2-trifluoro-*N*-(4,6-dideutero-5-hydroxy-2-methylphenyl)acetamide (4.43):** To protected phenol **4.42** (2.13 g, 8.62 mmol) was added methylene chloride (5 mL) and sulfuric acid-d_2 (5 mL) and stirred at rt overnight. The resulting product was poured onto a solution of saturated sodium carbonate (100 mL) and brought to pH 7 with conc. sulfuric acid. The mixture was then extracted with methylene chloride (2 x 40 mL). The organic layers were combined, dried over magnesium sulfate, filtered, and concentrated. The resulting deuterated product **4.43** (1.08 g, 50%) was used without further purification. ^{1}H NMR (300 MHz, $CDCl_3$): δ = 7.12 (d, *J* = 8.5 Hz, 1H), 6.86 (dd, *J* = 8.4 Hz, 0.25H, residual H not exchanged for D), 6.69 (s, 0.25H, residual H not exchanged for D), 4.27–4.16 (m, 1H), 3.24–3.12 (m, 1H), 2.14 (s, 3H), 1.19 (t, *J* = 7.2 Hz, 3H) ppm. ^{19}F NMR (272 MHz, $CDCl_3$): δ = -68.91 ppm. ^{13}C NMR (75 MHz, $CDCl_3$): δ = 157.86, 157.38, 156.91, 156.44, 154.43, 137.52, 131.87, 126.93, 121.96, 118.14, 116.77, 116.39, 114.33, 110.51, 77.10, 46.07, 16.53, 11.74 ppm.


^{1}H NMR, $CDCl_3$
9.29
8.63
8.29
8.27
8.26
7.97
7.95
7.56
7.54
7.53
7.50
7.26
7.03
7.00
4.32
4.30
4.28
4.25
4.10
4.04
3.97
3.91
2.90
1.61
1.48
1.45
1.43
1.26
0.00
HO
O
O
N
N
N
N
N
S
HN
N
2-(4-((4-(dimethylamino)naphthalen-1-yl)carbamothioyl)piperazin-1-yl)-
8-ethyl-5-oxo-5,8-dihydropyrido[2,3-d]pyrimidine-6-carboxylic acid (4.2)
$CDCl_3$
H_2O
grease
0.88
0.97
1.01
1.00
2.95
1.01
2.00
8.02
6.10
3.12
f1 (ppm)

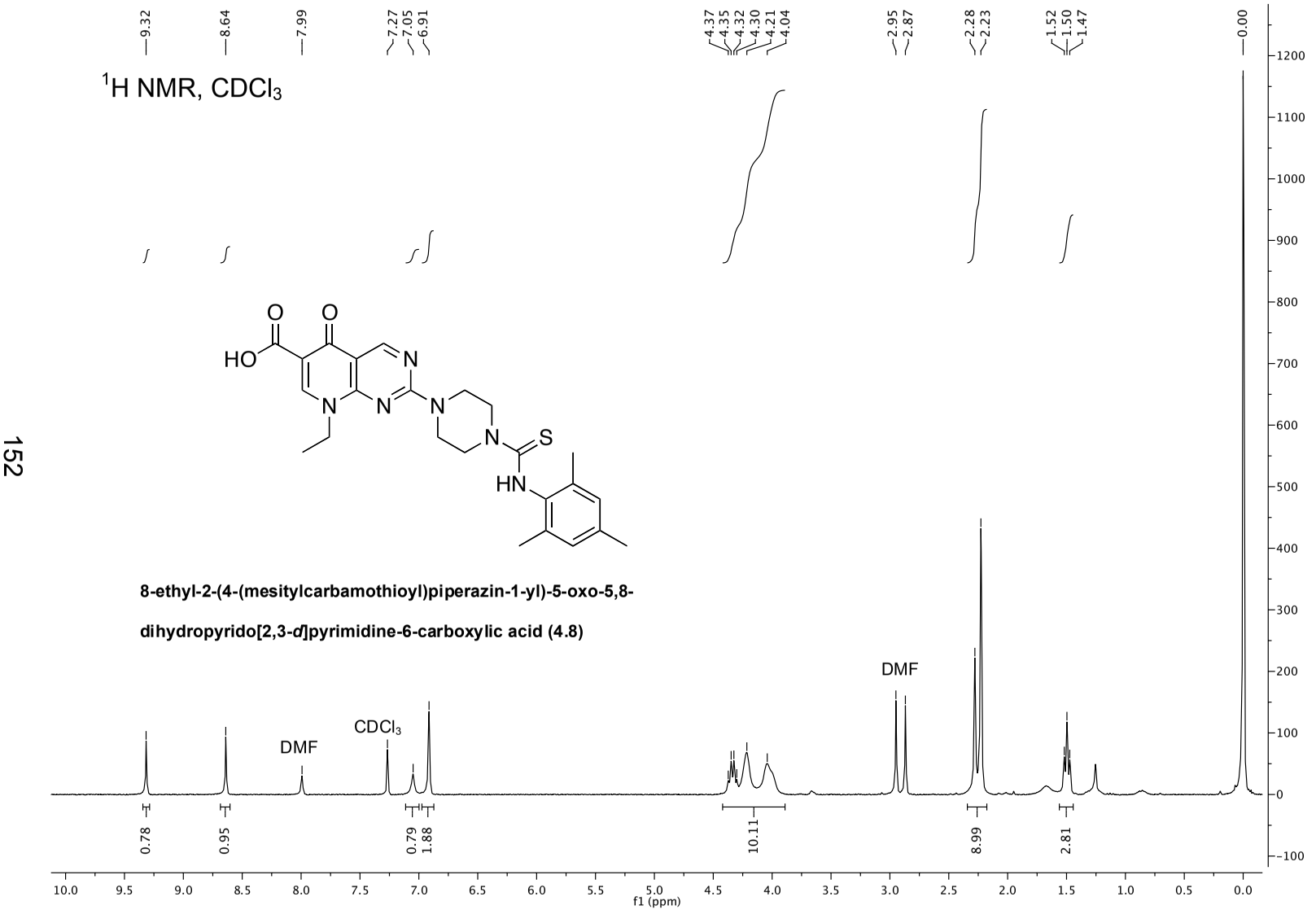


8-ethyl-2-(4-((4-iodophenyl)carbamothioyl)piperazin-1-yl)-5-oxo-5,8-dihydropyrido[2,3-*d*]pyrimidine-6-carboxylic acid (4.3)

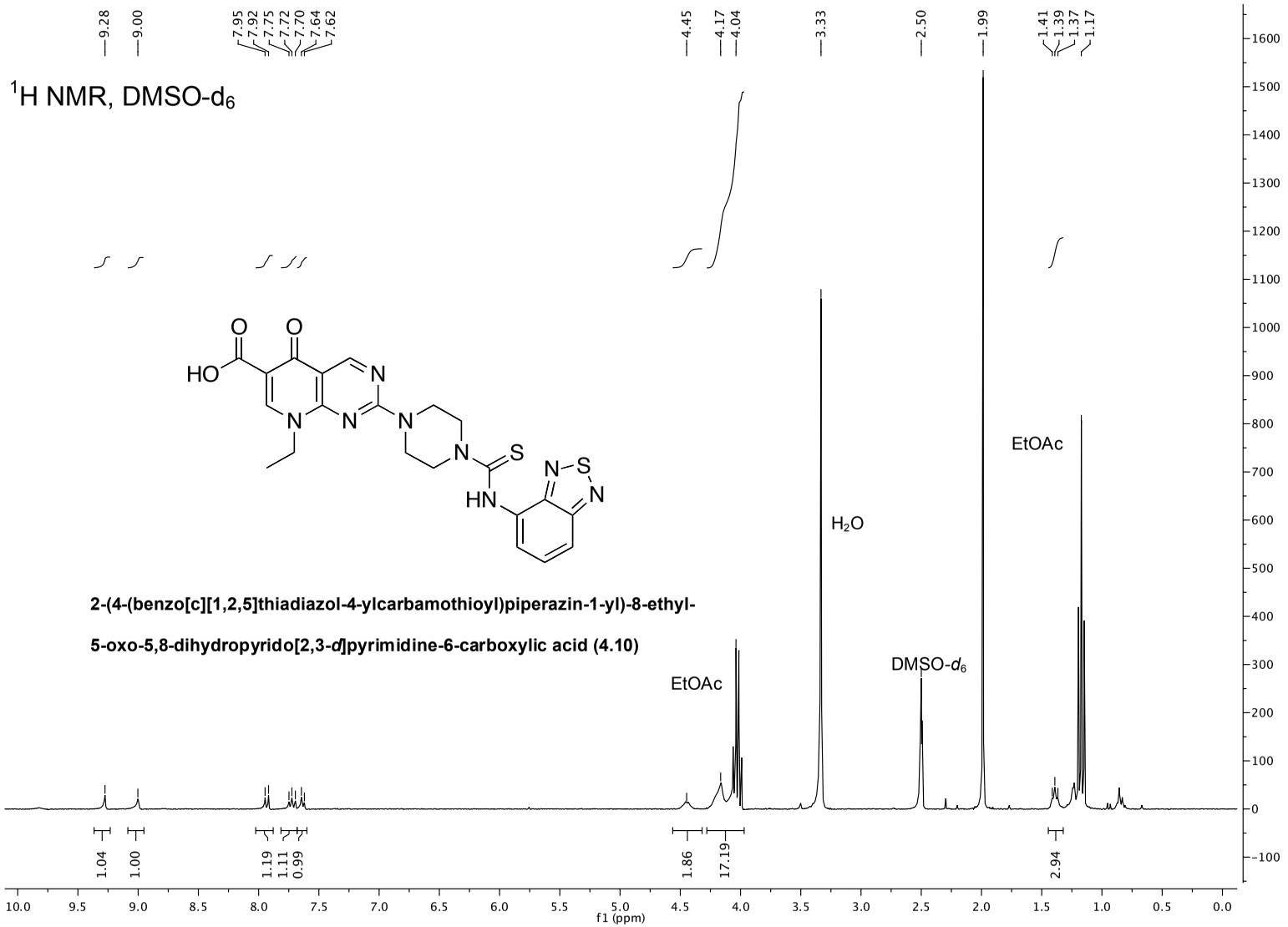

9.70
9.24
8.98
7.88
7.85
7.51
7.48
4.43
4.41
4.10
4.03
3.35
3.17
2.50
2.08
1.40
1.38
1.36
1.23
^{1}H NMR, DMSO-d$_6$
HO
O
O
N
N
N
N
N
S
HN
OH
O
2-(4-((4-carboxyphenyl)carbamothioyl)piperazin-1-yl)-8-ethyl-5-oxo-5,8-dihydropyrido[2,3-*d*]pyrimidine-6-carboxylic acid (4.4)
DMSO-d_6
acetone
H_2O
grease
0.80
0.84
0.91
2.18
1.87
2.00
7.75
3.12
f1 (ppm)



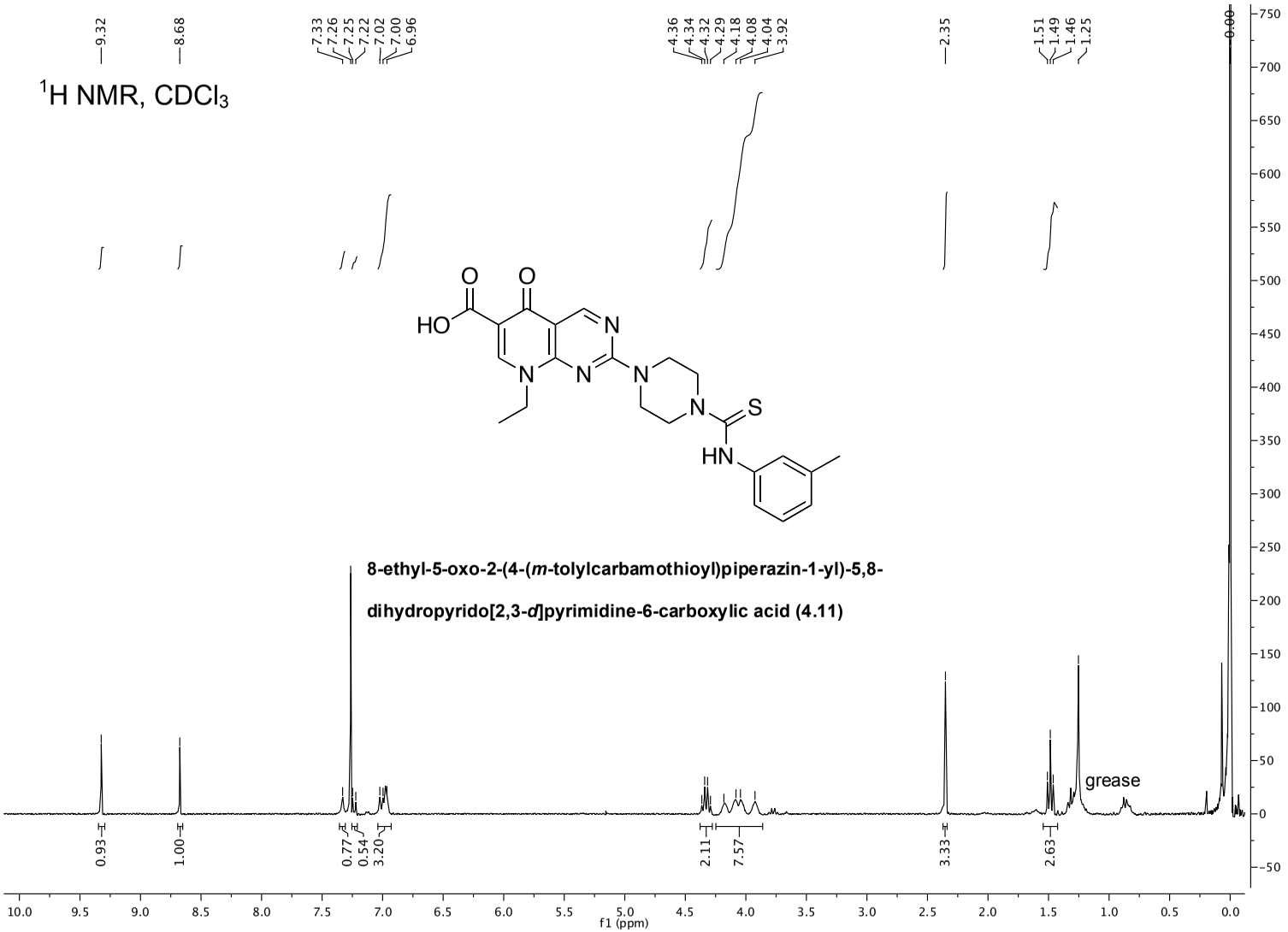
8-ethyl-2-(4-((2-(methoxycarbonyl)phenyl)carbamothioyl)piperazin-1-yl)-5-oxo-5,8-dihydropyrido[2,3-*d*]pyrimidine-6-carboxylic acid (4.5)

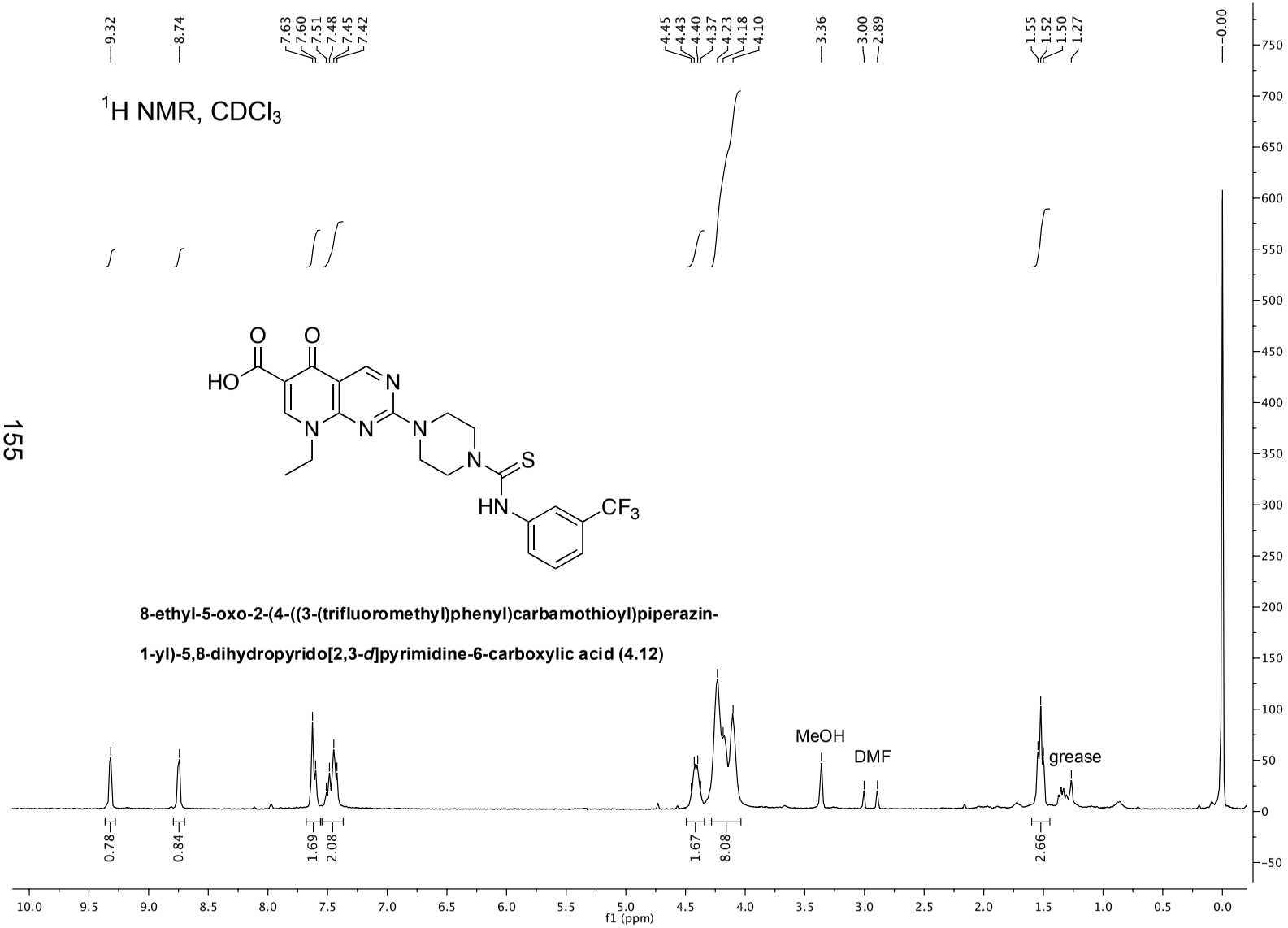


8-ethyl-2-(4-(mesitylcarbamothioyl)piperazin-1-yl)-5-oxo-5,8-dihydropyrido[2,3-*d*]pyrimidine-6-carboxylic acid (4.8)

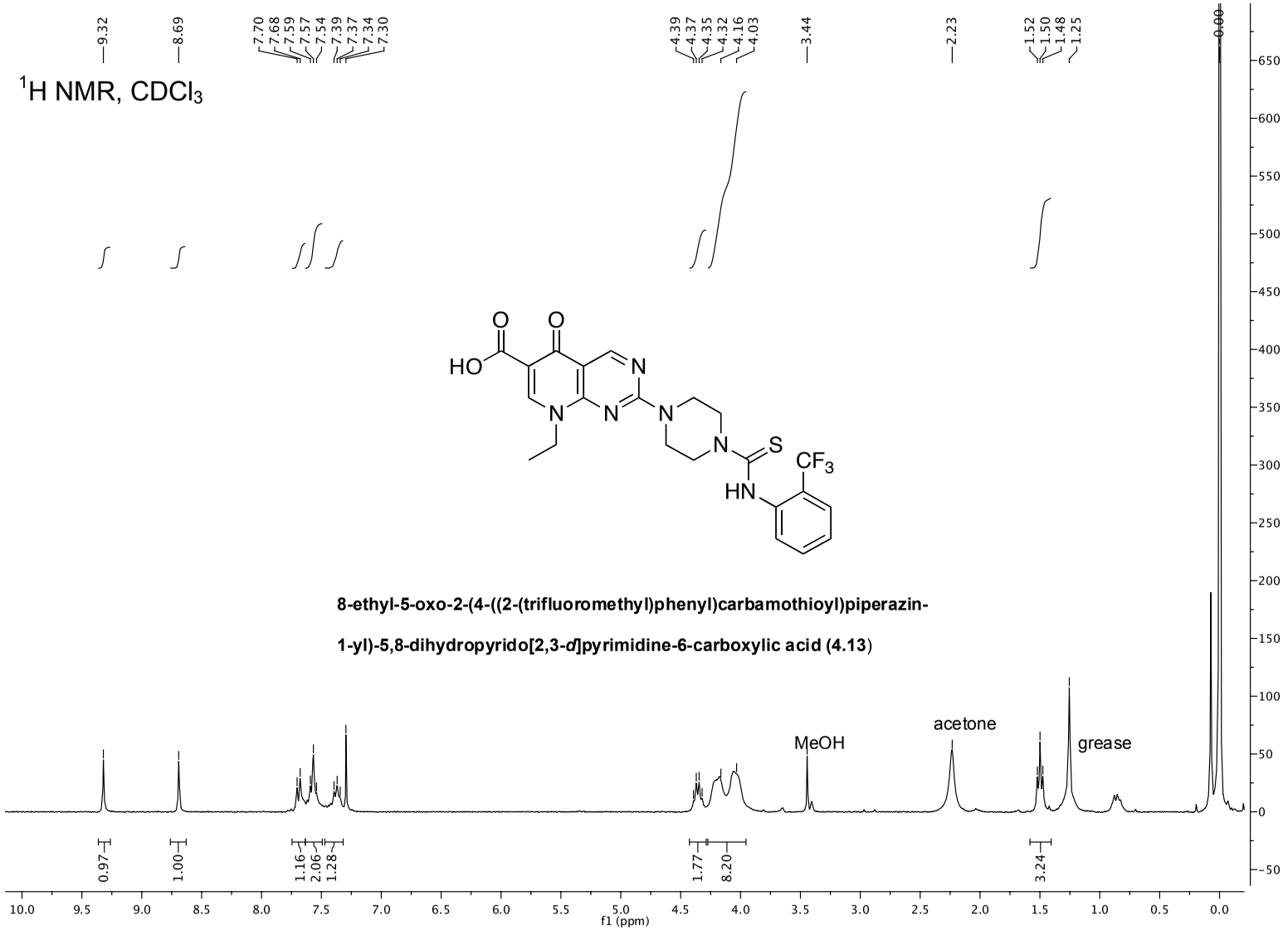


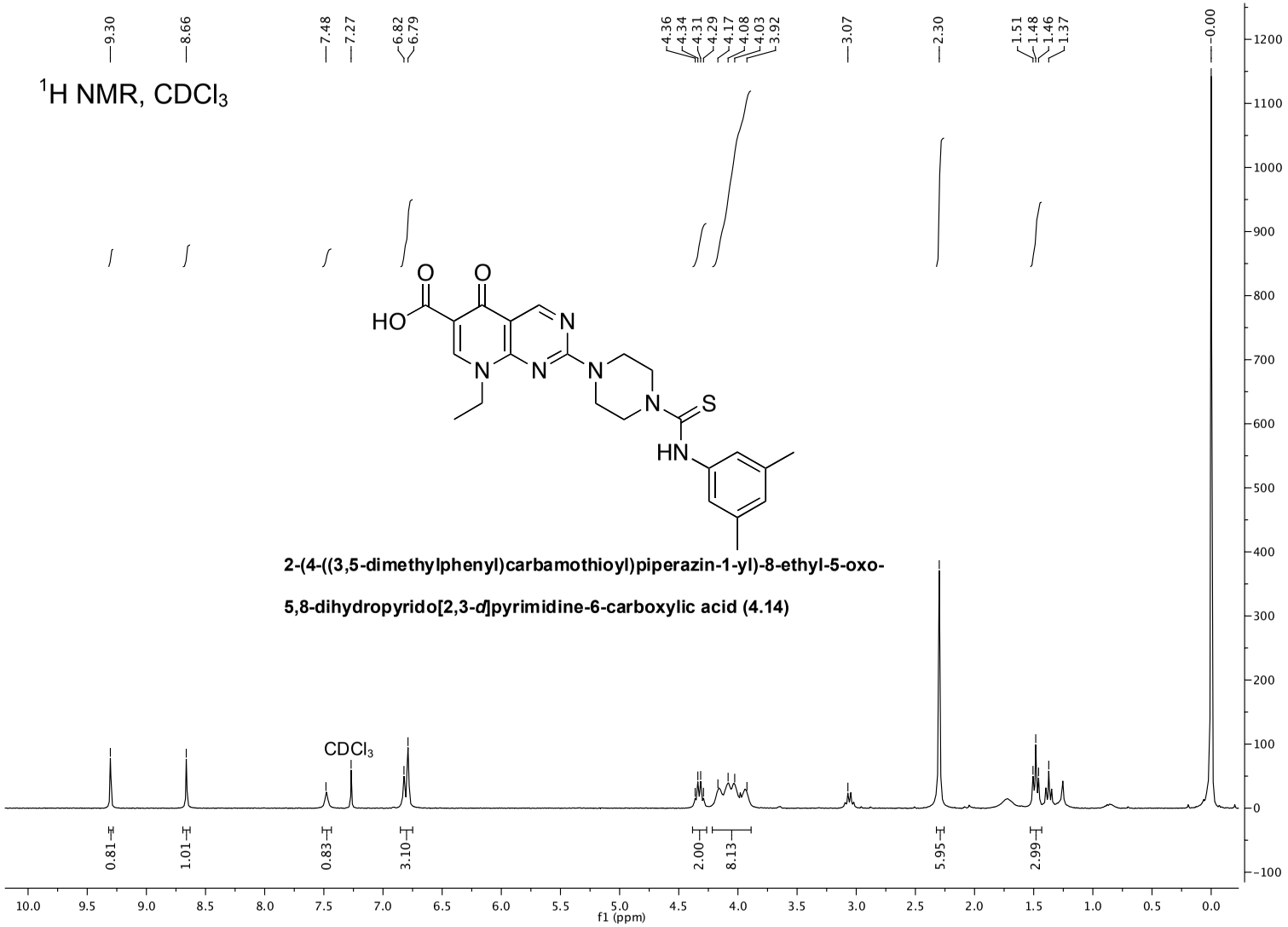
2-(4-(benzo[c][1,2,5]thiadiazol-4-ylcarbamothioyl)piperazin-1-yl)-8-ethyl-5-oxo-5,8-dihydropyrido[2,3-*d*]pyrimidine-6-carboxylic acid (4.10)


^{1}H NMR, $CDCl_3$
9.32
8.68
7.33
7.26
7.25
7.22
7.02
7.00
6.96
4.36
4.34
4.32
4.29
4.18
4.08
4.04
3.92
2.35
1.51
1.49
1.46
1.25
0.00
HO
O
O
N
N
N
N
N
S
HN
8-ethyl-5-oxo-2-(4-(*m*-tolylcarbamothioyl)piperazin-1-yl)-5,8-dihydropyrido[2,3-*d*]pyrimidine-6-carboxylic acid (4.11)
grease
0.93
1.00
0.77
0.54
3.20
2.11
7.57
3.33
2.63
f1 (ppm)

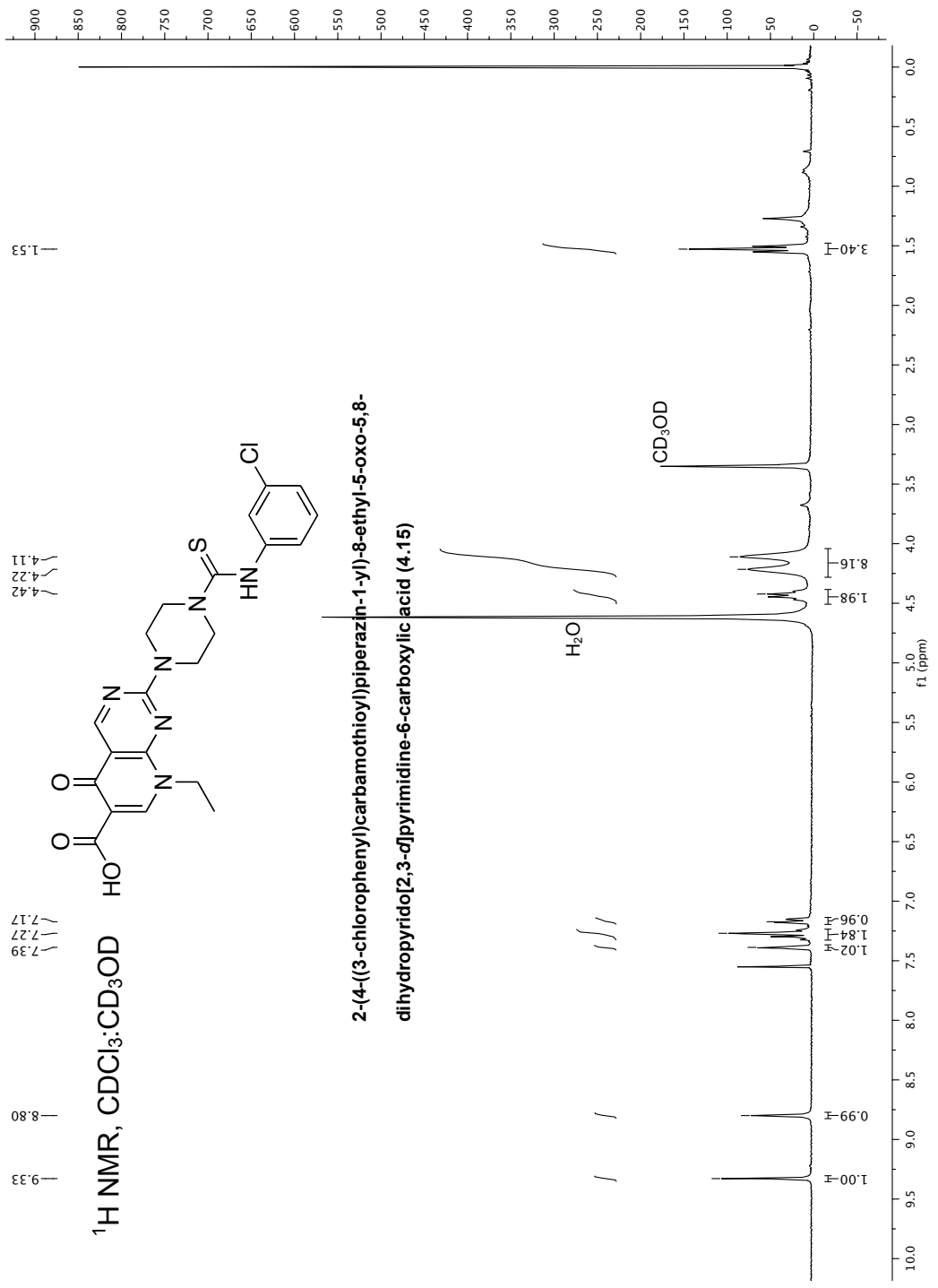


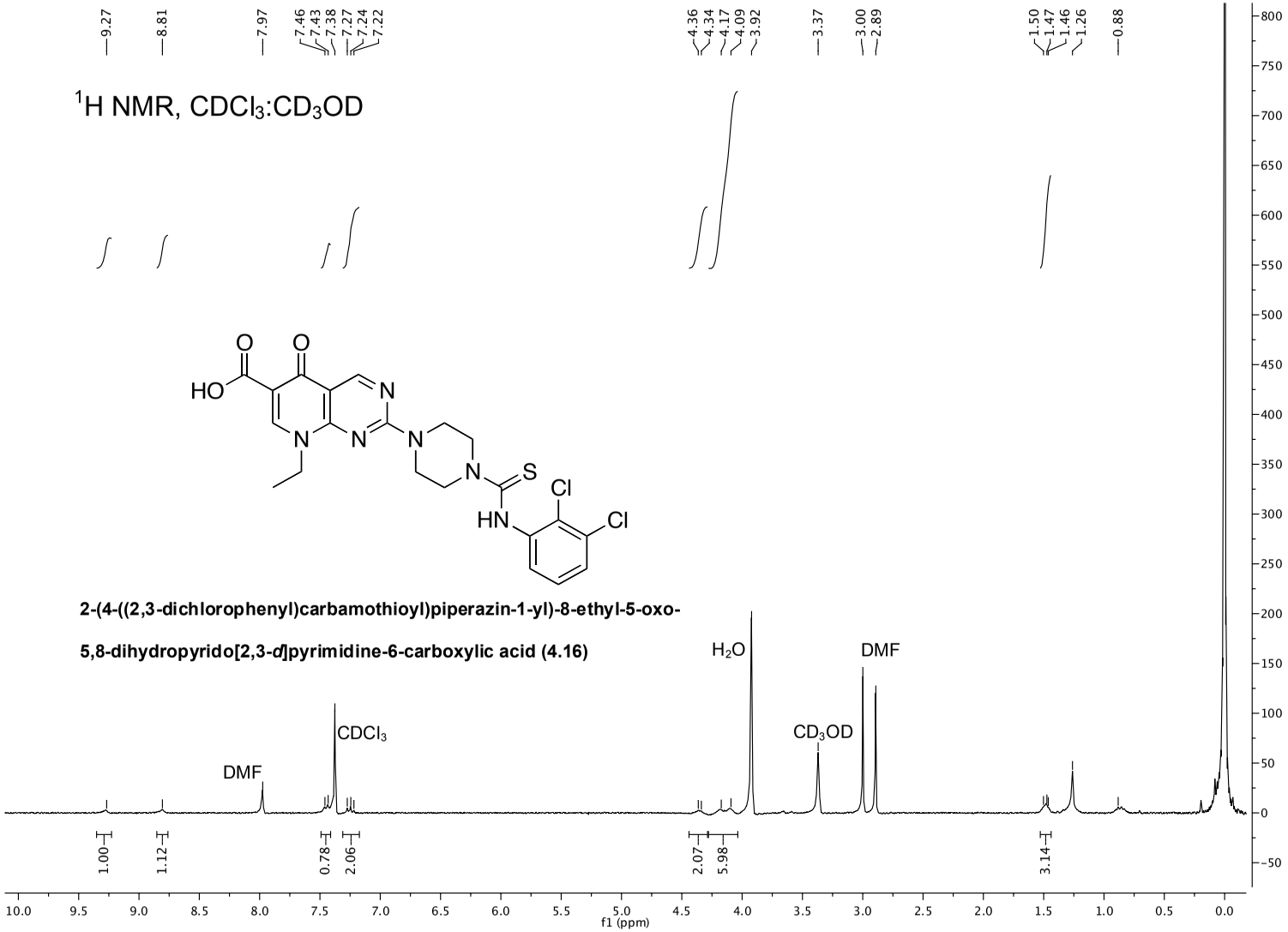
8-ethyl-5-oxo-2-(4-((3-(trifluoromethyl)phenyl)carbamothioyl)piperazin-1-yl)-5,8-dihydropyrido[2,3-*d*]pyrimidine-6-carboxylic acid (4.12)

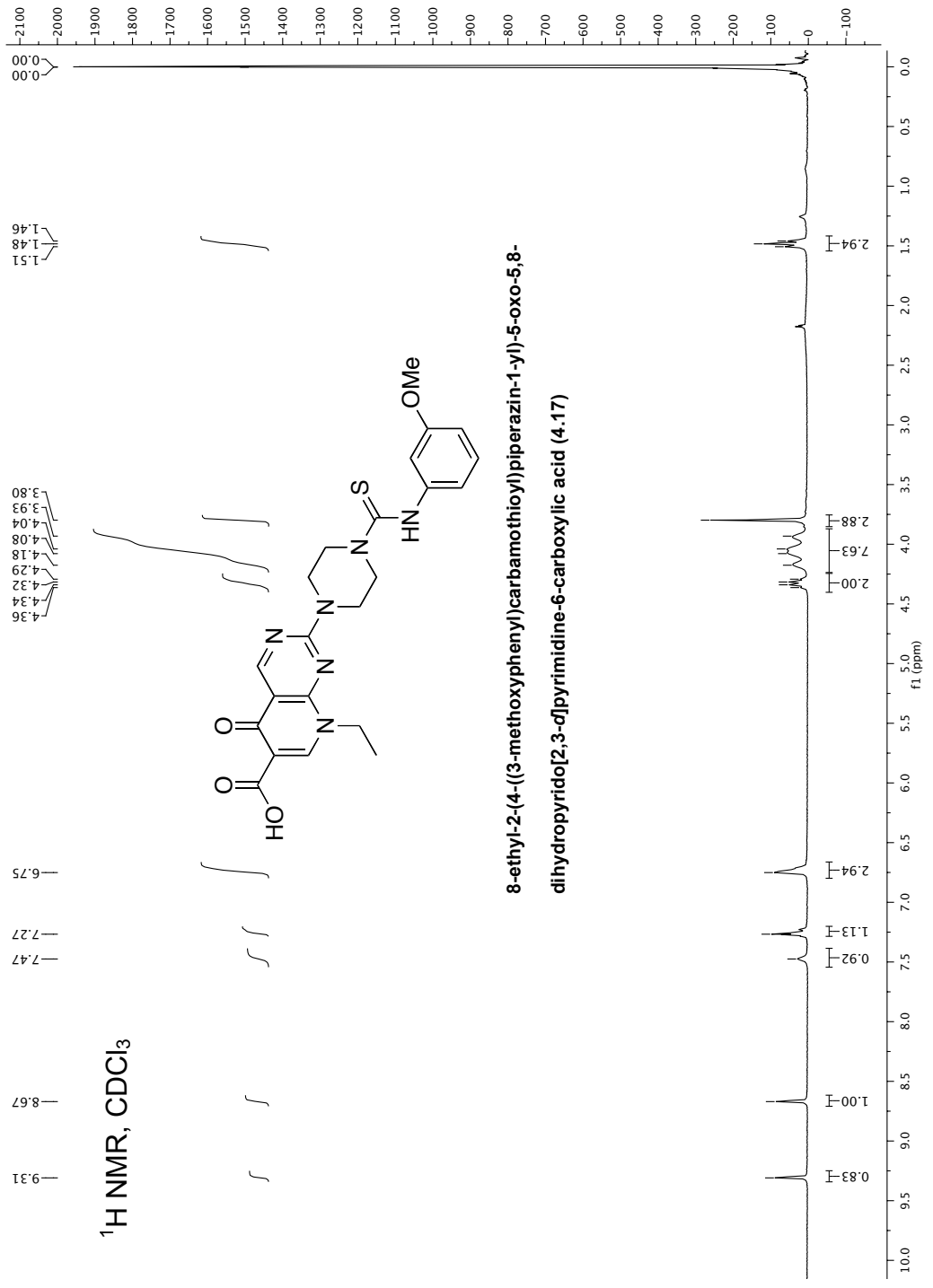

^{1}H NMR, CDCl$_3$
9.32
8.69
7.70
7.68
7.59
7.57
7.54
7.39
7.37
7.34
7.30
4.39
4.37
4.35
4.32
4.16
4.03
3.44
2.23
1.52
1.50
1.48
1.25
0.00
HO
O
O
N
N
N
N
N
S
CF$_3$
HN
8-ethyl-5-oxo-2-(4-((2-(trifluoromethyl)phenyl)carbamothioyl)piperazin-1-yl)-5,8-dihydropyrido[2,3-*d*]pyrimidine-6-carboxylic acid (4.13)
MeOH
acetone
grease
0.97
1.00
1.16
2.06
1.28
1.77
8.20
3.24
f1 (ppm)

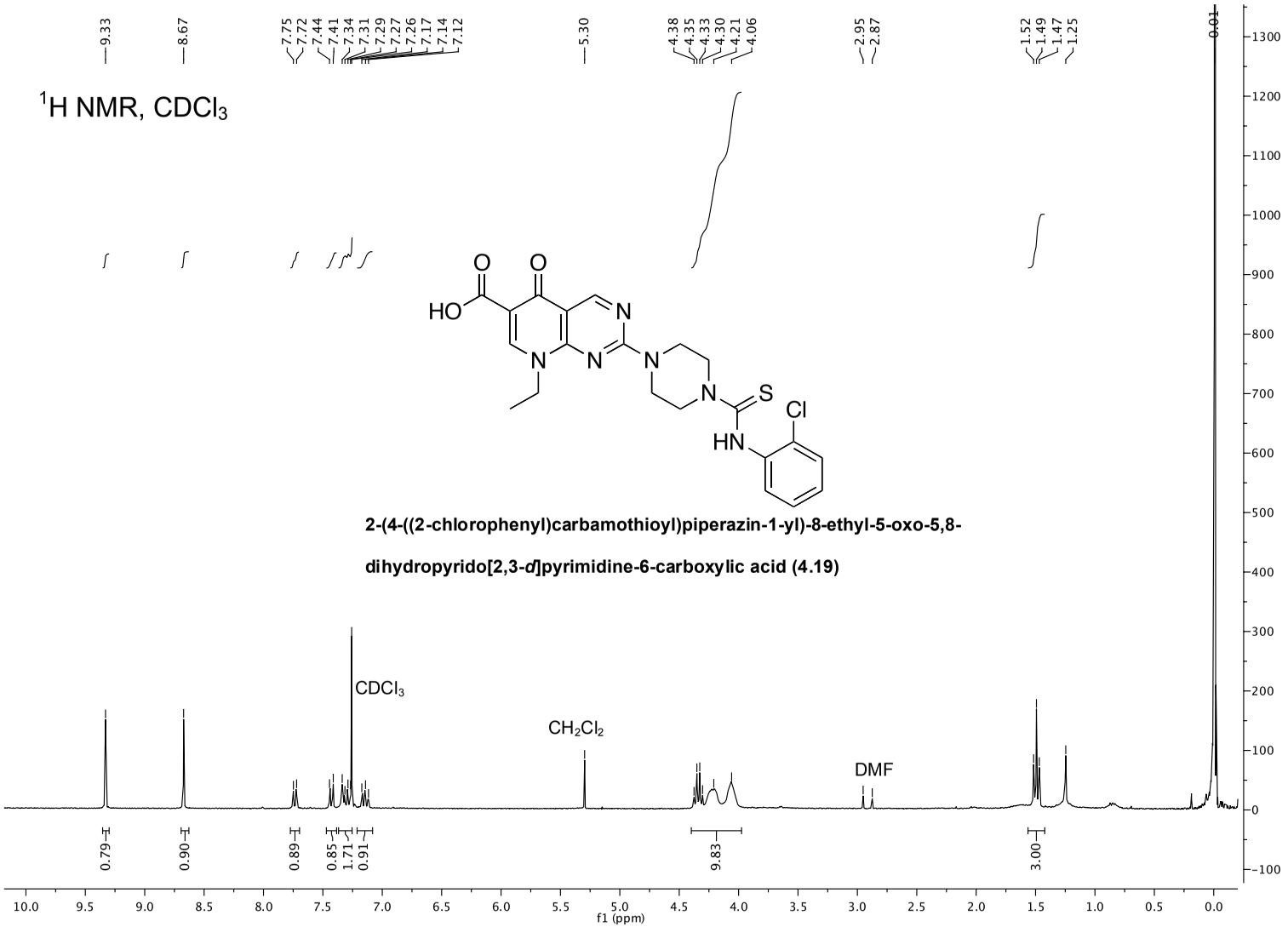


2-(4-((3,5-dimethylphenyl)carbamothioyl)piperazin-1-yl)-8-ethyl-5-oxo-5,8-dihydropyrido[2,3-*d*]pyrimidine-6-carboxylic acid (4.14)

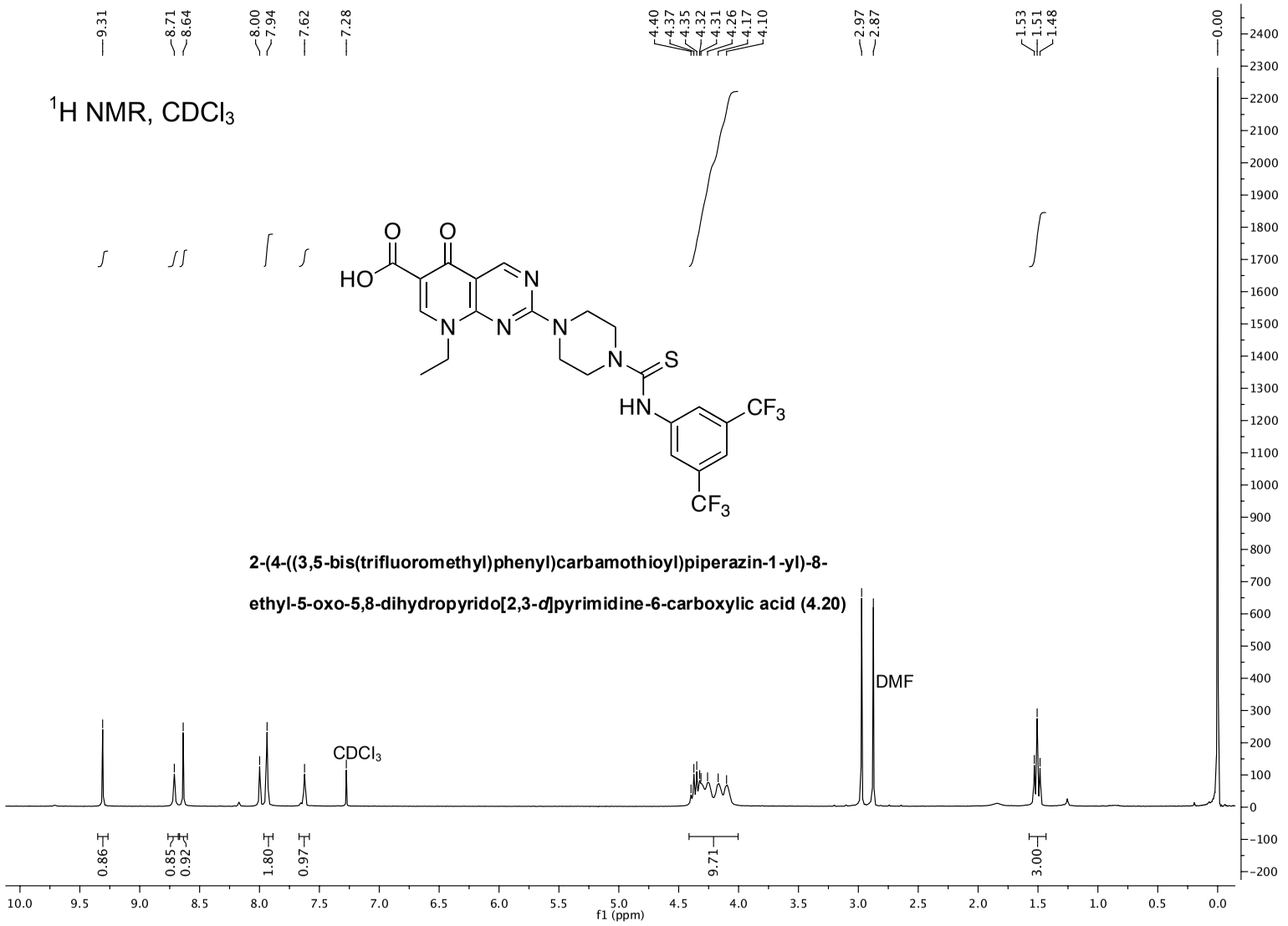

^{1}H NMR, $CDCl_3$:CD_3OD
2-(4-((3-chlorophenyl)carbamothioyl)piperazin-1-yl)-8-ethyl-5-oxo-5,8-dihydropyrido[2,3-d]pyrimidine-6-carboxylic acid (4.15)
H_2O
CD_3OD
f1 (ppm)

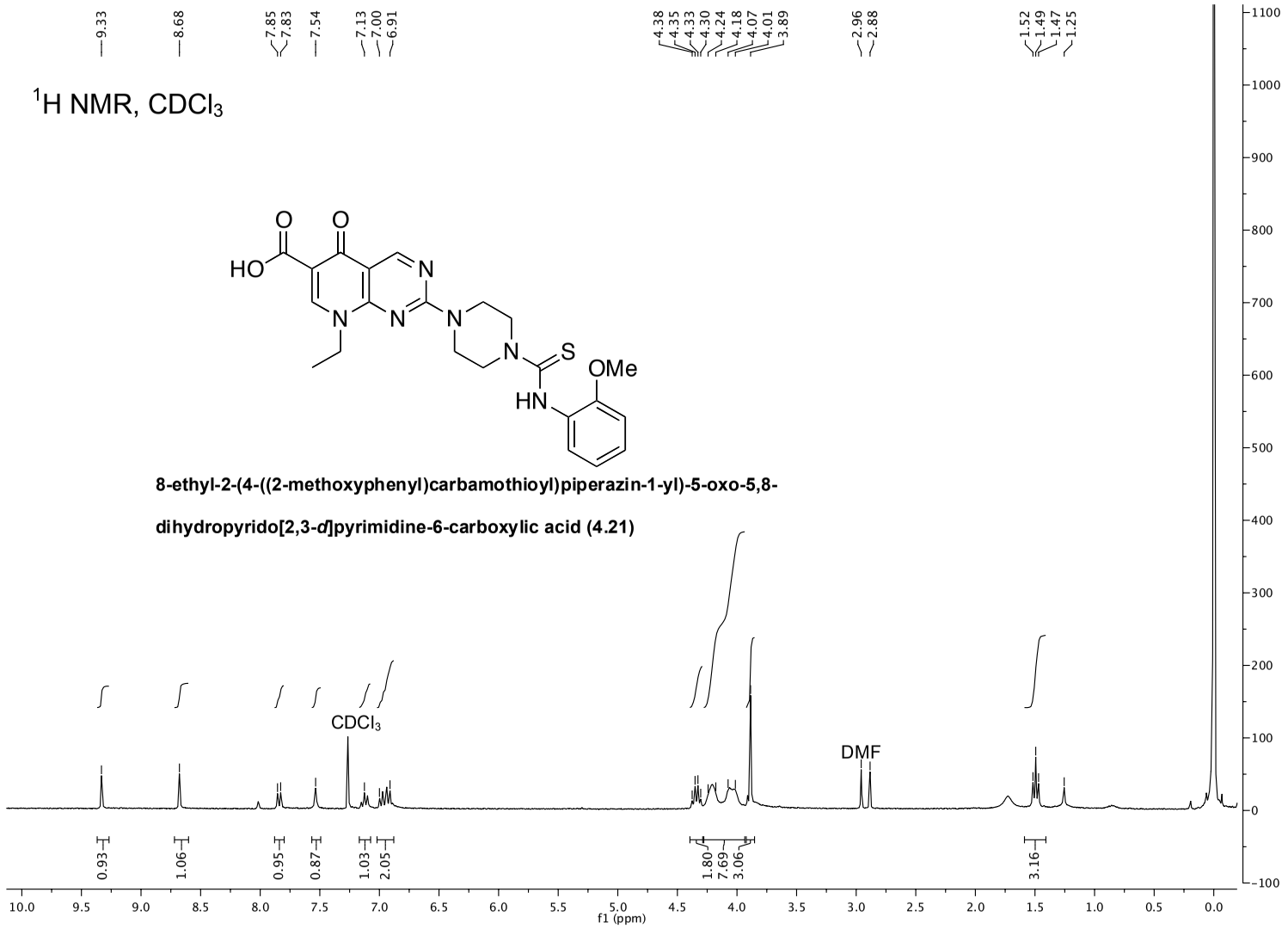

9.27
8.81
7.97
7.46
7.43
7.38
7.27
7.24
7.22
4.36
4.34
4.17
4.09
3.92
3.37
3.00
2.89
1.50
1.47
1.46
1.26
0.88
^{1}H NMR, $CDCl_3$:CD_3OD
O
O
HO
N
N
N
N
N
S
HN
Cl
Cl
2-(4-((2,3-dichlorophenyl)carbamothioyl)piperazin-1-yl)-8-ethyl-5-oxo-
5,8-dihydropyrido[2,3-d]pyrimidine-6-carboxylic acid (4.16)
DMF
$CDCl_3$
H_2O
CD_3OD
DMF
1.00
1.12
0.78
2.06
2.07
5.98
3.14
f1 (ppm)

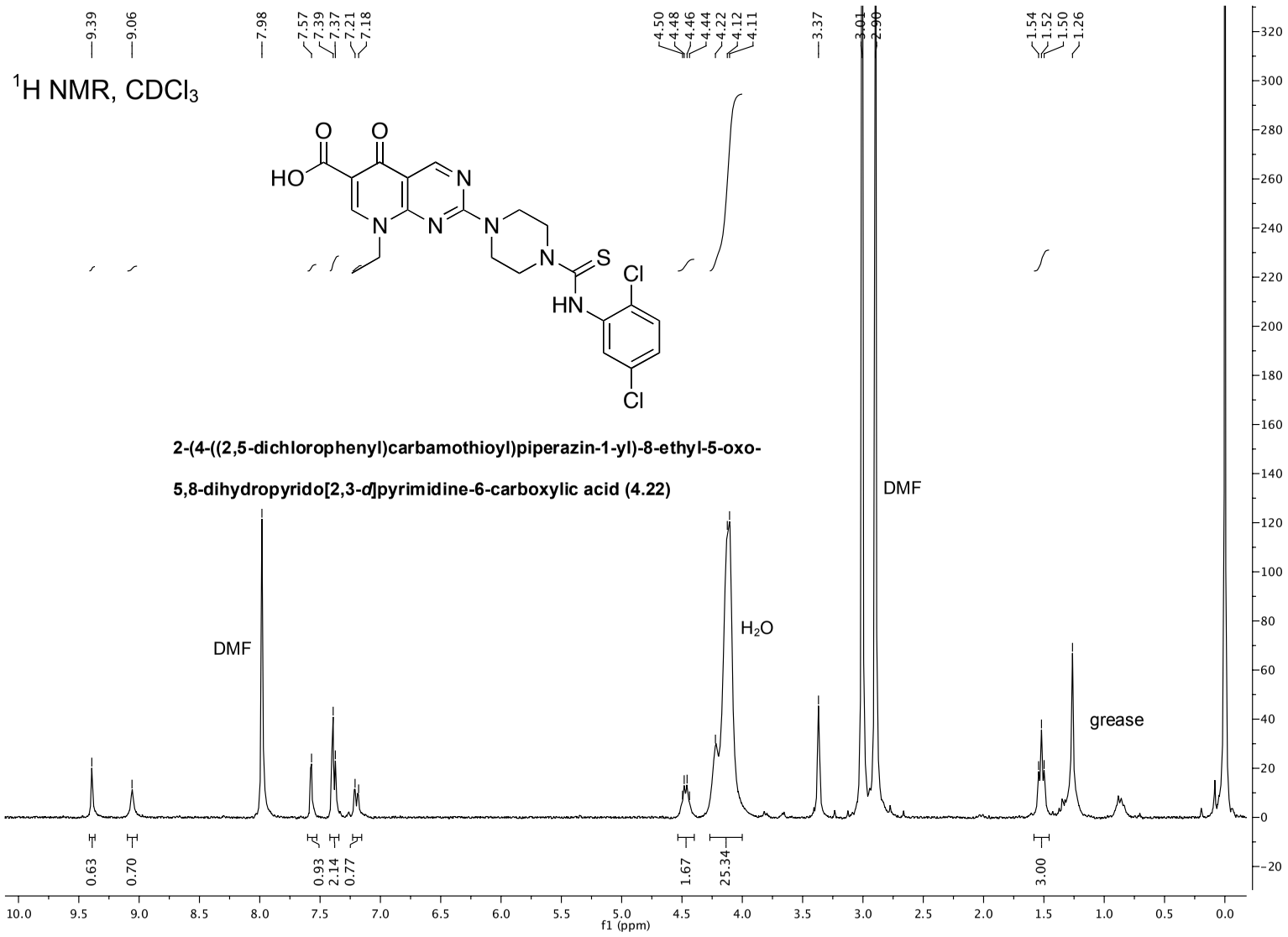

1H NMR, CDCl3
8-ethyl-2-(4-((3-methoxyphenyl)carbamothioyl)piperazin-1-yl)-5-oxo-5,8-dihydropyrido[2,3-d]pyrimidine-6-carboxylic acid (4.17)
f1 (ppm)

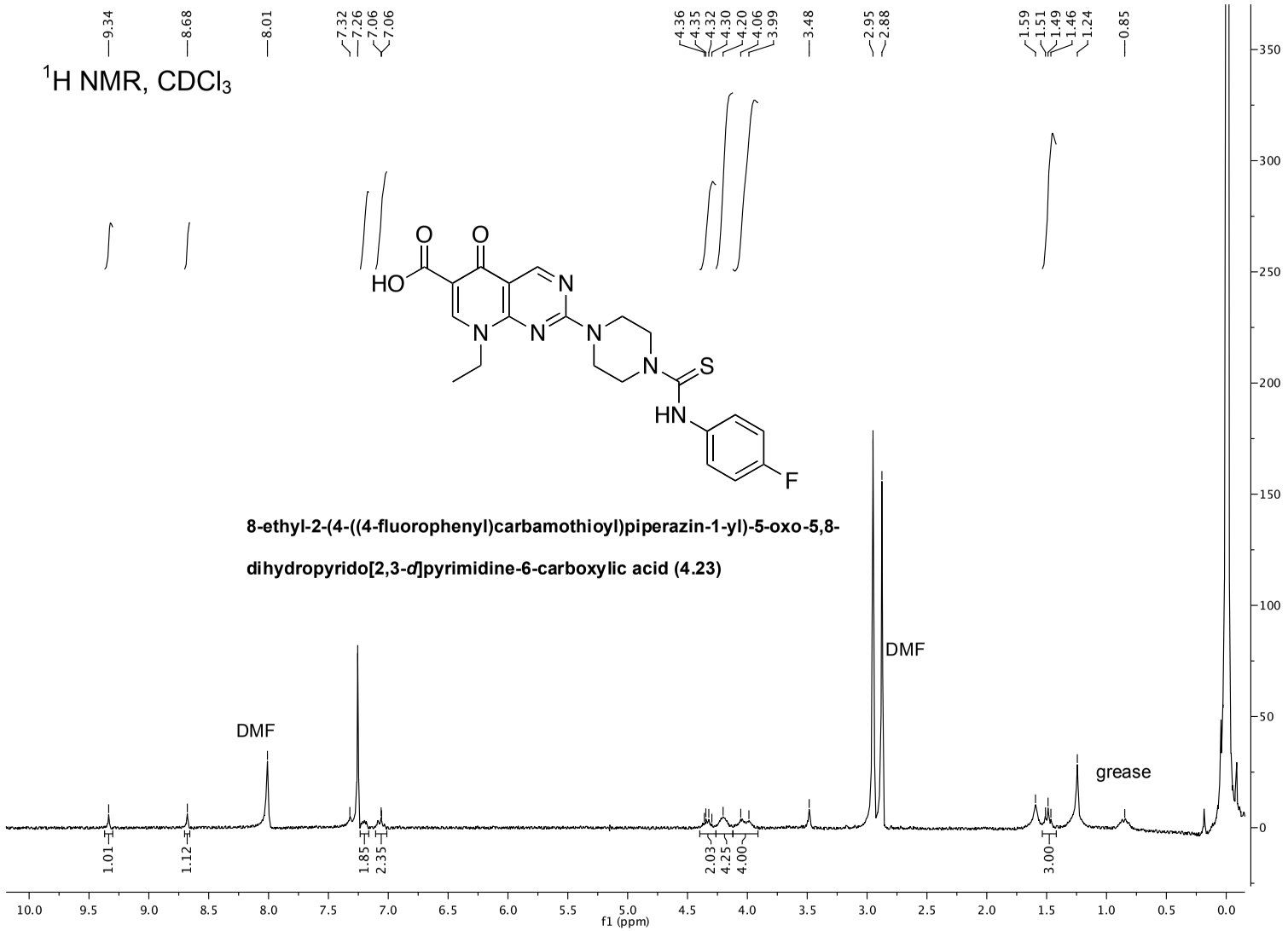


2-(4-((2-chlorophenyl)carbamothioyl)piperazin-1-yl)-8-ethyl-5-oxo-5,8-dihydropyrido[2,3-*d*]pyrimidine-6-carboxylic acid (4.19)

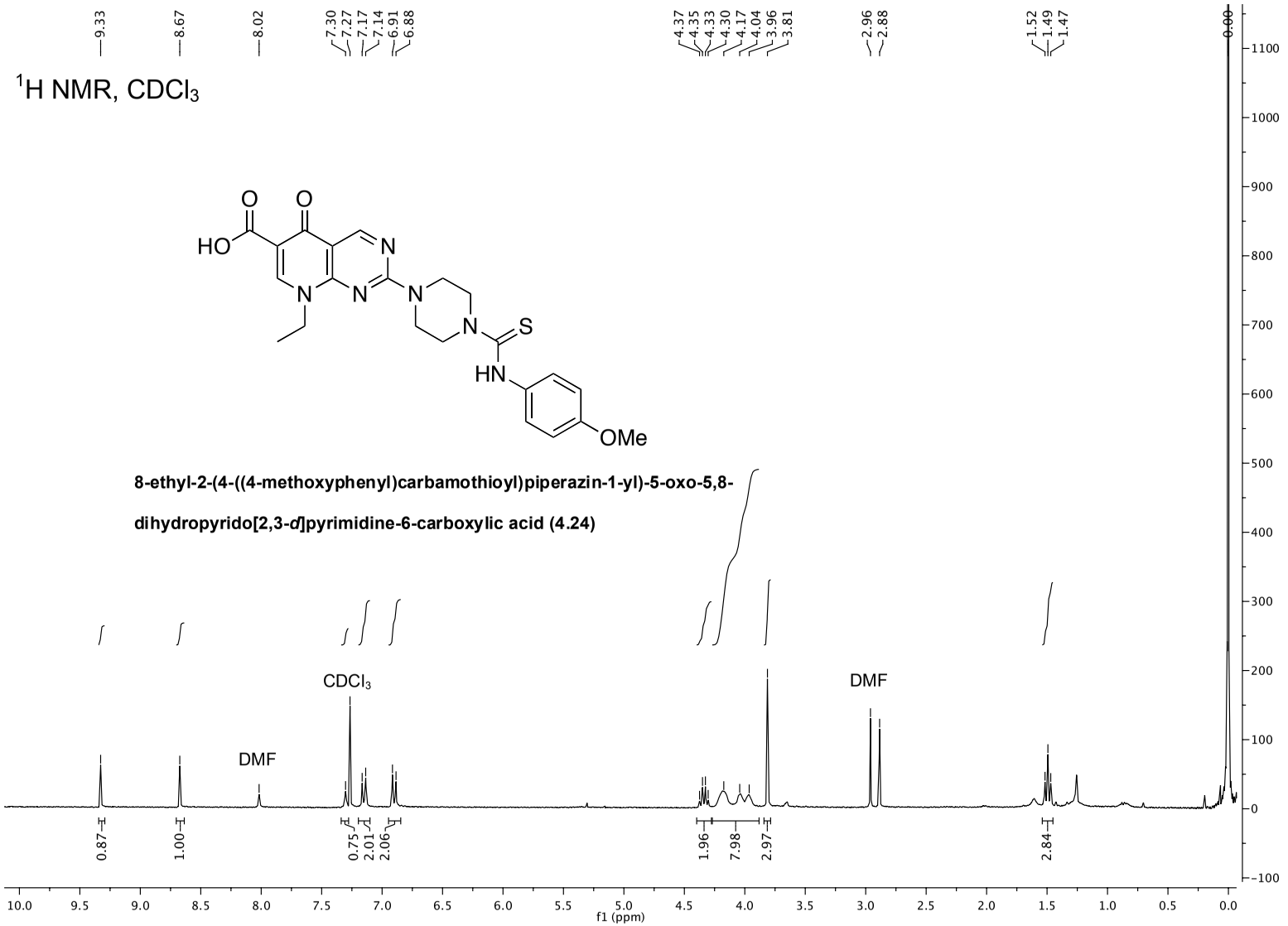

^{1}H NMR, $CDCl_3$
9.31
8.71
8.64
8.00
7.94
7.62
7.28
4.40
4.37
4.35
4.32
4.31
4.26
4.17
4.10
2.97
2.87
1.53
1.51
1.48
0.00
HO
O
O
N
N
N
N
N
S
HN
CF_3
CF_3
2-(4-((3,5-bis(trifluoromethyl)phenyl)carbamothioyl)piperazin-1-yl)-8-ethyl-5-oxo-5,8-dihydropyrido[2,3-d]pyrimidine-6-carboxylic acid (4.20)
DMF
$CDCl_3$
0.86
0.85
0.92
1.80
0.97
9.71
3.00
f1 (ppm)

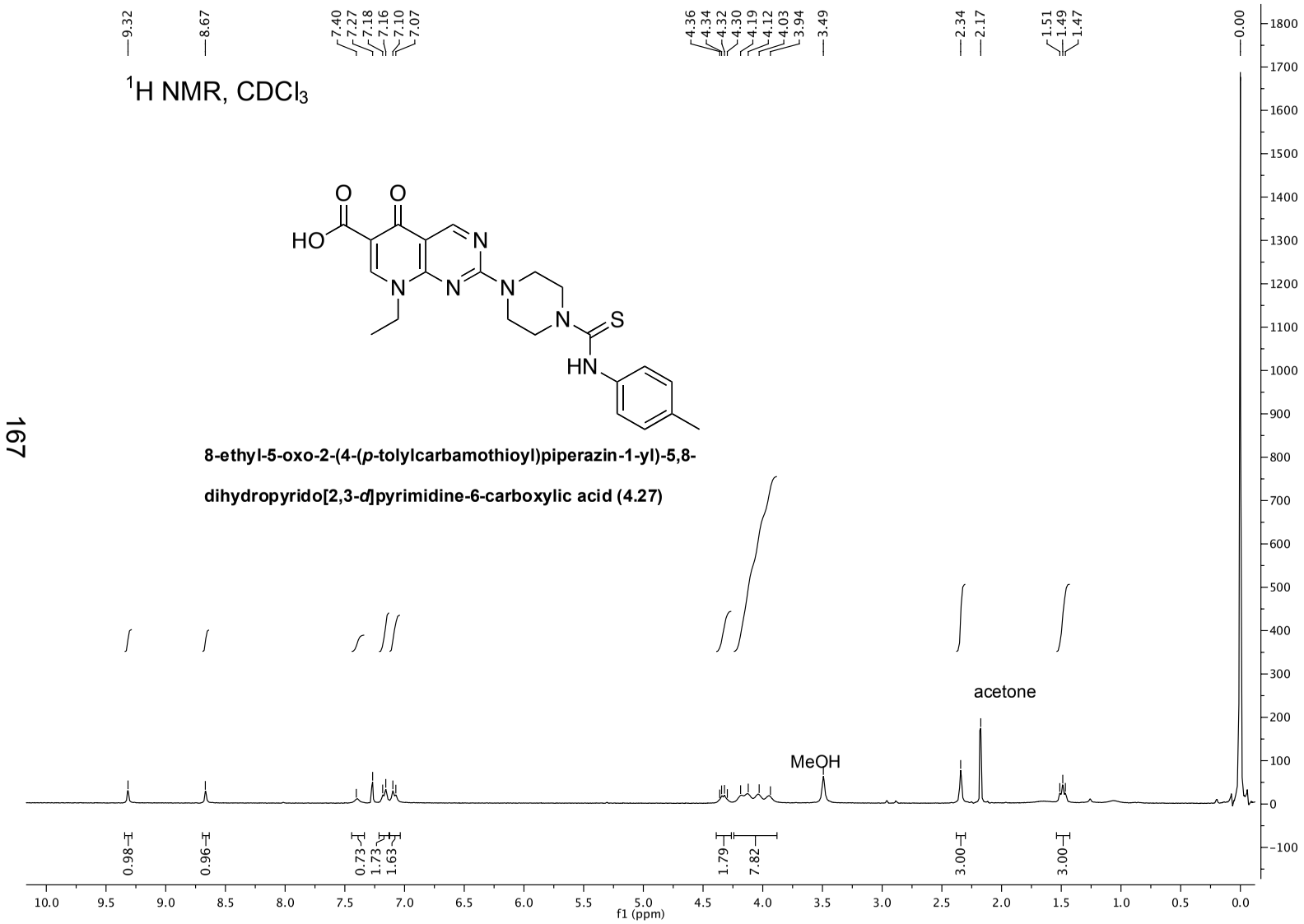

9.33
8.68
7.85
7.83
7.54
7.13
7.00
6.91
4.38
4.35
4.33
4.30
4.24
4.18
4.07
4.01
3.89
2.96
2.88
1.52
1.49
1.47
1.25
^{1}H NMR, $CDCl_3$
HO
O
O
N
N
N
N
N
S
OMe
HN
8-ethyl-2-(4-((2-methoxyphenyl)carbamothioyl)piperazin-1-yl)-5-oxo-5,8-dihydropyrido[2,3-*d*]pyrimidine-6-carboxylic acid (4.21)
$CDCl_3$
DMF
0.93
1.06
0.95
0.87
1.03
2.05
1.80
7.69
3.06
3.16
f1 (ppm)

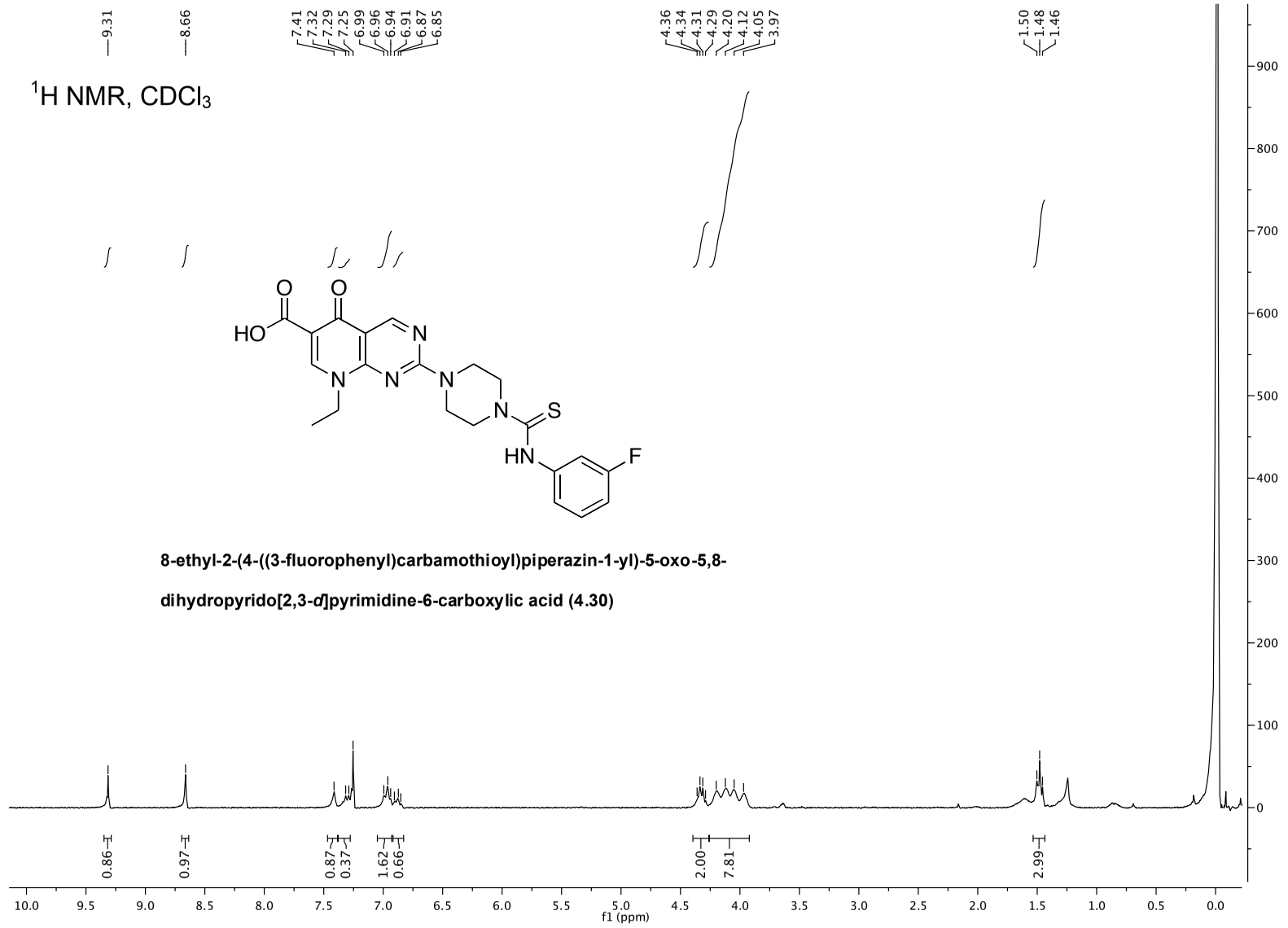

^{1}H NMR, $CDCl_3$
9.39
9.06
7.98
7.57
7.39
7.37
7.21
7.18
4.50
4.48
4.46
4.44
4.22
4.12
4.11
3.37
3.01
2.90
1.54
1.52
1.50
1.26
O
O
HO
N
N
N
N
N
S
HN
Cl
Cl
2-(4-((2,5-dichlorophenyl)carbamothioyl)piperazin-1-yl)-8-ethyl-5-oxo-
5,8-dihydropyrido[2,3-d]pyrimidine-6-carboxylic acid (4.22)
DMF
DMF
H_2O
grease
0.63
0.70
0.93
2.14
0.77
1.67
25.34
3.00
f1 (ppm)



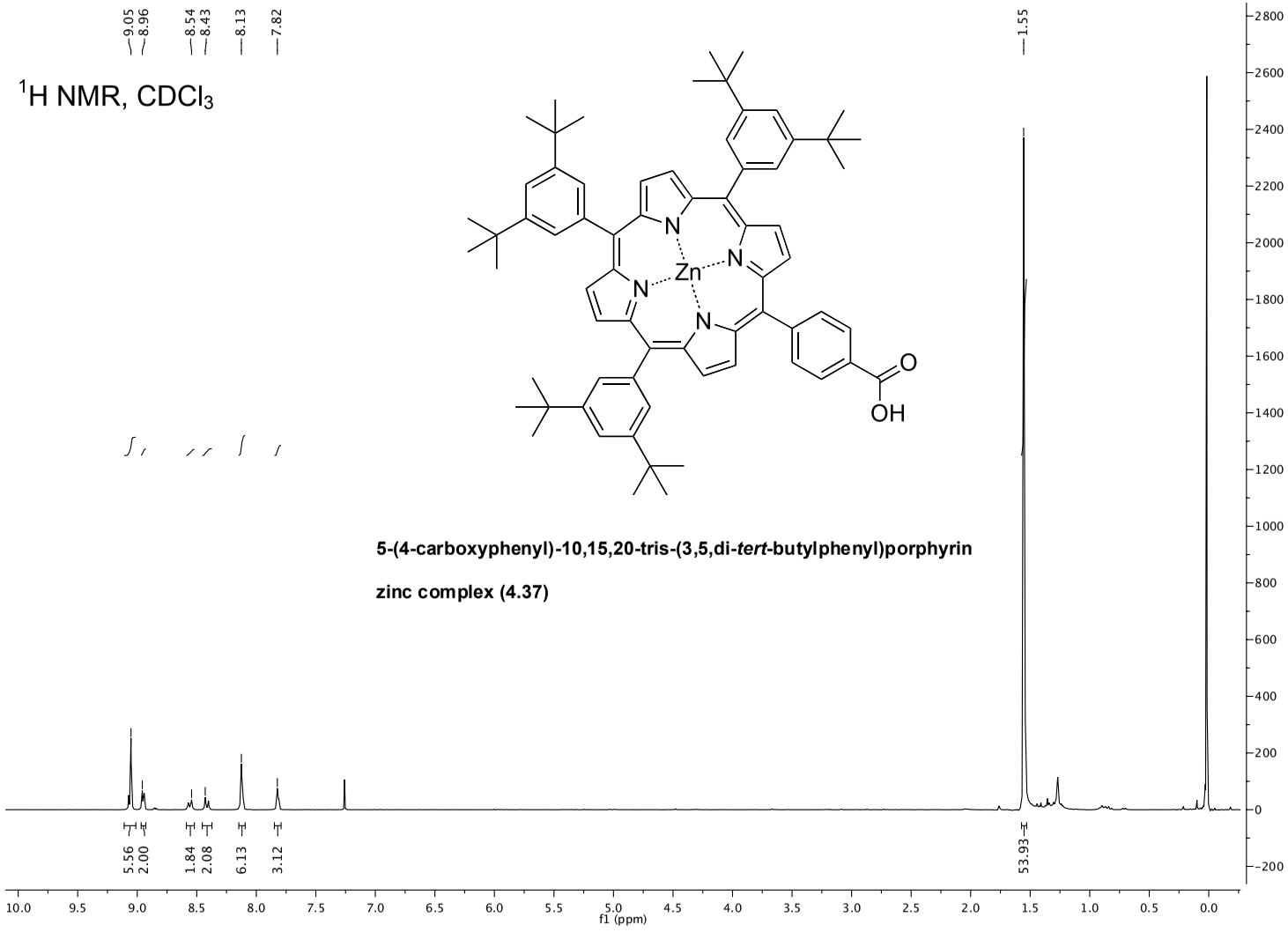
8-ethyl-2-(4-((4-fluorophenyl)carbamothioyl)piperazin-1-yl)-5-oxo-5,8-dihydropyrido[2,3-*d*]pyrimidine-6-carboxylic acid (4.23)


9.33
8.67
8.02
7.30
7.27
7.17
7.14
6.91
6.88
4.37
4.35
4.33
4.30
4.17
4.04
3.96
3.81
2.96
2.88
1.52
1.49
1.47
0.00
^{1}H NMR, $CDCl_3$
8-ethyl-2-(4-((4-methoxyphenyl)carbamothioyl)piperazin-1-yl)-5-oxo-5,8-dihydropyrido[2,3-d]pyrimidine-6-carboxylic acid (4.24)
CDCl3
DMF
DMF
0.87
1.00
0.75
2.01
2.06
1.96
7.98
2.97
2.84
f1 (ppm)

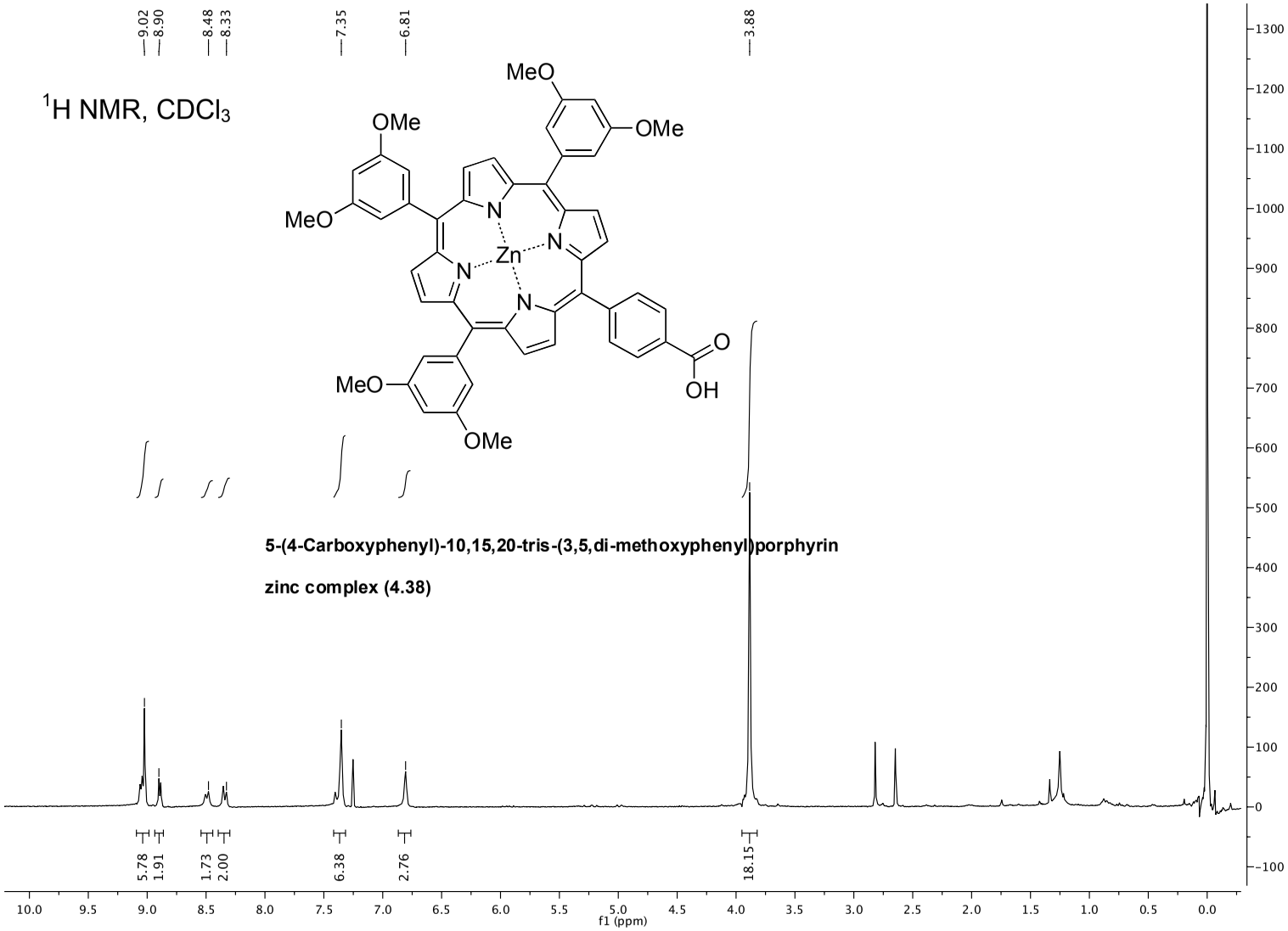

9.32
8.67
7.40
7.27
7.18
7.16
7.10
7.07
4.36
4.34
4.32
4.30
4.19
4.12
4.03
3.94
3.49
2.34
2.17
1.51
1.49
1.47
0.00
^{1}H NMR, CDCl$_3$
O
O
HO
N
N
N
N
N
S
HN
8-ethyl-5-oxo-2-(4-(*p*-tolylcarbamothioyl)piperazin-1-yl)-5,8-dihydropyrido[2,3-*d*]pyrimidine-6-carboxylic acid (4.27)
acetone
MeOH
0.98
0.96
0.73
1.73
1.63
1.79
7.82
3.00
3.00
f1 (ppm)

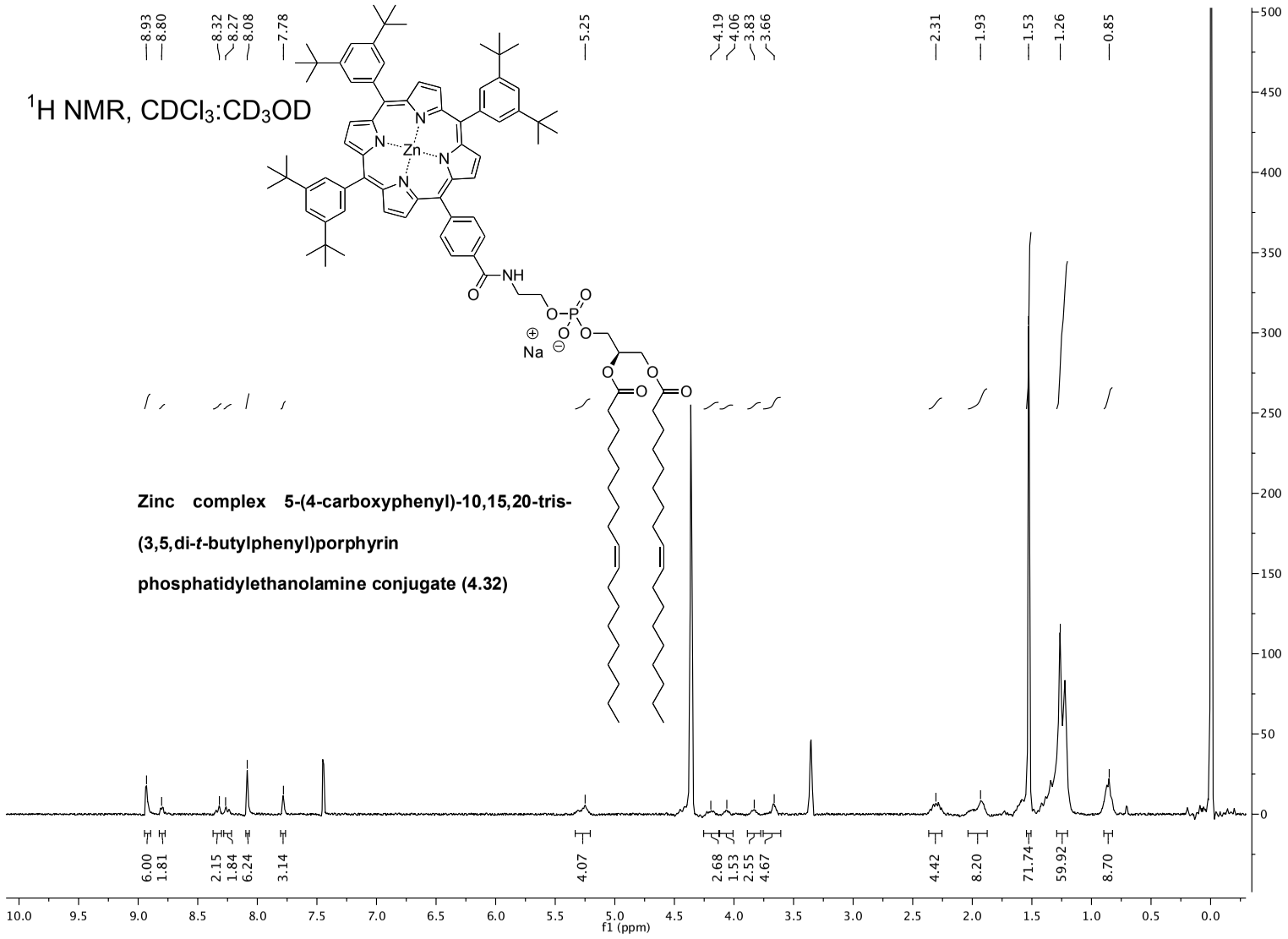


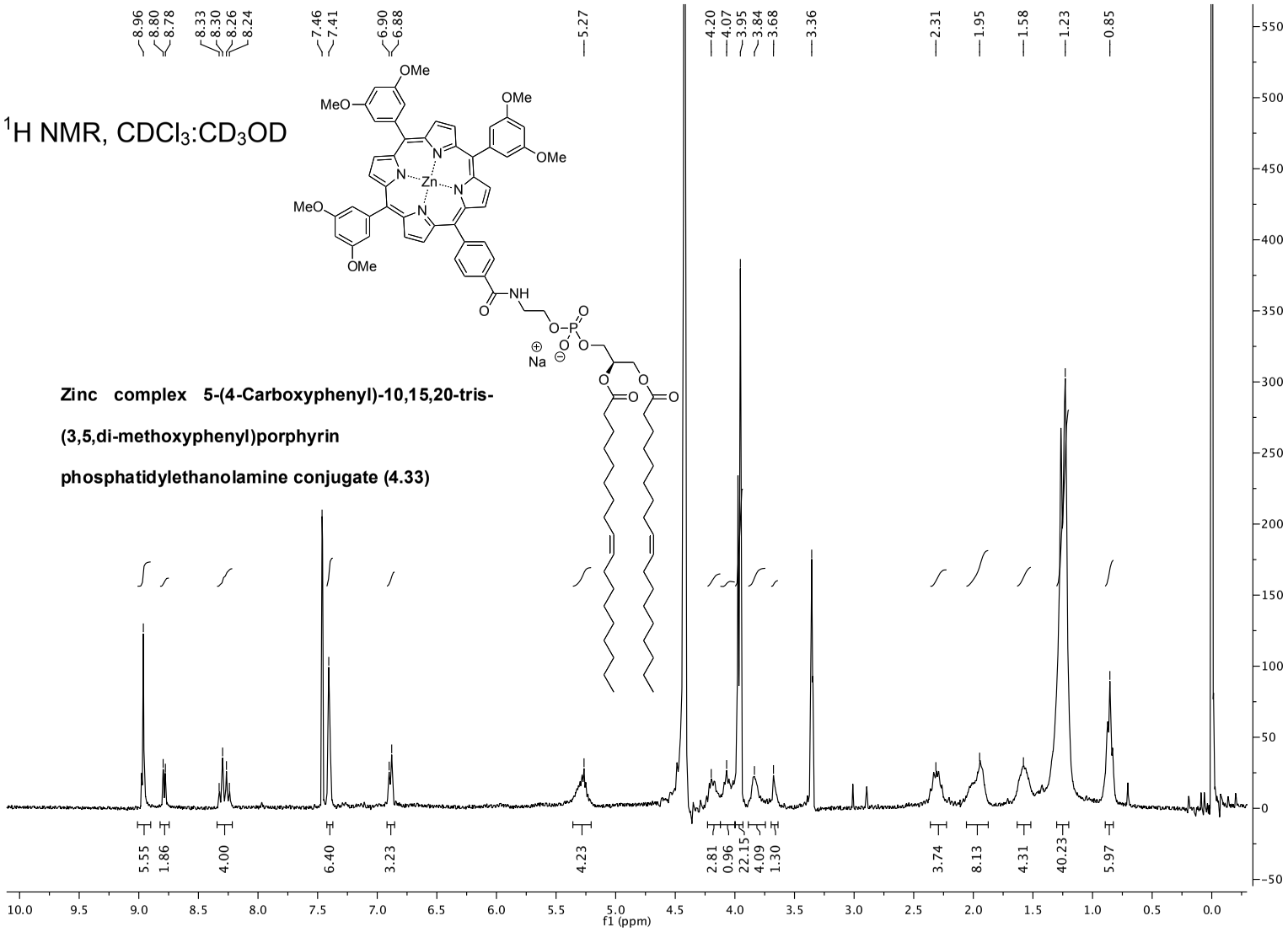
8-ethyl-2-(4-((3-fluorophenyl)carbamothioyl)piperazin-1-yl)-5-oxo-5,8-dihydropyrido[2,3-*d*]pyrimidine-6-carboxylic acid (4.30)



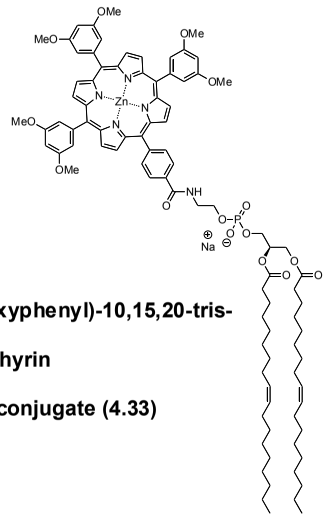
5-(4-carboxyphenyl)-10,15,20-tris-(3,5,di-*tert*-butylphenyl)porphyrin zinc complex (4.37)


^{1}H NMR, $CDCl_3$
9.02
8.90
8.48
8.33
7.35
6.81
3.88
MeO
OMe
OMe
MeO
N
N
Zn
N
N
O
OH
MeO
OMe
5-(4-Carboxyphenyl)-10,15,20-tris-(3,5,di-methoxyphenyl)porphyrin
zinc complex (4.38)
5.78
1.91
1.73
2.00
6.38
2.76
18.15
f1 (ppm)

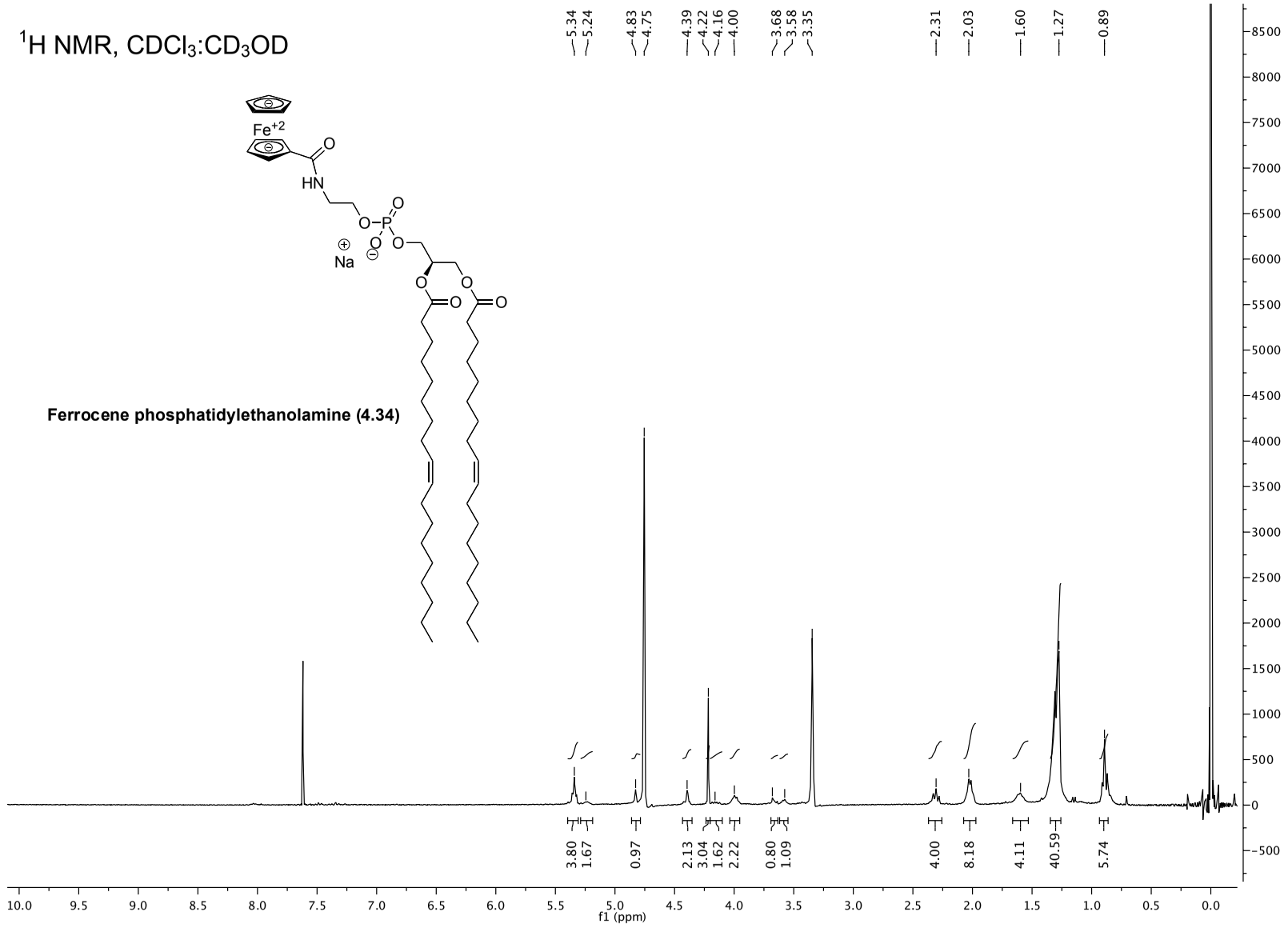

^{1}H NMR, $CDCl_3$:CD_3OD
Zinc complex 5-(4-carboxyphenyl)-10,15,20-tris-(3,5,di-*t*-butylphenyl)porphyrin phosphatidylethanolamine conjugate (4.32)
f1 (ppm)


^{1}H NMR, $CDCl_3$:CD_3OD
Zinc complex 5-(4-Carboxyphenyl)-10,15,20-tris-(3,5,di-methoxyphenyl)porphyrin phosphatidylethanolamine conjugate (4.33)
8.96
8.80
8.78
8.33
8.30
8.26
8.24
7.46
7.41
6.90
6.88
5.27
4.20
4.07
3.95
3.84
3.68
3.36
2.31
1.95
1.58
1.23
0.85
5.55
1.86
4.00
6.40
3.23
4.23
2.81
0.96
22.15
4.09
1.30
3.74
8.13
4.31
40.23
5.97
f1 (ppm)

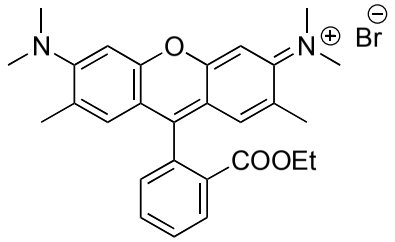
^{31}P NMR, $CDCl_3$:CD_3OD



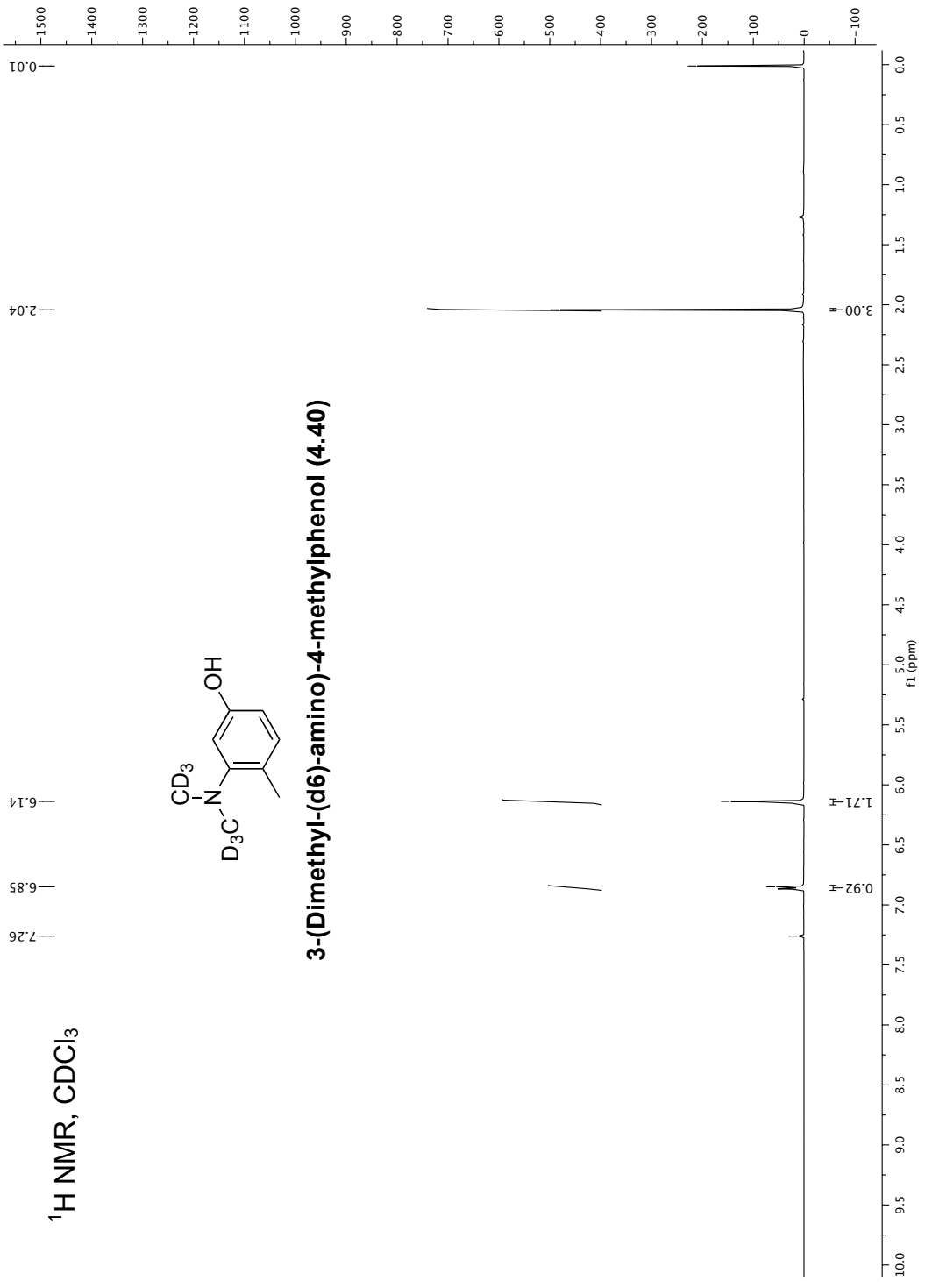
Zinc complex 5-(4-Carboxyphenyl)-10,15,20-tris-(3,5,di-methoxyphenyl)porphyrin phosphatidylethanolamine conjugate (4.33)


^{1}H NMR, $CDCl_3$:CD_3OD
Ferrocene phosphatidylethanolamine (4.34)
5.34
5.24
4.83
4.75
4.39
4.22
4.16
4.00
3.68
3.58
3.35
2.31
2.03
1.60
1.27
0.89
3.80
1.67
0.97
2.13
3.04
1.62
2.22
0.80
1.09
4.00
8.18
4.11
40.59
5.74
f1 (ppm)

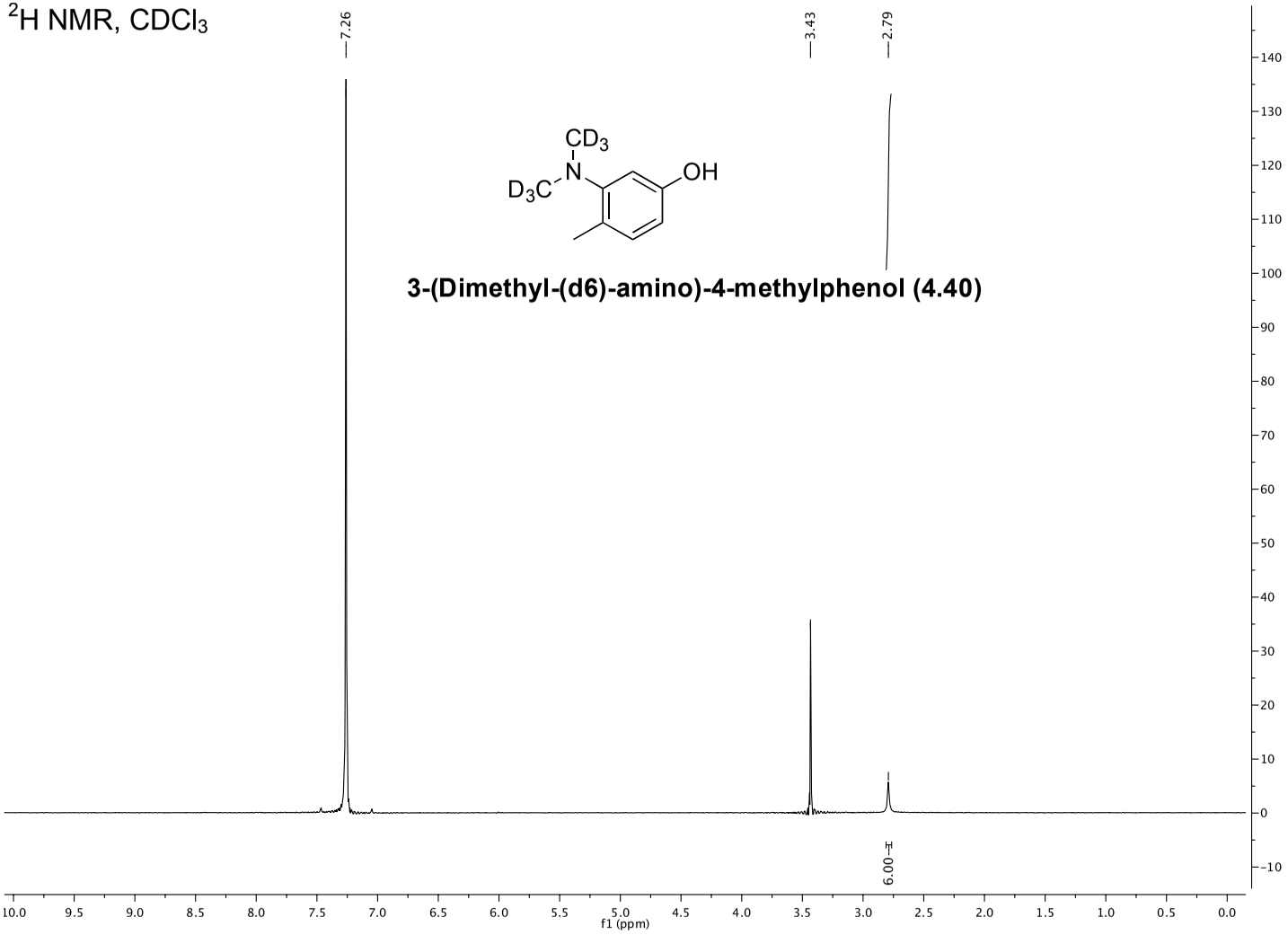
^{1}H NMR, $CDCl_3$



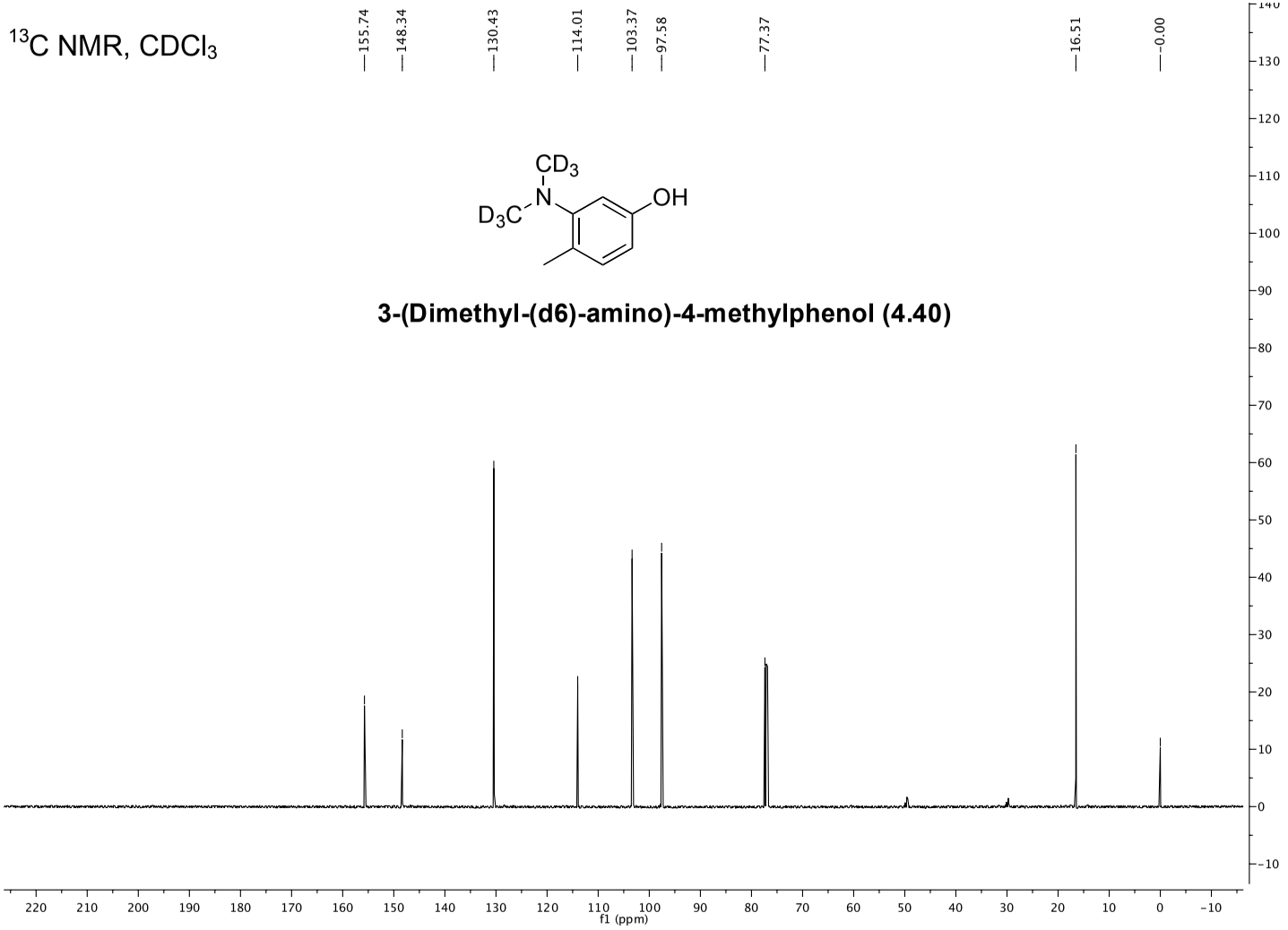
Tetramethylrhodamine (4.39)


3-(Dimethyl-(d6)-amino)-4-methylphenol (4.40)
^{1}H NMR, $CDCl_3$
OH
CD_3
N
D_3C
7.26
6.85
6.14
2.04
0.01
0.92
1.71
3.00
f1 (ppm)

^{2}H NMR, $CDCl_3$

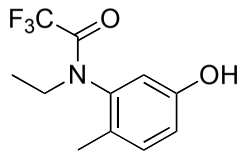

7.26
3.43
2.79
CD3
N
D3C
OH
3-(Dimethyl-(d6)-amino)-4-methylphenol (4.40)
6.00
f1 (ppm)

^{13}C NMR, $CDCl_3$



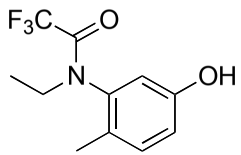
3-(Dimethyl-(d6)-amino)-4-methylphenol (4.40)

^{1}H NMR, $CDCl_3$

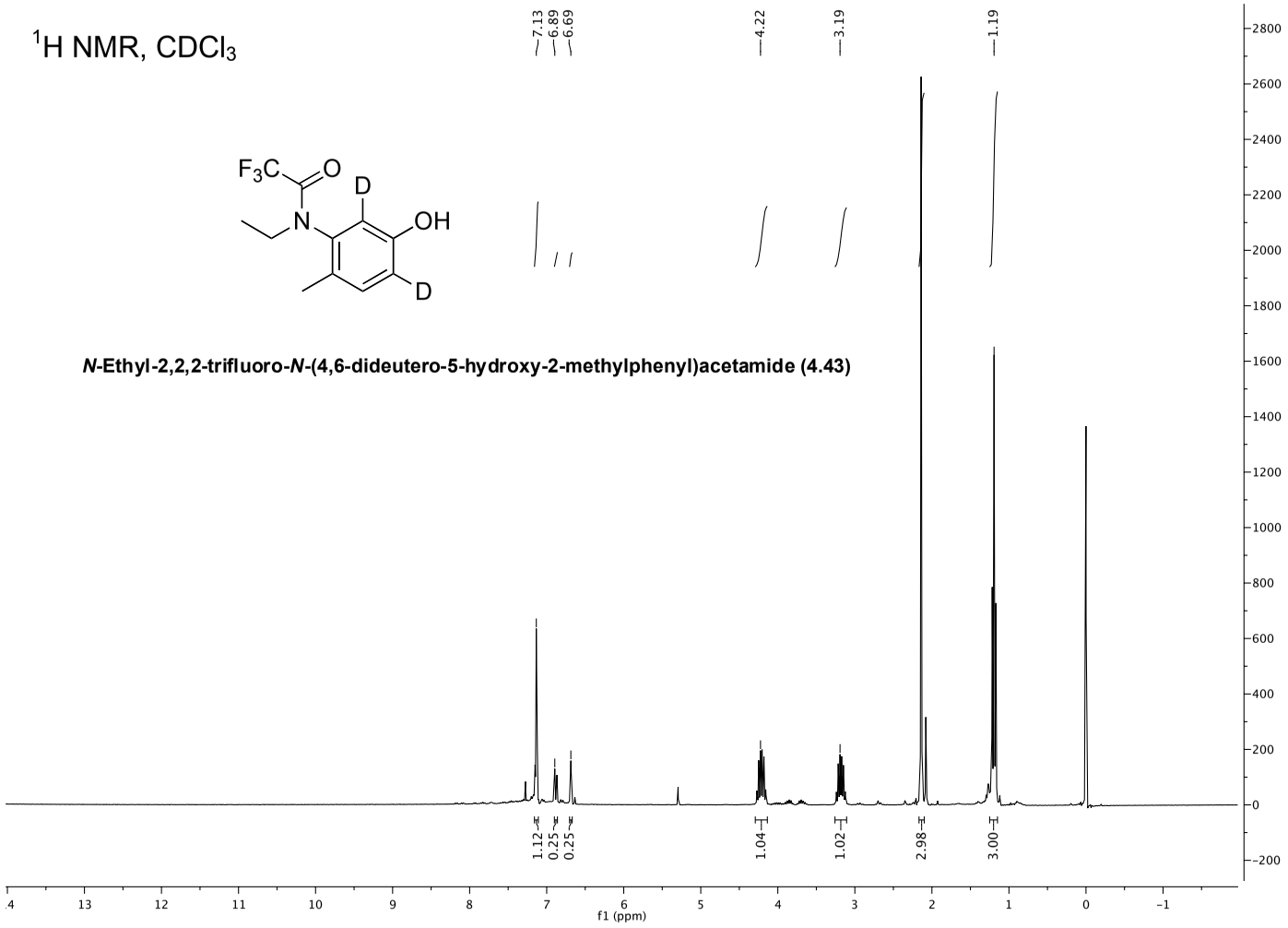


***N*-Ethyl-2,2,2-trifluoro-*N*-(5-hydroxy-2-methylphenyl)acetamide (4.42)**

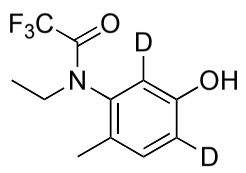
^{19}F NMR, $CDCl_3$



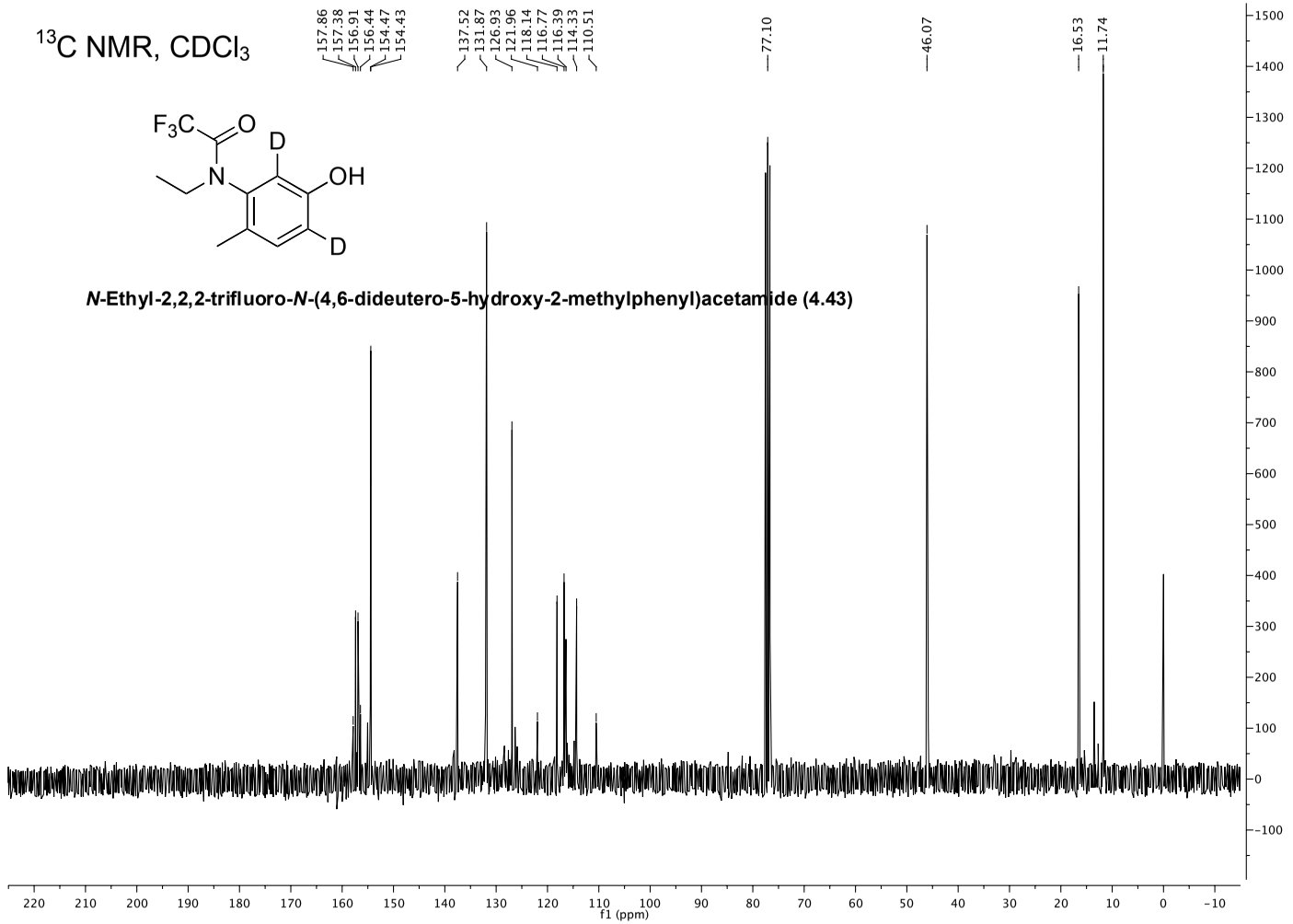
_N_-Ethyl-2,2,2-trifluoro-_N_-(5-hydroxy-2-methylphenyl)acetamide (4.42)

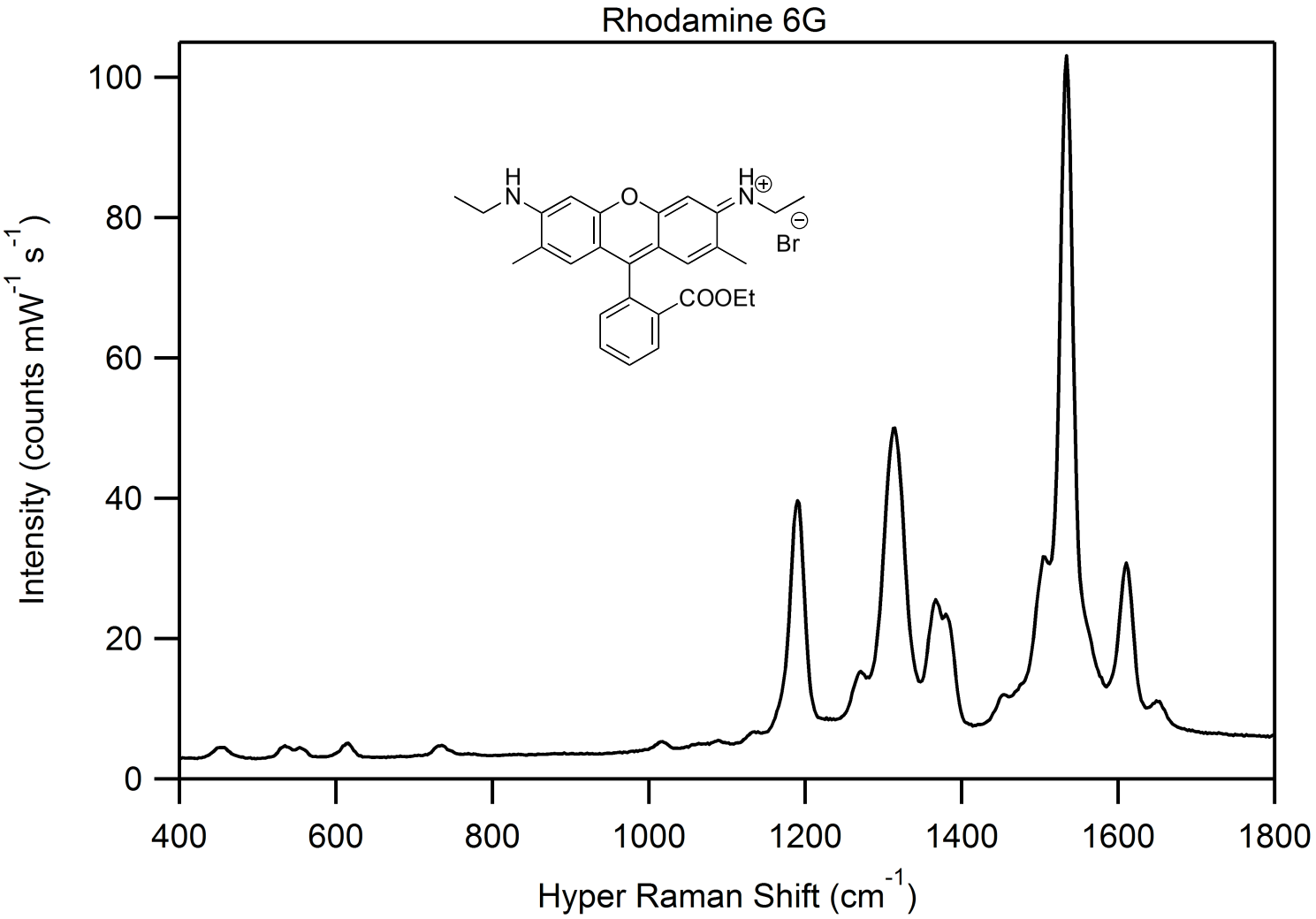

^{1}H NMR, $CDCl_3$
7.13
6.89
6.69
4.22
3.19
1.19
F_3C
O
N
D
OH
D
N-Ethyl-2,2,2-trifluoro-*N*-(4,6-dideutero-5-hydroxy-2-methylphenyl)acetamide (4.43)
1.12
0.25
0.25
1.04
1.02
2.98
3.00
f1 (ppm)

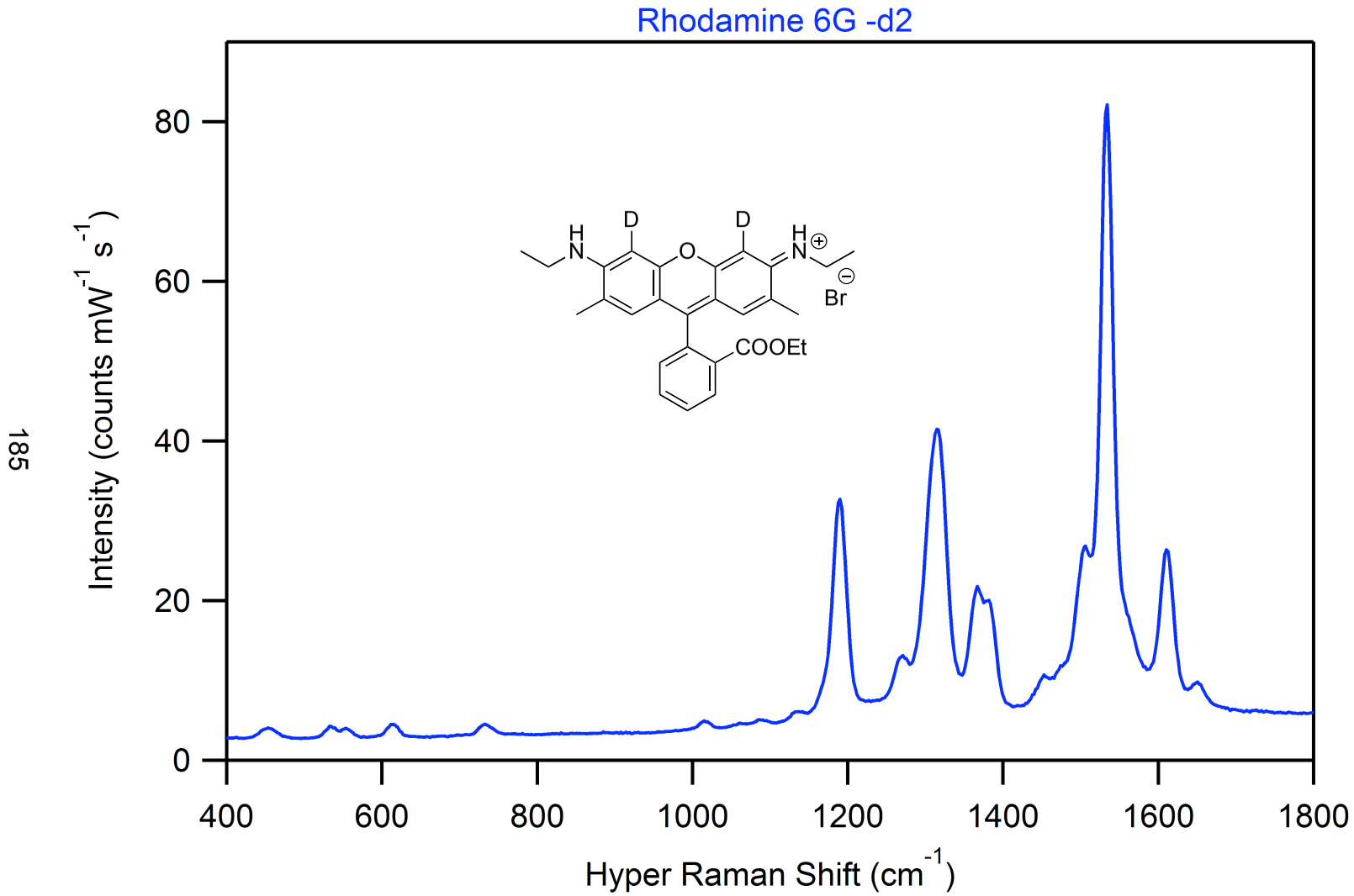
^{19}F NMR, $CDCl_3$

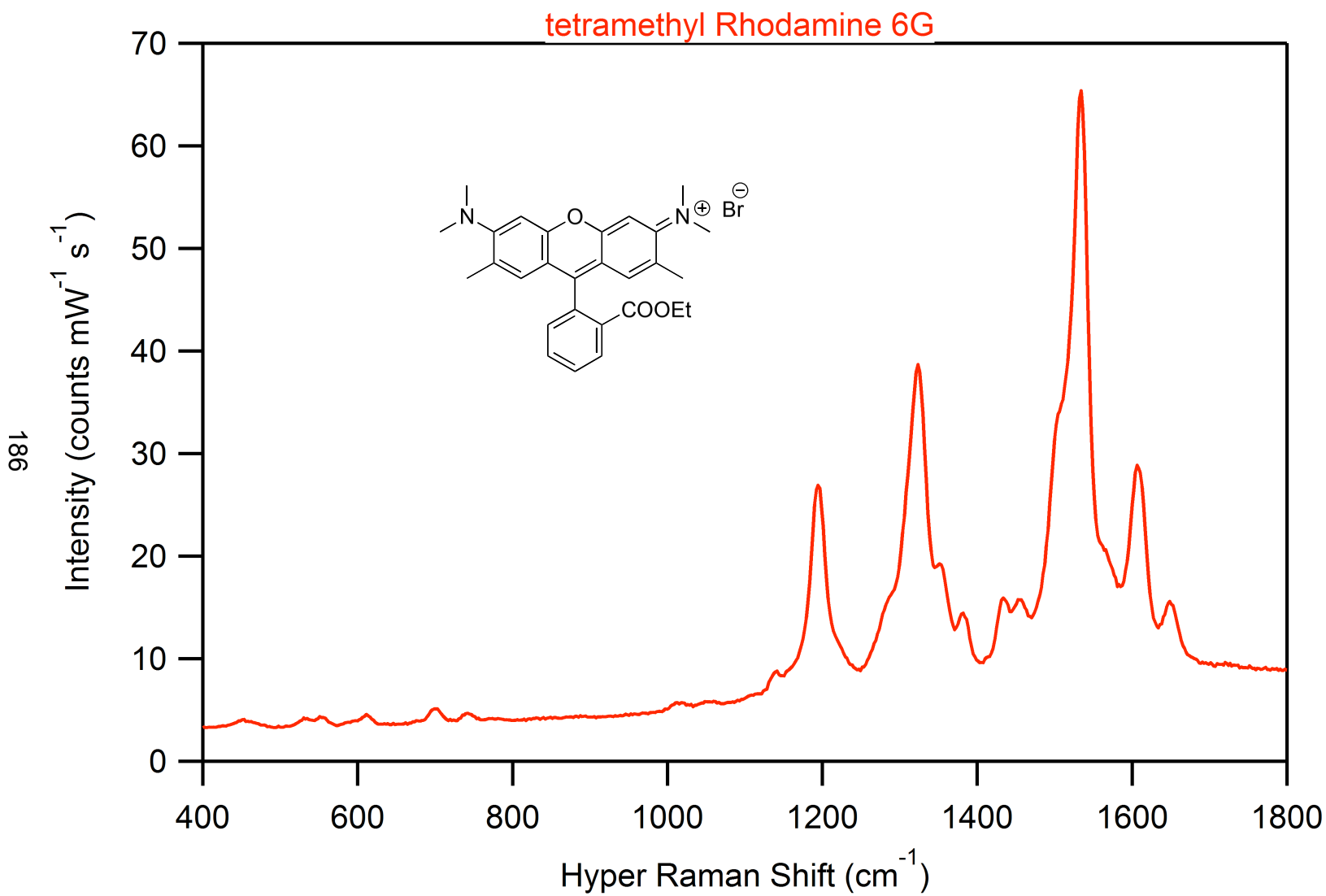


***N*-Ethyl-2,2,2-trifluoro-*N*-(4,6-dideutero-5-hydroxy-2-methylphenyl)acetamide (4.43)**


^{13}C NMR, CDCl$_3$
157.86
157.38
156.91
156.44
154.47
154.43
137.52
131.87
126.93
121.96
118.14
116.77
116.39
114.33
110.51
77.10
46.07
16.53
11.74
F$_3$C
O
D
N
OH
D
N-Ethyl-2,2,2-trifluoro-N-(4,6-dideutero-5-hydroxy-2-methylphenyl)acetamide (4.43)
f1 (ppm)


Rhodamine 6G
Intensity (counts mW^{-1} s^{-1})
Hyper Raman Shift (cm^{-1})
0
20
40
60
80
100
400
600
800
1000
1200
1400
1600
1800
H
N
O
H
N
Br
COOEt


Rhodamine 6G -d2
Intensity (counts mW-1 s-1)
Hyper Raman Shift (cm-1)
0
20
40
60
80
400
600
800
1000
1200
1400
1600
1800
H
N
D
O
D
H
N
Br
COOEt


tetramethyl Rhodamine 6G
Intensity (counts mW-1 s-1)
Hyper Raman Shift (cm-1)
0
10
20
30
40
50
60
70
400
600
800
1000
1200
1400
1600
1800
N
O
N
Br
COOEt

References

1. Cho, W.; Stahelin, R. V., Membrane-Protein Interactions in Cell Signaling and Membrane Trafficking. *Annu. Rev. Biophys. Biomol. Struct.* **2005,** *34* (1), 119-151.
2. Pendaries, C.; Tronchère, H.; Plantavid, M.; Payrastre, B., Phosphoinositide Signaling Disorders in Human Diseases. *FEBS Lett.* **2003,** *546* (1), 25-31.
3. Sprong, H.; van der Sluijs, P.; van Meer, G., How Proteins Move Lipids and Lipids Move Proteins. *Nat. Rev. Mol. Cell Biol.* **2001,** *2* (7), 504-513.
4. Lemmon, M. A., Membrane Recognition by Phospholipid-Binding Domains. *Nat. Rev. Mol. Cell Biol.* **2008,** *9* (2), 99-111.
5. Best, M. D.; Rowland, M. M.; Bostic, H. E., Exploiting Bioorthogonal Chemistry to Elucidate Protein-Lipid Binding Interactions and Other Biological Roles of Phospholipids. *Acc. Chem. Res.* **2011,** *44* (9), 686-698.
6. Best, M. D.; Zhang, H.; Prestwich, G. D., Inositol Polyphosphates, Diphosphoinositol Polyphosphates and Phosphatidylinositol Polyphosphate Lipids: Structure, Synthesis, and Development of Probes for Studying Biological Activity. *Nat. Prod. Rep.* **2010,** *27* (10), 1403-1430.
7. Jahn, R.; Lang, T.; Südhof, T. C., Membrane Fusion. *Cell* **2003,** *112* (4), 519-533.
8. Tamm, L. K.; Crane, J.; Kiessling, V., Membrane Fusion: A Structural Perspective on the Interplay of Lipids and Proteins. *Curr. Opin. Struct. Biol.* **2003,** *13* (4), 453-466.
9. Bonifacino, J. S.; Glick, B. S., The Mechanisms of Vesicle Budding and Fusion. *Cell* **2004,** *116* (2), 153-166.
10. Fahy, E.; Subramaniam, S.; Murphy, R. C.; Nishijima, M.; Raetz, C. R. H.; Shimizu, T.; Spener, F.; van Meer, G.; Wakelam, M. J. O.; Dennis, E. A., Update of the Lipid Maps Comprehensive Classification System for Lipids. *J. Lipid Res.* **2009,** *50* (Supplement), S9-S14.
11. Andreyev, A. Y.; Fahy, E.; Guan, Z.; Kelly, S.; Li, X.; McDonald, J. G.; Milne, S.; Myers, D.; Park, H.; Ryan, A.; Thompson, B. M.; Wang, E.; Zhao, Y.; Brown, H. A.; Merrill, A. H.; Raetz, C. R. H.; Russell, D. W.; Subramaniam, S.; Dennis, E. A., Subcellular Organelle Lipidomics in Tlr-4-Activated Macrophages. *J. Lipid Res.* **2010,** *51* (9), 2785-2797.
12. Shevchenko, A.; Simons, K., Lipidomics: Coming to Grips with Lipid Diversity. *Nat. Rev. Mol. Cell Biol.* **2010,** *11* (8), 593-598.
13. Tully, S. E.; Cravatt, B. F., Activity-Based Probes That Target Functional Subclasses of Phospholipases in Proteomes. *JACS* **2010,** *132* (10), 3264-3265.
14. Hanshaw, R. G.; Smith, B. D., New Reagents for Phosphatidylserine Recognition and Detection of Apoptosis. *Bioorg. Med. Chem.* **2005,** *13* (17), 5035-5042.
15. Bandyopadhyay, S.; Bong, D., Synthesis of Trifunctional Phosphatidylserine Probes for Identification of Lipid-Binding Proteins. *Eur. J. Org. Chem.* **2011,** *2011* (4), 751-758.
16. Narayan, K.; Lemmon, M. A., Determining Selectivity of Phosphoinositide-Binding Domains. *Methods* **2006,** *39* (2), 122-133.

17. Kavran, J. M.; Klein, D. E.; Lee, A.; Falasca, M.; Isakoff, S. J.; Skolnik, E. Y.; Lemmon, M. A., Specificity and Promiscuity in Phosphoinositide Binding by Pleckstrin Homology Domains. *J. Biol. Chem.* **1998,** *273* (46), 30497-30508.
18. Dowler, S.; Currie, R. A.; Downes, C. P.; Alessi, D. R., Dapp1: A Dual Adaptor for Phosphotyrosine and 3-Phosphoinositides. *Biochem. J.* **1999,** *342*, 7-12.
19. Stevenson, J. M.; Perera, I. Y.; Boss, W. F., A Phosphatidylinositol 4-Kinase Pleckstrin Homology Domain That Binds Phosphatidylinositol 4-Monophosphate. *J. Biol. Chem.* **1998,** *273* (35), 22761-22767.
20. Cho, W.; Bittova, L.; Stahelin, R. V., Membrane Binding Assays for Peripheral Proteins. *Anal. Biochem.* **2001,** *296* (2), 153-161.
21. Jain, M. K.; Egmond, M. R.; Verheij, H. M.; Apitzcastro, R.; Dijkman, R.; Dehaas, G. H., Interaction of Phospholipase-A2 and Phospholipid-Bilayers. *Biochim. Biophys. Acta* **1982,** *688* (2), 341-348.
22. Nalefski, E. A.; Slazas, M. M.; Falke, J. J., Ca2+-Signaling Cycle of a Membrane-Docking C2 Domain. *Biochemistry (Mosc).* **1997,** *36* (40), 12011-12018.
23. Qian, X. Q.; Zhou, C.; Roberts, M. F., Phosphatidylcholine Activation of Bacterial Phosphatidylinositol-Specific Phospholipase C toward Pi Vesicles. *Biochemistry (Mosc).* **1998,** *37* (18), 6513-6522.
24. Meers, P.; Daleke, D.; Hong, K.; Papahadjopoulos, D., Interactions of Annexins with Membrane Phospholipids. *Biochemistry (Mosc).* **1991,** *30* (11), 2903-2908.
25. Chapman, E. R.; Davis, A. F., Direct Interaction of a Ca2+-Binding Loop of Synaptotagmin with Lipid Bilayers. *J. Biol. Chem.* **1998,** *273* (22), 13995-14001.
26. Nalefski, E. A.; McDonagh, T.; Somers, W.; Seehra, J.; Falke, J. J.; Clark, J. D., Independent Folding and Ligand Specificity of the C2 Calcium-Dependent Lipid Binding Domain of Cytosolic Phospholipase a(2). *J. Biol. Chem.* **1998,** *273* (3), 1365-1372.
27. Nalefski, E. A.; Sultzman, L. A.; Martin, D. M.; Kriz, R. W.; Towler, P. S.; Knopf, J. L.; Clark, J. D., Delineation of 2 Functionally Distinct Domains of Cytosolic Phospholipase-a(2), a Regulatory Ca2+-Dependent Lipid-Binding Domain and a Ca2+-Independent Catalytic Domain. *J. Biol. Chem.* **1994,** *269* (27), 18239-18249.
28. Hixon, M. S.; Ball, A.; Gelb, M. H., Calcium-Dependent and -Independent Interfacial Binding and Catalysis of Cytosolic Group Iv Phospholipase a(2). *Biochemistry (Mosc).* **1998,** *37* (23), 8516-8526.
29. Bazzi, M. D.; Nelsestuen, G. L., Association of Protein-Kinase-C with Phospholipid-Vesicles. *Biochemistry (Mosc).* **1987,** *26* (1), 115-122.
30. Bazzi, M. D.; Nelsestuen, G. L., Protein-Kinase-C Interaction with Calcium - a Phospholipid-Dependent Process. *Biochemistry (Mosc).* **1990,** *29* (33), 7624-7630.
31. Pap, E. H. W.; Bastiaens, P. I. H.; Borst, J. W.; Vandenberg, P. A. W.; Vanhoek, A.; Snoek, G. T.; Wirtz, K. W. A.; Visser, A., Quantitation of the Interaction of Protein-Kinase-C with Diacylglycerol and Phosphoinositides by Time-Resolved Detection of Resonance Energy-Transfer. *Biochemistry (Mosc).* **1993,** *32* (48), 13310-13317.

32. Pap, E. H. W.; Vandenberg, P. A. W.; Borst, J. W.; Visser, A., The Interaction between Protein-Kinase-C and Lipid Cofactors Studied by Simultaneous Observation of Lipid and Protein Fluorescence. *J. Biol. Chem.* **1995,** *270* (3), 1254-1260.
33. Bazzi, M. D.; Nelsestuen, G. L., Proteins That Bind Calcium in a Phospholipid-Dependent Manner. *Biochemistry (Mosc).* **1991,** *30* (4), 971-979.
34. Bazzi, M. D.; Nelsestuen, G. L., Interaction of Annexin-Vi with Membranes - Highly Restricted Dissipation of Clustered Phospholipids in Membranes Containing Phosphatidylethanolamine. *Biochemistry (Mosc).* **1992,** *31* (42), 10406-10413.
35. Currie, R. A.; Walker, K. S.; Gray, A.; Deak, M.; Casamayor, A.; Downes, C. P.; Cohen, P.; Alessi, D. R.; Lucocq, J., Role of Phosphatidylinositol 3,4,5-Trisphosphate in Regulating the Activity and Localization of 3-Phosphoinositide-Dependent Protein Kinase-1. *Biochem. J.* **1999,** *337*, 575-583.
36. Bittova, L.; Stahelin, R. V.; Cho, W., Roles of Ionic Residues of the C1 Domain in Protein Kinase C-Alpha Activation and the Origin of Phosphatidylserine Specificity. *J. Biol. Chem.* **2001,** *276* (6), 4218-4226.
37. Stahelin, R. V.; Cho, W. H., Differential Roles of Ionic, Aliphatic, and Aromatic Residues in Membrane-Protein Interactions: A Surface Plasmon Resonance Study on Phospholipases a(2). *Biochemistry (Mosc).* **2001,** *40* (15), 4672-4678.
38. Jung, L. S.; Shumaker-Parry, J. S.; Campbell, C. T.; Yee, S. S.; Gelb, M. H., Quantification of Tight Binding to Surface-Immobilized Phospholipid Vesicles Using Surface Plasmon Resonance: Binding Constant of Phospholipase A2. *JACS* **2000,** *122* (17), 4177-4184.
39. Salamon, Z.; Lindblom, G.; Rilfors, L.; Linde, K.; Tollin, G., Interaction of Phosphatidylserine Synthase from E-Coli with Lipid Bilayers: Coupled Plasmon-Waveguide Resonance Spectroscopy Studies. *Biophys. J.* **2000,** *78* (3), 1400-1412.
40. Mehrotra, B.; Myszka, D. G.; Prestwich, G. D., Binding Kinetics and Ligand Specificity for the Interactions of the C2b Domain of Synaptogmin Ii with Inositol Polyphosphates and Phosphoinositides. *Biochemistry (Mosc).* **2000,** *39* (32), 9679-9686.
41. Schlattner, U.; Eder, M.; Dolder, M.; Khuchua, Z. A.; Strauss, A. W.; Wallimann, T., Divergent Enzyme Kinetics and Structural Properties of the Two Human Mitochondrial Creatine Kinase Isoenzymes. *Biol. Chem.* **2000,** *381* (11), 1063-1070.
42. Soulages, J. L.; Salamon, Z.; Wells, M. A.; Tollin, G., Low Concentrations of Diacylglycerol Promote the Binding of Apolipophorin-Iii to a Phospholipid-Bilayer - a Surface-Plasmon Resonance Spectroscopy Study. *Proc. Natl. Acad. Sci. U. S. A.* **1995,** *92* (12), 5650-5654.
43. Salamon, Z.; Tollin, G., Surface Plasmon Resonance Studies of Complex Formation between Cytochrome C and Bovine Cytochrome C Oxidase Incorporated into a Supported Planar Lipid Bilayer .1. Binding of Cytochrome C

to Cardiolipin/Phosphatidylcholine Membranes in the Absence of Oxidase. *Biophys. J.* **1996,** *71* (2), 848-857.

44. Ozawa, T.; Fukuda, M.; Nara, M.; Nakamura, A.; Komine, Y.; Kohama, K.; Umezawa, Y., How Can Ca2+ Selectively Activate Recoverin in the Presence of Mg2+? Surface Plasmon Resonance and Ft-Ir Spectroscopic Studies. *Biochemistry (Mosc).* **2000,** *39* (47), 14495-14503.
45. Sui, S. F.; Sun, Y. T.; Mi, L. Z., Calcium-Dependent Binding of Rabbit C-Reactive Protein to Supported Lipid Monolayers Containing Exposed Phosphorylcholine Group. *Biophys. J.* **1999,** *76* (1), 333-341.
46. Suurkuusk, M.; Singh, S. K., Formation of Hdl-Like Complexes from Apolipoprotein a-I-M and Dmpc. *Int. J. Pharm.* **2000,** *194* (1), 21-38.
47. Gasset, M.; Magdaleno, L.; Calvete, J. J., Biophysical Study of the Perturbation of Model Membrane Structure Caused by Seminal Plasma Protein Pdc-109. *Arch. Biochem. Biophys.* **2000,** *374* (2), 241-247.
48. Romsicki, Y.; Sharom, F. J., Interaction of P-Glycoprotein with Defined Phospholipid Bilayers: A Differential Scanning Calorimetric Study. *Biochemistry (Mosc).* **1997,** *36* (32), 9807-9815.
49. Dimitrova, M. N.; Matsumura, H.; Dimitrova, A.; Neitchev, V. Z., Interaction of Albumins from Different Species with Phospholipid Liposomes. Multiple Binding Sites System. *Int. J. Biol. Macromol.* **2000,** *27* (3), 187-194.
50. Bittova, L.; Sumandea, M.; Cho, W., A Structure-Function Study of the C2 Domain of Cytosolic Phospholipase a(2) - Identification of Essential Calcium Ligands and Hydrophobic Membrane Binding Residues. *J. Biol. Chem.* **1999,** *274* (14), 9665-9672.
51. Lichtenbergova, L.; Yoon, E. T.; Cho, W. W., Membrane Penetration of Cytosolic Phospholipase a(2) Is Necessary for Its Interfacial Catalysis and Arachidonate Specificity. *Biochemistry (Mosc).* **1998,** *37* (40), 14128-14136.
52. Boguslavsky, V.; Rebecchi, M.; Morris, A. J.; Jhon, D. Y.; Rhee, S. G.; McLaughlin, S., Effect of Monolayer Surface Pressure on the Activities of Phosphoinositide-Specific Phospholipase-C-Beta-1, Phospholipase-C-Gamma-1, and Phospholipase-C-Delta-1. *Biochemistry (Mosc).* **1994,** *33* (10), 3032-3037.
53. Rebecchi, M.; Boguslavsky, V.; Boguslavsky, L.; McLaughlin, S., Phosphoinositide-Specific Phospholipase C-Delta-1 - Effect of Monolayer Surface Pressure and Electrostatic Surface-Potentials on Activity. *Biochemistry (Mosc).* **1992,** *31* (51), 12748-12753.
54. Rebecchi, M.; Peterson, A.; McLaughlin, S., Phosphoinositide-Specific Phospholipase C-Delta-1 Binds with High-Affinity to Phospholipid-Vesicles Containing Phosphatidylinositol 4,5-Bisphosphate. *Biochemistry (Mosc).* **1992,** *31* (51), 12742-12747.
55. Snitko, Y.; Koduri, R. S.; Han, S. K.; Othman, R.; Baker, S. F.; Molini, B. J.; Wilton, D. C.; Gelb, M. H.; Cho, W. H., Mapping the Interfacial Binding Surface of Human Secretory Group Iia Phospholipase a(2). *Biochemistry (Mosc).* **1997,** *36* (47), 14325-14333.

56. Snitko, Y.; Han, S. K.; Lee, B. I.; Cho, W. W., Differential Interfacial and Substrate Binding Modes of Mammalian Pancreatic Phospholipases a(2): A Comparison among Human, Bovine, and Porcine Enzymes. *Biochemistry (Mosc).* **1999,** *38* (24), 7803-7810.
57. Lee, B. I.; Dua, R.; Cho, W. W., A Structural Determinant of the Unique Interfacial Binding Mode of Bovine Pancreatic Phospholipase a(2). *Biochemistry (Mosc).* **1999,** *38* (24), 7811-7818.
58. Jenco, J. M.; Becker, K. P.; Morris, A. J., Membrane-Binding Properties of Phospholipase C-Beta(1) and Phospholipase C-Beta 2: Role of the C-Terminus and Effects of Polyphosphoinositides, G-Proteins and Ca2+. *Biochem. J.* **1997,** *327*, 431-437.
59. Medkova, M.; Cho, W. H., Differential Membrane-Binding and Activation Mechanisms of Protein Kinase C-Alpha and -Epsilon. *Biochemistry (Mosc).* **1998,** *37* (14), 4892-4900.
60. Medkova, M.; Cho, W. W., Mutagenesis of the C2 Domain of Protein Kinase C-Alpha - Differential Roles of Ca2+ Ligands and Membrane Binding Residues. *J. Biol. Chem.* **1998,** *273* (28), 17544-17552.
61. Medkova, M.; Cho, W. H., Interplay of C1 and C2 Domains of Protein Kinase C-Alpha in Its Membrane Binding and Activation. *J. Biol. Chem.* **1999,** *274* (28), 19852-19861.
62. Mosior, M.; Newton, A. C., Mechanism of Interaction of Protein-Kinase-C with Phorbol Esters - Reversibility and Nature of Membrane Association. *J. Biol. Chem.* **1995,** *270* (43), 25526-25533.
63. Mosior, M.; Epand, R. M., Mechanism of Activation of Protein Kinase C: Roles of Diolein and Phosphatidylserine. *Biochemistry (Mosc).* **1993,** *32* (1), 66-75.
64. Kirsch, T.; Nah, H. D.; Demuth, D. R.; Harrison, G.; Golub, E. E.; Adams, S. L.; Pacifici, M., Annexin V-Mediated Calcium Flux across Membranes Is Dependent on the Lipid Composition: Implications for Cartilage Mineralization. *Biochemistry (Mosc).* **1997,** *36* (11), 3359-3367.
65. Bitto, E.; Cho, W. H., Roles of Individual Domains of Annexin I in Its Vesicle Binding and Vesicle Aggregation: A Comprehensive Mutagenesis Study. *Biochemistry (Mosc).* **1998,** *37* (28), 10231-10237.
66. Bitto, E.; Cho, W., Structural Determinant of the Vesicle Aggregation Activity of Annexin I. *Biochemistry (Mosc).* **1999,** *38* (42), 14094-14100.
67. Bitto, E.; Li, M.; Tikhonov, A. M.; Schlossman, M. L.; Cho, W., Mechanism of Annexin I-Mediated Membrane Aggregation. *Biochemistry (Mosc).* **2000,** *39* (44), 13469-13477.
68. Bazzi, M. D.; Youakim, A.; Nelsestuen, G. L., Importance of Phosphatidylethanolamine for Association of Protein-Kinase-C and Other Cytoplasmic Proteins with Membranes. *Biochemistry (Mosc).* **1992,** *31* (4), 1125-1134.
69. Ferrara, K. W.; Borden, M. A.; Zhang, H., Lipid-Shelled Vehicles: Engineering for Ultrasound Molecular Imaging and Drug Delivery. *Acc. Chem. Res.* **2009,** *42* (7), 881-892.

70. Mintzer, M. A.; Simanek, E. E., Nonviral Vectors for Gene Delivery. *Chem. Rev.* **2008,** *109* (2), 259-302.
71. Vermette, P.; Meagher, L.; Gagnon, E.; Griesser, H. J.; Doillon, C. J., Immobilized Liposome Layers for Drug Delivery Applications: Inhibition of Angiogenesis. *J. Controlled Release* **2002,** *80* (1–3), 179-195.
72. Chan, Y. H. M.; Boxer, S. G., Model Membrane Systems and Their Applications. *Curr. Opin. Chem. Biol.* **2007,** *11* (6), 581-587.
73. Jelinek, R.; Silbert, L., Biomimetic Approaches for Studying Membrane Processes. *Mol. BioSyst.* **2009,** *5* (8), 811-818.
74. Saxon, E.; Luchansky, S. J.; Hang, H. C.; Yu, C.; Lee, S. C.; Bertozzi, C. R., Investigating Cellular Metabolism of Synthetic Azidosugars with the Staudinger Ligation. *JACS* **2002,** *124* (50), 14893-14902.
75. Kohn, M.; Breinbauer, R., The Staudinger Ligation - a Gift to Chemical Biology'. *Angew. Chem. Int. Ed.* **2004,** *43* (24), 3106-3116.
76. Nilsson, B. L.; Kiessling, L. L.; Raines, R. T., High-Yielding Staudinger Ligation of a Phosphinothioester and Azide to Form a Peptide. *Org. Lett.* **2001,** *3* (1), 9-12.
77. Nilsson, B. L.; Kiessling, L. L.; Raines, R. T., Staudinger Ligation: A Peptide from a Thioester and Azide. *Org. Lett.* **2000,** *2* (13), 1939-1941.
78. Saxon, E.; Armstrong, J. I.; Bertozzi, C. R., A "Traceless" Staudinger Ligation for the Chemoselective Synthesis of Amide Bonds. *Org. Lett.* **2000,** *2* (14), 2141-2143.
79. Hang, H. C.; Yu, C.; Pratt, M. R.; Bertozzi, C. R., Probing Glycosyltransferase Activities with the Staudinger Ligation. *JACS* **2003,** *126* (1), 6-7.
80. Lin, F. L.; Hoyt, H. M.; van Halbeek, H.; Bergman, R. G.; Bertozzi, C. R., Mechanistic Investigation of the Staudinger Ligation. *JACS* **2005,** *127* (8), 2686-2695.
81. Schilling, C. I.; Jung, N.; Biskup, M.; Schepers, U.; Brase, S., Bioconjugation Via Azide-Staudinger Ligation: An Overview. *Chem. Soc. Rev.* **2011,** *40* (9).
82. Wu, C.-Y.; Wong, C.-H., Chemistry and Glycobiology. *Chem. Commun.* **2011,** *47* (22).
83. Zhang, H.; Ma, Y.; Sun, X.-L., Chemically-Selective Surface Glyco-Functionalization of Liposomes through Staudinger Ligation. *Chem. Commun.* **2009,** (21).
84. Laughlin, S. T.; Bertozzi, C. R., Imaging the Glycome. *Proc. Natl. Acad. Sci. U. S. A.* **2009,** *106* (1), 12-17.
85. Mahal, L. K.; Yarema, K. J.; Bertozzi, C. R., Engineering Chemical Reactivity on Cell Surfaces through Oligosaccharide Biosynthesis. *Science* **1997,** *276* (5315), 1125-1128.
86. Moses, J. E.; Moorhouse, A. D., The Growing Applications of Click Chemistry. *Chem. Soc. Rev.* **2007,** *36* (8).
87. Best, M. D., Click Chemistry and Bioorthogonal Reactions: Unprecedented Selectivity in the Labeling of Biological Molecules. *Biochemistry (Mosc).* **2009,** *48* (28), 6571-6584.

88. Debets, M. F.; van der Doelen, C. W. J.; Rutjes, F. P. J. T.; van Delft, F. L., Azide: A Unique Dipole for Metal-Free Bioorthogonal Ligations. *ChemBioChem* **2010,** *11* (9), 1168-1184.
89. Kolb, H. C.; Finn, M. G.; Sharpless, K. B., Click Chemistry: Diverse Chemical Function from a Few Good Reactions. *Angew. Chem. Int. Ed.* **2001,** *40* (11), 2004-2021.
90. Tron, G. C.; Pirali, T.; Billington, R. A.; Canonico, P. L.; Sorba, G.; Genazzani, A. A., Click Chemistry Reactions in Medicinal Chemistry: Applications of the 1,3-Dipolar Cycloaddition between Azides and Alkynes. *Med. Res. Rev.* **2008,** *28* (2), 278-308.
91. Link, A. J.; Mock, M. L.; Tirrell, D. A., Non-Canonical Amino Acids in Protein Engineering. *Curr. Opin. Biotechnol.* **2003,** *14* (6), 603-609.
92. van Hest, J. C. M.; Kiick, K. L.; Tirrell, D. A., Efficient Incorporation of Unsaturated Methionine Analogues into Proteins in Vivo. *JACS* **2000,** *122* (7), 1282-1288.
93. Kirshenbaum, K.; Carrico, I. S.; Tirrell, D. A., Biosynthesis of Proteins Incorporating a Versatile Set of Phenylalanine Analogues. *ChemBioChem* **2002,** *3* (2-3), 235-237.
94. Kiick, K. L.; Van Hest, J. C. M.; Tirrell, D. A., Expanding the Scope of Protein Biosynthesis Via Introduction of a Mutant Methionyl-Trna Synthetase. *Abstr Pap Am Chem S* **2000,** *219*, U216-U216.
95. Kiick, K. L.; Saxon, E.; Tirrell, D. A.; Bertozzi, C. R., Incorporation of Azides into Recombinant Proteins for Chemoselective Modification by the Staudinger Ligation. *Proc. Natl. Acad. Sci. U. S. A.* **2002,** *99* (1), 19-24.
96. Xie, J. M.; Schultz, P. G., Adding Amino Acids to the Genetic Repertoire. *Curr. Opin. Chem. Biol.* **2005,** *9* (6), 548-554.
97. Wang, L.; Xie, J.; Schultz, P. G., Expanding the Genetic Code. In *Annu. Rev. Biophys. Biomol. Struct.*, 2006; Vol. 35, pp 225-249.
98. Xie, J.; Schultz, P. G., Innovation: A Chemical Toolkit for Proteins - an Expanded Genetic Code. *Nat. Rev. Mol. Cell Biol.* **2006,** *7* (10), 775-782.
99. Wang, L.; Schultz, P. G., Expanding the Genetic Code. *Angew. Chem. Int. Ed.* **2005,** *44* (1), 34-66.
100. Wang, L.; Brock, A.; Herberich, B.; Schultz, P. G., Expanding the Genetic Code of Escherichia Coli. *Science* **2001,** *292* (5516), 498-500.
101. Chin, J. W.; Cropp, T. A.; Anderson, J. C.; Mukherji, M.; Zhang, Z. W.; Schultz, P. G., An Expanded Eukaryotic Genetic Code. *Science* **2003,** *301* (5635), 964-967.
102. Liu, W.; Brock, A.; Chen, S.; Chen, S.; Schultz, P. G., Genetic Incorporation of Unnatural Amino Acids into Proteins in Mammalian Cells. *Nat. Methods* **2007,** *4* (3), 239-244.
103. Hanson, S. R.; Greenberg, W. A.; Wong, C. H., Probing Glycans with the Copper(I)-Catalyzed 3+2 Azide-Alkyne Cycloaddition. *QSAR Comb. Sci.* **2007,** *26* (11-12), 1243-1252.
104. Bryan, M. C.; Fazio, F.; Lee, H. K.; Huang, C. Y.; Chang, A.; Best, M. D.; Calarese, D. A.; Blixt, C.; Paulson, J. C.; Burton, D.; Wilson, I. A.; Wong, C. H.,

Covalent Display of Oligosaccharide Arrays in Microtiter Plates. *JACS* **2004,** *126* (28), 8640-8641.
105. Fazio, F.; Bryan, M. C.; Blixt, O.; Paulson, J. C.; Wong, C. H., Synthesis of Sugar Arrays in Microtiter Plate. *JACS* **2002,** *124* (48), 14397-14402.
106. Huang, C. Y.; Thayer, D. A.; Chang, A. Y.; Best, M. D.; Hoffmann, J.; Head, S.; Wong, C. H., Carbohydrate Microarray for Profiling the Antibodies Interacting with Globo H Tumor Antigen. *Proc. Natl. Acad. Sci. U. S. A.* **2006,** *103* (1), 15-20.
107. Besanceney-Webler, C.; Jiang, H.; Zheng, T.; Feng, L.; Soriano del Amo, D.; Wang, W.; Klivansky, L. M.; Marlow, F. L.; Liu, Y.; Wu, P., Increasing the Efficacy of Bioorthogonal Click Reactions for Bioconjugation: A Comparative Study. *Angew. Chem. Int. Ed.* **2011,** *50* (35), 8051-8056.
108. Agard, N. J.; Prescher, J. A.; Bertozzi, C. R., A Strain-Promoted [3 + 2] Azide−Alkyne Cycloaddition for Covalent Modification of Biomolecules in Living Systems. *JACS* **2004,** *126* (46), 15046-15047.
109. Meier, H.; Petersen, H.; Kolshorn, H., Die Ringspannung Von Cycloalkinen Und Ihre Spektroskopischen Auswirkungen. *Chem. Ber.* **1980,** *113* (7), 2398-2409.
110. Agard, N. J.; Prescher, J. A.; Bertozzi, C. R., A Strain-Promoted [3 + 2] Azide,Àíalkyne Cycloaddition for Covalent Modification of Biomolecules in Living Systems [J. Am. Chem. Soc. 2004, 126, 15046,Àí15047]. *JACS* **2005,** *127* (31), 11196-11196.
111. Agard, N. J.; Baskin, J. M.; Prescher, J. A.; Lo, A.; Bertozzi, C. R., A Comparative Study of Bioorthogonal Reactions with Azides. *ACS Chem. Biol.* **2006,** *1* (10), 644-648.
112. Baskin, J. M.; Prescher, J. A.; Laughlin, S. T.; Agard, N. J.; Chang, P. V.; Miller, I. A.; Lo, A.; Codelli, J. A.; Bertozzi, C. R., Copper-Free Click Chemistry for Dynamic in Vivo Imaging. *Proceedings of the National Academy of Sciences* **2007,** *104* (43), 16793-16797.
113. Codelli, J. A.; Baskin, J. M.; Agard, N. J.; Bertozzi, C. R., Second-Generation Difluorinated Cyclooctynes for Copper-Free Click Chemistry. *JACS* **2008,** *130* (34), 11486-11493.
114. Ning, X.; Guo, J.; Wolfert, M. A.; Boons, G.-J., Visualizing Metabolically Labeled Glycoconjugates of Living Cells by Copper-Free and Fast Huisgen Cycloadditions. *Angew. Chem. Int. Ed.* **2008,** *47* (12), 2253-2255.
115. Sletten, E. M.; Bertozzi, C. R., A Hydrophilic Azacyclooctyne for Cu-Free Click Chemistry. *Org. Lett.* **2008,** *10* (14), 3097-3099.
116. Debets, M. F.; van Berkel, S. S.; Schoffelen, S.; Rutjes, F. P. J. T.; van Hest, J. C. M.; van Delft, F. L., Aza-Dibenzocyclooctynes for Fast and Efficient Enzyme Pegylation Via Copper-Free (3+2) Cycloaddition. *Chem. Commun.* **2010,** *46* (1).
117. Laughlin, S. T.; Baskin, J. M.; Amacher, S. L.; Bertozzi, C. R., In Vivo Imaging of Membrane-Associated Glycans in Developing Zebrafish. *Science* **2008,** *320* (5876), 664-667.
118. Chang, P. V.; Prescher, J. A.; Hangauer, M. J.; Bertozzi, C. R., Imaging Cell Surface Glycans with Bioorthogonal Chemical Reporters. *JACS* **2007,** *129* (27), 8400-8401.

119. Ning, X.; Temming, R. P.; Dommerholt, J.; Guo, J.; Ania, D. B.; Debets, M. F.; Wolfert, M. A.; Boons, G.-J.; van Delft, F. L., Protein Modification by Strain-Promoted Alkyne–Nitrone Cycloaddition. *Angew. Chem. Int. Ed.* **2010,** *49* (17), 3065-3068.
120. Boons, G.-J., Bioorthogonal Chemical Reporter Methodology for Visualization, Isolation and Analysis of Glycoconjugates. In *Carbohydr. Chem.*, The Royal Society of Chemistry: 2010; Vol. 36.
121. Poloukhtine, A. A.; Mbua, N. E.; Wolfert, M. A.; Boons, G.-J.; Popik, V. V., Selective Labeling of Living Cells by a Photo-Triggered Click Reaction. *JACS* **2009,** *131* (43), 15769-15776.
122. Sandbhor, M. S.; Key, J. A.; Strelkov, I. S.; Cairo, C. W., A Modular Synthesis of Alkynyl-Phosphocholine Headgroups for Labeling Sphingomyelin and Phosphatidylcholine. *J. Org. Chem.* **2009,** *74* (22), 8669-8674.
123. Jao, C. Y.; Roth, M.; Welti, R.; Salic, A., Metabolic Labeling and Direct Imaging of Choline Phospholipids in Vivo. *Proc. Natl. Acad. Sci. U. S. A.* **2009,** *106* (36), 15332-15337.
124. O'Neil, E. J.; DiVittorio, K. M.; Smith, B. D., Phosphatidylcholine-Derived Bolaamphiphiles Via Click Chemistry. *Org. Lett.* **2007,** *9* (2), 199-202.
125. Lampkins, A. J.; O'Neil, E. J.; Smith, B. D., Bio-Orthogonal Phosphatidylserine Conjugates for Delivery and Imaging Applications. *J. Org. Chem.* **2008,** *73* (16), 6053-6058.
126. Smith, B. A.; O'Neil, E. J.; Lampkins, A. J.; Johnson, J. R.; Lee, J.-J.; Cole, E. L.; Smith, B. D., Evaluation of Fluorescent Phosphatidylserine Substrates for the Aminophospholipid Flippase in Mammalian Cells. *J. Fluoresc.* **2012,** *22* (1), 93-101.
127. Neef, A. B.; Schultz, C., Selective Fluorescence Labeling of Lipids in Living Cells. *Angew. Chem. Int. Ed.* **2009,** *48* (8), 1498-1500.
128. Rowland, M. M.; Bostic, H. E.; Gong, D.; Speers, A. E.; Lucas, N.; Cho, W.; Cravatt, B. F.; Best, M. D., Phosphatidylinositol 3,4,5-Trisphosphate Activity Probes for the Labeling and Proteomic Characterization of Protein Binding Partners. *Biochemistry (Mosc).* **2011,** *50* (51), 11143-11161.
129. Losey, E. A.; Smith, M. D.; Meng, M.; Best, M. D., Microplate-Based Analysis of Protein−Membrane Binding Interactions Via Immobilization of Whole Liposomes Containing a Biotinylated Anchor. *Bioconj. Chem.* **2009,** *20* (2), 376-383.
130. Smith, M. D.; Sudhahar, C. G.; Gong, D.; Stahelin, R. V.; Best, M. D., Modular Synthesis of Biologically Active Phosphatidic Acid Probes Using Click Chemistry. *Mol. BioSyst.* **2009,** *5* (9).
131. Smith, M. D.; Gong, D.; Sudhahar, C. G.; Reno, J. C.; Stahelin, R. V.; Best, M. D., Synthesis and Convenient Functionalization of Azide-Labeled Diacylglycerol Analogues for Modular Access to Biologically Active Lipid Probes. *Bioconj. Chem.* **2008,** *19* (9), 1855-1863.
132. Masson, L.; Mazza, A.; Brousseau, R., Stable Immobilization of Lipid Vesicles for Kinetic Studies Using Surface Plasmon Resonance. *Anal. Biochem.* **1994,** *218* (2), 405-412.

133. Di Paolo, G.; De Camilli, P., Phosphoinositides in Cell Regulation and Membrane Dynamics. *Nature* **2006,** *443* (7112), 651-657.
134. Lemmon, M. A., Phosphoinositide Recognition Domains. *Traffic* **2003,** *4* (4), 201-213.
135. Vicinanza, M.; D'Angelo, G.; Di Campli, A.; De Matteis, M. A., Phosphoinositides as Regulators of Membrane Trafficking in Health and Disease. *Cell. Mol. Life Sci.* **2008,** *65* (18), 2833-2841.
136. Wymann, M. P.; Schneiter, R., Lipid Signalling in Disease. *Nat. Rev. Mol. Cell Biol.* **2008,** *9* (2), 162-176.
137. Prestwich, G. D., Touching All the Bases: Synthesis of Inositol Polyphosphate and Phosphoinositide Affinity Probes from Glucose. *Acc. Chem. Res.* **1996,** *29* (10), 503-513.
138. Painter, G. F.; J. A. Grove, S.; H. Gilbert, I.; B. Holmes, A.; R. Raithby, P.; L. Hill, M.; T. Hawkins, P.; R. Stephens, L., General Synthesis of 3-Phosphorylated Myo-Inositol Phospholipids and Derivatives. *J. Chem. Soc., Perkin Trans. 1* **1999,** (8), 923-936.
139. Kubiak, R. J.; Bruzik, K. S., Comprehensive and Uniform Synthesis of All Naturally Occurring Phosphorylated Phosphatidylinositols. *J. Org. Chem.* **2003,** *68* (3), 960-968.
140. Dreef, C. E.; Elie, C. J. J.; Hoogerhout, P.; van der Marel, G. A.; van Boom, J. H., Synthesis of 1-O-(1,2-Di-O-Palmitoyl-Sn-Glycero-3-Phospho)-D-Myo-Inositol 4,5-Bisphosphate: An Analogue of Naturally Occurring (Ptd)Ins(4,5)P2. *Tetrahedron Lett.* **1988,** *29* (49), 6513-6515.
141. Pietrusiewicz, K. M.; Salamończyk, G. M.; Bruzik, K. S.; Wieczorek, W., The Synthesis of Homochiral Inositol Phosphates from Myo-Inositol. *Tetrahedron* **1992,** *48* (26), 5523-5542.
142. Kishta Reddy, K.; Rizo, J.; Falck, J. R., Concise Synthesis of L-A-Phosphatidyl-D-Myo-Inositol 3,4-Bisphosphate, an Intracellular Second Messenger. *Tetrahedron Lett.* **1997,** *38* (27), 4729-4730.
143. Watanabe, Y.; Inada, E.; Jinno, M.; Ozaki, S., Phosphonium Salt Methodology for the Synthesis of Phosphoric Monoesters and Diesters and Its Application to Selective Phosphorylation. *Tetrahedron Lett.* **1993,** *34* (3), 497-500.
144. Vishwakarma, R. A.; Vehring, S.; Mehta, A.; Sinha, A.; Pomorski, T.; Herrmann, A.; Menon, A. K., New Fluorescent Probes Reveal That Flippase-Mediated Flip-Flop of Phosphatidylinositol across the Endoplasmic Reticulum Membrane Does Not Depend on the Stereochemistry of the Lipid. *Org. Biomol. Chem.* **2005,** *3* (7).
145. Rukavishnikov, A. V.; Ryan, M.; Griffith, O. H.; Keana, J. F. W., A Chromogenic Substrate for the Continuous Assay of Mammalian Phosphoinositide-Specific Phospholipase C. *Bioorg. Med. Chem. Lett.* **1997,** *7* (10), 1239-1242.
146. Gu, Q.-M.; Prestwich, G. D., Synthesis of Phosphotriester Analogues of the Phosphoinositides Ptdins(4,5)P2 and Ptdins(3,4,5)P3. *J. Org. Chem.* **1996,** *61* (24), 8642-8647.

147. Han, F.; Hayashi, M.; Watanabe, Y., Regioselective Phosphorylation of Vicinal 3,4-Hydroxy Myo-Inositol Derivative Promoted Practical Synthesis of D-Ptdins(4,5)P2 and D-Ins(1,4,5)P3. *Tetrahedron* **2003,** *59* (39), 7703-7711.
148. Han, F.; Hayashi, M.; Watanabe, Y., Chemical Resolution of 1,2-O-Cyclohexylidene-3,4-O-(Tetraisopropyldisiloxane-1,3-Diyl)-Myo-Inositol and Synthesis of Phosphatidyl-D-Myo-Inositol 3,5-Bisphosphate from Both L- and D-Enantiomers. *Eur. J. Org. Chem.* **2004,** *2004* (3), 558-566.
149. Morgan, A. J.; Komiya, S.; Xu, Y.; Miller, S. J., Unified Total Syntheses of the Inositol Polyphosphates: D-I-3,5,6p3, D-I-3,4,5p3, D-I-3,4,6p3, and D-I-3,4,5,6p4 Via Catalytic Enantioselective and Site-Selective Phosphorylation. *J. Org. Chem.* **2006,** *71* (18), 6923-6931.
150. Morgan, A. J.; Wang, Y. K.; Roberts, M. F.; Miller, S. J., Chemistry and Biology of Deoxy-Myo-Inositol Phosphates: Stereospecificity of Substrate Interactions within an Archaeal and a Bacterial Impase. *JACS* **2004,** *126* (47), 15370-15371.
151. Sculimbrene, B. R.; Miller, S. J., Discovery of a Catalytic Asymmetric Phosphorylation through Selection of a Minimal Kinase Mimic: A Concise Total Synthesis of D-Myo-Inositol-1-Phosphate. *JACS* **2001,** *123* (41), 10125-10126.
152. Sculimbrene, B. R.; Morgan, A. J.; Miller, S. J., Enantiodivergence in Small-Molecule Catalysis of Asymmetric Phosphorylation: Concise Total Syntheses of the Enantiomeric D-Myo-Inositol-1-Phosphate and D-Myo-Inositol-3-Phosphate. *JACS* **2002,** *124* (39), 11653-11656.
153. Sculimbrene, B. R.; Xu, Y.; Miller, S. J., Asymmetric Syntheses of Phosphatidylinositol-3-Phosphates with Saturated and Unsaturated Side Chains through Catalytic Asymmetric Phosphorylation. *JACS* **2004,** *126* (41), 13182-13183.
154. Anderson, R. J.; Osborne, S. L.; Meunier, F. A.; Painter, G. F., Regioselective Approach to Phosphatidylinositol 3,5-Bisphosphates: Syntheses of the Native Phospholipid and Biotinylated Short-Chain Derivative. *J. Org. Chem.* **2010,** *75* (11), 3541-3551.
155. Catimel, B.; Schieber, C.; Condron, M.; Patsiouras, H.; Connolly, L.; Catimel, J.; Nice, E. C.; Burgess, A. W.; Holmes, A. B., The Pi(3,5)P2 and Pi(4,5)P2 Interactomes. *J. Proteome Res.* **2008,** *7* (12), 5295-313.
156. Catimel, B.; Yin, M.-X.; Schieber, C.; Condron, M.; Patsiouras, H.; Catimel, J.; Robinson, D. E. J. E.; Wong, L. S. M.; Nice, E. C.; Holmes, A. B.; Burgess, A. W., Pi(3,4,5)P3 Interactome. *J. Proteome Res.* **2009,** *8* (7), 3712-3726.
157. Conway, S. J.; Miller, G. J., Biology-Enabling Inositol Phosphates, Phosphatidylinositol Phosphates and Derivatives. *Nat. Prod. Rep.* **2007,** *24* (4), 687-707.
158. Krugmann, S.; Anderson, K. E.; Ridley, S. H.; Risso, N.; McGregor, A.; Coadwell, J.; Davidson, K.; Eguinoa, A.; Ellson, C. D.; Lipp, P.; Manifava, M.; Ktistakis, N.; Painter, G.; Thuring, J. W.; Cooper, M. A.; Lim, Z. Y.; Holmes, A. B.; Dove, S. K.; Michell, R. H.; Grewal, A.; Nazarian, A.; Erdjument-Bromage, H.; Tempst, P.; Stephens, L. R.; Hawkins, P. T., Identification of Arap3, a Novel Pi3k Effector

Regulating Both Arf and Rho Gtpases, by Selective Capture on Phosphoinositide Affinity Matrices. *Mol. Cell* **2002,** *9* (1), 95-108.
159. Lim, Z. Y.; Thuring, J. W.; Holmes, A. B.; Manifava, M.; Ktistakis, N. T., Synthesis and Biological Evaluation of a Ptdins(4,5)P-2 and a Phosphatidic Acid Affinity Matrix. *J. Chem. Soc., Perkin Trans. 1* **2002,** (8), 1067-1075.
160. Manifava, M.; Thuring, J.; Lim, Z. Y.; Packman, L.; Holmes, A. B.; Ktistakis, N. T., Differential Binding of Traffic-Related Proteins to Phosphatidic Acid- or Phosphatidylinositol (4,5)-Bisphosphate-Coupled Affinity Reagents. *J. Biol. Chem.* **2001,** *276* (12), 8987-8994.
161. Osborne, S. L.; Wallis, T. P.; Jimenez, J. L.; Gorman, J. J.; Meunier, F. A., Identification of Secretory Granule Phosphatidylinositol 4,5-Bisphosphateinteracting Proteins Using an Affinity Pulldown Strategy. *Molecular & Cellular Proteomics* **2007,** *6* (7), 1158-1169.
162. Painter, G. F.; Thuring, J. W.; Lim, Z. Y.; Holmes, A. B.; Hawkins, P. T.; Stephens, L. R., Synthesis and Biological Evaluation of a Ptdins(3,4,5)P-3 Affinity Matrix. *Chem. Commun.* **2001,** (7), 645-646.
163. Pasquali, C.; Bertschy-Meier, D.; Chabert, C.; Curchod, M.-L.; Arod, C.; Booth, R.; Mechtler, K.; Vilbois, F.; Xenarios, I.; Ferguson, C. G.; Prestwich, G. D.; Camps, M.; Rommel, C., A Chemical Proteomics Approach to Phosphatidylinositol 3-Kinase Signaling in Macrophages. *Molecular & Cellular Proteomics* **2007,** *6* (11), 1829-1841.
164. Ferguson, C. G.; James, R. D.; Bigman, C. S.; Shepard, D. A.; Abdiche, Y.; Katsamba, P. S.; Myszka, D. G.; Prestwich, G. D., Phosphoinositide-Containing Polymerized Liposomes: Stable Membrane-Mimetic Vesicles for Protein−Lipid Binding Analysis. *Bioconj. Chem.* **2005,** *16* (6), 1475-1483.
165. Richer, S. M.; Stewart, N. K.; Tomaszewski, J. W.; Stone, M. J.; Oakley, M. G., Nmr Investigation of the Binding between Human Profilin I and Inositol 1,4,5-Triphosphate, the Soluble Headgroup of Phosphatidylinositol 4,5-Bisphosphate. *Biochemistry (Mosc).* **2008,** *47* (51), 13455-13462.
166. Richer, S. M.; Stewart, N. K.; Webb, S. A.; Tomaszewski, J. W.; Oakley, M. G., High Affinity Binding to Profilin by a Covalently Constrained, Soluble Mimic of Phosphatidylinositol-4,5-Bisphosphate Micelles. *ACS Chem. Biol.* **2009,** *4* (9), 733-739.
167. Kalyankar, N. D.; Sharma, M. K.; Vaidya, S. V.; Calhoun, D.; Maldarelli, C.; Couzis, A.; Gilchrist, L., Arraying of Intact Liposomes into Chemically Functionalized Microwells. *Langmuir* **2006,** *22* (12), 5403-5411.
168. Elkin, S. K.; Ivanov, D.; Ewalt, M.; Ferguson, C. G.; Hyberts, S. G.; Sun, Z. Y. J.; Prestwich, G. D.; Yuan, J. Y.; Wagner, G.; Oettinger, M. A.; Gozani, O. P., A Phd Finger Motif in the C Terminus of Rag2 Modulates Recombination Activity. *J. Biol. Chem.* **2005,** *280* (31), 28701-28710.
169. Webb, S. A.; Stewart, N. K.; Belcher, L. J.; Mechref, Y.; Tomaszewski, J. W.; Wu, G.; Novotny, M. V.; Oakley, M. G., Synthesis and Characterization of Covalent Mimics of Phosphatidylinositol-4,5-Bisphosphate Micelles. *Biomacromolecules* **2007,** *8* (6), 1790-1793.

170. Lassing, I.; Lindberg, U., Specific Interaction between Phosphatidylinositol 4,5-Bisphosphate and Profilactin. *Nature* **1985,** *314* (6010), 472-474.
171. Goldschmidt-Clermont, P.; Machesky, L.; Baldassare, J.; Pollard, T., The Actin-Binding Protein Profilin Binds to Pip2 and Inhibits Its Hydrolysis by Phospholipase C. *Science* **1990,** *247* (4950), 1575-1578.
172. Sathish, K.; Padma, B.; Munugalavadla, V.; Bhargavi, V.; Radhika, K. V. N.; Wasia, R.; Sairam, M.; Singh, S. S., Phosphorylation of Profilin Regulates Its Interaction with Actin and Poly (L-Proline). *Cell. Signal.* **2004,** *16* (5), 589-596.
173. Lambrechts, A.; Jonckheere, V.; Dewitte, D.; Vandekerckhove, J.; Ampe, C., Mutational Analysis of Human Profilin I Reveals a Second Pi(4,5)-P2 Binding Site Neighbouring the Poly(L-Proline) Binding Site. *BMC Biochem.* **2002,** *3*, 12.
174. Machesky, L. M.; Goldschmidtclermont, P. J.; Pollard, T. D., The Affinities of Human Platelet and Acanthamoeba Profilin Isoforms for Polyphosphoinositides Account for Their Relative Abilities to Inhibit Phospholipase-C. *Cell Regul.* **1990,** *1* (12), 937-950.
175. Lu, P. J.; Shieh, W. R.; Rhee, S. G.; Yin, H. L.; Chen, C. S., Lipid Products of Phosphoinositide 3-Kinase Bind Human Profilin with High Affinity. *Biochemistry (Mosc).* **1996,** *35* (44), 14027-14034.
176. Liang, P.-H.; Wang, S.-K.; Wong, C.-H., Quantitative Analysis of Carbohydrate−Protein Interactions Using Glycan Microarrays: Determination of Surface and Solution Dissociation Constants. *JACS* **2007,** *129* (36), 11177-11184.
177. Liang, P.-H.; Wu, C.-Y.; Greenberg, W. A.; Wong, C.-H., Glycan Arrays: Biological and Medical Applications. *Curr. Opin. Chem. Biol.* **2008,** *12* (1), 86-92.
178. Oyelaran, O.; Gildersleeve, J. C., Glycan Arrays: Recent Advances and Future Challenges. *Curr. Opin. Chem. Biol.* **2009,** *13* (4), 406-413.
179. Oyelaran, O.; Li, Q.; Farnsworth, D.; Gildersleeve, J. C., Microarrays with Varying Carbohydrate Density Reveal Distinct Subpopulations of Serum Antibodies. *J. Proteome Res.* **2009,** *8* (7), 3529-3538.
180. Oyelaran, O.; McShane, L. M.; Dodd, L.; Gildersleeve, J. C., Profiling Human Serum Antibodies with a Carbohydrate Antigen Microarray. *J. Proteome Res.* **2009,** *8* (9), 4301-4310.
181. Prestwich, G. D., Phosphoinositide Signaling: From Affinity Probes to Pharmaceutical Targets. *Chemistry & Biology* **2004,** *11* (5), 619-637.
182. Conway, S. J.; Gardiner, J.; Grove, S. J. A.; Johns, M. K.; Lim, Z.-Y.; Painter, G. F.; Robinson, D. E. J. E.; Schieber, C.; Thuring, J. W.; Wong, L. S. M.; Yin, M.-X.; Burgess, A. W.; Catimel, B.; Hawkins, P. T.; Ktistakis, N. T.; Stephens, L. R.; Holmes, A. B., Synthesis and Biological Evaluation of Phosphatidylinositol Phosphate Affinity Probes. *Org. Biomol. Chem.* **2010,** *8* (1).
183. Ferguson, K. M.; Lemmon, M. A.; Schlessinger, J.; Sigler, P. B., Structure of the High-Affinity Complex of Inositol Trisphosphate with a Phospholipase-C Pleckstrin Homology Domain. *Cell* **1995,** *83* (6), 1037-1046.
184. Garcia, P.; Gupta, R.; Shah, S.; Morris, A. J.; Rudge, S. A.; Scarlata, S.; Petrova, V.; McLaughlin, S.; Rebecchi, M. J., The Pleckstrin Homology Domain of

Phospholipase C-Delta(1) Binds with High Affinity to Phosphatidylinositol 4,5-Bisphosphate in Bilayer Membranes. *Biochemistry (Mosc).* **1995,** *34* (49), 16228-16234.
185. Hirose, K.; Kadowaki, S.; Tanabe, M.; Takeshima, H.; Iino, M., Spatiotemporal Dynamics of Inositol 1,4,5-Trisphosphate That Underlies Complex Ca2+ Mobilization Patterns. *Science* **1999,** *284* (5419), 1527-1530.
186. Lemmon, M. A.; Ferguson, K. M.; Obrien, R.; Sigler, P. B.; Schlessinger, J., Specific and High-Affinity Binding of Inositol Phosphates to an Isolated Pleckstrin Homology Domain. *Proc. Natl. Acad. Sci. U. S. A.* **1995,** *92* (23), 10472-10476.
187. Kutateladze, T. G., Phosphatidylinositol 3-Phosphate Recognition and Membrane Docking by the Fyve Domain. *Biochim. Biophys. Acta, Mol. Cell Biol. Lipids* **2006,** *1761* (8), 868-877.
188. Bravo, J.; Karathanassis, D.; Pacold, C. M.; Pacold, M. E.; Ellson, C. D.; Anderson, K. E.; Butler, P. J. G.; Lavenir, I.; Perisic, O.; Hawkins, P. T.; Stephens, L.; Williams, R. L., The Crystal Structure of the Px Domain from P40(Phox) Bound to Phosphatidylinositol 3-Phosphate. *Mol. Cell* **2001,** *8* (4), 829-839.
189. Vivanco, I.; Sawyers, C. L., The Phosphatidylinositol 3-Kinase-Akt Pathway in Human Cancer. *Nat. Rev. Cancer* **2002,** *2* (7), 489-501.
190. Assinder, S. J.; Dong, Q.; Kovacevic, Z.; Richardson, D. R., The Tgf-Beta, Pi3k/Akt and Pten Pathways: Established and Proposed Biochemical Integration in Prostate Cancer. *Biochem. J.* **2009,** *417*, 411-421.
191. Duronio, V., The Life of a Cell: Apoptosis Regulation by the Pi3k/Pkb Pathway. *Biochem. J.* **2008,** *415*, 333-344.
192. Engelman, J. A.; Luo, J.; Cantley, L. C., The Evolution of Phosphatidylinositol 3-Kinases as Regulators of Growth and Metabolism. *Nat. Rev. Genet.* **2006,** *7* (8), 606-619.
193. Manning, B. D.; Cantley, L. C., Akt/Pkb Signaling: Navigating Downstream. *Cell* **2007,** *129* (7), 1261-1274.
194. Yuan, T. L.; Cantley, L. C., Pi3k Pathway Alterations in Cancer: Variations on a Theme. *Oncogene* **2008,** *27* (41), 5497-5510.
195. Salmena, L.; Carracedo, A.; Pandolfi, P. P., Tenets of Pten Tumor Suppression. *Cell* **2008,** *133* (3), 403-414.
196. Katso, R.; Okkenhaug, K.; Ahmadi, K.; White, S.; Timms, J.; Waterfield, M. D., Cellular Function of Phosphoinositide 3-Kinases: Implications for Development, Immunity, Homeostasis, and Cancer. *Annu. Rev. Cell. Dev. Biol.* **2001,** *17* (1), 615-675.
197. Chow, L. M. L.; Baker, S. J., Pten Function in Normal and Neoplastic Growth. *Cancer Lett.* **2006,** *241* (2), 184-196.
198. Maehama, T.; Dixon, J. E., The Tumor Suppressor, Pten/Mmac1, Dephosphorylates the Lipid Second Messenger, Phosphatidylinositol 3,4,5-Trisphosphate. *J. Biol. Chem.* **1998,** *273* (22), 13375-13378.
199. Samuels, Y.; Wang, Z.; Bardelli, A.; Silliman, N.; Ptak, J.; Szabo, S.; Yan, H.; Gazdar, A.; Powell, S. M.; Riggins, G. J.; Willson, J. K. V.; Markowitz, S.; Kinzler,

K. W.; Vogelstein, B.; Velculescu, V. E., High Frequency of Mutations of the Pik3ca Gene in Human Cancers. *Science* **2004,** *304* (5670), 554.
200. Gong, D.; Smith, M. D.; Manna, D.; Bostic, H. E.; Cho, W.; Best, M. D., Microplate-Based Characterization of Protein-Phosphoinositide Binding Interactions Using a Synthetic Biotinylated Headgroup Analogue. *Bioconj. Chem.* **2009,** *20* (2), 310-316.
201. Das, A.; Base, C.; Manna, D.; Cho, W.; Dubreuil, R. R., Unexpected Complexity in the Mechanisms That Target Assembly of the Spectrin Cytoskeleton. *J. Biol. Chem.* **2008,** *283* (18), 12643-12653.
202. Kojima, T.; Fukuda, M.; Watanabe, Y.; Hamazato, F.; Mikoshiba, K., Characterization of the Pleckstrin Homology Domain of Btk as an Inositol Polyphosphate and Phosphoinositide Binding Domain. *Biochem. Biophys. Res. Commun.* **1997,** *236* (2), 333-339.
203. Lockyer, P. J.; Bottomley, J. R.; Reynolds, J. S.; McNulty, T. J.; Venkateswarlu, K.; Potter, B. V. L.; Dempsey, C. E.; Cullen, P. J., Distinct Subcellular Localisations of the Putative Inositol 1,3,4,5-Tetrakisphosphate Receptors Gap1(Ip4bp) and Gap1(M) Result from the Gap1(Ip4bp) Ph Domain Directing Plasma Membrane Targeting. *Curr. Biol.* **1997,** *7* (12), 1007-1010.
204. Schäfer, R.; Nehls-Sahabandu, M.; Grabowsky, B.; Dehlinger-Kremer, M.; Schulz, I.; Mayr, G. W., Synthesis and Application of Photoaffinity Analogues of Inositol 1,4,5-Trisphosphate Selectively Substituted at the 1-Phosphate Group. *Biochem. J.* **1990,** *272* (3), 817-825.
205. Prestwich, G. D.; Marecek, J. F.; Mourey, R. J.; Theibert, A. B.; Ferris, C. D.; Danoff, S. K.; Snyder, S. H., Tethered Ip3 - Synthesis and Biochemical Applications of the 1-O-(3-Aminopropyl) Ester of Inositol 1,4,5-Trisphosphate. *JACS* **1991,** *113* (5), 1822-1825.
206. Marecek, J. F.; Estevez, V. A.; Prestwich, G. D., New Tetherable Derivatives of Myoinositol 2,4,5-Trisphosphates and 1,3,4-Trisphosphates. *Carbohydr. Res.* **1992,** *234*, 65-73.
207. Tegge, W.; Ballou, C. E., Syntheses of D-Myo-Inositol 1,4,5-Trisphosphate Affinity Ligands. *Carbohydr. Res.* **1992,** *230* (1), 63-77.
208. Henne, V.; Mayr, G. W.; Grabowski, B.; Koppitz, B.; Soling, H. D., Semisynthetic Derivatives of Inositol 1,4,5-Trisphosphate Substituted at the 1-Phosphate Group - Effects on Calcium Release from Permeabilized Guinea-Pig Parotid Acinar-Cells and Comparison with Binding to Aldolase-A. *Eur. J. Biochem.* **1988,** *174* (1), 95-101.
209. Dorman, G.; Chen, J.; Prestwich, G. D., Synthesis of D-Myo-P-1-(O-Aminopropyl)-Inositol-1,4,5-Trisphosphate Affinity Probes from Alpha-D-Glucose. *Tetrahedron Lett.* **1995,** *36* (48), 8719-8722.
210. Nakanishi, W.; Kikuchi, K.; Inoue, T.; Hirose, K.; Iino, M.; Nagano, T., Hydrophobic Modifications at 1-Phosphate of Inositol 1,4,5-Trisphosphate Analogues Enhance Receptor Binding. *Biorg. Med. Chem. Lett.* **2002,** *12* (6), 911-913.

211. Inoue, T.; Kikuchi, K.; Hirose, K.; Iino, M.; Nagano, T., Synthesis and Evaluation of 1-Position-Modified Inositol 1,4, 5-Trisphosphate Analogs. *Biorg. Med. Chem. Lett.* **1999,** *9* (12), 1697-1702.
212. Olszewski, J. D.; Dorman, G.; Elliott, J. T.; Hong, Y.; Ahern, D. G.; Prestwich, G. D., Tethered Benzophenone Reagents for the Synthesis of Photoactivatable Ligands. *Bioconj. Chem.* **1995,** *6* (4), 395-400.
213. Rowland, M. M.; Gong, D.; Bostic, H. E.; Lucas, N.; Cho, W.; Best, M. D., Microarray Analysis of Akt Ph Domain Binding Employing Synthetic Biotinylated Analogs of All Seven Phosphoinositide Headgroup Isomers. *Chem. Phys. Lipids* **2012,** *165* (2), 207-215.
214. Lewallen, D. M.; Siler, D.; Iyer, S. S., Factors Affecting Protein–Glycan Specificity: Effect of Spacers and Incubation Time. *ChemBioChem* **2009,** *10* (9), 1486-1489.
215. Gong, D.; Bostic, H. E.; Smith, M. D.; Best, M. D., Synthesis of Modular Headgroup Conjugates Corresponding to All Seven Phosphatidylinositol Polyphosphate Isomers for Convenient Probe Generation. *Eur. J. Org. Chem.* **2009,** (24), 4170-4179.
216. Bruzik, K. S.; Salamończyk, G. M., Synthesis of the Enantiomeric 1,4,5,6-Tetra-O-Benzyl-Myo Inositols. *Carbohydr. Res.* **1989,** *195* (1), 67-73.
217. Bruzik, K. S.; Tsai, M. D., Efficient and Systematic Syntheses of Enantiomerically Pure and Regiospecifically Protected Myo-Inositols. *JACS* **1992,** *114* (16), 6361-6374.
218. Frech, M.; Andjelkovic, M.; Ingley, E.; Reddy, K. K.; Falck, J. R.; Hemmings, B. A., High Affinity Binding of Inositol Phosphates and Phosphoinositides to the Pleckstrin Homology Domain of Rac Protein Kinase B and Their Influence on Kinase Activity. *J. Biol. Chem.* **1997,** *272* (13), 8474-8481.
219. Manna, D.; Albanese, A.; Park, W. S.; Cho, W., Mechanistic Basis of Differential Cellular Responses of Phosphatidylinositol 3,4-Bisphosphate- and Phosphatidylinositol 3,4,5-Trisphosphate-Binding Pleckstrin Homology Domains. *J. Biol. Chem.* **2007,** *282* (44), 32093-32105.
220. James, S. R.; Downes, C. P.; Gigg, R.; Grove, S. J. A.; Holmes, A. B.; Alessi, D. R., Specific Binding of the Akt-1 Protein Kinase to Phosphatidylinositol 3,4,5-Trisphosphate without Subsequent Activation. *Biochem. J.* **1996,** *315*, 709-713.
221. Wang, C.-C.; Huang, Y.-L.; Ren, C.-T.; Lin, C.-W.; Hung, J.-T.; Yu, J.-C.; Yu, A. L.; Wu, C.-Y.; Wong, C.-H., Glycan Microarray of Globo H and Related Structures for Quantitative Analysis of Breast Cancer. *Proceedings of the National Academy of Sciences* **2008,** *105* (33), 11661-11666.
222. Wu, C.-Y.; Liang, P.-H.; Wong, C.-H., New Development of Glycan Arrays. *Org. Biomol. Chem.* **2009,** *7* (11), 2247-2254.
223. Wang, S. K.; Liang, P. H.; Astronomo, R. D.; Hsu, T. L.; Hsieh, S. L.; Burton, D. R.; Wong, C. H., Targeting the Carbohydrates on Hiv-1: Interaction of Oligomannose Dendrons with Human Monoclonal Antibody 2g12 and Dc-Sign. *Proc. Natl. Acad. Sci. U. S. A.* **2008,** *105* (10), 3690-3695.

224. Jiang, T.; Sweeney, G.; Rudolf, M. T.; Klip, A.; Traynor-Kaplan, A.; Tsien, R. Y., Membrane-Permeant Esters of Phosphatidylinositol 3,4,5-Trisphosphate. *J. Biol. Chem.* **1998,** *273* (18), 11017-11024.
225. Torchilin, V. P., Recent Advances with Liposomes as Pharmaceutical Carriers. *Nat Rev Drug Discov* **2005,** *4* (2), 145-160.
226. Sawant, R. R.; Torchilin, V. P., Liposomes as 'Smart' Pharmaceutical Nanocarriers. *Soft Matter* **2010,** *6* (17).
227. Allen, T. M.; Cullis, P. R., Drug Delivery Systems: Entering the Mainstream. *Science* **2004,** *303* (5665), 1818-1822.
228. Said Hassane, F.; Frisch, B.; Schuber, F., Targeted Liposomes: Convenient Coupling of Ligands to Preformed Vesicles Using “Click Chemistry”. *Bioconj. Chem.* **2006,** *17* (3), 849-854.
229. Cavalli, S.; Tipton, A. R.; Overhand, M.; Kros, A., The Chemical Modification of Liposome Surfaces Via a Copper-Mediated [3 + 2] Azide-Alkyne Cycloaddition Monitored by a Colorimetric Assay. *Chem. Commun.* **2006,** (30).
230. Rijkers, D. T. S.; van Vugt, H. H. R.; Jacobs, H. J. F.; Liskamp, R. M. J., A Convenient Synthesis of Azido Peptides by Post-Assembly Diazo Transfer on the Solid Phase Applicable to Large Peptides. *Tetrahedron Lett.* **2002,** *43* (20), 3657-3660.
231. Mehvar, R., Recent Trends in the Use of Polysaccharides for Improved Delivery of Therapeutic Agents: Pharmacokinetic and Pharmacodynamic Perspectives. *Curr. Pharm. Biotechnol.* **2003,** *4* (5), 283-302.
232. van Lengerich, B.; Rawle, R. J.; Boxer, S. G., Covalent Attachment of Lipid Vesicles to a Fluid-Supported Bilayer Allows Observation of DNA-Mediated Vesicle Interactions. *Langmuir* **2010,** *26* (11), 8666-8672.
233. Chan, Y.-H. M.; Lenz, P.; Boxer, S. G., Kinetics of DNA-Mediated Docking Reactions between Vesicles Tethered to Supported Lipid Bilayers. *Proc. Natl. Acad. Sci. U. S. A.* **2007,** *104* (48), 18913-18918.
234. Kumar, A.; Erasquin, U. J.; Qin, G.; Li, K.; Cai, C., "Clickable", Polymerized Liposomes as a Versatile and Stable Platform for Rapid Optimization of Their Peripheral Compositions. *Chem. Commun.* **2010,** *46* (31).
235. Kumar, A.; Kolar, S. S.; Zao, M.; McDermott, A. M.; Cai, C., Localization of Antimicrobial Peptides on Polymerized Liposomes Leading to Their Enhanced Efficacy against Pseudomonas Aeruginosa. *Mol. BioSyst.* **2011,** *7* (3).
236. Loosli, F.; Doval, D. A.; Grassi, D.; Zaffalon, P.-L.; Favarger, F.; Zumbuehl, A., Clickosomes-Using Triazole-Linked Phospholipid Connectors to Fuse Vesicles. *Chem. Commun.* **2012,** *48* (10).
237. Jewett, J. C.; Sletten, E. M.; Bertozzi, C. R., Rapid Cu-Free Click Chemistry with Readily Synthesized Biarylazacyclooctynones. *JACS* **2010,** *132* (11), 3688-3690.
238. Kuzmin, A.; Poloukhtine, A.; Wolfert, M. A.; Popik, V. V., Surface Functionalization Using Catalyst-Free Azide−Alkyne Cycloaddition. *Bioconj. Chem.* **2010,** *21* (11), 2076-2085.
239. Jewett, J. C.; Bertozzi, C. R., Cu-Free Click Cycloaddition Reactions in Chemical Biology. *Chem. Soc. Rev.* **2010,** *39* (4).

240. Bostic, H. E.; Smith, M. D.; Poloukhtine, A. A.; Popik, V. V.; Best, M. D., Membrane Labeling and Immobilization Via Copper-Free Click Chemistry. *Chem. Commun.* **2012,** *48* (10), 1431-1433.
241. Ma, Y.; Zhang, H.; Gruzdys, V.; Sun, X.-L., Azide-Reactive Liposome for Chemoselective and Biocompatible Liposomal Surface Functionalization and Glyco-Liposomal Microarray Fabrication. *Langmuir* **2011,** *27* (21), 13097-13103.
242. Umezu-Goto, M.; Kishi, Y.; Taira, A.; Hama, K.; Dohmae, N.; Takio, K.; Yamori, T.; Mills, G. B.; Inoue, K.; Aoki, J.; Arai, H., Autotaxin Has Lysophospholipase D Activity Leading to Tumor Cell Growth and Motility by Lysophosphatidic Acid Production. *The Journal of Cell Biology* **2002,** *158* (2), 227-233.
243. Tokumura, A.; Majima, E.; Kariya, Y.; Tominaga, K.; Kogure, K.; Yasuda, K.; Fukuzawa, K., Identification of Human Plasma Lysophospholipase D, a Lysophosphatidic Acid-Producing Enzyme, as Autotaxin, a Multifunctional Phosphodiesterase. *J. Biol. Chem.* **2002,** *277* (42), 39436-39442.
244. Tanaka, M.; Okudaira, S.; Kishi, Y.; Ohkawa, R.; Iseki, S.; Ota, M.; Noji, S.; Yatomi, Y.; Aoki, J.; Arai, H., Autotaxin Stabilizes Blood Vessels and Is Required for Embryonic Vasculature by Producing Lysophosphatidic Acid. *J. Biol. Chem.* **2006,** *281* (35), 25822-25830.
245. Hoeglund, A. B.; Bostic, H. E.; Howard, A. L.; Wanjala, I. W.; Best, M. D.; Baker, D. L.; Parrill, A. L., Optimization of a Pipemidic Acid Autotaxin Inhibitor. *J. Med. Chem.* **2010,** *53* (3), 1056-1066.
246. Zhan, W.; Jiang, K.; Smith, M. D.; Bostic, H. E.; Best, M. D.; Auad, M. L.; Ruppel, J. V.; Kim, C.; Zhang, P., Photocurrent Generation from Porphyrin/Fullerene Complexes Assembled in a Tethered Lipid Bilayer. *Langmuir* **2010,** *26* (19), 15671-15679.

Vita

Heidi Elizabeth Bostic was born in Gaffney, South Carolina. In 2003, she began her undergraduate studies at Wofford College in Spartanburg, SC, where she earned a B.S. in Chemistry, a B.A. in Computer Science, a minor in Mathematics, and an Emphasis in Computational Science. She came to the University of Tennessee in 2007 and joined the lab of Dr. Michael Best where her research interests have included the application of bioorthogonal chemistry to study membrane systems.